Nano/micromaterials and motors in (bio)sensing applications

Maria Guix Noguera

PhD Thesis

PhD in Chemistry

Director

Prof. Arben Merkoçi

Chemistry Department

Science Faculty

2013

Memòria presentada per aspirar al Grau de Doctor per Maria Guix Noguera

Maria Guix Noguera

Vist i plau

Prof. Dr. Arben Merkoçi (director)

Investigador ICREA
Nanobioelectronics & Biosensors Group
Institut Català de Nanotecnologia (ICN)
Catalan Institute of Nanoscience and Nanotechnology (ICN2)

Prof. Dr. Josep Ros Badosa (tutor)

Catedràtic de Química Inorgànica
Universitat Autònoma de Barcelona

Bellaterra, 30 de Juny de 2013

The present thesis research has been carried out at the Nanobioelectronics and Biosensors Group at Catalan Institute of Nanoscience Nanotechnology (ICN2) and the Chemistry Department of Universitat Autònoma de Barcelona (UAB).

According to the decision of the PhD Comission of the Autonomous University of Barcelona, taken on March 13th, 2013, this PhD thesis is presented as a compendium of the following publications:

"Nanomaterials for Electroanalysis" Arben Merkoçi, Adriano Ambrosi, Alfredo de la Escosura-Muñiz, Briza Pérez-López, Maria Guix, Marisa Maltez and Sergio Marin Chapter at Encyclopedia of Analytical Chemistry, John Willey & Sons 2010.

"Structural characterization by confocal laser scanning microscopy and electrochemical study of multi-walled carbon nanotube tyrosinase matrix for phenol detection" Maria Guix, Briza Pérez-López, Melike Sahin, Mònica Roldán, Adriano Ambrosi and Arben Merkoçi. *Analyst* **2010**, *135*, 1918-1925.

"Stable and sensitive flow-through monitoring of phenol using a carbon nanotube based screen printed biosensor" Georgina Alarcón, Maria Guix, Adriano Ambrosi, Maria Teresa Ramirez Silva, Manuel Eduardo Palomar Pardavé and Arben Merkoçi. *Nanotechnology* **2010**, *21*, 245502-245511.

"Bismuth Film Combined with Screen-Printed Electrode as Biosensing Platform for Phenol Detection" Arben Merkoçi, Ulku Anik, Serdar Çevik, Meliha Çubukçu and Maria Guix. *Electroanalysis* **2010**, *22*, 1429 – 1436.

"Bimetallic nanowires as electrocatalysts for nonenzymatic real-time impedancimetric detection of glucose" Carmen Clotilde Mayorga-Martinez, Maria Guix, Rossana Elena Madrid and Arben Merkoçi. *Chem, Commun.* **2012**, *48*, 1686–168.

"Compact Microcubic Structures Platform based on Self-Assembly Prussian Blue Nanoparticles with Highly Tuneable Conductivity" Welter Cantanhêde Silva, Maria Guix, Georgina Alarcón Angeles and Arben Merkoçi. *Phys. Chem. Chem. Phys.* **2010**, *12*, 15505-15511.

"In-chip magnetic and electrokinetic manipulations for bead based immunosensing applications" Adriano Ambrosi, Maria Guix and Arben Merkoçi. *Electrophoresis* **2010**, *32*, 1-9.

"Superhydrophobic Alkanethiol-Coated Microsubmarines for Effective Removal of Oil" Maria Guix, Jahir Orozco, Miguel García, Wei Gao, Sirilak Sattayasamitsathit, Arben Merkoçi, Alberto Escarpa and Joseph Wang. *ACS Nano* **2012**, *5*, 4445-4451.

ACKNOWLEDGEMENTS

In the following section I would like to thank to all the people who have been supporting me during all this hard, but enriching, period of my life. Part of the section will be written in Catalan (my mother tongue) and Spanish, as I will express myself in the language I feel like when memories with each people come back.

M'agradaria no oblidar-me de ningú, de poder expressar com d'agraïda n'estic de tots els moments viscuts, de tot el suport rebut i òbviament, de tots els coneixements adquirits durant tot aquest temps. Crec poder dir amb certesa que aquest no ha estat un camí fàcil, però tot i així ha estat agradable seguir-lo, sentint-me acompanyada en tot moment tant en el meu camí científic com personalment.

El primer agraïment és pel Dr. Arben Merkoçi, qui més enllà d'haver estat un director excel·lent en la meva tesi, ha intentat sempre donar-me suport i ha fet gala d'aquella empatia que tots els qui hem treballat amb ell coneixem. Gràcies per saber pressionar quan era necessari, per fer sempre el que ha estat millor per mi essent d'una manera indubtable el millor pare científic que hauria pogut tenir. Perquè mai podré agrair-li prou els valors transmesos barrejats amb l'entusiame científic i la confiança que moltes vegades ens fan falta.

Gràcies a tots els que hi van ser-hi des de bon principi, a en Josep Ros, que em va acollir i va deixar-me endinsar en el món de les nanopartícules. A en Leo, la Bet, en Toni, en Sergi, la Maica, en Jordi, en Joan, en Jordi i en Miguel, per fer que al recordar les llargues jornades a inorgànica sempre em robin un somriure. Jornades que es combinaven amb un Màster on vaig poder créixer com a persona gràcies a companys com la Irene, en Joan, la Míriam, en Carlos, en Cornelius, l'Alfonso, la Lorena i la Maria.

Donant pas a l'entrada al grup, al meu grup de nom difícil de recordar però amb gent difícil d'oblidar. Porque en Nanobioelectronics & Biosensors Group he vivido con intensidad todo lo qué significa trabajar en ciencia, y sobretodo con gente. Acogiéndome des del principio, tal y como hicieron Briza, Tere, Anna, Gemma, Alfredo, Adriano, Marisa y Sergi. Dejando que los que iban llegando, como Mariana, Claudio, Anne, Miquel, Helena, Melike, Pinar, Gina, Welter, Tiziana, Deniz, Serdar, Wilanee, Luis, Lourdes, Carmen, Sandrine, Marisol, Adaris, Álex, Flavio y Edén, se convirtieran en una parte más de mi vida. Porque no somos un grupo, sino una gran familia en la que también están Carlos, Dulce, Anabel, Rosa, Marta y Montse, haciendo que todo sea mucho más fácil.

Gràcies a tot el Servei de Microscòpia de la Universitat Autònoma de Barcelona, per la seva professionalitat i paciència, a l'Onofre, en Pablo, l'Emma i en Marcos, i sobretot a la Mònica per ajudar-me tantíssim en el meu primer article.

I wouldn't like to forget the people I had the pleasure to know during my short, but intense, internship in Switzerland, working at EMPA (Thun). It was a pleasure to have as a supervisor Dr. Laetitia Philippe, but also to share such an amazing time with Mikäel, Aleksandra, Ali, Matthias, Sebastian, Jamil, Juan, Edin, Sergio, Christoph, Kotaru, Rudy, James, Vera, Eveline and Katrin. Thanks for such tasteful chocolate at coffee breaks and thrilling frisbee plays.

Then I flew to San Diego and thanks to Dr. Wang and all his amazing team I could finally see micromotors literally flying. At the UCSD I had the great pleasure to be a part of the so-called Spanish team, with Susana, Jahir and Miguel, but working at the same time with great people like Gabriela, Wei, Sirilak, Filiz, Josh, Aoife, Cawas, Amay, Alexandra, Serguey, Dan, Beke, Ming, Jonathan, Victor, Younge, Vinci, Wenzhao, Allan, Ashley, Aysegul, Allen, Jordi, Aakash, Deisy and Laura. Thanks to all of them for being my American family and specially to Azu and Raj, who were taking care of me since the first moment, as well as all the catalan people who taught me knitting while they made me feel that I was not so far away.

Al llarg d'aquest del camí he conegut a molta gent, però voldria agrair a tots aquells que hi eren ja abans, que segueixin sent-hi tot i les meves múltiples absències, sobretot els darrers mesos. A les meves nenes, la Laura, l'Ingrid, la Mariona, les Núries i la Maria. A l'Elisenda, incansable. A l'Amàlia, la Rosa, la Cris i en Víctor, per haver-me fet costat des del primer dia, sempre. A tota la gent que he tingut el plaer de conèixer i tenir al meu costat entre pis i pis, la Irene, l'Ali, l'Anna, la Bruna, la Sílvia, l'Ángeles i la Núria.

A Juan, por estar siempre a mi lado, incluso estando al otro lado del charco, sacando mi lado más optimista en los momentos más complicados.

I finalment vull donar les gràcies a aquells que sempre, sense excepció, han estat al meu costat: la meva petita però incondicional família. Començant pels meus pares, Joan i Assumpta, la tieta Lourdes i l'avi Ventura, però en especial a la iaia Paquita, que no podrà veure el final d'aquest camí aquí, al meu costat. Gràcies per haver-hi estat sempre, expulsant-me les meves pors i donant-me la llibertat per créixer i per a ser millor persona, mentre m'acompanyàveu fent-me costat a cada pas.

ACKNOWLEDGEMENTS FOR THE FINANCING SUPPORT

The main scope of the thesis is the study of the implementation of various nano/micromaterials into biosensing and moving platforms , not only to improve their performance but also to achieve novel sensing and actuation capabilities. The use of well-known carbon nanomaterials, conveniently modified with biological entities, offered new possibilities to biosensing platforms.

Different enzyme immobilization techniques so as to develop miniaturized electrochemical platforms, such as screen-printed electrodes (SPE), with interest for various biosensing applications have been developed.

The use of modified-SPE coupled to different operational systems including a Flow Injection Analysis (FIA) one, permitted the development of a biosensing device with a better analytical performance while being used for phenol detection with interest for environmental applications.

In addition a versatile lab-on-a-chip system for immunosensing-related applications, by coupling the classical electrophoresis approach to the magnetic manipulation of modified magnetic beads to electrochemically detect rabbit Immunoglobulin G (IgG) protein used as proof of concept model analyte also has been developed.

Finally one step further has been done by the integration of nano/micromaterials with micromotors platforms with interest also for environmental-related issues. Beyond the devices motion studies, interesting sensing and environmental applications have been reported, envisioning such engines even as the future platforms for *in situ* theranostic issues.

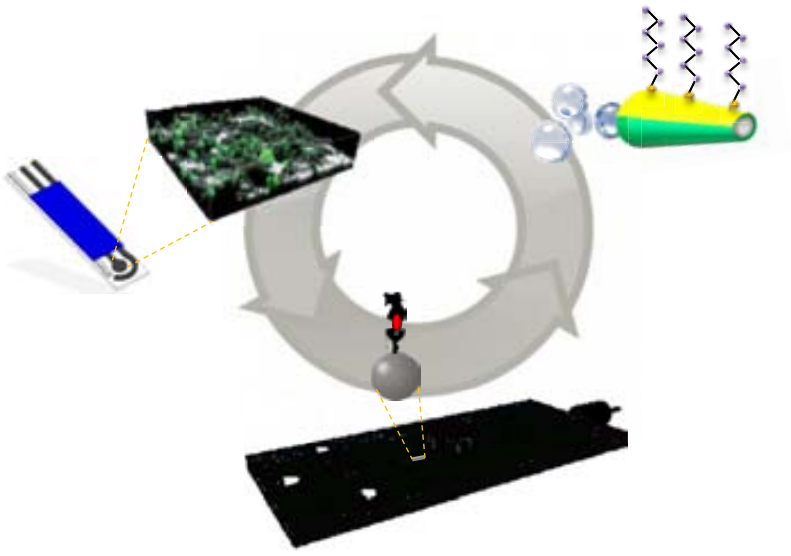

SPE	screen-printed electrode
FIA	flow injection analysis
NPs	nanoparticles
DNA	deoxyribonucleic acid
QDs	quantum dots
CNTs	carbon nanotubes
TEM	transmission electron microscopy
SEM	scanning electron microscopy
HRTEM	high-resolution transmission electron microscopy
AFM	atomic force microscopy
CLSM	confocal fluorescence microscopy
XRD	X-ray diffraction
Ag	antigen
Ab	antibody
DPV	differential pulse voltammetry
GOX	glucose oxidase
HRP	horseradish peroxidase
AuNP	gold nanoparticle
SWCNT	singlewall carbon nanotubes
MWCNT	multiwall carbon nanotubes
CVD	chemical vapor deposition
DMSO	dimethyl sulfoxide
H_2O	water
APTES	3-aminopropyltriethoxysilane
NADH	nicotinamide adenine dinucleotide
PVC	polyvinyl chloride
GA	glutaraldehyde
ALP	alkaline phosphatase
PCR	polymerase chain reaction
1D	one dimension
Au	gold
Pt	platinum
IME	interdigitated microelectrodes
Ni	nickel
Ag	silver
CNT	carbon nanotubes

CMOS	complementary metal-oxide-semiconductor
PDMS	polydimethylsiloxane
PLGA	poly-D,L-lactic-*co*-glycolic acid
PPy	polypyrrole
UV	ultraviolet
DNA	deoxyribonucleic acid
RNA	ribonucleic acid
HRP	horseradish peroxidase
3-D	three dimensional space
DSG	dynamic shadowing growth
TiO_2	titanium dioxide
SDS	sodium dodecyl sulphate
Fe	iron
CAD	catecholaminergic-a-differentiated
SAM	self-assembled monolayers
anti-CEA	antibody against the carcinoembryonic antigen
mAb	monoclonal antibody
Ga	gallium
As	arsenic
PANI	polyaniline
PEDOT	poly(3,4-ethylenedioxythiophene)
PAPBA	poly(3-aminophenylboronic) acid
FIB	focus ion beam
Ag/AgCl	silver/silver chloride
WE	working electrode
RE	reference electrode
AE	auxiliar electrode
THF	tetrahydrofuran
ROI	region of interest
Bi	bismuth
BiFE	bismuth film electrode
CV	cyclic voltammetry
LOD	limit of detection
LOQ	limit of quantification
FIA	flow injection analytical
Glu	glutaraldehyde
EPA	Environment Protection Agencies

GOx	glucose oxidase
GDH	glucose dehydrogenase
CIT	chronoimpedance technique
NW	nanowire
EEIZ	electrode–electrolyte interface impedance
IrOx	iridium oxide
H_2O_2	hydrogen peroxide
O_2	oxygen
UA	uric acid
AA	ascorbic acid
CA	citric acid
LbL	layer-by-layer
CDC	constitutional dynamic chemistry
PB	prussian blue
β-CD	β-cyclodextrin
PAH	polyallylamine
KCl	potassium chloride
AP	alkaline phosphatase
EC	electrochemical
MB	magnetic bead
p-NPP	p-nitrophenyl phosphate

INTRODUCTION

RESULTS AND DISCUSSION

CHAPTER 1

GENERAL INTRODUCTION

THESIS OVERVIEW

The development of more sensible and robust analytical platforms if of great interest nowadays, especially for the development of miniaturized systems designed to perform *in situ* measurements in environmental monitoring and assessment. Regarding electrochemical sensing techniques, the integration of nano/micro materials could especially enhance their analytical performance.

Several nano/micro materials as for example carbon nanotubes, bimetallic nanowires or Prussian blue nanoparticles have been studied. The present PhD thesis is focused on the implementation of such nano/materials coupled to biological entities (e.g. enzymes, antibodies) to improved biosensing platforms. Different sensing platforms, starting by the miniaturized screen-printed electrodes to lab-on-a-chip systems, to obtain versatile analytical platforms for sensing of pollutants and other analytes of interest, such as glucose or dopamine have been developed.

Beyond the classical batch and lab-on-a-chip sensing systems, an alternative and challenging approach based on the use of tubular catalytic micromotors as dynamic analytical platform is presented. Their implementation in environmental and analytical issues is of special importance, as they are envisioned as key components in future diagnostic systems.

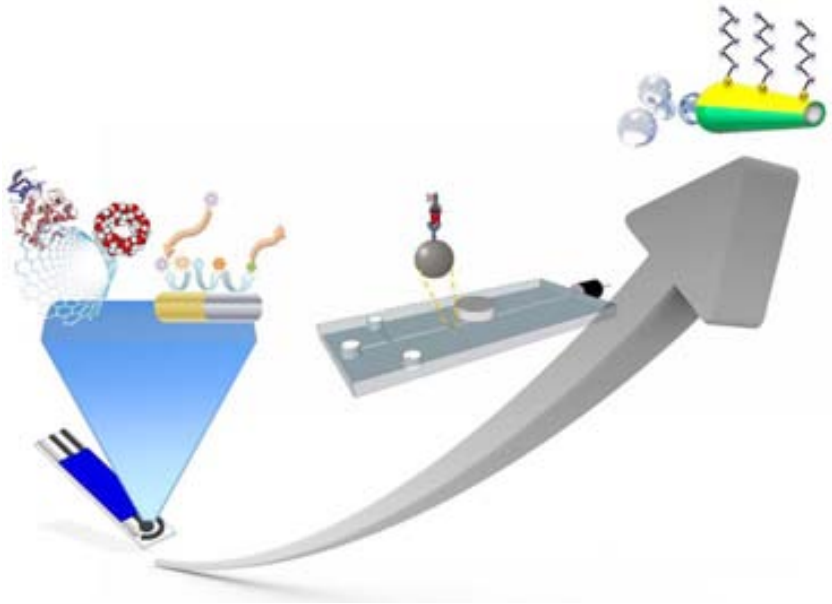

Scheme 1.1. General schematic of the main research fields of the thesis showing the batch systems coupled to different biological entities followed by more complex platforms (FIA and lab-on-a-chip systems) and micromotors for environmental issues.

General aspects and experimental results related to the present PhD thesis are divided into six main chapters, including the introduction, thesis objectives, results and discussions and general conclusions and perspectives.

Chapter 1 entitled *"General Introduction"*, hereby presented, is divided into three main parts. A general overview of the present thesis with a brief introduction of the related research fields and concepts with interest for the experimental work of this PhD thesis, followed by a short summary of the included six chapters. The second part is focused on the full-comprehension of the state-of-the-art regarding nano/micro materials and their applications in electroanalysis, in addition to a general presentation of the mechanisms and principal applications of catalytic micro/nano motors autonomously moved in presence of hydrogen peroxide.

Chapter 2 entitled *"Objectives of the thesis"*, presents the different objectives of the PhD thesis. The principal aim of the present thesis is the integration of different nano/micro materials to different analytical platforms so as to obtain more robust and efficient sensing systems. Along with the main purpose of the thesis, particular objectives related to each developed platform, starting by screen-printed electrode platforms to lab-on-a-chip devices or micromotors, and the different nanomaterials involved in, are depicted.

Chapter 3 entitled *"Batch detection platforms"* consider all the studies based on screen-printed electrodes (SPE) modified with nano/micro materials, as carbon nanotubes or nanowires, to further be implemented on the detection of certain analytes of interest (e.g. phenol, glucose). The results of an extensive characterization of the SPE platforms, concerning not only their morphology, but also how enzymatic species are distributed along their matrices are given. Regarding enzyme immobilization, different approaches that depend on the system requirements and lead to an improvement of the SPE stability and sensibility towards phenol detection are described. The integration of modified-SPE in a flow system demonstrating future real applications in monitoring systems is also considered. Additionally, other hybrid platforms of interest, which are envisioned as potential host-guest systems in dependent electrochemical biosensing designs are presented. All these studies demonstrate the contribution of nano/micromaterials to obtaining of simple and robust

miniaturized systems with better responses and to opening the door to more efficient sensing strategies for monitoring applications.

Chapter 4 entitled "*Lab-on-a-chip platforms"* deals with the development of bead-based protein analysis in lab-on-a-chip devices. The integration of microscale magnetic beads in such platforms, coupled with electrochemical detection, resulted in an extremely efficient immunosensing application. The different optimizations of key parameters involved in the development of such electrophoretic and magnetic-based chip, of great interest for environmental and biosensing applications for its versatility and low reagent consumption, are presented.

Chapter 5 entitled "*Micromotors*" describes the main features of template-based tubular micromotors, along with their evolution in different applications related to biosensing and environmental issues. It is specially emphasized the development of superhydrophobic micromotors and their further application in water-oil contaminated water due to their oil-sorption properties. The objective of such micromotors is in line with previously described batch platforms for environmental issues (ex. phenol detection) given the fact that these devices aim to be autonomously moving microscale entities envisioned as future *in situ* monitoring and cleaning systems thanks to their small size, versatility and moving efficiency in complex matrix.

Concluding remarks of the present thesis in addition to future perspectives regarding the different results and research fields explored during the PhD thesis are enclosed at the **Chapter 6**.

NANOMATERIALS FOR ELECTROANALYSIS

Related Publication

"Nanomaterials for Electroanalysis" Arben Merkoçi, Adriano Ambrosi, Alfredo de la Escosura-Muñiz, Briza Pérez-López, Maria Guix, Marisa Maltez, Sergio Marin. Chapter at Encyclopedia of Analytical Chemistry, John Willey & Sons **2010**.

1. 2. 1. Introduction

Nanotechnology is the term used to describe the creation and exploitation of materials with structural features in between those of atoms and bulk materials, with at least one dimension in the nanometer range (1nm = 10^{-9} m). The properties of materials with nanometric dimensions are significantly different from those of atoms or bulk materials. Suitable control of the properties of nanometer-scale structures can lead to new science as well as new products, devices, and technologies.[1]

There has been explosive growth of nanoscience and technology in the last decade, primarily because of the availability of new methods of synthesizing nanomaterials, as well as tools for characterization and manipulation. Several innovative methods for the synthesis of NPs and nanotubes, and their assemblies, are now available. In addition, there is a better understanding of the size-dependent electrical, optical, and magnetic properties of individual nanostructures of semiconductors, metals, and other materials.[2]

Besides the established techniques of electron microscopy, crystallography, and spectroscopy, scanning probe microscopies have provided powerful tools for the study of nanostructures. Novel methods of fabricating patterned nanostructures, as well as new device and fabrication concepts, are constantly being discovered.

The immediate goals of the science and technology of nanomaterials must be to fully master the synthesis of isolated nanostructures (building blocks) and their ensembles and assemblies with the desired properties, to explore and establish nanodevice concepts and systems architecture, to generate new classes of high performance materials, including biologically inspired systems, to connect nanoscience to molecular electronics and biology, and to improve known investigative methods while discovering better tools for the characterization of nanostructures.[3]

Table 1 lists typical nanomaterials of different dimensionalities commonly used in electroanalysis. Nanotubes, NPs, nanowires, and nanocomposite and nanostructurated materials have already been used to fabricate a large number of electrochemical devices, ranging from chemical sensors and enzyme-based biosensors to DNA sensors, exhibiting higher sensitivity, stability, and selectivity due to the presence of

functionalized nanomaterials used as catalytic tools, as immobilization platforms, or as labels for the sensitive recognition events.[4]

Table 1. Typical nanomaterials used in electroanalysis

	Size	Materials
Nanoparticles, quantum dots	1–100nm	Metals, semiconductors, magnetic materials, ceramic oxides
Nanotubes, nanocomposites	Diameter 1–100 nm; length 1 nm – 15μm	Metals, semiconductors, oxides, sulfides, nitrides, carbon
Nanowires	Diameter 1–100 nm; length 2 nm – 20μm	Metals, semiconductors, oxides, sulfides, nitrides, carbon
Nanochannels, nanopores	Several square nanometers to square micrometers	Metals, oxides, carbon

Various nanostructures have been investigated to determine their properties and possible applications in electroanalysis. NPs, quantum dots (QDs), carbon nanotubes (CNTs), nanowires, and nanochannels of different sizes and materials have been applied and integrated to electrochemical platforms with functions depending on the specific features of the nanomaterials. They have been applied to improve immobilization of (bio)molecules onto electrode surfaces, to catalyze reactions, to record higher transducing signals, to enhance specificity of reactions, to miniaturize analytical systems, and speed up processes.

A detailed description of the most commonly used nanomaterials in electrochemical detecting tools, their general properties, and their most successful applications in electrochemical analysis are given in the following sections.

1. 2. 2. Nanoparticles

Metal and semiconductor NPs are certainly the most studied and applied in electrochemical analysis.[5] Owing to their small size (normally in the range of 1–100 nm), NPs exhibit unique chemical, physical, and electronic properties that are different from those of bulk materials, and can be used to construct novel and improved sensing devices; in particular, electrochemical sensors and biosensors. Such properties strongly depend on the number and kind of atoms that make up the particle. The properties of the particles generally depend on their size, shape, distribution, and stabilizing agents, which are controlled by the preparation conditions.[6]

Metal NPs can be prepared by physical and chemical methods. The physical methods consist of using a low-pressure evaporation of the metal, followed by a controlled condensation in a stream of inert gas. Chemical procedures consist of the chemical reduction of metal ions to metal atoms in the presence of a stabilizer (capping agent such as citrate or thiol) that binds to their surface to impart high stability and rich linking chemistry and provide the desired charge and solubility properties. The latter preparative method is more suitable to obtain small and uniform NPs than the former; moreover, the size and uniformity of the NPs depend on the kind and amount of the reducing agent employed.[7]

NPs from metallic materials such as gold,[8] silver,[9] cobalt,[10] and platinum[11] can be synthesized. The surface plasmon absorption band can provide information of the development of the band structure in metals[12,13] and has led to a plethora of studies on the size-dependent optical properties of metal particles, particularly those of silver and gold.[14,15] The optical response of these metal NPs is both size- and shape dependent and locally variable.[16] This sensitivity to morphology makes precise control over the growth of these NPs and knowledge of their external and internal structures essential.

Plasmonic metal NPs also show potential for biosensing[17] and cancer therapy.[18] Nanoscale shells of gold surrounding a silica core can be selectively tuned to convert near-infrared photo energy into thermal energy – nanofurnace that efficiently targets and destroys cells.[19] While some bulk metals have similar properties, only those with nanodimensions offer such tunable, and deliverable, possibilities.

Different kinds of techniques can be used to characterize the NPs depending on the kind of the application. Table 2 shows several characterization techniques and the parameters that can be obtained from each.

Table 2. Techniques used for nanoparticles characterization

Techniques	Characterization
Transmission electron microscopy (TEM)	Size and shape (>10 nm) Crystalline structure (poor)
High-resolution transmission electron microscopy (HRTEM)	Size and shape (>0.1 nm) Crystalline structure (poor) Crystalline lattice

	Microanalysis (poor)
Atomic force microscopy (AFM)	Size and shape (>0.01 nm) Size distribution
Confocal fluorescence microscopy (CLSM)	Size and shape (>100 nm) Fluorescence properties
X-ray diffraction (XRD)	Crystalline structure (exact)
Z-potential	Electrical charge Size (poor)
Electrochemical	Concentration Redox potential

Many types of NPs of different sizes and compositions are now available, which facilitate their application in electroanalysis, bringing important advantages: (i) their immobilization on electrode surfaces generates a roughened conductive high surface area interface that enables the sensitive electrochemical detection of molecular and biomolecular analytes; (ii) NPs act as effective labels for the amplified electrochemical analysis of the respective analytes; (iii) the conductivity properties of metal NPs enable the design of biomaterial architectures with predesigned and controlled electrochemical functions.

Applications

Several applications of NPs ranging from their use for biomolecule labelling, modification of electrode surfaces, enhancement of electron-transfer, and catalysis with interest for electroanalysis are described in the following sections.

The labelling of biomolecules, such as antigen, antibody, and DNA with NPs plays an increasingly important role in developing sensitive electrochemical biosensors. Biomolecules labelled with NPs can retain their bioactivity and interact with their counterparts, and based on the electrochemical detection of those NPs, the amount or concentration of analytes can be determined.

The use of biomolecules labelled with NPs offers novel opportunities for (bio) detection systems.[20] The electrochemical detection of NPs offers highly sensitive detection alternatives besides being the easiest and cheapest technique comparing to optical detections such as fluorescence spectroscopy among others. The use of NPs as detecting labels is applied to improve the DNA and protein analysis.

DNA analysis DNA biosensors represent a very important type of affinity biosensors in which the biorecognition molecules are oligonucleotides of known sequence and the recognition event is the hybridization with the complementary sequences. Among the various types of DNA sensors, the electrochemical sensor has some advantage such as the use of very simple equipment to perform measurements, low cost, and possibility of miniaturization in order to obtain high-density arrays. DNA biosensors based on DNA hybridization are playing an increasing role in DNA analysis.[21,22]

Protein analysis immunosensors and immunoanalysis are affinity ligand-based analytical tools that use antibodies as the biospecific sensing element with the immunochemical reaction coupled to a transducer. These biosensors are based on the ability of an antibody to form complexes with the corresponding antigen.[23,24]

Immunoassays are among the most specific of the analytical techniques. They provide extremely low detection limits and can be used for a wide range of substances. As research moves into the era of proteomic, such assays become extremely useful for identifying and quantifying proteins. Immunosensors are based on immunological reactions involving the shape recognition of the antigen (AG) by the antibody (AB)-binding site to form the AB/AG stable complex:

$$AB + AG \leftrightarrow AB/AG \quad (1)$$

Immunoassays, based on the specific reaction of ABs with the target substances (AGs) to be detected, have been widely used for the measurement of targets at low concentration in clinical samples such as urine and blood and the detection of the trace amounts of drugs and chemicals such as pesticides in biological and environmental samples.

Direct detection of NPs consists of a so-called solid state analysis, where the metals forming the NPs are detected electrochemically without any preliminary dissolution step to liberate the metal ions in solution. However, this type of detection needs a direct contact between the electrode surface and the metal itself and excludes from detection a large portion of non-touching particles. Despite the loss of sensitivity that could result from this phenomenon, in comparison with techniques exploiting the total

NPs dissolution and all metal ions detected, direct detections achieve more rapid responses and still considerable limit of detections.

Solid-state detection of NPs has been applied in numerous immunoassays analysis exploiting the intrinsic electrochemical properties of the metal NPs used as tracers. Ambrosi et al. recently used magnetic particles as platform to perform the immunological interactions. After the specific interaction with the secondary NP labeled antibody, these magnetic particles were collected onto the electrode surface by means of a permanent magnet inserted inside the electrode body. Differential pulse voltammetry (DPV) analyses were performed to quantify the metal NPs collected through the biospecific interaction and that are related to the target analyte concentration (protein). Very low limits of detection were achieved using this magnetic particle collection, reaching the lowest value of 260 pgmL−1 human IgG protein.[25]

Modification of Electrode Surfaces

Owing to their large specific surface area and high surface free energy, NPs can adsorb biomolecules strongly and once introduced onto the surface of a proper transducer would play an important role in the immobilization of biomolecules and consequently improve the biosensor performance. Generally, the adsorption of biomolecules directly onto naked surfaces of bulk materials may frequently result in their denaturation and loss of bioactivity. However, the adsorption of such biomolecules onto the surfaces of NPs can retain their bioactivity. Having comparable dimensions, biomolecules conjugated to NPs maintain the natural conformation/structure and hence the functionality.

Figure 7 is a schematic that show three different mechanisms that can be used to functionalize NPs with biomolecules:

1. Electrostatic adsorption.

2. Chemisorption of thiol derivatives.

3. Specific affinity interactions.

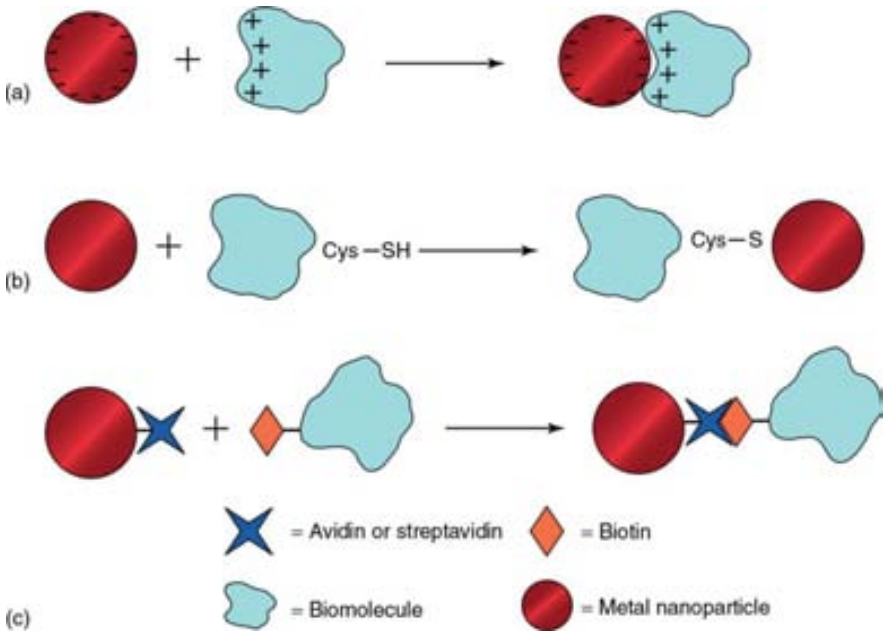

Figure 1.2.1. Schematic of different strategies used to couple NPs with biomolecules. (a) Electrostatic interaction of biomolecules with metal nanoparticles; (b) covalent interaction of biomolecules through thiol groups with metal nanoparticles; (c) bioconjugation of metal nanoparticles by the use of bioaffinity interactions upon (strept)avidin–biotin binding.

Concerning enzyme immobilization, in the early 1990s, Crumbliss et al. immobilized several kinds of enzymes with gold NPs and further fabricated different enzyme electrodes with retained enzymatic activity.[26] Chen *et al.* first attached gold NPs to gold electrodes modified with cysteamine monolayer, and then successfully immobilized horseradish peroxidase on these NPs.[27] They also studied the effect of nanoparticle size on the performance of the prepared biosensors. NPs with smaller size were found to be more suitable for enzyme immobilization. Many similar studies have been reported for the construction of biosensors based on the immobilization of different enzymes such as horseradish peroxidase, [28, 29] microperoxidase-11, [30] tyrosinase,[31] and hemoglobin[32] with gold NPs.

The electrostatic deposition of biomolecules, particularly proteins or enzymes, can also be extended to multilayer-level assemblies.[33] Proteins that are electrostatically attracted to the charged NPs can provide an interface for the further deposition of an oppositely charged polyelectrolyte polymer, which again allows the deposition of a secondary protein layer. Multilayer films of glucosidase,[34] glucose oxidase (GOX),[35] urease, [36] and HRP [37] have been assembled on polystyrene NPs by the alternate deposition of the proteins and an oppositely charged synthetic polyelectrolyte as a linker, e.g. positively charged poly(diallyldimethylammonium) chloride or negatively

charged poly(sodium 4-styrenesulfonate). The protein/polymer multilayer shell could be varied from several to hundreds of nanometers in thickness. This strategy permits the preparation of functional films on NPs with a high density of enzyme molecules.

Chemisorption of proteins onto AuNP surface can originate from the binding of thiol groups from cysteine residues that exist in the proteins to the Au surface. If no thiolated residues are available in the native proteins, thiol groups can be incorporated by chemical means; for example, with 2-iminothiolane [38] or through genetic engineering. [39] For example, the immobilization of endoglucanase enzyme onto AuNPs through the covalent bonds formed between the Au atoms and the cysteine residues of the protein has been reported.[40]

Nanoparticles are considered enhancers of electron transfer, as the electrical contacting of redox enzymes with electrodes is a key process in the design of enzyme electrodes for bioelectronic applications such as biosensors, [41] or biofuel cell elements.[42] Enzymes usually lack direct electrical communication with electrodes due to the fact that their active centers are surrounded by considerably thick insulating protein shells, which, therefore, block the direct electron transfer. The conductive properties of NPs – mostly metal NPs at nanoscale dimensions – make them suitable for enhancing the electron transfer between the enzyme active centers and electrodes, thus acting as ‘‘mediators’’ or ‘‘electrical wires’’.

1.2.3. Carbon nanotubes

The discovery in 1985 of buckminsterfullerene opened a new era for the chemistry of carbon and for novel materials. Sumi Ijima, the Japanese physicist, discovered the nanotubes in 1991.[43] CNTs have generated great interest for various applications based on their field emission and electronic transport properties, their high mechanical strength, and their chemical properties.[43] From this arises an increasing potential for use as fieldemission devices,[44] nanoscale transistors,[45] tips for scanning microscopy,[46] or components for composite materials.[47]

In this context, CNT are considered particular nanomaterials that have generated a considerable interest owing to their unique structure-dependent electronic and mechanical properties.[48]

CNTs can be divided into single-wall carbon nanotubes (SWCNT) and multiwall carbon nanotubes (MWCNT)[49] (Figure 8). SWCNT (Figure 8a) possess a cylindrical nanostructure formed by rolling a single graphite sheet into a tube. SWCNT can thus be viewed as molecular wires with every atom on the surface. MWCNT (Figure 8b) comprise of an array of such nanotubes that are concentrically nested like rings of a tree trunk.[50]

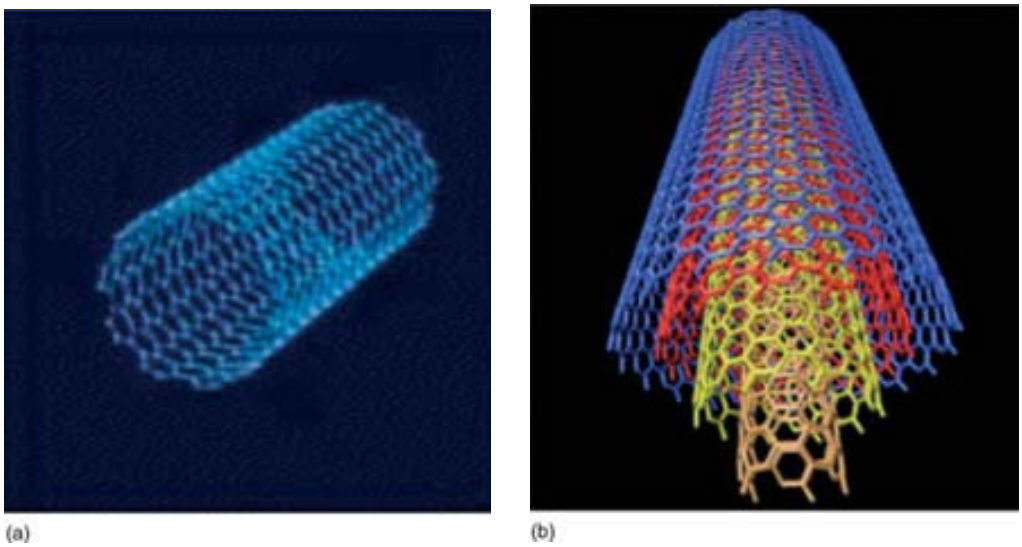

Figure 8. Schematics of an individual (a) SWCNT and (b) MWCNT. (Adapted from Ref. 49. Elsevier, 2005.)

CNTs are one of the most commonly used building blocks of nanotechnology. With 100 times the tensile strength of steel, thermal conductivity better than all but copper, but with the ability to carry much higher currents, CNTs seem to be a wonder material.

Concerning carbon nanotubes production, there are several methods to form CNTs: arc method, laser methods, chemical vapor deposition (CVD), etc. However, in order to use CNTs in novel devices, it is necessary to produce these materials with a high crystallinity on a large scale economically. In this context, the catalytic CVD method is considered to be the optimum for producing large amounts of CNTs, particularly with the use of a floating-catalyst method.[51] This technique is more controllable and cost efficient compared to arc-discharge and other methods.

Extensive research has been dedicated to the purification of CNTs in order to remove foreign NPs that modify the physicochemical properties of CNTs. Chemical methods

have been applied for purifying CNTs. SWNT purification developed by Smalley and coworkers [52] consists of refluxing as-grown SWNTs in nitric acid solutions. Subsequently, more-effective purification techniques have been developed with minor physical damage of the tubes.[53,54] The other method was reported by Martinez *et al.*[55] and consists in a technique of high-temperature air oxidation in conjunction with microwave acid treatments, for removing a high portion of metal particles in relatively short periods of time. The most effective methods for MWNTs purification are high-temperature treatments in an inert atmosphere (graphitization or annealing) and removing structural defects (heptagons and heptagon–pentagon pairs) or impurities such as metallic compounds.[56]

Carbon nanotubes dispersion is of key importance before their further implementation in certain applications, as it is necessary to transform them into a "soluble" product. The preparation of homogeneous dispersions of CNTs, suitable for their use in thin films or for other applications, is of a great importance. Various methods can be used for this purpose. End[57] and/or sidewall[58] functionalization, use of surfactants with sonication,[59] polymer wrapping of nanotubes,[60,61] and protonation by superacids[62] have been reported. Although these methods are quite successful, they often related to CNTs cut into smaller pieces (sonication and/or functionalization), thus partly losing the high aspect ratio of SWCNTs.

Kim *et al.*[63] provided an example of CNT solubilization. They developed a simple, efficient process for solubilizing CNTs with amylose in dimethyl sulfoxide–H_2O (DMSO–H_2O) mixture as well as in pure water. This process requires two important conditions, presonication of CNTs in water and subsequent treatment of the fine CNT dispersion with amylose in a specified DMSO–H_2O mixture, followed by a postsonication. The best solvent composition was found to be 10–20% DMSO, in which amylose assumes an interrupted loose helix. The resulting colloidal solution was stable and exhibited no precipitation over several weeks.

CNT solubilization by covalent modification was reported by Luong *et al.* [64] MWCNTs were solubilized in a mixture of 3-aminopropyltriethoxysilane (APTES) and Nafion-perfluorinated ion-exchange resin and ethanol. Uniformly dispersed MWCNTs were obtained after 20 min sonication and used for sensor applications.

Applications

CNTs have a wide range of properties that we are still in process of discovering with an ambitious variety of applications. In this case, we focus on the application of CNT-modified electrodes in bioelectroanalysis, which mainly includes electrochemical studies on neurotransmitters, proteins, nucleic acids, and other molecules.

In recent years, CNT-modified electrodes show the properties of electrocatalytic activity due to its unique electronic properties and CNTs can promote electrontransfer reactions,[65] which can be applied for the detection of analytes in a low concentration or in the complex matrix. The CNT-modified electrodes usually include CNT paste electrode,[66] CNT coating electrode,[67] or CNT embedded in a polymeric matrix.[68] Generally, CNT-modified electrodes contain an electrochemical analysis and biosensor applications.[69,70]

Modifications of Electrodes Surfaces

The derivatization of carbon surfaces allows electrochemists to design tailor-made electrodes, which offer distinct advantages for catalysis, analysis and biological applications, and the area of electrochemistry has attracted considerable attention over the last few years,[71] it has aroused great interest in modifying electrode surfaces, for example Pérez *et al.* integrated CNTs onto a GC electrode and use this for reduced nicotinamide adenine dinucleotide (NADH) detection. The use of polyvinyl chloride (PVC) as a matrix for CNTs dispersion aimed to ensure better mechanical/robustness properties of the sensor membrane compared to an unmodified GC electrode. Additionally, with the use of glutaraldehyde (GA) as a matrix linker, their design offer future alternatives for biosensors applications due to the ability of the developed design to aid in covalent binding of biological molecules[72] (Figure 9).

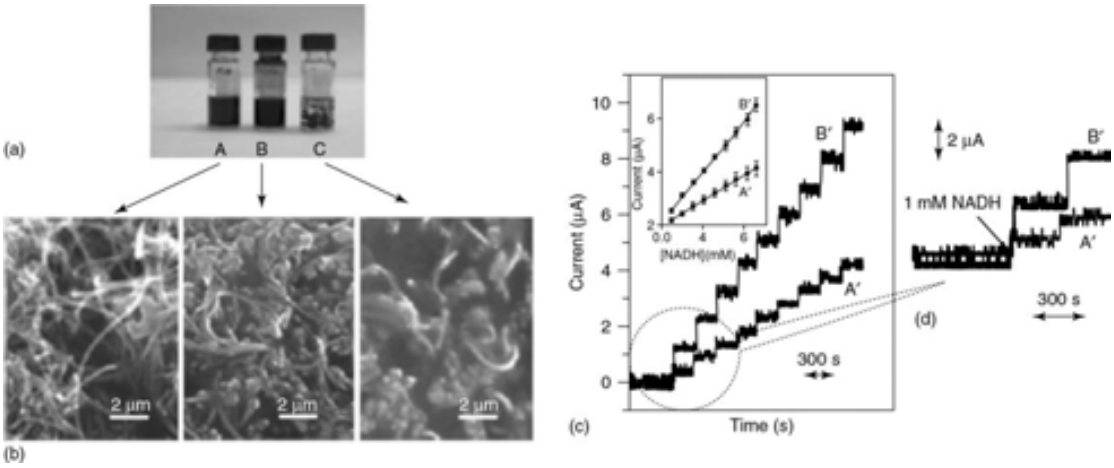

Figure 9 (a) Images of the MWCNTs in tetrahydrofuran (THF) (A), THF+PVC (B), and in THF+PVC+GA solution (C). (b) Scanning electron microscope (SEM) images of the same solutions as in the upper images. (c) Current – time recordings including (as inset) the corresponding calibration plots obtained from amperometric experiments at unmodified (A') and at modified (B') GC electrode for successive additions of 1mM NADH in 0.1M phosphate buffer pH 7. Working potential: +0.7V. (d) The stability of the response (as zoom of the recordings in (c)) is shown for each electrode used. (Adapted from Ref. 127. Wiley-VCH, 2008.)

Carbon Nanotubes as ''Carriers/Amplifiers''

A strategy for dramatically amplifying enzyme-linked electrical detection of proteins and DNA using CNTs as carrying enzymes has been developed by Wang *et al.*,[73] amplifying electrical detection and producing an ultrasensitive bioelectronic detection of DNA hybridization. First, the alkaline phosphatase (ALP) enzyme tracer was immobilized on CNTs using 1-ethyl-3-(3-dimethylaminopropyl) carbodiimide as linker. Such coupling of several CNT-derived amplification processes results in highly sensitive detection of proteins and DNA and hence indicates great promise for PCR-free DNA assays and for assembling controllable nanoscale systems.

The loading of multiple peroxidase enzyme tracers onto CNTs "carriers" has recently been exploited by Rusling's team for highly sensitive immunodetection of cancer biomarkers in serum and tissue lysates.[74]

1.2.4. Nanowires

Nanowires are attractive materials because of their small size, high surface-to-volume ratios, and/or electronic, optical, and magnetic properties, which can differ markedly from those observed for bulk or thin film materials as the nanowire cross-sectional diameter decreases. Because of the high surface-to-volume ratio and novel electron

transport properties of these nanostructures, their electronic conductance is strongly influenced by minor surface perturbations (such as those associated with the binding of macromolecules). Such 1D materials thus offer the prospect of rapid (real-time) and sensitive label-free bioelectronic detection, and massive redundancy in nanosensor arrays. Metal and conducting polymer nanowires can be readily prepared by a template directed electrochemical synthesis involving electrodeposition into the pores of a membrane template.[75]

Nanowires show promise in a number of different sensing strategies, including optical,[76] electrical,[77] electrochemical[78] and mass-based[79] approaches. Recent results suggest the possibility of incorporating large numbers of nanowires into large-scale arrays and complex hierarchical structures for high-density biosensors, electronics, and optoelectronics.[80]

1.2.5. Conclusions and future perspectives

Nanomaterials ranging from NPs, CNTs and nanowires are proving to be very interesting alternatives to conventional materials in a broad range of electrochemical sensing and biosensing systems. Their integration into electrochemical platforms depends on their different sizes, forms, and constituting materials.

NPs have been applied to improve immobilization of (bio)molecules onto electrode surfaces, to catalyze reactions, and to enhance transducing signals. In addition, owing to their small size and electrochemical properties (i.e. heavy metal-based QDs or even gold NPs), these are showing to be excellent labelling tags as alternative to conventional ones like dyes or enzymes.

Although most of the electrochemical strategies for DNA analysis reported to date suffered from the fact that the hybridization event is still separated from the detection, there is a lot of on going effort is to integrate the whole electrochemical assay in a classical biosensor model with real applications for the future. The electrochemical properties of NPs make them extremely easy to detect (in both direct and indirect detection modes) by using simple instrumentation. The electrochemical coding technology is thus expected to open new opportunities for DNA diagnostics, and for bioanalysis, in general, with a special interest for in-field low-cost applications.

There are various advantages that CNTs bring in the electrochemical analysis. CNTs composites seem to be an attractive alternative material in electrochemical sensors. The developed biosensors based on this kind of materials are showing clear advantages in terms of sensor operability (sensitivity, detection limit, stability, etc.) due, overall, to an improvement of electron transfer that leads to a lowering of working potential and consequently a significant remove of interferences during a real sample analysis.

The application of the above-mentioned nanomaterials in relation to electroanalysis is already a consolidated research field not only for electroanalysis but also for the current nanoscience and nanotechnology. The experiences acquired so far in the field of electrochemistry are successfully coupled with the knowledge of new nanomaterials. This synergy is already offering interesting alternatives for several important analytical chemistry applications in fields like clinical analysis, environmental industry, safety as well as other industries.

1.2.6. References

[1] Ratner, M.; Ratner, D. "Nanotechnology: A Gentle Introduction to the Next Big Idea", 1st edition, Prentice Hall PTR, New Jersey, USA, **2003**.

[2] Rao, C. N. R.; Cheetham, A. K. *J. Mater. Chem.* **2001**,*11*, 2887.

[3] Coontz, R.; Szuromi, P. *Science* **2000**, *290*, 1523.

[4] Wang, J. *Analyst* **2005**, *130*, 421.

[5] Penn, S. G.; He, L.; Natan, M. J. *Curr. Opin. Chem. Biol.* **2003**, *7*, 609.

[6] Bonnemann, H.; Richards, F. J.M. *Eur. J. Inorg. Chem.* **2001**, *2001*, 2455.

[7] Niemeyer, C. M. *Angew. Chem. Int. Ed. Engl.* **2001**, *40*, 4128.

[8] Brust, M.; Fink, J.; Bethell, D.; Schiffrin, D. J.; Kiely, C. *J. Chem. Soc. Chem. Commun.* **1995**, *117*, 1655.

[9] Quaroni, L.; Chumanov, G. *J. Am. Chem. Soc.* **1999**, *121*, 10642.

[10] Ershov, B. G.; Sukhov, N. L.; Janata, E. *J. Phys. Chem. B* **2000**, *104*, 6138.

[11] Vidal-Iglesias, F. J.; Solla-Gullon, J.; Rodriguez, P.; Herrero, E.; Montiel, V.; Feliu, J. M.; Aldaz, A. *Electrochem. Commun.* **2004**, *6*, 1080.

[12] Scott, A. B.; Smith, W. A.; Thompson, M. A. *J. Phys. Chem.* **1953**, *57*, 757.

[13] Doyle, W. T. *Phys. Rev.* **1958**, *111*, 1067.

[14] Lee, K. S.; El-Sayed, M. A. *J. Phys. Chem. B* **2006**, *110*, 19220.

[15] Hanauer, M.; Pierrat, S.; Zins, I.; Lotz, A.; Snnichsen, C. *Nano Lett.* **2007**, *7*, 2881.

[16] Nelayah, J.; Kociak, M.; Sthéphan, O.; García, F. J.; Tencé, M.; Henrard, L.; Taverna, D.; Pastoriza-Santos, I.; Liz-Marzán, L. M.; Colliex, C. *Nat. Phys.* **2007**, *3*, 348.

[17] Willets, K. A.; Van Duyne, R. P. *Annu. Rev. Phys. Chem.* **2007**, *58*, 267.

[18] Jain, P. K.; El-Sayed, I. H.; El-Sayed, M. A. *Nano Today* **2007**, *2*, 18.

[19] Hirsch, L. R.; Stafford, R. J.; Bankson, J. A.; Sershen, S. R.; Rivera, B.; Price, R. E.; Hazle, J. D.; Halas, N. J.; West, J. L. *Proc. Natl. Acad. Sci. U.S.A.* **2003**, *100*, 13549.

[20] Murphy, L. *Curr. Opin. Chem. Biol.* **2006**, *10*, 177.

[21] Ozsoz, M.; Erdem, A.; Kerman, K.; Ozkan, D.; Tugrul, B.; Topcuoglu, N.; Ekren, H.; Taylan, M. *Anal. Chem.* **2003**, *75*, 2181.

[22] Park, S. J.; Taton, T. A.; Mirkin, C. A. *Science* **2002**, *295*, 1503.

[23] Luppa, P. B.; Sokoll, L. J.; Chan, D. W. *Clin. Chim. Acta*, **2001**, *314*, 1.

[24] Shankaran, D. R.; Gobi, K. V.; Miura, N. *Sens. Actuators B* **2007**, *121*, 158.

[25] Ambrosi, A.; Castañeda, M. T.; Killard, A. J.; Smyth, M. R.; Alegret, S.; Merkoçi, A. *Anal. Chem.* **2007**, *79*, 5232.

[26] Crumbliss, A. L.; Perine, S. C.; Stonehuerner, J.; Tubergen, K. R.; Zhao, J.; Henkens, R. W. *Biotechnol. Bioeng.***1992**, *40*, 483.

[27] Xiao, Y.; Ju, H. X.; Chen, H. Y. *Anal. Chim. Acta* **1999**, *391*, 73.

[28] Jia, J. B.; Wang, B. Q.; Wu, A. G.; Cheng, G. J.; Li, Z.; Dong, S. J. *Anal. Chem.* **2002**, *74*, 2217.

[29] Luo, X. L.; Xu, J. J.; Zhang, Q.; Yang, G. J.; Chen, H. Y. *Biosens. Bioelectron.* **2005**, *21*, 190.

[30] Patolsky, F.; Gabriel, T.; Willner, I. *J. Electroanal. Chem.* **1999**, *479*, 69.

[31] Liu, Z. M.; Wang, H.; Yang, Y. ; Yang, H .F.; Hu, S. Q.; Shen, G. L.; Yu, R. Q. *Anal. Lett.* **2004**, *37*, 1079.

[32] Gu, H. Y.; Yu, A. M.; Chen, H. Y. *J. Electroanal. Chem.* **2001**, *516*, 119.

[33] Caruso, F. *Adv. Mater.* **2001**, *13*, 11.

[34] Caruso, F.; Fiedler, H.; Haage, K. *Colloids Surf. A* **2000**, *169*, 287.

[35] Schüler, C.; Caruso, F. *Macromol. Rapid Commun.* **2000**, *21*, 750.

[36] Lvov, Y.; Caruso, F. *Anal. Chem.* **2001**, *73*, 4212.

[37] Caruso, F.; Schüler, C. *Langmuir* **2000**, *16*, 9595.

[38] Droz, E.; Taborelli, M.; Descouts, P.; Wells, T. N. C.; Werlen, R. C. *J. Vac. Sci. Technol. B* **1996**, *14*, 1422.

[39] Kanno, S.; Yanagida, Y.; Haruyama, T.; Kobatake, E.; Aizawa, M. *J. Biotechnol.* **2000**, *76*, 207.

[40] Gole, A.; Vyas, S.; Phadtare, S.; Lachke, A.; Sastry, M.; *Colloids Surf. B:Biointerf.* **2002**, *25*, 129.

[41] Armstrong, F. A.; Wilson, G. S. *Electrochim. Acta* **2000**, *45*, 2623.

[42] Willner, I.; Arad, G.; Katz, E. *Bioelectrochem. Bioenerg.* **1998**, *44*, 209.

[43] Iijima, S.; *Nature* **1991**, *56*, 354.

[44] Choi, W.B.; Chung, D. S.; Kang, J.H.; Kim, H. Y.; Jin, Y. W.; Han, I. T.; Lee, Y. H.; Jung, J. E.; Lee, N. S.; Park, G. S.; Kim, J. M. *Appl. Phys. Lett.* **1999**, *75*, 3129.

[45] Tans, S. J.; Verschueren, A. R. M.; Dekker, C. *Nature* **1998**, *393*, 49.

[46] Dai, H.; Hafner, J.H.; Rinzler, A. G.; Colbert, D. T.; Smalley, R. E. *Nature* **1996**, *384*, 147.

[47] Shaffer, M. S.; Fan, S.; Windle, A. H. *Carbon* **1998**, *36*, 1603.

[48] De Gani, Y.; Heller, A. *J. Phys. Chem.* **1987**, *91*, 1285.

[49] Merkoçi, A.; Pumera, M.; Llopis, X.; Pérez, B.; del Valle, M.; Alegret, S. *Trends Anal. Chem.* **2005**, *24*, 826.

[50] Heller, A.; *J. Phys. Chem. Res.* **1992**, *96*, 3579.

[51] Endo, M.; Hayashi, T.; Kim, Y. A.; Terrones, M.; Dresselhaus, M. S. *Philos. Trans. R. Soc. London Ser. A* **2004**, *362*, 2223.

[52] Liu, J.; Rinzler, A. G.; Dai, H.; Hafner, J.H.; Bradley, R. K.; Boul, P. J.; Lu, A.; Iverson, T.; Shelimov, K.; Huffman, C. B.; Rodriguez-Macias, F.; Shon, Y. S.; Lee, T. R.; Colbert, D. T.; Smalley, R. E. *Science* **1998**, *280*, 1253.

[53] Rinzler, A. G.; Liu, J.; Dai, H.; Nikolaev, P.; Huffman, C. B.; Rodriguez-Marcias, F. J. *Appl. Phys. A* **1998**, *67*, 29,

[54] Dillon, A. C.; Gennett, T.; Jones, K. M.; Alleman, J. L.; Parilla, P. A.; Heben, M. J. *Adv. Mater.* **1999**, *11*, 1354.

[55] Martinez, M. T.; Callejas, M. A.; Benito, A. M.; Maser, W. K.; Cochet, M.; Andres, J. M.; Schreiber, J.; Chauvet, O.; Fierro, J. L.; *Chem. Commun.* **2002**, *9*, 1000.

[56] Andrews, R.; Jacques, D.; Qian, D.; Dickey, E. C. *Carbon* 2001, *39*, 1681.

[57] Chen, J.; Hamon, M. A.; Hu, H.; Chen, Y.; Rao, A. M.; Eklund, P.C.; Haddon, R. C. *Science* **1998**, *282*, 95.

[58] Tasis, D.; Tagmatarchis, N.; Georgakilas, V.; Prato, M. *Chem. Eur. J.* **2003**, *9*, 4000.

[59] Islam, M. F.; Rojas, E.; Bergey, D. M.; Johnson, A. T.; Yodh, A. G. *Nano Lett.* **2003**, *3*, 269.

[60] O'Connell, M. J.; Boul, P.; Ericson, L. M.; Huffman, C.; Wang, Y.; Haroz, E.; Kuper, C.; Tour, J.; Ausman, K. D.; Smalley, R. E. *Chem. Phys. Lett.* **2001**, *342*, 265.

[61] Chen, J.; Liu, H.; Weimer, W. A.; Halls, M. D.; Waldeck, M. D. H.; Walker, G. C. *J. Am. Chem. Soc.* **2002**, *124*, 9034.

[62] Ramesh, S.; Ericson, L. M.; Davis, V. A.; Saini, R. K.; Kittrell, C.; Pasquali, M.; Billups, W. E.; Adams, W.; Hauge, R. H.; Smalley, R. E. *J. Phys. Chem. B* **2004**, *108*, 8794.

[63] Kim, O. K.; Je, J.; Baldwin, J. W.; Kooi, S.; Pehrsson, P. E.; Buckley, L. J. *J. Am. Chem. Soc.* **2003**, *125*, 4426.

[64] Luong, J. H. T.; Hrapovic, S.; Wang, D.; Bensebaa, F.; Simard, B. *Electroanalysis*

2004, *16*, 132.

[65] Yue-Rong, W.; Ping, H.; Qiong-Lin, L; Guo-An, L.; Yi-Ming, W. *Chin. J. Anal. Chem.* 2008, *36*, 1011.

[66] Britto, P. J.; Santhanam, K. S. V.; Ajayan, P. M. *Bioelectrochem. Bioenerg.* **1996**, *41*, 121.

[67] Wang, Z. H.; Liu, J.; Liang, Q. L.; Wang, Y. M.; Luo, G. A. *Analyst* **2000**, *127*, 653.

[68] Pérez López, B.; Sola, J.; Alegret, S.; Merkoçi, A. *Electroanalysis* **2008**, *20*, 603.

[69] Pérez, B.; Pumera, M.; del Valle, M.; Merkoçi, A.; Alegret, A. *J. Nanosci. Nanotechnol.* **2005**, *5*, 1694.

[70] Pérez-López, B.; Merkoçi, A. *Analyst* **2009**, *134*, 60.

[71] Pandurangappa, M.; Lawrence, N. S.; Jiang, L.; Jones, T. G. J.; Compton, R. G. *Analyst* **2003**, *128*, 473.

[72] Pérez López, B.; Sola, J.; Alegret, S.; Merkoçi, A. *Electroanalysis* **2008**, *20*, 603.

[73] Wang, J.; Liu, G.; Jan, M. R. *J. Am. Chem. Soc.* **2004**, *126*, 3010.

[74] Yu, X.; Munge, B.; Patel, V.; Jensen, G.; Bhirde, A.; Gong, J. D.; Kim, S. N.; Gillespie, J.; Gutkind, J. S.; Papadimitrakopoulos, F.; Rusling, J. F. *J. Am. Chem. Soc.* **2006**, *128*, 11199.

[75] Martin, C. R. *Acc. Chem. Res.* **1995**, *28*, 61.

[76] Brunker, S. E.; Cederquist, K. B.; Keating, C. D.; *Nanomedicine* **2007**, *2*, 695.

[77] Patolsky, F.; Timko, B. P.; Zheng, G.; Lieber, C. M. *MRS Bull.* **2007**, *32*, 142.

[78] Wang, J. *Analyst* **2005**, *130*, 421.

[79] Carrascosa, L. G.; Moreno, M.; Alvarez, M.; Lechuga, L. M. *Trends Anal. Chem.* **2006**, *25*, 196.

[80] Lieber, C. M.; Wang, Z. L. *MRS Bull.* **2007**, *32*, 99.

CATALYTIC NANO/MICRO MOTORS AND APPLICATIONS

1.3.1. Introduction

Nano/micromotors propelled by the presence of certain chemical fuels owe their motion to the specific chemical reaction taking place in the interface between the catalytic material (part of the nano/micromotor) and the fuel, which can be added to the reaction or be inherently present in the operation medium. Depending on the reaction taking place, nano/micromotors motion can be due to the bubble production, inducing the so-called bubble recoil mechanism, or to a certain gradient of concentration involving the selphoretic mechanisms. Among the different fuels reported up to date, the most extensively used in the synthetic autonomous systems has been hydrogen peroxide. However, it should be remarked that it has been of special interest the use of alternative fuels, like water or acid/basic induced locomotive systems, which can promote their motion and at the same time be biocompatible. Although micromotors moving in presence of hydrogen peroxide do not present the same potentiality for *in situ* biological applications, they are efficient and present long-life performance, which make them suitable for certain miniaturized systems (e.g. lab-on-a-chip devices) or environmental-related monitoring systems.

1.3.2. Hydrogen peroxide fuel

Hydrogen peroxide has largely been employed to propel nano/micromotors and to further study the basic mechanisms governing their motion. The different parameters determining the motion and directionality including related applications are will be described. Two groups of hydrogen peroxide fuel-based autonomous nanomotors corresponding to the two main principle mechanisms, selfphoretic or bubble-based ones, along with the evolution on their design, motion capabilities and related applications, will be presented.

1.3.2.1. Selfphoretic mechanisms

Since the first reported micro/nanomotors there was the concern of attributing a mechanism that could perfectly describe their motion, ideally one that could be applied to all the autonomously moving systems. Although the first autonomous motors were reported to move by means of bubble expulsion from the catalytic section,[1] further studies based on bimetallic rod-shape particles showed a different behavior towards hydrogen peroxide presence, which indicates that for each case

different mechanistic pathways govern their motion patterns, influencing both the parameters that enhance their velocity and their motion direction.

Pt/Au nanorods [2] synthesis, conceived as nanomotors, was based on the electrochemical deposition of the corresponding metals on alumina membranes, followed by nanorods release. Nanomotors movement was clearly observed to be non-Brownian and the motion direction was toward the platinum end. Initially, the interfacial tension gradient model was supposed to fit the system requirements, as the movement was induced by both the gradients of solute, in this case an oxygen concentration gradient, and temperature due to the exothermic decomposition of hydrogen peroxide at the platinum end. The oxygen was produced at the platinum end, where its concentration remained constant as it was generated at a constant rate, while the real gradient took place at the opposite gold segment, where the oxygen concentration decreased and took place the relevant interfacial tension, giving rise to a net axial force that propels the motion toward the platinum side. However, the interfacial tension model itself did not justify the motion direction, which in this case was attributed to the polarity of the gold surface.

Inspired by how a cell would maintain a dynamic electric field, the self electrophoresis mechanism [3] based on the electrochemical hydrogen peroxide decomposition at both the platinum and gold ends of the nanomotor was proposed. This mechanism would represent a flux of electrons, as well as protons, inside the particle, behaving as a short-circuited galvanic cell. According to the mechanism, as a cathodic section the oxidation of hydrogen peroxide takes place preferentially on the platinum end, while the reduction of hydrogen peroxide and oxygen occurs at the Au side, which could be considered the anodic section (Figure 5AI).[2] Further studies by using interdigitated microelectrodes (IME), demonstrated that effectively nanomotors presented a catalytically generated electric fields that induced electroosmotic fluid pumping. [4] By combining different metals pairs in the bimetallic nanomotor configuration and studying the reaction that was taking place in each metal section as if it was a half-cell reaction, the motion direction showed a clear correlation with the mixed potentials of individual catalytic metals.[5] Not only the direction motion could be perfectly predicted, but also the reaction rate, as nanomotors with a metal pair with higher potential differences exhibit higher speeds. This way, the self-electrophoresis mechanism, so-called bipolar electrophoresis mechanism, was confirmed.

However, there was one particular case whose movement was based on sustained interfacial tension gradient, the gold gear-like structures with platinum deposited on the tooth region.[6] The hydrophobic character of the section next to the catalytic region is crucial for the optimal rotational movement of the gear, therefore the gold surface was judiciously functionalized to exhibit such hydrophobic behavior. Although the whole microfabricated structure was bigger than the nanomotors entities already mentioned, this system was conceived as a synergy between different pieces or catalytic section of a motion system, where micrometric asymmetric scale pieces were moved to accomplish an ultimate useful work.

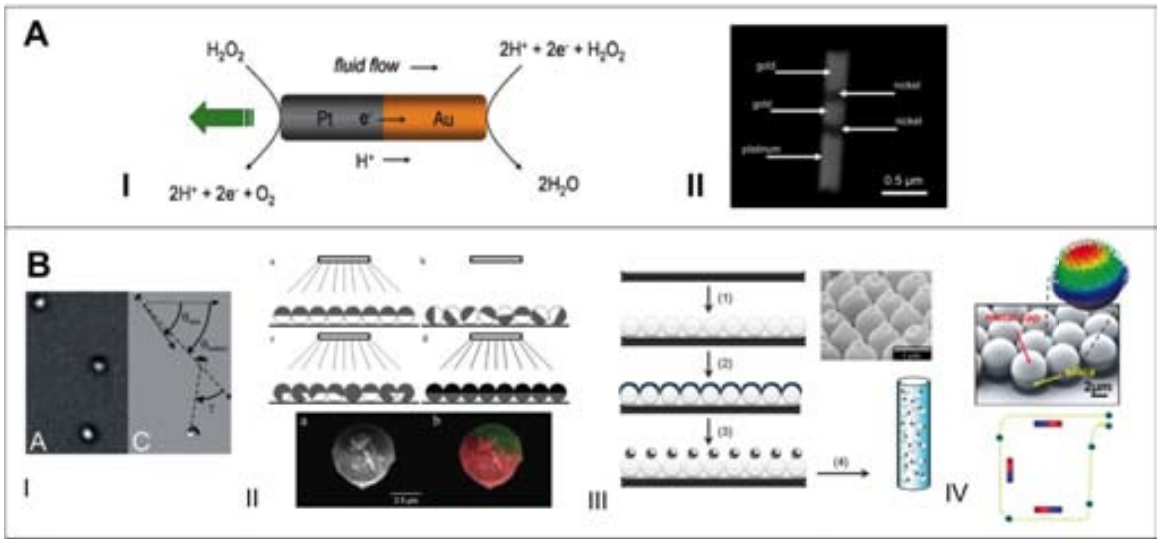

Figure 5. Autonomously moving nano/micromotors by means of selfphoretic mechanisms. (A) Rod-shape Au/Pt bimetallic nanomotor based on selfelectrophoresis mechanism (I) (Reprinted with the permission from Ref. 2. Copyright 2004 ACS) and its magnetically guided counterpart with ferromagnetic nickel segments (II). Reprinted with the permission from Ref. 25. Copyright 2005 Willey-VCH. (B) Spherical shape particles whose movement is attributed to selfdiffusiophoresis mechanism and demonstration of the motion orientation of asymmetrically platinum-coated polystyrene particles (I) (Reprinted with the permission from Ref. 9. Copyright 2010 ACS), faster and more versatile method of synthesis for bimetallic spherical particles (II) (Reprinted with the permission from Ref. 16. Copyright 2010 ACS), catalytic sphere dimer showing quasi-linear and quasi-circular trajectories (III) (Reprinted with the permission from Ref. 17. Copyright 2010 Willey-VCH) and colloidal Janus particles with magnetic cap that leads to the first fine magnetic guidance of spherical catalytic particles (IV). Reprinted with the permission from Ref. 28. Copyright 2010 Willey-VCH.

Apart from the mechanism, the shape and symmetry of the nanomotor entity is crucial for determining how the translational or rotational motion events will take place. For example, Pt/Au nanomotors move in the direction of long axis, where the drag force is minimized.[2] However, for the perfect spherical particles, being totally symmetric, the net force created in case of a gradient would essentially be cancelled out. Therefore, symmetry breaking is the clue in the movement of such catalytic

nano/micromotors, starting up from the rod-shape nanomotors, whose asymmetry is coming from their shape itself, to the well-known spherical Janus particles, which owe the movement to their asymmetry in surface properties.[7] Additionally, it must be noticed that the particles developed by Golestanian and co-workers,[7] with an asymmetric distribution of catalyst on its surface, were moving by means of a self-diffusiophoretic mechanism. This model doesn't imply any electrochemical reaction, like the self-electrophoresis mechanism previously described, but is directly related to the gradient concentration of products created at the catalytic section. Such Janus particles demonstrated to self-assemble resulting into doublets or even higher order aggregates, showing a different trajectories and morphologies (the majority rotated, while linear translators were exceptional).[8] Directionality of spherical nanomotors was firstly described by the study of asymmetrically platinum-coated polystyrene particles, where it was demonstrated that the platinum-coated region was oriented opposite to the direction of motion (Figure 5BI).[9] The direction of their motion shows to be highly correlated with the particle orientation, which is not affected by the particle-surface interactions. Although particles generally move in the same general direction, infrequent large directional changes bring major changes to the particle trajectory.

Nano/micromotors that moves by means of electrophoretic or diffusiophoretic mechanisms are especially affected by the ionic strength and the viscosity of the medium, this last parameter being decisive when motion is evaluated at the nanoscale where nanomotors are propelled according to the fluid dynamics at the low Reynolds numbers[10]. Although the autonomous moving of Pt/Au nanorods at viscous interfaces have been studied due to their anomalous translational and rotational diffusion patterns,[11] demonstrating that their movement can be modulated from active motion towards passive diffusion depending on the surfactant concentration, in general the motion studies related to Pt/Au nanorods have been performed in non-viscous mediums and limited to low-ionic strength environments. To optimize and improve their performance, several approaches that particularly affect their composition and/or morphology have been reported.

Regarding rod-shape nanomotors, the importance of the cathodic and anodic section length ratio was demonstrated by early experimental studies in Au/Pt nanomotors, where the surface area of the catalytic platinum segment limited oxygen production.[3]

However, further research stated that 1:1 axial ratio gave the faster axial motion for a given pair of rods, being preferred the shorter ones to minimize the fluid drag and the sliding friction along the glass surface, which in turn decrease their velocity.[5]

With the objective to obtain a higher potential difference between the metal pair and consequently a higher speed, diverse improvements have been achieved by changing the composition or the morphology of the cathodic or anodic end (Figure 6A). On the one hand, more active materials toward oxygen reduction have been introduced in the cathodic end instead of platinum, such as carbon nanotubes[12], as well as the substitution of gold by Ag/Au alloy[13] at the anodic end. In both cases it has been demonstrated an enhance in the electron transfer reactions, which resulted in an acceleration of nanomotor's speed up to 51μm/s in the case of Au/Ni/Au/Pt-CNT and 150μm/s in the case of Ag-Au/Pt compared to the classical Au/Pt bimetallic nanomotors, which in presence of 2-3% of hydrogen peroxide showed speeds of 8μm/s (10 body lengths/second).[2] From the morphological point of view, enhanced surface roughness of the catalytic segment, and therefore a higher surface-to-area ratio, resulted in faster Au/Ni nanomotors.[14] Apart from playing with the inherent composition of the bimetallic nanomotor, energy-rich chemical reactions were achieved by adding hydrazine to the hydrogen peroxide fuel and showing a doubling of the nanomotors speed in the case of CNT-modified ones.[12] After obtaining the desired speed by tailoring their morphology, composition and their surrounding medium, the next logical step was the real control over their motion. A first approach of this fine control was reported by Wang *et al.* by presenting electrochemical activation of the nanomotor's motion, which not only permits to control nanomotors speed but also achieves an interesting "on" and "off" electrochemical activation system by means of applying a reversible voltage, held by a gold-fiber working electrode located next to the nanomotors plane.[15]

Regarding the synthetic approaches to obtain bimetallic spherical motors, several improvement have been reported, showing a faster and more versatile method for the synthesis of the bimetallic ones[16] and demonstrating that their velocity decreases with the sphere radius (Figure 5BII). In addition, the development of new systems such as catalytic sphere dimer[17] showed quasi-linear and quasi-circular trajectories in presence of hydrogen peroxide, which could be easily tuned by changing the size of the two spheres or their internuclear separation (Figure 5BIII). These factors were key

to understand the propulsion mechanism and explore more complex motor designs based on building blocks that are suspected to create dynamic structures and devices by means of self-assembly mechanisms.

However, one of the most challenging contributions to nanomotors field had been the possibility to perform the magnetic guidance of their motion. Concerning rod-shape nanomotors, Sen *et al.* [18] achieved their magnetic control by adding a ferromagnetic nickel segment that can be transversally magnetized due to its size, which must be shorter than the diameter of the rod (Figure 5AII). It is important to notice that the applied magnetic field only aligns the rods by orienting their net magnetic moments and doesn't add any additional force to the motion, which really opened the door to the real manipulation of the nanomotors and their further implementation in sensing devices. In the case of spherical particles, their high symmetry complicated the control of their directionality by magnetic means, as the fixed orientation of the magnetic moment generally relies on the magnetic shape anisotropy. Therefore, one first logical approach was the introduction of asymmetry to the perfectly spherical particles, by converting them in ellipsoids. [19] After sputtering of a thin layer of platinum onto the microellipsoids, a preferred magnetization direction along its axis was achieved. However, the real control of spherical particles came by Schmidt *et al.*, [20] that reported the fabrication of Janus particles with a magnetic cap structure based on ultrathin magnetic multilayers onto the spheres (Figure 5BIV). In case of in-plane (x- or y- axis), orientation of the magnetic field the motors will perform a deterministic propulsion with a certain speed, but in case of out-of-plane orientation, the motor will immediately stop. This approach eliminates the rotational diffusion of the Janus particles and also permits a real control over the motion of the spherical particles, leading to a perfect guidance of their trajectory and the possibility to stop their motion on demand.

The possibility to magnetically control the nanomotors directionality motivated the design of different systems. CMOS (complementary metal-oxide-semiconductor) chip where arrays magnetic nanoparticles or nanorods (Au/Ni/Au/Ni/Pt) were integrated demonstrating their successful manipulation, even giving raise to trapping events. Two different CMOS designs were implemented, the ring trap chip, which employs a magnetic steering scheme, and the wire array chip, where the steering electromagnetic field produced by an array of parallel wire line was digitally controlled. By using both

systems, optical and electromagnetic measurements were done, demonstrating the basic control of the magnetic nanostructures by the applied currents.[21] In addition, the directional control of CNT-modified nanomotors by using a weak external magnet to sort out different features in PDMS platforms was successfully achieved in absence of bulk fluid flow (Figure 6CI), in addition to the dynamic loading, including both the pick-up and drop-off events by means of the magnetic-torque based method.[22] The transport of magnetic cargo over predefined paths showed the versatility and potential possibilities of nanomotors in lab-on-a-chip systems. Additional improvements (beside the control of the directionality of nanomotors) were focused on thermal modulation of nanomotors motion by applying short heat pulses to accelerate or slow down their motion. In addition, other changes associated to the activation of the redox reactions where hydrogen peroxide fuel was involved were studied, showing the decrease of medium viscosity in case of raising the temperature.[23]

Nanomotors motion-related capabilities to perform transport and delivery events in a controlled way have been extensively studied. First approach permitted the pick-up, transport and release of magnetic particles, which were captured by taking advantage of the paramagnetic nickel segment present in the nanomotor. Further studies brought the possibility of substituting this magnetic particles by magnetic liposomes or biodegradable polymeric particle (poly-D,L-lactic-*co*–glycolic acid (PLGA) particles) (Figure 6CII).[24] Apart from presenting a magnetic behavior, they are of special interest for both being potential drug carriers, especially liposomes, which can carry both hydrophilic and lipophilic therapeutic agents and present and on-demand drug release by mechanically or chemically breaking them. Cargo manipulation by magnetically controlled spherical motors have been demonstrated by applying a magnetic field that will not only control the trajectory of the motor, but it will also induce a magnetic dipole-dipole moments between the particles and the cargo.[28] In case of changing the magnetic field orientation, such interaction will disappear, leading to the unloading of the cargo, and the motor will stop their motion. This cargo manipulation has been also depicted in chip studies, fully controlling the trajectory of the spherical motors, which in addition could sort out several microobjects in the channels. However, more sophisticated systems that involved specific or more complex interactions were developed. Clear examples are the nanomotors synthesized by Sen *et. al* depicted in Figure 6CIII. Their interaction with the particle of interest

was on the one hand based on the electrostatic interaction between the positively charged cargo (positively charged polystyrene amidine microspheres) and a Pt-Au nanomotor with a negatively charged polypyrrole (PPy) tail,[25] and on the other hand took advantage of the biotin-streptavidin specific binding by functionalizing the Pt-Au nanomotors with a biotin-terminated disulfide and capturing an streptavidin-coated cargo. Compared to the magnetic-based capture methods, the ones held through chemical bonding or electrostatic interactions lacked easy methods for the cargo unloading. Improved nanomotors were synthesized with the capacity of not only capturing and transporting, but also releasing of the cargo with a high degree of precision through UV-light-stimulated methods.[26] The dissolution of the silver segment of the Pt/Au/Ag/Au/PPy nanomotor in presence of UV light, whose cargo was attached through electrostatic interactions at the PPy end, and the selective dissolution of the photocleavable bifunctional linker used to attach the motor to the cargo by photolysis upon UV illumination, promoted the drop-off events.

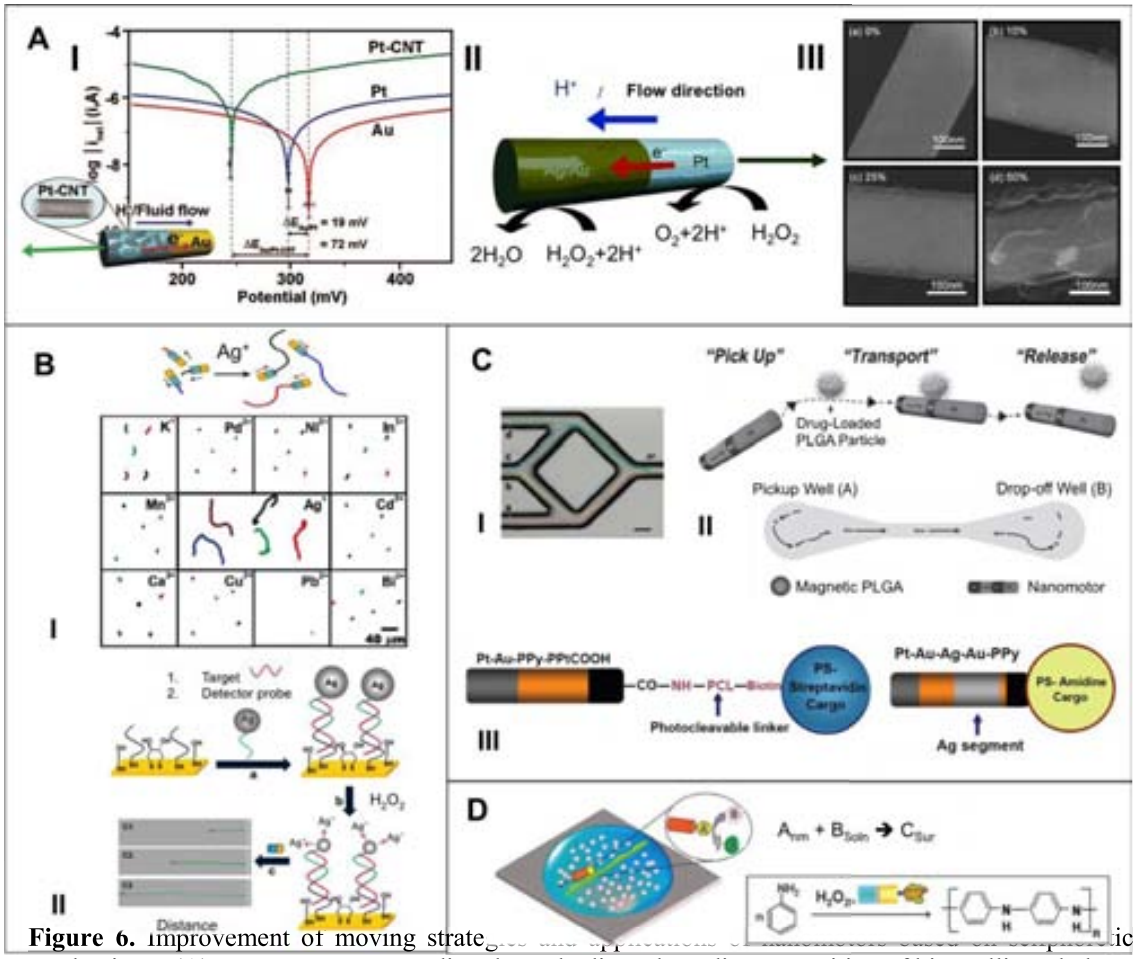

Figure 6. Improvement of moving strategies and applications of nanomotors based on synthetic mechanisms. (A) Improvements regarding the cathodic and anodic composition of bimetallic rod-shape nanomotors. Incorporation of carbon nanotubes to the cathodic end (I) (Reprinted with the permission from Ref. 12. Copyright 2008 ACS) or the substitution of Ag/Au alloy at the anodic end (II) (Reprinted

with the permission from Ref. 13. Copyright 2008 Willey-VCH) and, as well as an enhanced surface roughness of the catalytic section (III), resulted on an acceleration of nanomotor's speed. Reprinted with the permission from Ref. 14. Copyright 2009 RSC. (B) Motion-sensing applications of nanomotors by towards the trace silver (I) (Reprinted with the permission from Ref. 27. Copyright 2009 ACS) and to determine DNA and bacterial ribosomal RNA (I). Reprinted with the permission from Ref. 28. Copyright 2010 Nature. (C) Nanomotors motion-related capabilities to perform transport and delivery event in PDMS platforms by magnetic-torque based method (I) (Reprinted with the permission from Ref. 22, Copyright 2008 ACS) as well as to transport magnetic liposomes or biodegradable polymeric particles (II) (Reprinted with the permission from Ref. 24. Copyright 2008 Willey-VCH); in addition, drop-off events were finely tuned by UV-light-stimulated methods, in case of using a photocleavable bifunctional linker (III). Reprinted with the permission from Ref. 26. Copyright 2008 Willey-VCH. (D) Creation of *in-situ* surface microstructure by nanomotors moving by selfeletrophoretic mechanism. Reprinted with the permission from Ref. 29. Copyright 2010 RSC.

Nanomotors have been regarded as a potential clue on the future biosensing platforms due not only to the possibility to better control its trajectory and speed, but also because promising motion-sensing applications have been reported (Figure 6B). Although Au-Pt bimetallic nanomotors movement in presence of hydrogen peroxide is compromised by high-ionic mediums, a faster speed in presence of trace silver ions have been observed.[27] This motion-based chemical sensing is related to the underpotential deposition of silver on both the gold and platinum segments in presence of silver ions, which in the case of the gold section results on an increase of the mixed potentials between the cathodic and anodic segments, and in the case of the platinum section it showed a more catalytically active surface. A clear correlation between nanomotors speed in presence of hydrogen peroxide and silver ions concentration with a silver detection range from 0.5 to 100 μM was observed. Nanomotors enhanced speed in presence of silver ions also permitted the development of a simple, sensitive and fast method to determine DNA and bacterial ribosomal RNA.[28] The detector probe used in the hybridization sandwich assay is tagged with a silver nanoparticle, which will be lately dissolved obtaining in the solution a certain silver ions concentration that can be correlated with the hybridization event. Once the unmodified bimetallic nanomotors swam in the silver enriched fuel, their speed was enhanced, finding out that longer the signal distances were, higher the concentration of the nucleic target was, reaching detection limits up to the attomole level.

It should be mentioned that apart from the cargo transport and their potential application in sensing platforms, nanomotors that moves by means of phoretic mechanisms had been applied also to create *in situ* surface microstructures. Peroxide-driven horseradish peroxidase (HRP)-functionalized nanomotor were magnetically guided in presence of aniline monomer, performing a localized deposition/precipation

of polyaniline (Figure 6D).[29] Although resolution is limited to nanomotor diameter, the generation of predefined patterns is of great interest for surface chemistry, as well as to be considered as an additional key functionality for future self-assembly systems or other biosensing platforms that nanomotors could provide.

1.3.2.2. Bubble induced propulsion based mechanism

Bubble induced propulsion mechanism can be considered as the first reported locomotion principle although a long way since achieving the full control of the engines while moving by means of bubble propulsion was necessary. Such nano/micromotors design showed a really fast decomposition rate of hydrogen peroxide into water and oxygen in presence of different transition metals, as for example platinum, silver, manganese or nickel. The choice of the appropriate geometry, in addition to other parameters optimizations, have overcome some of the problems that selfphoretic motion-based nano/micromotors present, like ionic-strength limitations associated to their movement, in addition to perform novel trajectories that bring novel mechanized-related functions at the nanoscale.

First micromotors developed by Whitesides *et al.* were fabricated by rapid prototyping and based on hemicylindrical plates with a small platinum area on the surface, which in presence of hydrogen peroxide were clearly moving by the bubbles generated at their platinum section (Figure 8A). Recoil force is a result of a momentum conservation generated from the bubbles expulsed from the platinum surface determined both the movement and the direction of the micro/nanomotors.[1] In addition, the hydrophobic character of each region of the motor, which induced capillary interaction between menisci, resulted in spontaneous attraction between the hydrophobic edges of the plates being the first demonstration of "collective behaviour" by self-assembly chiral structures in the autonomous motors field.

Further lithography techniques were implemented to synthesize new micromotor structures more efficient towards rotary motion. Although template-based bimetallic Au/Ni nanowires with their gold segment anchored to the surface of a silicon wafer (Figure 7A)[30] have shown fairly good clockwise and counterclockwise rotations in presence of hydrogen peroxide fuel, alternative approaches which include lithographic techniques have shown higher rotational speeds. Mirkin *et al.* tailored

nanorod architecture by using on-wire lithography (OWL) upon template-directed synthesis of Au-Pt nanorod, which allowed coating one face of the nanorod with gold (Figure 7BI).[31] It should be noticed that in this nanomotor configuration an anchorage was needed to obtain a rotating behavior. Pure rotary motion was obtained in presence of hydrogen peroxide by working with a similar design, improved by the deposition of a platinum layer by vapor-deposition onto an Au-Ru bimetallic rod (Figure 7BII).[32] In the trimetallic structure, the force is generated along two axes that do not intersect at the center of the drag, which results in a rotary speed ten times faster.

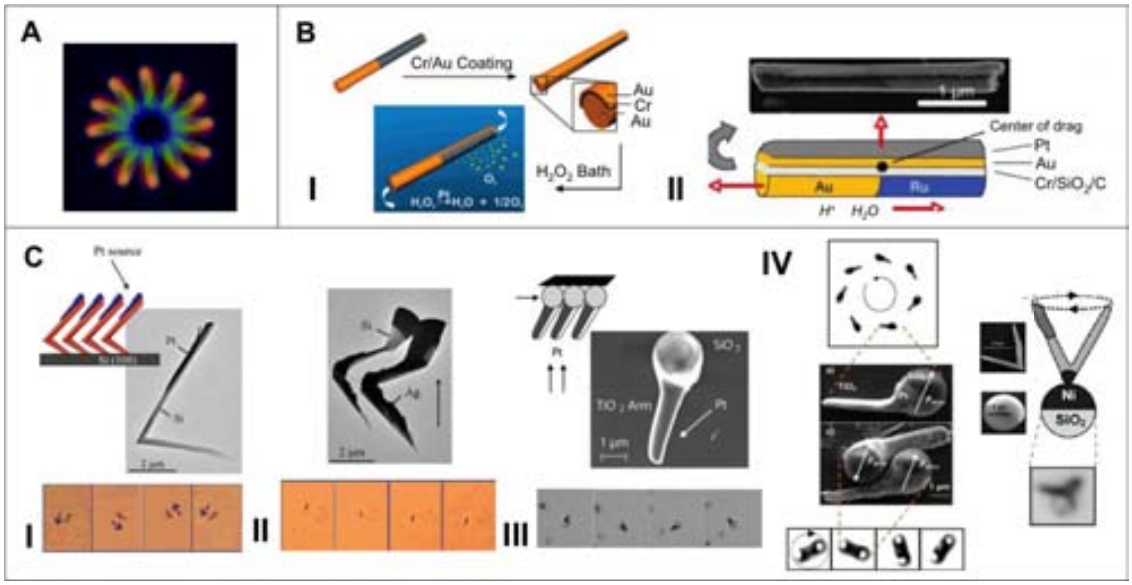

Figure 7. Rotary nano/micromotors based on bubble propulsion mechanism. (A) Au/Ni nanowires with their gold segment anchored to a silicon wafer surface. Reprinted with the permission from Ref. 30. Copyright 2005 RSC. (B) Improved rotation nanomotors fabricated by on-wire template direct synthesis of Au-Pt nanorod with an addition gold coating onto one face (I) (Reprinted with the permission from Ref. 31. Copyright 2007 ACS) and deposition of a Pt layer by vapor-deposition onto Au/Ru bimetallic rod (II). Reprinted with the permission from Ref. 32. Copyright 2009 ACS. (C) Heterogeneous self-motile structures fabricated by dynamic shadowing growth (DSG), achieving L-shaped Si/Pt structures (I) and Si/Ag nanospring structures (II) (Reprinted with the permission from Ref. 33. Copyright 2007 ACS); Pt-coated TiO_2 nanoarms grown on silica microbeads (III) (Reprinted with the permission from Ref. 34. Copyright 2009 Willey-VCH) and self-assembled clusters based on V-shaped nanomotor and microbeads (IV). Reprinted with the permission from Ref. 35. Copyright 2010 Willey-VCH.

Another lithographic technique extensively used for its versatility to fabricate 3-D heterogeneous self-motile structures was dynamic shadowing growth (DSG), as depicted in Figure 3C. The key rule design for these catalytic motors is the asymmetric deposition of a catalytic section, as it was reported for rotary Si/Pt and Si/Ag nanorods, rotary L-shaped Si/Pt or rolling Si/Ag nanospring.[33] L-shaped geometry showed both clockwise and counterclockwise rotation patterns, but in any case rotation was held from the long arms to the short ones, demonstrating that

nanomotors were pushed from the Pt side (Figure 7CI). Nanospring design was conceived taking into consideration the motion patterns observed in the L-shaped structures, expecting that the nanomotor would not only rotate but also would be moving downward, giving raise to the rolling and translational motions at the same time (Figure 7CII). The most challenging multicomponent catalytic nano/micromotors developed by DSG were based on Pt-coated titanium dioxide (TiO_2) nanoarms grown upon silica microbeads (Figure 7CIII).[34] More important than the design itself, was the potential of such entities to self-organize presenting tadpole-like structures by the assembly of two nanomotors, inspiring other clusters that spontaneously self-assemble through magnetic interactions forming a helicopter-like nanomotor, a V-shaped like nanomotor and a microbead, both magnetized (Figure 7CIV).[35] In addition, their rotational frequency was parabolically increased due to the addition of the sodium dodecyl sulphate (SDS) surfactant that lowers the surface tension. This frequency enhance agrees with the nanobubble-ejection model. It firstly demonstrated in the case of hydrogen peroxide decomposition by Pt-coated spherical silica catalytic microbeads that the propelling force was attributed to the momentum change via oxygen bubbles detachment from the catalytic surface and that it was specially influenced by the fuel concentration and the surface tension of the solution.[36] The possibility to have systems that organize themselves in more complex arrangements without external forces is crucial for future real application where several independent parts would work in coordination to give rise to new potential applications.

Further studies based on spherical-shape nano/micromotors showed alternative composition and designs that can bring different strategies to control their motion as shown in Figure 8B. Bubble formation and the study of the buoyancy force governing the movement of polymer resin beads coated with palladium nanoparticles at different viscosity conditions, resulted in tailoring the vertical velocity leading to horizontal motion (Figure 8BI).[37] Molecular motors induced autonomous motion to silica microparticles covalently tethered to synthetic manganese catalase,[38] which showed efficient translational motion that in addition to some autonomous rotary motion were attributed to the structure anisotropy (Figure 8BII). Such molecular motor was further used to functionalize bare silica and glass surfaces, demonstrating that the translation motion of modified glass microsized fibers moved due to oxygen bubbles growth.[39] The study of such bubble growth effect and how it contributes in to the motion of big

spherical Janus micromotors, suggested a quasioscillatory translational motion for such catalytic micromotors,[40] in contrast to the reported mechanism by Zhao *et al.*[34] Therefore, bubble growth and burst events generates a competition that leads to a net forward motion produced by the growth force moving the micromotor forward and the burst force inducing a local pressure that pulls the micrometer backward (Figure 8BIII). One last example of the advances in self-propelled Janus micromotors have recently fabricated by using a template-assisted layer-by-layer self-assembly and microcontact printing method by Li and coworkers (Figure 8BIV). Polyelectrolyte multilayer hollow capsules partially coated with platinum nanoparticles showed both the autonomous circular and spiral motions, as well as a very interesting delivery capability based on the controllable encapsulation and triggered release in response to certain external stimuli, which tunes their permeability.[41]

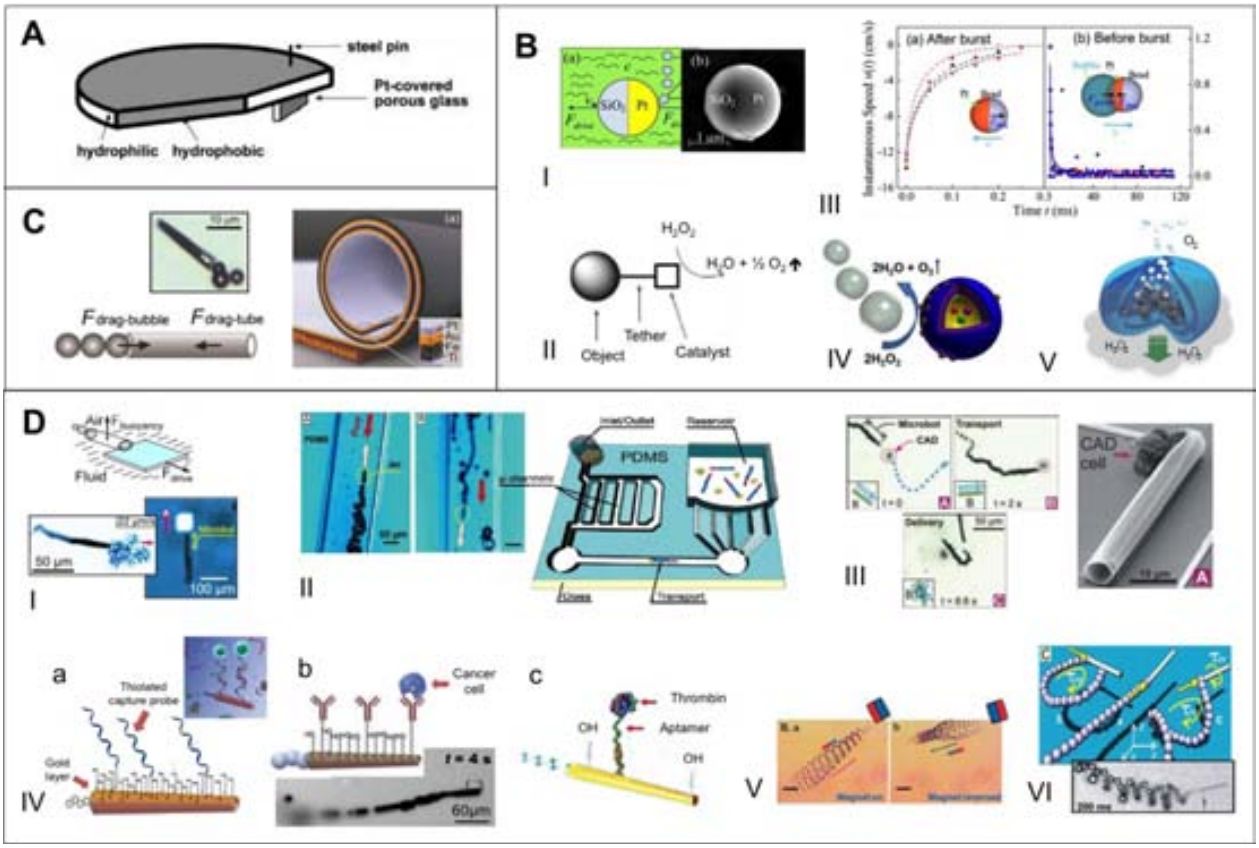

Figure 8. Improvement strategies and applications of autonomously moving nano/micromotors by means of bubble propulsion mechanisms fabricated by photolithographic processes. (A) First micromotor developed by Whitesides *et al.* based on PDMS plates with a small platinum area on one surface. Reprinted with the permission from Ref. 1. Copyright 2002 Willey-VCH. (B) Schematic representation of rolled-up catalytic miromotors, synthesized through strain engineering strategy. Reprinted with the permission from Ref. 42. Copyright 2008 Willey-VCH. (C) Non tubular shape nano/micromotors. Regarding the spherical shape motors, Pt-coated spherical silica microbeads (I) (Reprinted with the permission from Ref. 36. Copyright 2009 AIP) and silica particles tethered to a synthetic manganese catalase (II) (Reprinted with the permission from Ref. 38. Copyright 2008 RSC) and polyelectrolyte multilayer hollow capsules partially coated with platinum nanoparticles (IV)

(Reprinted with the permission from Ref. 41. Copyright 2012 ACS), showed autonomous movement in presence of H_2O_2, in addition bubble growth effect on big spherical catalytic nan/micromotors was also studied (III) (Reprinted with the permission from Ref. 40. Copyright 2008 AIP); stomatocyte-like structure obtained by supramolecular assembly of amphiphilic block copolymers which entrapped Pt nanoparticles (V) (Reprinted with the permission from Ref. 52. Copyright 2013 Nature). (D) Applications of rolled-up micromotors, selectively loading, transporting and delivering polystyrene particles and thin metallic films (I) (Reprinted with the permission from Ref. 44. Copyright 2010 Willey-VCH); swimming in a controlled manner in microfluidic systems, even against flowing streams (II) (Reprinted with the permission from Ref. 45. Copyright 2011 ACS); capturing and delivering murine CAD cells (III) (Reprinted with the permission from Ref. 46. Copyright 2011 RSC); modifying their outer surface by self-assembly monolayers to perform on-the-flight hybridization to selective isolation of nucleic acids (IVa) (Reprinted with the permission from Ref. 47. Copyright 2011 ACS) tumor cells (IVb) (Reprinted with the permission from Ref. 48. Copyright 2011 Willey-VCH) or thrombin (IVc) (Reprinted with the permission from Ref. 49, Copyright 2011 ACS) all the processes held in raw biological samples; controlling their directionalities according to an external field and behaving as a permanent magnet (V) (Reprinted with the permission from Ref. 50. Copyright 2012 RSC); showing crowscrew-like trajectories that allow them to perform mechanized functions (VI). Reprinted with the permission from Ref. 51. Copyright 2012 ACS.

However, the great leap on nano/micromotors moved by means of bubble induced propulsion came with the rolled-up catalytic micromotors. Their synthesis is based in strain engineering strategy, which rearrange in a controlled fashion nanomembranes intro three dimensional micro/nano structures (See Figure 8C).[42] Although material choice is limited, because of the parameters related to the relaxation and generation of stress involved in the roll-up procedure, this simple and reproducible technique offers the possibility to obtain different tube geometries with an inner catalytic layer in addition to its simple mas production possibility. First reported tubular micromotor based on Ti/Fe/Au/Ag nanotube had an inner silver catalytic surface and achieved speeds up to 720-150 nm/ms,[42] which was propelled by a recoiling mechanism produced by expelled microbubbles. Further studies integrated not only an inner platinum surface, more active towards hydrogen peroxide decomposition, but also a magnetic layer that permits the magnetic guidance of the micromotors by applying external rotating magnetic fields.[43] Although their lengths is considerable large compared to the nanomotors moving by selfphoretic mechanisms, such micromotors present speeds up to 2 mm/s, in addition to different trajectories that can easily be identified by the microbubble tails, revealing curved, circular and self-rotating motions.

The control of rolled-up micromotors trajectory and their high speeds in presence of hydrogen peroxide and certain surfactants, led to the performance of several tasks. Self-propelled catalytic Ti/Fe/Pt micromotors have been reported to selectively loading, transporting and delivering polystyrene particles and thin metallic films

(Figure 8DI).[44] This transport-and-delivery capabilities were further optimized in microchannels of microfluidic systems, where micromotors swam in a controlled manner to perform the corresponding tasks by sucking the cargo toward its front opening and propelling themselves even against the flowing streams (Figure 8DII).[45] Taking advantage that micromotors moving by bubble recoil mechanisms are not limited by high-ionic mediums, controlled manipulation of murine CAD cells (cathecolaminergic cell line from the central nervous system) was held not only transporting it, but also delivering the cell in the location of interest by rapidly rotating the magnet (Figure 8DIII). [46] By applying a custom-modified photolithography process, microrockets were sputtered with a gold layer, offering the opportunity to more selectively perform pick-up and delivery events (Figure 8DIV). Outer gold surface was functionalized by means of mixed self-assembly monolayers (SAM) to be further modified with single-strand DNA probe, performing an on-the-fly hybridization that permits the selective isolation of target nucleic acids from raw biological samples, such as serum, crude *Escherichia coli* lisate, urine or saliva.[47] Moreover, it was demonstrated that the hybrization process was enhanced by the locally induced convection associated to the bubbles generated during the micromotor motion and it was not compromised by the peroxide fuel and the surfactant presence in the solution. The selective binding and isolation of tumor cells in non-preprocessed biological samples was also demonstrated for micromotors with their outer gold modified with a binary SAM conjugated to anti-carcinoembryonic antigen (anti-CEA) monoclonal antibody (mAb), a specific antibody for the proteins expressed on cancer cells.[48] Following the same principles, an aptamer-modified micromotor was implemented for the selective isolation of target proteins, demonstrating the rapid loading, transport and controlled release of thrombin in complex biological samples, such as serum or plasma.[49]

In addition rolled-up tubular micromotors have recently been reported to align the directionalities of their movement according to the external field (Figure 8DV).[50] After being exposed to strong magnetic field the micromotor become magnetized, behaving as a permanent magnet with well-defined polarities and bringing the opportunity to sense and follow magnetic fields. Although cylindrical rolled-up micromotors showed a straight direction, asymmetrically GaAs/(Cr)Pt rolled-up microtubes have shown novel corkscrew-like trajectory that allow them to perform

mechanized functions, such as drilling (Figure 8DVI).[51] In addition, the asymmetric sharp tip that this structures present let them embed themselves into biomaterials, such as soft cellular material.

Designs that resemble structures already present in nature were also reported by polymer deformation, creating polymer vesicles that mimic natural stomatocytes (Figure 8DV). Such synthetic structures were obtained by supramolecular assembly of amphiphilic block copolymers, selectively entrapping preformed platinum nanoparticles within the nanocavities present inside the polymeric stomatocyte.[52] In presence of hydrogen peroxide, the catalytic decomposition of the fuel takes places inside the cavity promoting a rapid discharge that induces thrust and directional movement through the controlled opening of the cavity. It should be noted that although the direct observation of bubbles was possible in the case of the micron-size polymeric structures, both bubble propulsion and self-diffusiophoresis are feasible, as a gradient of oxygen concentration is also self-generated, consistent with the studies performed by Howse *et al.*, [53] where such synergy on the mechanisms was demonstrated for nonconductive 2μm Janus particles.

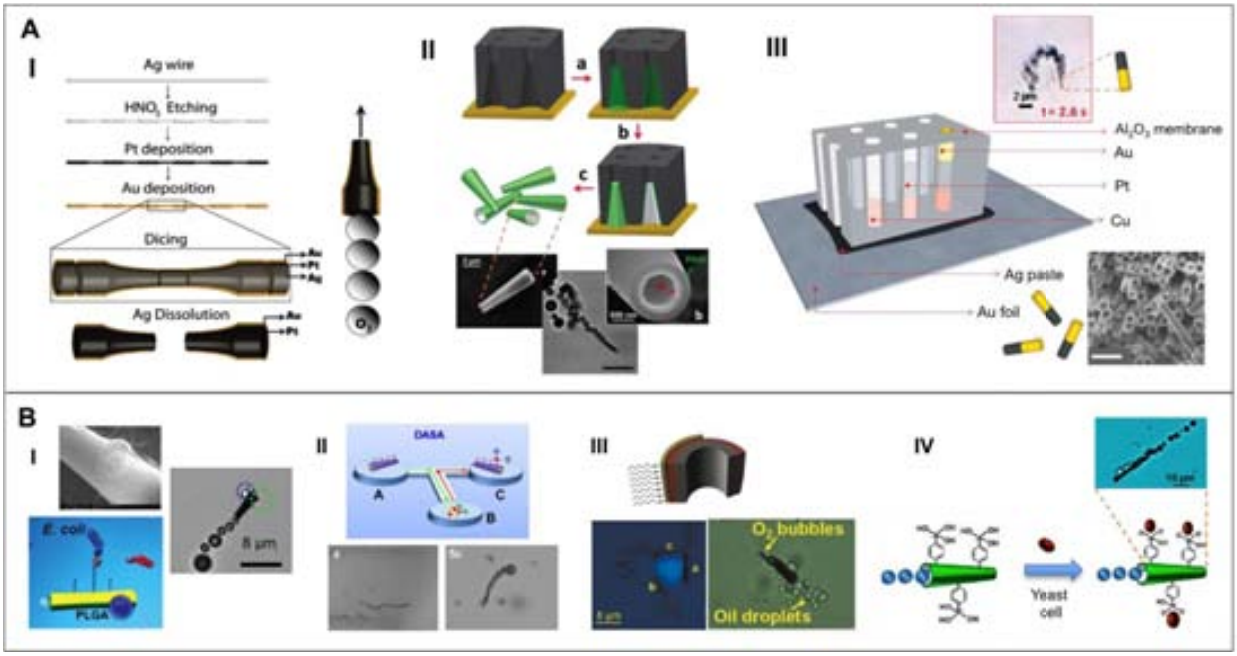

Figure 9. Improvement strategies and applications of autonomously moving tubular nano/micromotors by means of bubble propulsion mechanisms fabricated by template-based methods. (A) Schematic representation of the different template methods used to synthesize nano/micromotors: template-assisted layering approach for the direct deposition of the different layers onto a silver wire, which is further diced and dissolved to obtain the tubular micromotors (I) (Reprinted with the permission from Ref. 54. Copyright 2010 ACS); direct sequential deposition of PANI/Pt tubular micromotors onto conically shaped membranes, which are further dissolved (II) (Reprinted with the permission from Ref. 55. Copyright 2011 ACS); silver is firstly deposited in alumina template membranes, which enables the

further metal depositions of the metals onto the membrane walls and the desired tubular nanomotors (III). Reprinted with the permission from Ref. 57. Copyright 2013 RSC. (B) Applications of the tubular template-based micromotors: direct optical optical visualization of pick-up, transport and delivery of *E. Coli* bacteria and polymeric drug-carrier spheres (I) (Reprinted with the permission from Ref. 58. Copyright 2012 ACS); in-chip immunoassays for the *in-situ* capture and transport of target proteins (II) (Reprinted with the permission from Ref. 59. Copyright 2013 RSC); absorption and capture of oil thanks to the superhydrophobic-modified outer layer (III) (Reprinted with the permission from Ref. 60. Copyright 2012 ACS); selective recognition of monosaccharides for the capture and release of yeast cells (IV). Reprinted with the permission from Ref. 61. Copyright 2012 ACS.

Alternative template-based methods have been developed to fabricate conical tubular miromotors, starting by simplified template-assisted layering approaches to the direct deposition of the different layers confining the tubular engine (see Figure 9A). The very first approach was based on the sequential deposition of platinum and gold onto an etched silver wire, used as a template, to further dicing the wire and dissolving it (Figure 9AI).[54] The degree of concavity was controlled by the etching conditions, obtaining micromotors with an optimal smooth cone geometry that could be magnetically guided in case of plating an intermediate nickel layer, which also allows the pick-up and transport of magnetic cargo. However, much efficient tubular micromotors have been synthesized by direct sequential electrodeposition of polyaniline (PANI) and platinum, using as a template polycarbonate membranes with conically shaped pores (Figure 9AII).[55] The outer polymeric layer permitted the layer-by-layer electrodeposition, being used as a conductive template to obtain the desired tubular micromotors, such as the magnetic PANI/Ni/Pt that can be magnetically guided. PANI/Pt tubular micromotors exhibit similar velocities to their rolled-up counterparts, but their dimensions are appreciably smaller. A wide range of polymeric micromotors by using different polymeric precursors to electrodeposit their outer layer, including polypyrrole (PPy) or poly(3,4-ethylenedioxythiophene) (PEDOT), and varying their inner catalytic metal surface, demonstrating the different morphologies and locomotion patterns depending on the chosen combination have been developed.[56] In any case, the use of surfactants during micromotors motion led to a decrease on the surface tension, creating dense smaller bubbles that induce smoother propulsion. Although the micromotors present slower speed, such controllable movement for real applications was preferred.

Smaller bubble-recoil nano/micromotors fabricated by template-based methods have been reported by Pumera *et al.*,[57] presenting similar dimensions to the nanomotors moved by selfphoretic mechanisms (Figure 9AIII). Although being fabricated by

using the same alumina membranes as the rod-shape nanomotors, they present a tubular shape due to firstly deposited outer silver surface, which enables the further metal depositions only onto the walls of the membranes. Such tubular nanomotors present different trajectories like straight, screw-like and circular motion, and speed up to 40 body lengths per second.

Interesting applications for self-propelled micromotors fabricated by template-based methods due to their high speed at very low fuel concentration (down to 0.2% of hydrogen peroxide) and their dimensions, similar to the analyte of interest were reported (Figure 9B). One first example is the functionalization of Au/Ni/PANI/Pt micromotors with Concanavalin A (ConA), which selectively captures pathogenic bacteria from fuel-enhanced real samples.[58] The direct label-free optical visualization of the pick-up, transport and delivery events could be observed due to the similar dimensions of both the micromotor and the bacteria. The simultaneous transport of both the pathogenic bacteria and polymeric magnetic drug-carrier spheres envisions attractive motion-based theranostics strategy. In addition, antibody-functionalized synthetic catalytic micromotors have been implemented for in-chip immunoassays by the active *in-situ* capture and transport of target proteins between different reservoirs in fuel-enhanced environments, avoiding the washing steps in common antibody-based protein bioassays.[59] Self-propelled micromotors have also been used for assessing environmental issues, such as the remediation of oil-contaminaed water by using microengines conveniently functionalizated by long chain of self-assembled monolayers on their outer gold rough surface to obtain a superhydrophobic layer able to absorb and capture oil.[60] Alternative materials to the mentioned polymers have been reported, bringing not only the desired conductive conical template, but also directly providing the target recognition without the need of additional external functionalization. Poly(3-aminophenylboronic acid) (PAPBA)/Ni/Pt tubular micromotors selectively recognize monosaccharides, bringing the possibility of capture and release yeast cells.[61]

New techniques have been implemented to obtain precisely geometries for the catalytic motors in the nanoscale. Focus Ion Beam (FIB) etching has recently been used to fabricate a sophisticated nanomotor that swims in certain orbits, demonstrating the easy fabrication of catalytic entities and their convenient manipulation.[62] Although this technique is has not mass-production capability, it

opens to door to the design of almost any shape, bringing new locomotion patterns and future new functionalities.

1.3.3. Conclusions and future perspectives

Concerning catalytic nano/micromotors moving in presence of hydrogen peroxide, remarkable advances related to their composition and shape had led to more efficient entities, which had permitted a better understanding of their motion patterns and their implementation in real systems. Although the use of hydrogen peroxide is hindered by their toxicity, such devices are still the most efficient ones, with great interest for miniaturized systems (e. g. lab-on-a-chip) and applications held in non-biological environments.

However, the main focus of the research in this field has been searching of efficient motors in terms of the used fuel /motion source, their composition and structure beside the versatility in applications. While catalytic nano/micromotors propelled in presence of hydrogen peroxide have been widely studied, future applications towards motors moving in presence of external stimulus (e. g. light, electric source, magnetic source, etc.) or alternative biocompatible fuels, such as water or moving in basic/acid environments are envisioned. Hydrogen peroxide has been the very first example of what it can be achieved and what parameters must be considered regarding nano/micromotors motion. This kind of nanomotors opened the door to the development of many new nano/micromotors designs with the capacity to freely moving and performing complex tasks in biological samples without compromising their stability, leading to real theranostic applications (sensing and therapy at the same platform).

References

[1] Ismagilov, R. F.; Schwartz, A.; Bowden, N.; Whitesides, G. M. *Angew. Chem. Int. Ed.* **2002**, *41*, 652.

[2] Paxton, W. F.; Kistler, K. C.; Olmeda, C. C.; Sen, A.; St. Angelo, S. K.; Cao, Y.; Mallouk, T. E.; Lammert, P. E.; Crespi, V. H. *J. Am. Chem. Soc.* **2004**, *126*, 13424.

[3] Paxton, W. F.; Sen, A.; Mallouk, T. E. *Chem. Eur. J.* **2005**, *11*, 6462.

[4] Paxton, W. F.; Baker, P. T.; Kline, T. R.; Wang, Y.; Mallouk, T. E.; Sen, A. J. Am. Chem. Soc. **2006**, *128*, 14881.

[5] Wang, Y.; Hernandez, R. M.; Bartlett, D. J.; Bingham, J. M.; Kline, T. R.; Sen, A; Mallouk, T. E. *Langmuir* **2006**, *22*, 10451.

[6] Catchmark, J. M.; Subramanian, S.; Sen, A. *Small* **2005**, *1*, 202.

[7] Howse, J. R.; Jones, R. A. L; Ryan, A. J.; Gough, T.; Vafabakhsh, R.; Golestanian, R. *Phys. Rev. Lett.* **2007**, *99*, 048102.

[8] Ebbens, S.; Jones, R. A. L.; Ryan, A. J.; Golestanian, R.; Howse, J. R. *Phys. Rev. E* **2010**, *82*, 015304.

[9] Ke, H.; Ye, S.; Carroll, R. L.; Showalter, K. *J. Phys. Chem. A* **2010**, *114*, 5462.

[10] Purcell, E. M. Am. J. Phys. **1977**, *45*, 3.

[11] Dhar, P.; Fischer, Th. M.; Wang, Y.; Mallouk, T. E.; Paxton, W. F.; Sen, A. *Nano Lett.* **2006**, *6*, 66.

[12] Laocharoensuk, R; Burdick, J.; Wang, J. *ACS Nano* **2008**, *2*, 1069.

[13] Demirok, U. K.; Laocharoensuk, R.; Manesh, K. M.; Wang, J. *Angew. Chem. Int. Ed.* **2008**, *47*, 9349.

[14] Zacharia, N .S.; Sadeq, Z. S.; Ozin, G. A. *Chem. Commun.* **2009**, *39*, 5856.

[15] Calvo-Marzal, P.; Manesh, K. M.; Kagan, D.; Balasubramanian, S.; Cardona, M.; Flechsig, G. U.; Posner, J.; Wang, J. *Chem. Commun.* **2009**, 30, 4509.

[16] Wheat, P. M.; Marine, N. A.; Moran, J. L.; Posner, J. D. *Langmuir* **2010**, 26, 13052.

[17] Valadares, L. F.; Tao, Y. G.; Zacharia, N. S.; Kitaev, V.; Galembeck, F.; Kapral, R.; Ozin, G. A. *Small* **2010**, *6*, 565.

[18] Kline, T. R.; Paxton, W. F.; Mallouk, T. E.; Sen, A. *Angew. Chem. Int. Ed.* **2005**, *44*, 744.

[19] Tierno, P.; Albalat, R.; Sagués, F. *Small* **2010**, *6*, 1749.

[20] Baraban, L.; Makarov, D.; Streubel, R.; Mönch, I.; Grimm, D.; Sanchez, S.; Schmidt, O. G. *ACS Nano* **2012**, *6*, 3383.

[21] Choi, E.; Gut, Z.; Gracias, D.; Andreou, A. G. *ISCAS* **2006**, 1319.

[22] Burdick, J.; Laocharoensuk, R.; Wheat, P. M.; Posner, J. D.; Wang, J. *J. Am.. Chem. Soc.* **2008**, *130*, 8164.

[23] Balasubramanian, S.; Kagan, D.; Manesh, K. M.; Calvo-Marzal, P.; Flechsig, G. U.; Wang, J. *Small* **2009**, *5*, 1569.

[24] Kagan, D.; Laocharoensuk, R.; Zimmerman, M.; Clawson, C.; Balasubramanian, S.; Kang, D.; Bishop, D.; Sattayasamitsathit, S.; Zhang, L.; Wang, J. *Small* **2010**, *6*, 2741.

[25] Sundararajan, S.; Lammert, P. E.; Zudans, A. W.; Crespi, V. H.; Sen, A. *Nano Lett.*, **2008**, *8*, 1271.

[26] Sundararajan, S.; Sengupta, S.; Ibele, M. E.; Sen, A. *Small* **2010**, *6*, 1479.

[27] Kagan, D.; Calvo-Marzal, P.; Balasubramanian, S.; Sattayasamitsathit, S.; Manesh, K. M.; Flechsig, G. U.; Wang J. *J. Am. Chem. Soc.* **2009**, *131*, 12082.

[28] Wu, J.; Balasubramanian, S.; Kagan, D.; Manesh, K. M.; Campuzano, S.; Wang, J. *Nat. Commun.* **2010**, *36*, 1.

[29] Manesh, K. M.; Balasubramanian, S.; Wang J. *Chem. Commun*. **2010**, *46*, 5704.

[30] Fournier-Bidoz, S.; Arsenault, A. C.; Manners, I.; Ozin, G. A. *Chem. Commun.* **2005**, *4*, 441.

[31] Qin, L.; Banholzer, M. J.; Xu, X.; Huang, L.; Mirkin, C. A. *J. Am. Chem,. Soc.* **2007**, *129*, 14870.

[32] Wang, Y.; Fei, S.; Byun, Y. M.; Lammert, P. E.; Crespi, V. H.; Sen, A.; Mallouk, T. E. *J. Am. Chem. Soc* **2009**, *131*, 9926.

[33] He, Y.; Wu, J.; Zhao, Y. *Nano Lett.* **2007**, *7*, 1369.

[34] Gibbs, J. G.; Zhao, Y. P. *Small* **2009**, *5*, 2304.

[35] Gibbs, J. G.; Zhao, Y. *Small* **2010**, *6*, 1656.

[36] Gibbs, J. G.; Zhao, Y. P. *Appl. Phys. Lett.* **2009**, *94*, 163104.

[37] Agrawal, A.; Dey, K. K.; Paul, A.; Basu, S.; Chattopadhyay A. *J. Phys. Chem. C* **2008**, *112*, 2797.

[38] Vicario, J.; Eelkema, R.; Browne, W. E.; Meetsma, A.; La Crois, R. M.; Feringa, B. L. *Chem. Commun.* **2005**, *31*, 3936–3938.

[39] Stock, C.; Heureux, N.; Browne, W. R.; Feringa, B. L. *Chem. Eur. J.* **2008**, *14*,

3146.

[40] Manjare, M.; Yang, B.; Zhao, Y. P. *Phys. Rev. Lett.* **2012**, *109*, 128305.

[41] Wu, Y.; Wu, Z.; Lin, X.; He, Q.; Li, J. *ACS Nano* **2012**, *6*, 10910.

[42] Mei, Y.; Huang, G.; Solovev, A. A.; Bermúdez-Ureña, E.; Mönch, I.; Ding, F.; Reindl, T.; Fu, R. K. Y.; Chu, P. K.; Schmidt, O. G. *Adv. Mater.* **2008**, *20*, 4085.

[43] Solovev, A. A.; Mei, Y.; Bermúdez Ureña, E.; Huang, G.; Schmidt, O. G. *Small* **2009**, *5*, 1688.

[44] Solovev, A. A.; Sanchez, S.; Pumera, M.; Mei, Y. F.; Schmidt, O. G. *Adv. Funct. Mater.* **2010**, *20*, 2430.

[45] Sanchez, S.; Solovev, A. A.; Harazim, S. M.; Schmidt, O. G. *J. Am. Chem. Soc.* **2011**, *133*, 701.

[46] Sanchez, S.; Solovev, A. A.; Schulze, S.; Schmidt, O. G. *Chem. Commun.*, **2011**, *47*, 698.

[47] Kagan, D.; Campuzano, S.; Balasubramanian, S.; Kuralay, F.; Flechsig, G. U.; Wang, J. *Nano Lett.* **2011**, *11*, 2083.

[48] Balasubramanian, S.; Kagan, D.; Hu, C. M. J.; Campuzano, S.; Lobo-Castañon, M. J.; Lim, N.; Kang, D. Y.; Zimmerman, M.; Zhang, L.; Wang, J. *Angew. Chem. Int. Ed.* **2011**, *50*, 4161.

[49] Orozco, J.; Campuzano, S.; Kagan, D.; Zhou, M.; Gao, W.; Wang, J. *Anal. Chem.* **2011**, *83*, 7962.

[50] Zhao, G.; Sanchez, S.; Schmidt, O. G.; Pumera M. *Chem. Commun.*, **2012**, *48*, 10090.

[51] Solovev, A. A.; Xi, W.; Gracias, D. H.; Harazim, S. M.; Deneke, C.; Sanchez, S.; Schmidt, O. G. *ACS Nano* **2012**, *6*, 1751.

[52] Wilson, D. A.; Nolte, R. J. M.; van Hest, J. C. M. Nature 2013, DOI: 10.1038/NCHEM.1281.

[53] Ebbens, S. J.; Howse, J. R. *Langmuir* **2011**, *27*, 12293.

[54] Manesh, K. M.; Cardona, M.; Yuan, R.; Clark, M.; Kagan, D.; Balasubramanian, S.; Wang, J. *ACS Nano* **2010**, *4*, 1799.

[55] Gao, W.; Sattayasamitsathit, S.; Orozco, J.; Wang, J. *J. Am. Chem. Soc.* **2011**, *133*, 11862.

[56] Gao, W.; Sattayasamitsathit, S.; Uygun, A.; Pei, A.; Ponedal, A.; Wang, J. *Nanoscale*. **2012**, *4*, 2447.

[57] Zhao, G.; Ambrosi, A.; Pumera, M. *Nanoscale* **2013**, DOI: 10.1039/C2NR31566A.

[58] Campuzano, S.; Orozco, J.; Kagan, D.; Guix, M.; Gao, W.; Sattayasamitsathit, S.; Claussen, J. C.; Merkoçi, A.; Wang, J. *Nano Lett.*, **2012**, *12*, 396.

[59] García, M.; Orozco, J.; Guix, M.; Gao, W.; Sattayasamitsathit, S.; Escarpa, A.; Merkoçi, A.; Wang, J. *Nanoscale* **2013**, *5*, 1325.

[60] Guix, M.; Orozco, J.; García, M.; Gao, W.; Sattayasamitsathit, S.; Merkoçi, A.; Escarpa, A.; Wang, J. *ACS Nano* **2012**, *6*, 4445.

[61] Kuralay, F.; Sattayasamitsathit, S.; Gao, W.; Uygun, A.; Katzenberg, A.; Wang, J. *J. Am. Chem. Soc.* **2012**, *134*, 15217.

[62] Bao, J.; Nakajima, M.; Yang, Z.; Kojimai, M.; Fukuda, T. Nanotechnology (IEEE-NANO), **2012** 12th IEEE Conference on**.**

CHAPTER 2

OBJETIVES OF THE THESIS

The development of efficient miniaturized analytical platforms for the detection of pollutants and other analytes of interest is of great concern nowadays both to address environmental and/or health related issues. The main objective of the present thesis is the implementation of nano/micromaterials in different miniaturized platforms with the aim of obtaining more efficient, robust and selective (bio)sensing and moving platforms/devices with interest for further integration in monitoring and cleaning/remediation systems.

More in details, the objectives of the thesis can be summarized as following:

1. **Design, fabrication and characterization of novel carbon nanotubes (CNT) modified screen-printed electrodes (SPE)**
    - 1.1. Study of CNT purification and dispersion for its further implementation in SPE.
    - 1.2. Characterization of CNT structure and composition by SEM microanalysis and TEM.
    - 1.3. Study CNT integration onto working electrode surface and characterization of its morphology through SEM and Confocal Scanning Laser Microscopy (CSLM).

2. **Study and applications of screen-printed and ITO electrodes.**
    - 2.1. Study different immobilization approaches and evaluate electrochemical behavior (including sensibility, sensitivity and stability between others) of the developed biosensing platform towards phenol detection. .
    - 2.2. Characterize the morphology and enzyme distribution through the matrix of biosensing platform by SEM and CSLM studies.
    - 2.3. Study the possible integration of the miniaturized SPE in monitoring systems.
    - 2.4. Integration of nano/micromaterials into an SPE, to evaluate its analytical platform towards glucose detection by impedancimetric methods.

2.5. Layer-by-layer modification of ITO to include nano/micromaterials which could enhance its electrochemical behavior, especially regarding applications for host-guest systems.

3. **Integration of nano/micromaterials in lab-on-a-chip platform for protein analysis.**
    3.1. Study of different nano/micromaterials, which could be of interest as dynamic platforms, with advanced and improved electrochemical response, for immunosensing applications..
    3.2. Study key parameters in electrophoresis: injection time, injection voltage or pumping voltage, related to the nano/micromaterials loading.
    3.3. Study and optimization of the electrochemical parameters for protein detection.

4. **Study and application of micromotors towards environmental and health issues.**
    4.1. Design, fabrication and characterization of template-based tubular micromotors.
    4.2. Judicious functionalization of micromotors outer surface with the idea to design novel environment remediation and health related applications.
    4.3. Motion studies related to the fuel concentration, matrix effect and lifetime.

RESULTS AND DISCUSSION

CHAPTER 3

BATCH DETECTION PLATFORMS

Related Publications

"Structural characterization by confocal laser scanning microscopy and electrochemical study of multi-walled carbon nanotube tyrosinase matrix for phenol detection" Maria Guix, Briza Pérez-López, Melike Sahin, Mònica Roldán, Adriano Ambrosi and Arben Merkoçi. *Analyst* **2010**, *135*, 1918-1925.

"Stable and sensitive flow-through monitoring of phenol using a carbon nanotube based screen printed biosensor" Georgina Alarcón, Maria Guix, Adriano Ambrosi, Maria Teresa Ramirez Silva, Manuel Eduardo Palomar Pardavé and Arben Merkoçi. *Nanotechnology* **2010**, *21*, 245502-245511.

"Bismuth Film Combined with Screen-Printed Electrode as Biosensing Platform for Phenol Detection" Arben Merkoçi, Ulku Anik, Serdar Çevik, Meliha Çubukçu and Maria Guix. *Electroanalysis* **2010**, *22*, 1429 – 1436.

"Compact Microcubic Structures Platform based on Self-Assembly Prussian Blue Nanoparticles with Highly Tuneable Conductivity" Welter Cantanhêde Silva, Maria Guix, Georgina Alarcón Angeles and Arben Merkoçi. *Phys. Chem. Chem. Phys.* **2010**, *12*, 15505-15511.

"Bimetallic nanowires as electrocatalysts for nonenzymatic real-time impedancimetric detection of glucose" Carmen Clotilde Mayorga-Martinez, Maria Guix, Rossana Elena Madrid and Arben Merkoçi. *Chem, Commun.* **2012**, *48*, 1686–168.

3.1. Introduction

Miniaturized biosensing batch platforms based on screen-printed electrodes have a great potential for a wide range of applications, basically due to their versatility and easy-functionalization. In the following sections the fabrication process, along with the different modifications and further enzyme immobilizations, of some of the developed platforms will be described. An overview of some of their applications in batch and flow through monitoring systems will also be given (more details can be seen in the published articles).

3.1.1. **Screen-printing** technology

Screen-printed technology is based on the sequential deposition of layers of different conductive or non-conductive inks on a variety of inert substrates. Nowadays, screen-printing microfabrication technology is well established for the mass production of thick film electrodes and it is widely applied to build biological or chemical sensors.[1] Screen-printed electrodes (SPE) represent one of the most important products of this technology.

Generally, inert substrates used in screen-printed processes are ceramic or polymeric substrates. In case of polymeric substrates, polyester substrate is the most common used for its durability, thermal and hydroscopic stability, clarity and stiffness. Exact composition of printing inks is uncertain, as they are commercial, but it is known that these inks are comprised mainly by synthetic grade graphite, vinyl or epoxy-based polymeric binder and solvents.

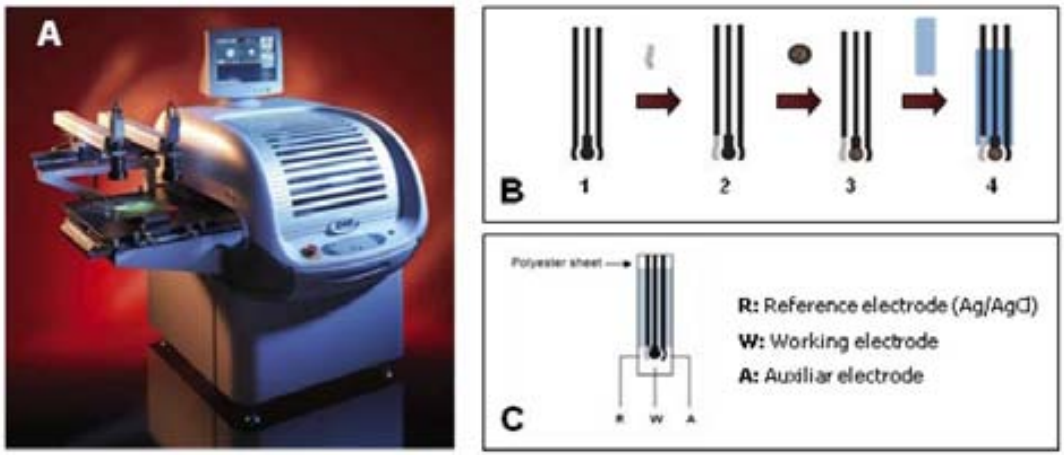

Figure 1. (A) Photography of the screen-printed machine DEK 248. (B) Scheme of the screen-printed process performed to produce home-made SPE. (C) Details, not in scale, of an SPE.

Screen-printing process for the fabrication of SPEs is based on four main steps (see Figure 1B): (1) deposition of graphite ink, (2) deposition of silver/silver chloride (Ag/AgCl) ink, (3) deposition of an addition layer onto the working electrode area for modification purposes, and (4) deposition of the insulating ink. Insulating substrate used is a polyester sheet where the deposition of each layer is performed by forcing the ink to pass through the open meshes of a net (composed by polyester mono-filament of 110 threats) using a silicon spatula (squeege).

After the deposition of each layer a drying process that consists on introducing the printed sheet into an oven during 15 minutes at 90ºC is applied. During this process the ink is adsorbed onto the sheet and the solvent almost evaporated.

The fabricated SPE is composed by three electrodes (see Figure 1C): working electrode (WE), reference electrode (RE) and auxiliar electrode (AE) printed in a single strip. In the WE is where the reaction occurs, the RE (composed by Ag/AgCl) provides a constant potential reference and the AE (or counter electrode) is used to ensure that current does not run through the reference electrode.

Screen-printing technology offers the opportunity for mass production of low cost biosensors. Several printing steps such as biomolecule (i.e. enzyme) layers as well as other species (i.e. mediators etc.) with interest for the normal operation of biosensors can be applied that makes this technology a versatile one for a broad range of applications.

3.1.2. Carbon-nanotubes modified screen-printed electrodes

Incorporating carbon nanotubes into sensing devices generally requires the dispersion of CNTs in certain solvents so they can be processed into thin films or other applications.[2] To control the properties of the CNTs it is necessary to remove foreign nanoparticles that modify the physico-chemical properties of carbon nanotubes. CNTs processing permit the elimination of non-nanotube material, dispersion of individual nanotubes and chemical functionalization.[3] Purification of CNTs by sonication can induce sidewall[4] or end[5] functionalization, which is of interest for facilitating their manipulations.[6] In our particular case, CNTs are dispersed into a suitable solvent in order to achieve their homogeneous distribution onto the working electrode surface.

Chemical oxidation (by previously stirring CNTs into 2 M nitric acid at 25 ºC for 24 h) and physical treatment (applying a sonication process at room temperature during 4 h) shorten the CNTs and lead to the partial oxidation of the CNTs to produce functional oxygenated groups at the open ends and defects along the sidewall.[7] Impurities and defects in CNTs were characterized by SEM microanalysis and showed that traces of iron (Fe), nickel (Ni) and potassium (K) from 0.5%, 1.6% and 1.5% were decreased to 0.1%, 0.9% and 0.4% after treatment with nitric acid.[8] CNTs were dispersed in tetrahydrofuran (THF) (1 mg of CNTs/1 ml THF) during four hours by sonication. The studies reveal a good dispersion of the CNTs in THF. At the same time, some impurities that are probably related to the remaining metals are observed in the different TEM images taken. Defects along the tubes can also be seen in addition to the impurities.

Screen-printed microfabrication is based on the sequential deposition of graphite ink, Ag/AgCl ink and insulating ink on a polyester substrate. After each layer is deposited a drying process is carried out, which consists on keeping the polyester substrate at 90 ºC for 15 min. Previously to their dispersion, CNTs were purified by stirring them in 2 M nitric acid at 25 ºC for 24 h. Multiwalled CNTs used have a purity of 95%.[9] The working surface area of a bare SPE was modified by depositing a 7 ml drop of MWCNTs suspension (1 mg MWCNTs/1 ml THF) onto the working electrode surface, followed by a drying process at room temperature for 24 h.

Once the modified SPE was prepared, an accurate and extensive characterization of the CNTs based matrix is especially important for understanding the improved response mechanisms and consequently a correct interpretation of the analytical platform responses. Although CNTs are usually characterized prior to application by electron microscopy (SEM and TEM), Raman spectroscopy, thermal analysis and absorption spectroscopy (UVVis-NIR), it is also important to evaluate their properties once they have been applied/integrated into a matrix where biological molecules will be further included. Careful testing with these techniques provides important information on the morphology, distribution and possible linkages of CNTs that led to significant improvements in CNTs based biosensors. The characterization process of the working electrode surface was performed by SEM to check if a homogeneous distribution of CNTs over the surface was achieved (Figure 2). SPE images of the

working electrode, with and without CNTs, were obtained by previously mounting the electrode onto adhesive carbon films and then coated with gold. Profile images were taken from electrodes that were previously immersed in liquid nitrogen and immediately cut with a knife. A more sponge-like structure of the MWCNTs modified surface (Figure 2C2) in comparison to bare SPE surface (Figure 2B2) can be observed. The cut view of the MWCNTs (Figure 2D) clearly shows the MWCNTs layer deposited over the previous imprinted carbon layer. The evident roughness would be with interest for biosensing application due to the increased sensing area.

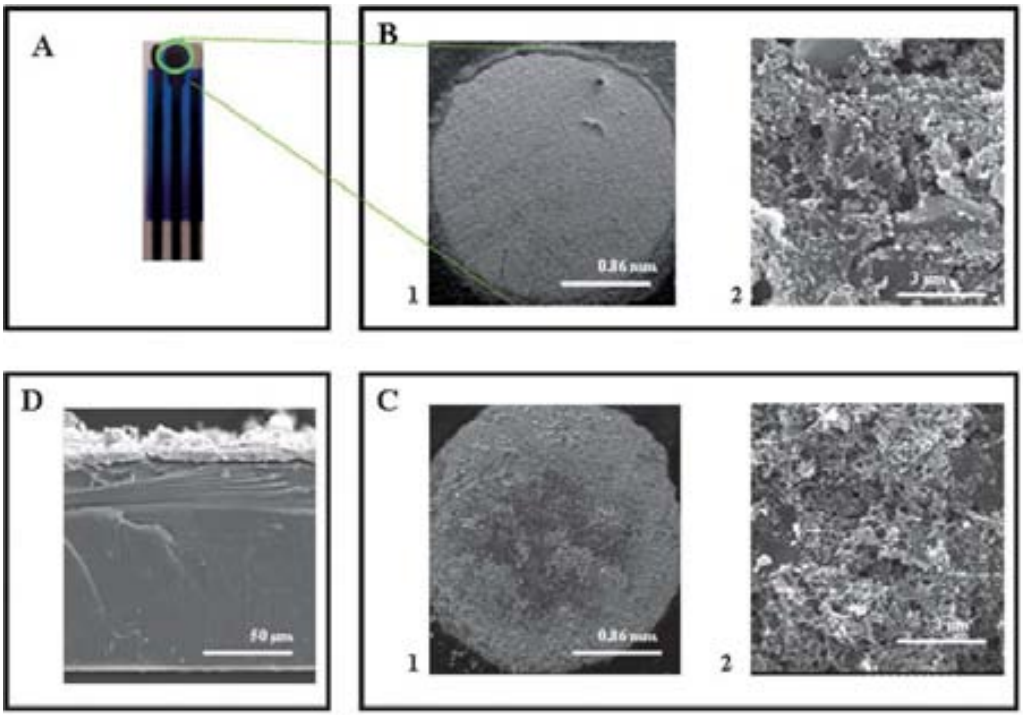

Figure 2. Image of the SPE (A) where the working surface area evaluated by SEM is circled in green. SEM images of the working surface area of a bare (B) and MWCNTs (C) modified SPE at different resolutions: 0.86 mm (B1 and C1) and 3 μm (B2 and C2). In the case of SPE modified with MWCNTs, a suspension of 7 μl of MWCNTs dispersion (1 mg MWCNT/1 ml THF) was dropped onto the working electrode area and left to be dried at room temperature during 24 h. SEM image of the profile of SPE modified with MWCNTs (D) is also shown.

A more accurate quantitative study of the sensor surface is done by calculating several statistical data that correspond to the studied sensor surfaces by using Confocal Laser Scanning Microscopy (CLSM) in reflection mode and three-dimensional analysis (topographic image) to assess the different parameters of roughness were used. Roughness parameters were calculated according to DIN-ENISO 4287 (1997).[10] Average roughness (Pa; arithmetic average of the profile ordinates within the measured section), root mean square (Pq; root mean square value of the profile

ordinates within the measured section), maximum values for the valleys (Pn, depth of the greatest profile valleys) and peaks (Pp; height of the highest profile peak) are measured. Although CLSM has less resolution than SEM, it is not limited to the surface characterization of the materials. Being a nondestructive method it can provide quantitative information on the roughness and the relative surface-to-area value of the different electrodes were evaluated (see Table 1). These values clearly indicate that quantitatively SPE modified with CNTs have a higher average roughness and a higher maximum values for the valleys and peaks compared to the carbon surface of the unmodified SPE.

SPE	Pa	Pq	Pn	Pp
Bare	1.51 ± 0.25	2.06 ± 0.57	14.57 ± 1.58	13.49 ± 3.14
CNTs modified	2.23 ± 0.39	3.03 ± 0.45	18.14 ± 1.62	15.52 ± 1.74

Table 1. Quantitative information over the roughness of different formulations evaluated by CLSM. Formulation evaluated were bare SPE and SPE modified with CNTs. Statistical data and its standard deviation are presented and consists of the average roughness (Pa), root mean square (Pq), maximum values for the valleys (Pn) and peaks (Pp). Seven fields for each surface (bare and CNTs modified) were studied using the reflection mode evaluated by DIN-EN-ISO 428726.

3.2. Enzyme-based screen-printed electrodes platforms for phenol detection

Phenolic compounds are on the priority pollutants list of the European Community and the environmental Protection Agency of the United States because of their toxicity and persistency in the environment. They are commonly used in resin manufacture, and polymer and pharmaceutical products.[11] As they are compounds of particular environmental significance, it is important to be able to quantify and monitor them on-site.

Phenolic compounds are classically determined by gas chromatography and spectrophotometric analyses,[12] but these techniques are expensive, time-consuming and difficult to be applied *in situ*. Electrochemical biosensors represent a promising alternative to the mentioned technique due to the extremely high sensitivity achievable, the simplicity of their use, very low cost and the fact that biosensors can be easily combined with miniaturized devices. Amperometric biosensors based on tyrosinase enzyme show high selectivity for phenol detection.

Different matrixes such as carbon paste,[13,14] graphite epoxy composite,[15,16] sol–gel composite,[17,18] graphite-teflon electrodes[19],[20] glassy carbon electrodes[21,22] and screen-printed electrodes (SPEs) [23 , 24] have been reported. Screen-printing is a well-established microfabrication technology for the mass production of thick film electrodes and it is widely applied to build biological or chemical sensors,[25] which can be used without complicated sample pretreatment and therefore are suitable for on-site monitoring.[26]

Confocal laser scanning microscopy (CLSM) is emerging as an indispensable tool that can provide valuable information related to the distribution of the incorporated enzyme within the sensing matrix layer.[27] CLSM can be useful for characterizing not only the outer layer of the biosensing surface but also its interior, and provide at the same time a relative quantification of the enzyme. These studies aim to obtain a better understanding and control of the structure, shape and composition of the CNTs based biosensing materials and could be of interest for further investigations including biofuel cells,[28,29] drug delivery[30,31] or biomarkers analysis,[32] between others.

3.2.1. Enzyme immobilization approaches

Immobilization of the enzyme represents the crucial point in obtaining adequate sensitivities and overall stability of the biosensor. Different approaches, based on adsorption, covalent binding[33] or entrapment in polymers,[34] have been performed to achieve better immobilization of the enzyme. Nanostructured materials can be used to improve the incorporation of the enzyme into the sensing matrix and avoid its leaking. Better responses in terms of the biosensor performance are related to the intrinsic properties of the nanostructured materials used. Carbon nanotubes (CNTs) have unique structure-dependent electronic and mechanical properties[35] that when coupled with the specific recognition properties of enzymes provide important improvements in biosensors.

Their advantages in electrochemical biosensing applications are mostly related to their capacity to mediate electron transfer reactions between electroactive species[36] and transducers thanks to their excellent electrical conductivity. Other exceptional properties of CNTs such as their mechanical strength and large surface area, which

make them a potential linking bridge to attach biomolecules to the biosensor transducer, have been reported.[37,38]

Coupling CLSM with the specificity of immunostaining techniques has been proved to be a good technique for evaluating the distribution of biological species in certain matrixes.[39] In case of Tyrosinase being immobilized by physical adsoption into the CNTs matrix, their distribution can be evaluated by CLSM by using optical sectioning through a material up to a 100 μm depth. Maximum height section studied was ca. 18.14 μm (corresponding to the electrode modified with CNTs). Taking several images of successive depth planes of the material allow three dimensional (3D) imaging of the matrix.

The possible autofluorescence of the different electrode constituents (i.e. polyester substrate and carbon ink) before and after applying the immunostaining protocol have been studied. The control of the possible autofluorescence coming from the different materials that constitute the biosensing area are also evaluated so as to avoid false positives. The used electrode materials didn't show any autofluorescence in the spectra of interest (results not shown). Consequently, the fluorescence of the studied sensors is only due to the presence of the tyrosinase in the different studied matrixes. This protocol allows the problems usually present in immunochemistry to be avoided.

CLSM is suitable to study the enzyme distribution through the working electrode surface. An *in situ* 3D representation of this distribution can be seen in Figure 3. A better distribution of tyrosinase onto the electrode surface as well as in depth is observed at the CNTs based SPE. Furthermore, it is possible to have been measured across all individual CLSM images of the stack. This value gives an idea of the sum of the total fluorescence in the frame scanned. As the fluorescence is proportional to the enzyme present in the sample, this integrated value can be related to the total enzyme adsorbed in this stack. Comparing the frame scanned for the bare and the modified SPE a quantity of the immobilized tyrosinase enzyme 1.96 times higher in the case of the MWCNTs modified SPE is found.

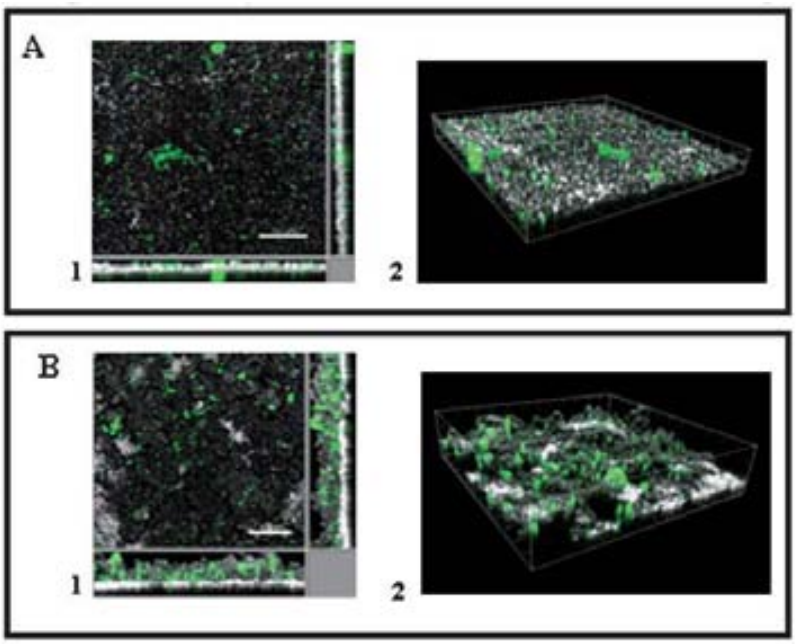

Figure 3. CLSM images of the sensor surfaces. (A) Distribution of tyrosinase in the SPE carbon matrix (1) and its corresponding 3D confocal images (2). (B) Distribution of tyrosinase in the SPE CNTs matrix (1), and its corresponding 3D confocal images (2). Scale bar 50 mm.

Additional information on the relation between the tyrosinase distribution and the roughness can be found by overlapping the signal obtained by the reflection mode and the fluorescence signal obtained in the same linear region of interest (ROI) (Figure 4). The graphics of the fluorescence versus the depth along the ROI (Figure 3 graphics) demonstrate that the enzyme distribution is directly affected by the roughness of the sample. Both Figure 2 and Figure 3 demonstrate qualitatively demonstrate that tyrosinase is well distributed within the surface and the depth of the CNTs based matrix.

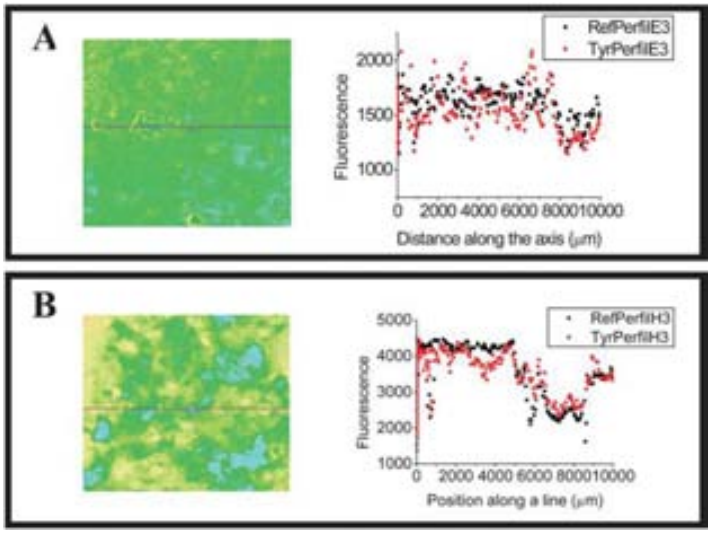

Figure 4. Confocal micrographs of bare SPE (A) and CNTs modified SPE (B), with their corresponding graph. Fluorescence of the Alexa Fluor! 488 dye (pink) is overlapped with the signal

obtained by working in the reflection mode (blue). ROI (linear region of interest) used for each surface is shown.

One of the biggest challenges in designing a new enzyme based biosensor is to find the optimal balance between stability and activity of the enzyme. Immobilization methods, such as cross-linking bonding,[40] covalent attachment,[41] polymer inclusion[42] and simple adsorption, have different effectiveness with regard to the stability of the signal generated, due to the fact that a higher or lower percentage of enzyme immobilized is lost during the measurement. On the other hand, better stability is generally obtained, paying the price of the loss of signal intensity related to a lower enzyme catalytic activity. A good combination of support material and immobilization method is of fundamental importance to achieve the desired performances from the sensing system. In our specific case, the first step was tyrosinase immobilization through physical absorption, as it was previously reported, followed by the casting of glutaraldehyde solution at 5% onto the working electrode surface and left to dry at room temperature. Such treatment led to the creation of a glutaraldehyde film, without compromising CNTs dispersion, as it can be clearly appreciated at the SEM images taken after the mentioned treatment (Figure 5).

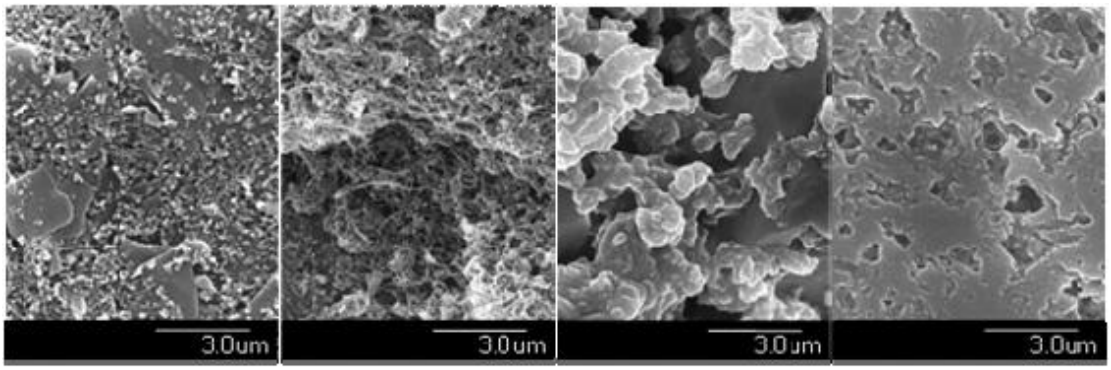

Figure 5. SEM images of the working surface area of (A) bare SPE, (B) SPE modified with MWCNTs, (C) SPE modified with MWCNT/Tyr and (D) SPE modified with MWCNT/Tyr/Glu. Images are taken at a resolution of 3 **μ**m and an acceleration voltage of 15 kV.

A third immobilization approach based on the mushroom tissue immobilization by via bismuth (Bi) deposition onto multiwalled carbon nanotube (MWCNT) modified SPE (SPE/MWCNT) offers a simple and stable biosensor design. Bismuth film electrode (BiFE) was developed as an alternative electrode material to mercury film electrode.[43] BiFE was easily formed by accumulation of Bi^{3+} ions on proper electrode surface by applying suitable potential at significant period of time. The novelty of the

immobilization procedure relays on the electrodeposition of tissue onto SPE surface with the aid of Bi^{3+} precursor thaIntt interacts with the tissue and got reduced onto the transducer surface. This represents an *in situ* Bi and tissue deposition/entrapment without using any other matrix like gelatin or binder glutaraldehyde.

Effects of Bi amount, deposition time and deposition potential have profound effect on accumulation of Bi^{3+}onto electrode surface. For this reason, these parameters were optimized for 50 mM phenol on plain SPE in the presence of proper amount of Bi^{3+} with 10 mL tissue, at a working potential was -0.8 V (see more details at annexes).

The Bi^{3+}-tissue interaction was studied by using UV-spectroscopy and evaluating the surface morphology by performing SEM studies. Spectroscopic methods revealed the creation of a complex only when bismuth was present, while SEM images shown a more complex structure of the Bi film in case of tissue presence (Figure 6).

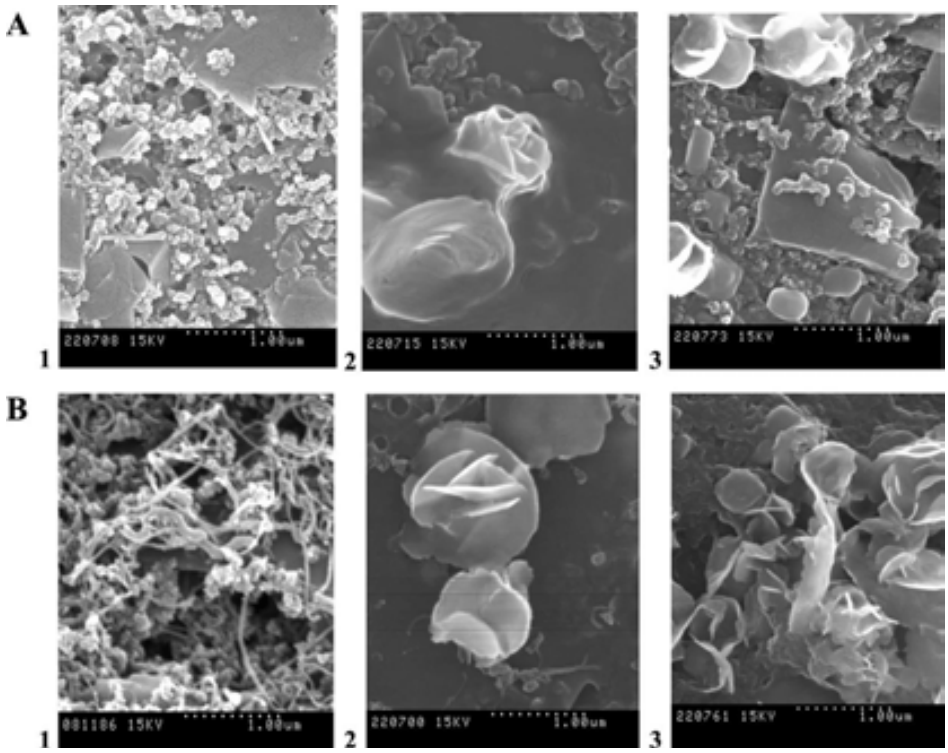

Figure 6. SEM images of plain-SPE (1A), BiFE on SPE (2A), SPE/Bi/Tissue (3A) and SEM images of MWCNT modified SPE (1B), BiFE on MWCNT/SPE (2B), SPE/MWCNT/Bi/Tissue (3B). Resolution of 1 μm, magnification of 30 k x and accelerating potential of 15 kV have been used.

3.2.2. Electrochemical measurements

Tyrosinase has hydroxylase activity, by which phenol can be hydroxylated to catechol using molecular oxygen, and then oxidase activity that can catalyze the oxidation of

catechol to o-quinone. At moderately negative potential the o-quinone product of phenol oxidation may be reduced electrochemically to catechol. Oxidation by the enzyme followed by reduction at the electrode may result in cycling between the catechol and o-quinone and yields a catalytically amplified current[16] (Figure 7A). Therefore, what is occurring at the electrode surface is the reduction of o-quinone to catechol (the working electrode acting as a cathode).

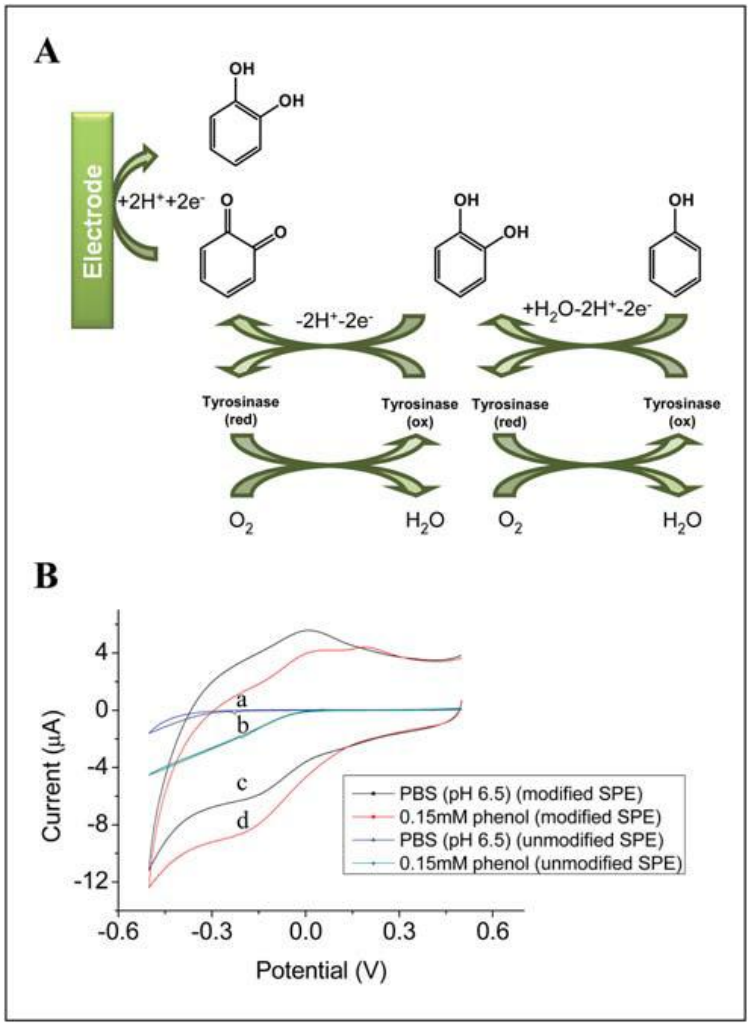

Figure 7. Schematic diagram displaying the electrode reactions involved in the detection of phenol at the SPE surface using the tyrosinase enzyme (A). Cyclic voltammograms recorded for unmodified and modified SPE in 0.1 M PBS (pH 6.5) (B). Without (a), and with (b) 0.15 mM phenol addition with the SPE/Tyr biosensor; without (c) and with (d) 0.15mM phenol addition with the SPE/MWCNT/Tyr. Conditions used in the cyclic voltammograms: starting potential of 0.5 V; scan rate of 0.05 V/s and switching potential of !0.5 V. Reproducibility of peak potential, 11%; reproducibility of peak current, 39%.

Regarding MWCNT/Tyrosinase matrix, where tyrosinase was immobilized by physical adsorption, in order to understand the phenol detection mechanism using the developed MWCNT/Tyrosinase matrix cyclic voltammetry studies have been performed. The developed matrixes (SPE/Tyr and SPE/MWCNT/Tyr) are studied in

the absence and presence of phenol substrate. While in the absence of phenol the SPE/Tyr did not give any significant response (Figures 7B, curve a) in the presence of phenol (Fig. 7B, curve b) a narrow shape CV characterized by a reduction peak without reaching a plateau has been observed. SPE/MWCNT/Tyr displays a CV (Figure 7B, curve c) with a broad shape and a peak at less negative potential (at -150 mV) in comparison to SPE/Tyr. In the presence of 0.15 mM of phenol an increase of the anodic current for SPE/MWCNT/Tyr (Figures 7B, curve d) can be observed. Additionally, working potential as well as enzyme loading have been studied, determining as the optimum value -0.2 V for SPE/MWCNT/Tyr and a Tyrosinase concentration of 1mg/50µl (see more details at annexes).

This matrix is especially interesting for low phenol concentration detection, due to the high stability of the signal and the rapid response of the biosensor at the working range. Moreover, phenol concentrations over 2.5 and 25 µM are of special interest in the field of environmental analysis. The analytical parameters related to our electrode formulation were a detection limit of 1.35 µM and a sensitivity of 47.4 $\mu A \cdot mM^{-1}$ within a linear response range of 2.5 to 75 µM phenol (Figure 8). The limit of quantification, calculated as 10 times the concentration corresponding to noise level current, was found to be 4.51 mM; standard deviation of slope, 0.005 µM/µA; standard deviation of intercept, 0.008 µA. A shelf lifetime study was also performed and showed very promising results, with a shelf lifetime of 68 days while being stored in the refrigerator.

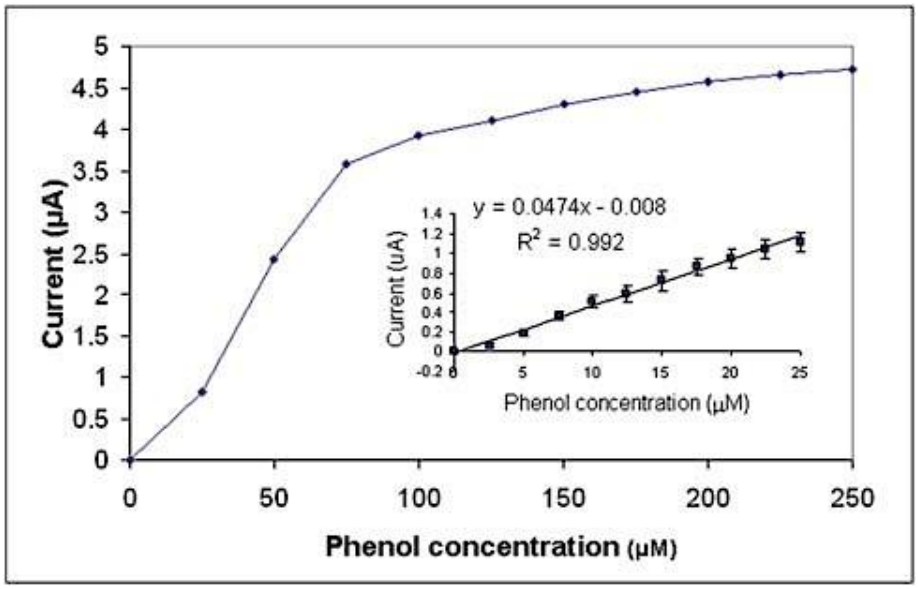

Figure 8. Calibration plot corresponding to successive additions of 5 ml of a 2.5 x 10^{-5} M phenol solution into a 20 ml 0.1 M PBS (pH 6.5) during stirring conditions with a Tyr/MWCNT/SPE

biosensor with tyrosinase concentration of 1 mg tyrosinase/50ml buffer. Inset: Calibration plot under the same conditions at the 2.5 to 25 mM range is shown.

In the third immobilization approach, where mushroom tissue is immobilized *via* Bi film onto SPE for phenol detection, considering electrocatalytic contribution of MWCNT, optimum potential study was investigated by using SPE/MWCNT/Bi/ Tissue. As a result, 800 mV shown the highest current value was obtained, like in the case of SPE/Bi/Tissue. Alhtough such working potential is expected to strip off the Bi-film from the electrode surface at this potential, UV spectroscopy studies demonstrated that the creation of a complex between Bi-film and mushroom tissue should have been formed. However, the presence of phenol during measurements resulted with more complex interactions, which require the application of a cleaning process between two measurements in order to decrease the background current. The effect of pH on the electrode response, as well as the effect of tissue amount, were studied, choosing an optimum pH 4.5 (Bi stays in its cationic form at acidic pH, enhancing the probability of being linked to negatively charged enzymes) and 5µl of tissue amount to obtain the highest response towards phenol detection.

Under optimum working conditions, SPE/Bi/Tissue system was compared with SPE/MWCNT/Bi/Tissue biosensor in terms of analytical characteristics. Introducing MWCNT into electrode structure provides wider linear range with better RSD value. This is probably related to the diffusion process of the electroactive specie undergoing oxidation onto the SPE electrode. On the other hand, plain SPE provides slightly better limit of detection (LOD) and limit of quantification (LOQ) values compared to MWCNT/SPE. Developed systems were also applied for phenol detection in synthetically prepared wastewater sample as described in experimental part. As a result, recoveries of 95.20% (SPE/Bi/Tissue) and 95.60% (SPE/MWCNT/Bi/Tissue) were obtained with the electrodes.

3.2.1.3. Integration in a flow system

A stable and sensitive biosensor for phenol detection based on a screen-printed electrode modified with tyrosinase, multiwall carbon nanotubes and glutaraldehyde (following the second enzyme immobilization approach already described in section 3.2.1.) is applied in a flow injection analytical (FIA) system.

An FIA setup (Figure 9) that uses a home-made flow-through cell of 20 μl was built and housed the SPE/MWCNT/Tyr/Glu biosensor, ensuring a stable operational analysis. In a typical measurement a 0.1 M buffer solution of pH 6.5 was introduced for 5 min at a flow rate of 3 ml min−1 by using a peristaltic pump (Perimax16/3). Volumes of phenol standard solutions from 0.5 to 25 μl were injected by using an automatic injector (Hamilton 36781). The injected phenol is passed through the electrochemical flow-through cell with the integrated SPE/MWCNT/Tyr/Glu biosensor. The measurements were performed under a flow-through regime by applying a working potential of −100 mV.

Figure 9. FIA setup based on home-made flow-through cell, peristaltic pump (Perimax16/3) and a model Ch-Instrument potentiostat 660A electrochemical workstation from CH Instruments Inc., Austin, TX.

Several parameters such as the working potential, pH of the measuring solution, biosensor response time, detection limit, linear range of response and sensitivity are studied. Parameters such as working potential, pH of the measuring solution, flow rate and injection time were analysed so as to find the optimum working conditions. The effect of applied potential on the phenol response of the biosensor was studied by the amperometric technique in the range of 0 to −500 mV. The highest signal-to-noise ratio was recorded applying a working potential of −100 mV, and therefore this potential was used for the further optimizations and studies.

The enzymatic activity is greatly influenced by the medium pH; therefore, the sensor response was investigated using pH ranging from 4.6 to 8.8. Figure 10 shows the FIA responses of the biosensor for different pH values. The biosensor response increased from pH 4.6 up to 6.5. A gradually decreased response was observed at pH values

above 6.5, which can be associated with a lower tyrosinase activity. The pH value of 6.5 was selected as optimal and used in all the following measurements.

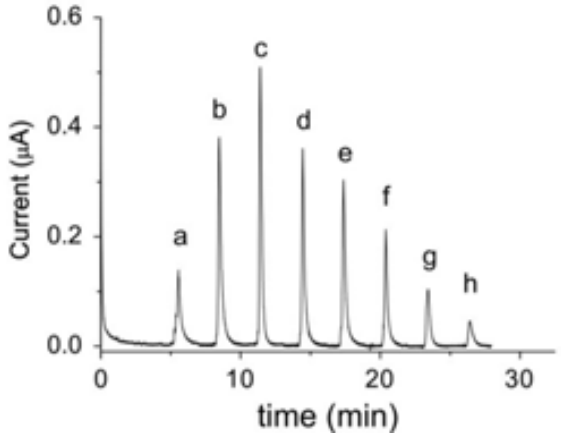

Figure 10. Amperometric responses of the SPE/MWCNT/Tyr/Glu biosensor at different pH values: (a) 4.67; (b) 5.99; (c) 6.50; (d) 7.16; (e) 7.53; (f) 8.18; (g) 8.52; (h) 8.82. Each peak corresponds to the injection of 20 **μ**l of 10 **μ**M of phenol solution at phosphate buffer 0.01 M, pH 6.5 at 25 ◦C; an operating potential of −100 mV versus Ag/AgCl was used. Other experimental conditions were as described in the text.

Parameters related to the FIA system were also optimized. The effect of injection time from 2 to 30 s on the amperometric response of the biosensor towards phenol was studied. A stable and reproducible response at 10 s injection time was obtained. For shorter injection times (t <10 s) the analytical response was not reproducible. A current decrease related to the short exposure time of the enzyme to the phenol substrate was observed. For longer injection times (10 s < t < 60 s) a saturation of the signal was observed. The heights of the peaks for retention times longer than 60 s remained almost constant but broadened, and therefore not adequate in terms of the time of analysis.

The study of the flow rate effect determined that the response time of the biosensor decreases at flow rates lower than 2 ml min−1. At higher rates the response time and the peak current increase. This is probably related to a more efficient diffusion process occurring under these conditions. This behaviour can be associated with chemical kinetics of the enzyme due to the fact that the response is better controlled by the enzymatic reaction at smaller volumes.[44] A flow rate of 3 ml min^{-1} was chosen as the best to get a fast, stable and repeatable response.

Electrochemical quantification of phenol using the FIA system was studied. The biosensor exhibited good response as a function of phenol concentration. The plot of

the cathodic current versus phenol concentration (Figure 11) in the range of 0.05–1 μM phenol shows a correlation coefficient of 0.99. The biosensor exhibits a sensitivity of 52.5 nA μM−1 and a detection limit of 0.14 μM phenol. The obtained detection limit is almost 500 times lower than the allowed levels of phenols in water as given by the EPA. The biosensor keeps its activity during continuous FIA measurements at room temperature, showing a stable response (RSD 5%) within a two weeks working period at room temperature. The stability of this biosensor during this working period is related to the good entrapment of the enzyme within the MWCNT/Glu matrix and also probably to the fact that MWCNT and Glu are able to minimize surface fouling of the biosensor surface.

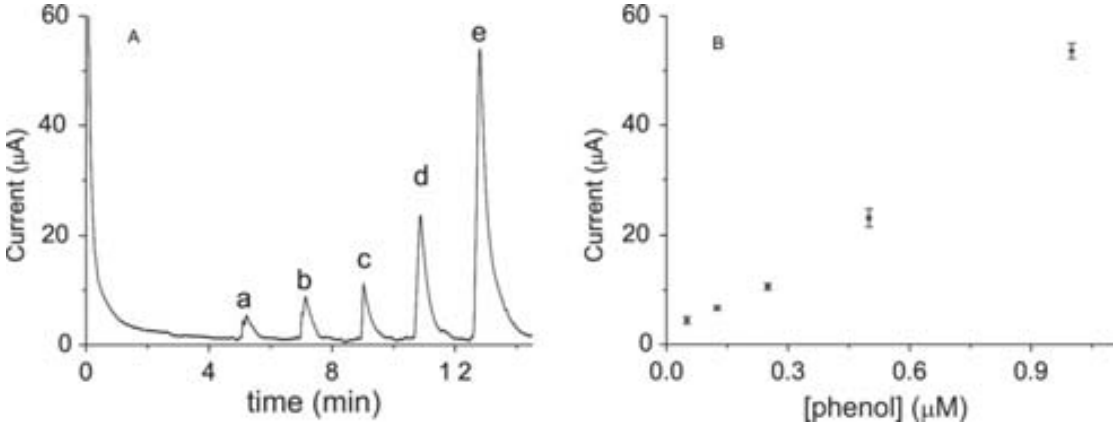

Figure 11. (A) FIA peaks obtained by chronoamperometric detection of phenol with concentrations of (a) 0.05, (b) 0.125, (c) 0.25, (d) 0.5, (e) 1 and (f) 1.25 μM. (B) Corresponding calibration curve of the current response versus phenol concentration. The error bars indicate the standard error for triplicate measurements. Conditions: temperature, 25 ◦C; operating potential, −100 mV versus Ag/AgCl reference; 0.01 M PBS solution at pH 6.5 is used as buffer. SPE/MWCNT/Tyr/Glu biosensor is used as detector.

The developed biosensor was also applied for phenol detection in seawater samples (see more details at annexes) and seems to be a promising alternative for automatic control of seawater contamination, being of interest for several other applications.

3.3. Nonenzymatic screen-printed electrode platforms for glucose detection

Although the most of the known amperometric glucose biosensors are based on glucose oxidase (GOx) or glucose dehydrogenase (GDH) immobilization,[45,46] in some applications it is necessary to have sensors which are stable when they are exposed to high temperatures or other aggressive environments.[47] Most of these nonenzymatic electrochemical glucose sensors rely on measuring the current response during the

direct glucose oxidation on the electrode surface. The use of noble metals such as Pt and Au to develop nonenzymatic sensors has been reported.[45] However, in the presence of glucose these electrodes quickly lose their activity due to accumulation of chemisorbed intermediates, which block the electrocatalytic surface.[45]

On the other hand the chronoimpedance technique (CIT) for real-time determination of glucose concentration in first and second generation glucose oxidase/carbon paste electrodes has been implemented. This technique allows continuous and rapid time response measurements and is only limited by the transient response of the biosensor. This new method is supposed to be applicable to any other biosensor system.[48,49] It has been reported that the nanostructured electrodes possess a very large surface to area activation ratio, favoring kinetically controlled reactions like electrocatalytic oxidation of glucose more than diffusion controlled reactions expecting a high sensitivity toward glucose detection.[50] For this reason we propose the combination of both materials and consequently the use of a bimetallic platinum/gold nanowire (Au–Pt NW) as a free-enzyme electrocatalyst for glucose detection. This is achieved through Au–Pt NW integration on the working electrode of a screen printed electrode (SPE) followed by CIT measurements performed for the first time in an integrated and miniaturized three electrode system. The use of an iridium oxide (IrOx) thin layer electrodeposited onto the working electrode surface was necessary to reduce the electrode–electrolyte interface impedance (EEIZ) for CIT measurements, as previously described.[51] Au–Pt NWs were immobilized onto the SPE working electrode surface by using the iridium oxide (IrOx) thin layer and the cross-linking agent glutaraldehyde.

Morphological and structural studies of bimetallic nanowires were performed by a Transmission Electron Microscope (TEM). Highly regular and uniform average diameter Au–Pt NWs of about 140 nm (Figure 12) can be observed. X-Ray microanalysis of nanowires was performed by TEM, showing an Au and Pt alloy at different proportions along the nanowire. Compositions in terms of Pt and Au percentages at different sections of the Au–Pt NW are given in the inset table of Fig. 12(A). A homogeneous distribution of the nanowires on the electrode surface can be observed by a Scanning Electron Microscopy (SEM) image (Figure 12B). Figure 12C

shows the effect of glutaraldehyde as a binding matrix, showing a good entrapment of the wires within the mentioned matrix.

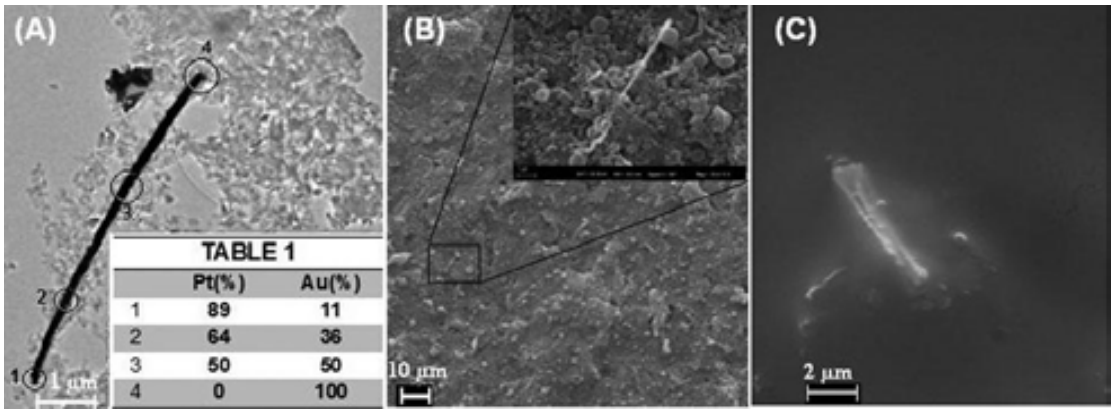

Figure 12. TEM image of a single (Au/Pt)NW(A). SEM micrographs of modified SPE with a (Au/Pt)NW (B). Effect of glutaraldehyde as a binding matrix for NW entrapment (C).

The electrocatalytic effect of Au–Pt NWs toward glucose detection was evaluated, were a current decrease was observed by increasing glucose concentration, indicating that Au–Pt NWs are exhibiting electrocatalytic activity toward glucose presence. glucose concentrations the catalytic effect of NWs in the range from 0 to 0.1 V.

In an electrode–electrolyte interface (EEI) the electric current flows due to the charge transfer occurring during the electrochemical reactions that take place between the electrode surface and the electrolyte. In our specific case, the electrochemical reaction on the SPE/IrOx/Au–Pt NW sensor surface can be described considering the different metallic surfaces present along the alloy (Figure 13). The mentioned mechanism based on the glucose oxidation on the gold surface and hydrogen peroxide (H_2O_2) reduction on the platinum surface is the reason why this sensor presents such a high sensitivity and a low linear range for glucose detection. It is well known that Au nanoclusters can behave as GOx mimicking units able to catalytically oxidize glucose and produce gluconates and H_2O_2.[52,53]

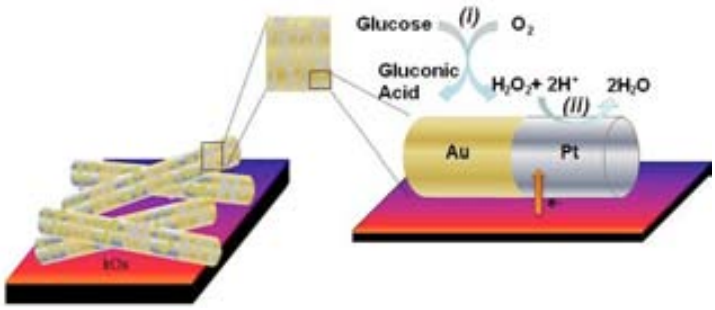

Figure 13. Proposed mechanism for the glucose electrocatalytic detection using a Au–Pt NW. (i)

Glucose is transported by convection to the gold surface, where it is oxidized to glucuronic acid by reducing O2 to H2O2, (ii) H2O2 decomposes into H2O on the platinum surface.

This process, catalysed by AuNPs, is similar to the one performed using the natural enzyme glucose oxidase, which also catalyzes the oxidation of glucose with the co-substrate oxygen (O_2). The recent implementation of an Au NW modified sensor for nonenzymatic glucose detection also has confirmed that nanostructured gold is able to act by mimicking the GOx activity.[54] On the other hand, Pt is a widely used electrode material for H_2O_2 detection and biosensor fabrication. Most of the platinum based biosensors detect H_2O_2 at relatively high potential (around 0.6 V). However, Pt NWs and Pt nanoparticles (NPs) were recently reported for H_2O_2 detection at 0 mV.[55,56] The use of a bimetallic gold–platinum nanowire as a free-enzyme electrocatalyst for glucose detection is a very interesting application due to the non-competitive mechanism taking place on the electroactive surface.

For a better elucidation of the glucose detection mechanism further impedance measurements were carried out. Measurements were performed under different experimental conditions (see more details at annexes), elucidating that SPE/IrOx/Au NW and SPE/IrOx sensors don't show any response toward either H_2O_2 or glucose. Results are consistent with the sensors composition, as in the first configuration platinum is not present to reduce H_2O_2 (product of glucose oxidation on the Au surface) and in the second configuration H_2O_2 is not catalyzed by iridium oxide at this potential value.[57,58]

The SPE/IrOx/Au–Pt NW sensor is the only one that exhibits response to glucose addition, showing an impedance change of around 150 Ω (Fig. 3A). This sensor can detect glucose because both metals (Pt and Au) are present and both reactions can be coupled, the oxidation of glucose to gluconic acid (Au surface) and reduction of hydrogen peroxide (Pt surface). Real-time determination of impedance changes (|Z|) in 50 mM NaOH solution during successive addition of glucose 20 mM was carried out by using a composed signal of 100 mV DC plus a 50 mV ac of 0.4 Hz (Figure 14). Impedance response shows a linear range up to 140 mm with 8557 Ω mM^{-1} of sensitivity, and 0.99 of correlation coefficient (inset of Figure 14). In order to compare the repeatability of 3 sensors, the normalized impedance (relative value to zero concentration of glucose) is evaluated. The results of triplicate sets, indicated by

error bars, show the repeatability and reproducibility corresponding to the measurements with a relative standard deviation (RSD) less than 5% for a glucose concentration range of 20–140 mM.

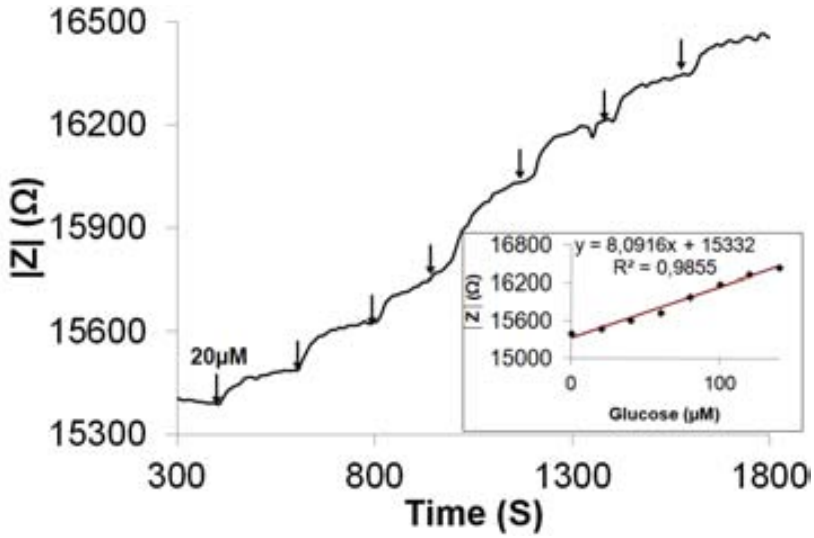

Figure 14. (A) Real-time impedancimetric response of the SPE/IrOx/ Au–PtNWsensor. (B) Sensor calibration given as impedance magnitude versus glucose concentration in the 0–140 mM range.

Selectivity is a very important parameter to be considered for nonenzymatic glucose sensors. To evaluate the selectivity of the sensor, impedancimetric response toward uric acid (UA) and ascorbic acid (AA) was measured. These interference species are normally present in real physiological samples and are usually examined in the presence of glucose. It must be considered that the concentration of glucose studied is at least 30 times lower than the one in human blood,[59] and in addition for this experiment the glucose concentration is 20 times higher than the concentration of interference species. Citric acid (CA) is also evaluated due to its presence as a preservative in soft drinks and other foods. Good selectivity of the SPE/IrOx/Au–PtNW sensor is shown toward glucose oxidation, because interference species (such as UA, AA and CA) can be neglected (see more details at annexes).

The low detection range obtained by this glucose sensor, in addition to its high repeatability and sensitivity, may allow applications to non-invasive detection of glucose in other biological fluids (saliva, sweat and urine) where glucose, where it is present at very low concentrations. Moreover, the results obtained show that the use of the CIT as a novel transduction platform coupled with bimetallic nanowires can bring advantages in the design of nonenzymatic sensors achieving improved

analytical performance besides the robustness and stability of the biosensing system with interest for applications in various fields.

3.4. Other approaches

Advanced functional materials have been constructed based on the combination of appropriate building blocks such as inorganic compounds, [60,61] biopolymers, [62] semiconductor quantum dots,[63] metallic nanoparticles,[64,65] and carbon nanotubes.[66,67] For this purpose, layer-by-layer (LbL) and self-assembled[68,69] structures provide an excellent approach, since several hybrid supramolecular nanodevices can be built combining suitable oppositely charged components.[68,69] In the LbL method, the self-assembly process is governed by individual immobilization of positively and negatively charged polyelectrolytes, which allow for design and control of the thickness and structural morphology aspects. In the context of nanoscience, constitutional dynamic chemistry (CDC) concepts[70] confer the means to interpret and control functional supramolecular entities, since dynamic character such as functional recognition and self-organization must be directly involved on the molecular level.[71]

Control of molecular and supramolecular properties is used to obtain a new advanced hybrid material based on Prussian blue nanoparticles (PB NPs). This hybrid material is obtained through a self-assembled Layer-by-Layer (LbL) approach combining the advantageous features of β-cyclodextrin (β-CD) polysaccharides, PB NPs and poly(allylamine hydrochloride) from electrostatic interaction between the deposited layers. The presence of cyclodextrin molecules confers a unique structural characteristic to the material, while Prussian blue (PB) iron(II) hexacyanoferrate(III) is defined as a mixed valence coordination compound [72,73] exhibiting unique electronic, electrochemical and structural features with a wide range of applications including molecular magnets, [74] sensors, [75,76] semiconductors, [77] electrochromic devices,[72,74] and biosensors.[78]

In order to obtain supramolecular structures with interest for both host–guest model and DNA probe applications,[79] PB nanoparticles protected by β -CD, designed as PB-CD NPs, have been reported that could improve the charge transfer inside the β -CD cavity producing an attractive nanocomposite.[80] To the best of our knowledge this is the first example of PB nanoparticles using β-CD polymer as a stabilizer, which opens

the way to develop new supramolecular devices with interest for sensing and biosensing applications.

A novel assembled nanoplatform is designed, which takes advantage of alternate layer depositions from PB-CD NPs with polyallylamine (PAH). It is obtained on a tin oxide substrate by using the LbL technique, which is able to control the nano/micro supramolecular structure and in this way tune its conductivity. Multilayer characterization and formation of compact microcube structures at the molecular level have been evidenced by optical and electrochemical experiments.

The characterization of the hybrid material by transmission electronic microscopy images suggested that PB NPs were protected by β-CD polysaccharides that prevent the aggregation phenomena. In addition, as confirmed by scanning electronic microscopy images, it was found that PB NPs are organized in microcubic supramolecular like structures via a mesoscale self-assembly process (Figure 15). Interestingly, the 3-bilayer {PAH/PB-CD} film exhibited a higher density of microcubic structures and a high electrochemical response with PB sites available for redox reactions at a supramolecular level.

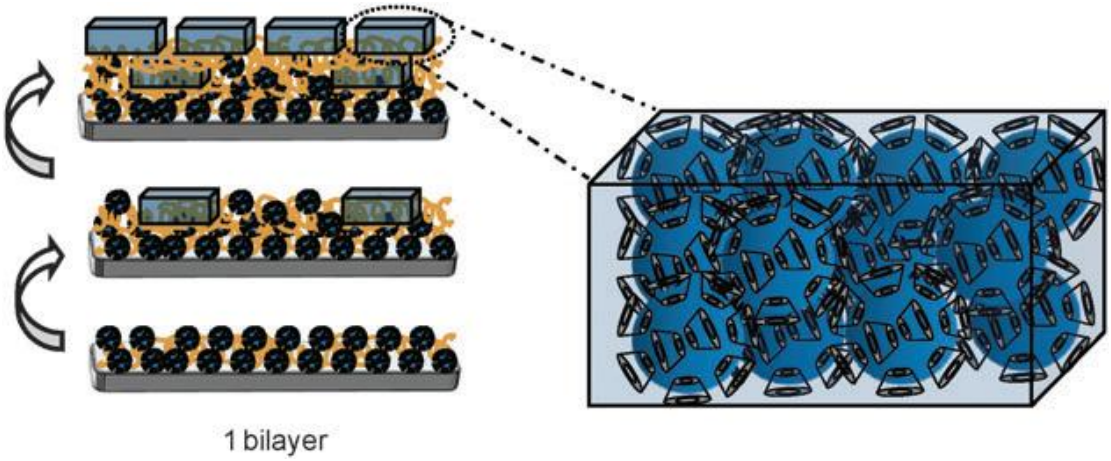

Figure 15. Self-assembly for 1, 2 and 3-bilayers based on interaction between Prussian blue nanoparticles protected by β-cyclodextrin (blue) and PAH polymer (orange). Detail: Microcubic structure.

The layer-by-layer assembly onto ITO electrodes from PAH and PB-CD NPs was performed (up to 4 bilayers) and monitored by cyclic voltammetry (after each deposition step) over a potential range of -0.3 to 1.1 V *vs.* Ag/AgCl in 0.2 mol L^{-1} of potassium chloride (KCl). As illustrated in Figure 16, typical j–E electrochemical responses were obtained for $\{PAH/PB\text{-}CD\}_n$ systems showing two well-defined

redox couples at 125 ($E_{(1/2)1}$) and 800 mV ($E_{(1/2)2}$) attributed to the conversion of Prussian white (PW) to Prussian blue (PB) and Prussian blue (PB) to Berlin green (BG), respectively, which are similar to those of PB species immobilized in LbL films reported previously.[78,81,82] Moreover, the cathodic and anodic peak currents increased with the number of bilayers. This last behavior indicates that PB nanoparticles are electrically connected within multilayers (see more details at annexes).

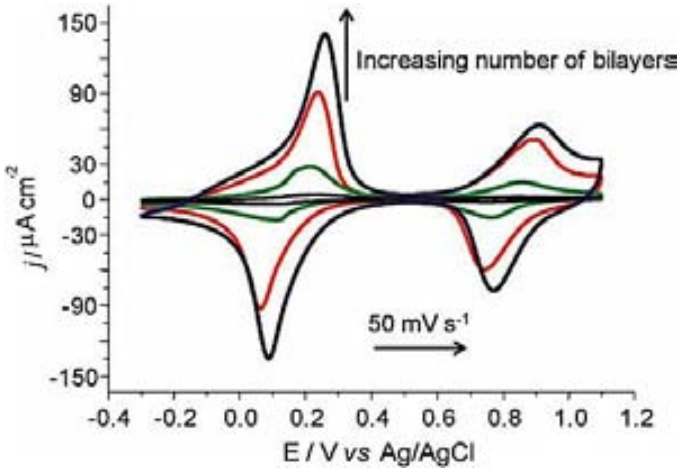

Figure 16. Cyclic voltammograms for self-assembly {PAH/PB-CD} multilayers onto ITO electrode containing 1, 2, 3, and 4 bilayers. Scan rate: 50 mV s^{-1}. Electrolyte: KCl, 0.2 mol L^{-1}, T = 25 ºC.

The developed platform is expected to have interesting applications in the sensing and biosensing fields, where highly conductive and tunable 'on-demand' platforms combined with biorecognition reactions are desirable. Additionaly, by utilizing fewer bilayers and consequently less material deposition, the formed {PAH/PB-CD} multilayer films of a tuneable conductivity can be expected to have interesting future applications for host–guest like dependent electrochemical biosensing designs.

3.5. Conclusions and future perspectives

Screen-printed electrodes modified with carbon-nanotubes have been characterized in depth, evaluating their structural characteristics and other parameters that play a key role on the further functionalization of the electrode surface and its analytical performance while being used in analytes monitoring. The developed device has shown several advantages in terms of cost, simplicity, analytical performances, being used in phenol detection.

Regarding phenol detection, several immobilization approaches for tyrosinase immobilization, starting by the physical adsorption of the enzyme have been successfully obtained and applied. The results obtained by CLSM studies particularly were remarkable. These results were not limited to the 3D visualization of the matrix, but also provided a statistical study to evaluate material roughness and its effect on enzyme distribution through the entire working electrode surface. Enzyme distribution and aggregation effects are considered to be of crucial importance for the electrochemical process, which has been demonstrated in the case of phenol detection.

Second immobilization approach, where a novel MWCNT/SPE biosensor that uses glutaraldehyde as the immobilization matrix of Tyrosinase (Tyr) is designed and applied for phenol analysis in a Flow Injection Analysis (FIA) system, have shown excellent results towards phenol detection (below EPA criteria), in addition to a long term stability of the biosensor. The developed biosensor exhibited relatively fast response time (15 s) and good performance in terms of sensitivity and detection limit when the Tyr enzyme is entrapped within the MWCNT/glutaraldehyde matrix. The proposed immobilization matrix is easy to be prepared and cheaper than other materials like nanorods,[83] nanoparticles, fibres[84] and polymers.[85] The developed SPE/MWCNT/Tyr/Glu biosensor seems to be an interesting alternative for phenol detection in water including its integration into automatic control systems for pollution control in water samples.

As a third enzyme immobilization approach, enzyme source mushroom tissue was electrochemically immobilized onto SPE or SPE/MWCNT/ surface with the aid of Bi film. This immobilization and complex formation of Bi^{3+}-ions with tissue were demonstrated with UV spectroscopy and SEM measurements. Then developed biosensor's working conditions were optimized and obtained system was subjected to phenol detection in synthetically prepared wastewater sample. Avoiding the usage of matrices like gelatin might be helpful to overcome diffusion problems caused by these membranes. On the other hand, stability of tissue was provided by means of Bi film that was formed during the accumulation procedure suggesting the usage of more specific enzyme like tyrosinase or laccase, which might provide more sensitive results for this system.

The designed nonenzymatic platforms, where Au–Pt NWs were immobilized onto the SPE working electrode surface by using the IrOx thin layer and the cross-linking agent glutaraldehyde, have been successfully implemented as a glucose sensor. The low detection range obtained by this glucose sensor, in addition to its high repeatability and sensitivity, may allow applications to non-invasive detection of glucose in other biological fluids (saliva, sweat and urine) where glucose is present at very low concentrations. Moreover, the results obtained show that the use of the CIT as a novel transduction platform coupled with bimetallic nanowires can bring advantages in the design of nonenzymatic sensors achieving improved analytical performance besides the robustness and stability of the biosensing system with interest for applications in various fields.

Apart from the modified MWCNT screen printed electrodes, where different biological entities were immobilized to achieve higher sensitivity and selectivity, and the SPE nonenzymatic platform, an alternative analytical platform that combines the advantageous features of β-CD polysaccharide, Prussian blue nanoparticles and the layer-by-layer process, have been prepared and characterized. It is envisaged that unique features arising from the nanostructured PAH/PB-CD LbL films and overall tuning of the conductivity upon LbL control may be exploited in several sensing and biosensing designs. The study of further applications of these materials in immunosensing systems is still in progress at our laboratories.

3.6. References

[1] Fanjul-Bolado, P.; Hernández-Santos, D.; Lamas-Ardisana, P. J. *Electrochim. Acta* **2008**, *53*, 3635.

[2] Luo, H.; Shi, Z.; Nangiang, L.; Zhennan, G.; Zhuang, Q. *Anal. Chem.* **2001**, *73*, 915.

[3] Yogeswaran, U.; Chen, S. M. *Anal. Lett.* **2008**, *41*, 210.

[4] Tasis, D.; Tagmatarchis, N.; Georgakilas, V.; Prato, M. *Chem.–Eur. J.* **2003**, *9*, 4001.

[5] Chen, J.; Hamon, M. A.; Hu, H.; Chen, Y.; Rao, A. M.; Eklund, P. C.; Haddon, R. C. *Science* **1998**, *282*, 95.

[6] Gong, K.; Yan, Y.; Zhang, M.; Su, L; Xiong, S.; Mao, L. *Anal. Sci.* **2005**, *21*, 1383.

[7] Kam, N. W. S.; Jessop, T. C.; Wender, P. A.; Dai, H.; *J. Am. Chem. Soc.* **2004**, *126*, 6850.

[8] Alarcón-Angeles, G.; Pérez-López, B.; Palomar-Pardave, M.; Ram**!**ırez-Silva, M. T. *Carbon* **2008**, *46*, 898.

[9] Pérez, B.; Pumera, M.; Valle, M.; Merkoçi, A.; Alegret, S. *J. Nanosci. Nanotechnol.* **2005**, *5*, 1694.

[10] ISO 4287. Geometrical product specifications (GPS)-surface texture: profile method-terms, definitions and surface texture parameters, International Organization for Standardization, Switzerland, 1997.

[11] Manahan, S. E. Environmental Chemistry; Lewis Publishers, Chelsea, MI, 1991.

[12] Janda, V.; Krijt, K.; *J. Chromatogr. A* **1984**, *283*, 309.

[13] Byfield, M. P.; Abuknestra, R. A. *Biosens. Bioelectron.* **1994**, *9*, 373.

[14] Rogers, K. R.; Becker, J. Y.; Cembrano, J. *Electrochim. Acta* **2000**, *45*, 4373–4379.

[15] Pérez, B.; Merkoçi, A. *Analyst* **2009**, *134*, 60.

[16] Serra, B.; Mateo, E.; Pedrero, M.; Reviejo, A. J.; Pingarrón, J. M. *Analusis* **1999**, *27*, 592.

[17] Rajesh, W. ; Kaneto, K. *React. Funct. Polym.* **2004**, *59*, 163.

[18] Kochana, J.; Gala, A.; Parczewski, A.; Adamski, J. *Anal. Bioanal. Chem.* **2008**, *391*, 1275.

[19] Serra, B.; Jiménez, S.; Mena, M. L.; Reviejo, A. J.; Pingarrón, J. M. *Biosens. Bioelectron.* **2002**, 17, 217.

[20] Carralero, V.; Mena, M. L.; Gonzalez-Cort**!**es, A.; Yáñez-Sedeño, P.; Pingarrón, J.

M. *Biosens. Bioelectron*. **2006**, *22*, 730.

[21] Shan, D.; Mousty, C.; Cosnier, S.; Mu, S. *Electroanalysis* **2003**, *15*, 1506.

[22] Zhang, T.; Tian, B.; Kong, J.; Yang, P.; Liu, B. *Anal. Chim. Acta* **2003**, *489*, 199.

[23] Solná, R.; Skládal, P. *Electroanalysis* **2005**, *17*, 2137.

[24] Montereali, M. R.; Vastarella, W.; Seta, L.; Pilloton, R. *Int. J. Environ. Anal. Chem.* **2005**, *85*, 795.

[25] Fanjul-Bolado, P.; Hernández-Santos, D.; Lamas-Ardisana, P. J. *Electrochim. Acta* **2008**, *53*, 3635.

[26] Poerschmann, J.; Zhang, A.; Kopinke, F. D.; Pawliszyn, T. *Anal. Chem.* **1997**, *69*, 597.

[27] Li, J.; Jiang, Z.; Wu, H.; Zhang, L.; Long, L.; Jiang, Y. *Soft Matter* **2010**, *6*, 542.

[28] Wang, S. C.; Yang, F.; Silva, M.; Zarow, A.; Wang, Y.; Iqbal, Z. *Electrochem. Commun.* **2009**, *11*, 34.

[29] Li, X.; Zhou, H.; Yu, P.; Su, L.; Ohsaka, T.; Mao, L. *Electrochem. Commun.* **2008**, *10*, 851.

[30] Kostarelos, K.; Bianco, A.; Prato, M. *Nat. Nanotechnol.* **2009**, *4*, 627-

[31] Liu, Z.; Fan, A. C.; Rakhra, K.; Sherlock, S.; Goodwin, A.; Chen, X.; Yang, Q.; Felsher, D. W.; Dai, H. *Angew. Chem. Int. Ed.* **2009**, *48*, 7668.

[32] Yu, X.; Munge, B.; Patel, V.; Jensen, G.; Bhirde, A.; Gong, J. D.; Kim, S. N.; Gillespie, J.; Gutking, J. S.; Papadimitrakopoulos, F.; Rusling, J. F. *J. Am. Chem. Soc.* **2006**, *128*, 11199.

[33] Montereali, M. R.; Vastarella, W.; Seta, L.; Pilloton, R. *Int. J. Environ. Anal. Chem.* **2005**, *85*, 795–806.

[34] Sánchez, S.; Roldán, M.; Pérez, S.; Fabregas, E. *Anal. Chem.* **2008**, *80*, 6508.

[35] Degani, Y.; Heller, A. *J. Phys. Chem.* **1987**, *91*, 1285,

[36] Zhang, X.; Ju, H.; Wang, J. Electrochemical Sensors, Biosensors and Their Biomedical Applications, Elsevier, Amsterdam, 2007.

[37] Sun, Y. P.; Fu, L. F.; Lin, Y.; Huang, W. J. *Acc. Chem. Res.* **2002**, *35*, 1096.

[38] Meyyappan, M. Carbon Nanotubes: Science and Applications, CRC Press, Boca Raton, 2005.

[39] Liu, H.; Kao, W. W. Y. *Mol. Vis.* **2009**, *15*, 505.

[40] Jung, D.; Paradiso, M. *J. Mater. Sci.* **2009**, 4, 6747

[41] Drevon, G. F.; Danielmeier, K.; Federspiel, W.; Stolz, D. B.; Wicks, D. A.; Yu, P.

C.; Russell, A. J. *Biotechnol. Bioeng.* **2002**, *79*, 785.

[42] Umran, Y.; Memet, V. K. *J. Appl. Polym. Sci.* **2009,** *114*. 3716.

[43] Wang, J.; Lu, J.; Hočevar, S. B.; Farias, P. A. M.; Ogorevc, B. *Anal. Chem.* **2000**, *72*, 3218.

[44] Martinez, N. A.; Messina, G. A.; Bertolino, F. A.; Salinas, E.; Raba, J. *Sensors Actuators B* **2008,** *133*, 256.

[45] Meng, L.; Jin, J.; Yang, G.; Lu, T.; Zhang, H.; Cai, C. *Anal. Chem*. **2009**, *81*, 7271.

[46] Chiua, J.-Y.; Yua, C.-M.; Yena, M.-J.; Chena, L.-C.*Biosens. Bioelectron.* **2009**, *24*, 2015.

[47] Kang, X.; Mai, Z.; Zou, X.; Cai, P.; Mo, J. *Anal. Biochem.* **2007**, 363, 143.

[48] Mayorga-Martinez, C. C.; Treo, E. F.; Madrid, R. E.; Felice, C. F. *Biosens. Bioelectron.* **2010**, *26*, 1239.

[49] Mayorga-Martinez, C. C.; Treo, E. F.; Madrid, R. E.; Felice, C. F. *Biosens. Bioelectron.* **2011**, *29*, 200..

[50] Lee, Y.-J.; Park, J.-Y. *Sens. Actuators B* **2011**, *155*, 134.

[51] Mayorga Martinez, C. C.; Madrid, R. E; Felice, C. J. *Sens. Actuators B* **2008**, *133*, 682.

[52] Luo, W.; Zhu, C.; Su, S.; Li, D.; He, Y.; Huang, Q.; Fan, C. *ACS Nano* **2010**, *4*, 7451.

[53] Zheng, X.; Liu, Q.; Jing, C.; Li, Y.; Li, D.; Luo, W.; Wen, Y.; He, Y.; Huang, Q.; Long, Y.-T.; Fan, C. *Angew. Chem. Int. Ed.* **2011**, *50*, 1.

[54] Cherevko, S.; Chung, C.-H. *Sens. Actuators B* **2009**, *142*, 216.

[55] Yang, M.; Qua, F. I.; Lua, Y.; Heb, Y.; Shena, G.; Yua, R. *Biomaterials* **2006**, *27*, 5944.

[56] Guo, S.; Wen, D.; Zhai, Y.; Dong, S.; Wang, E. *ACS Nano* **2010**, ***4***, 3959.

[57] Irhayem, E. A.; Elzanowska, H.; Jhas, A. S.; Skrzyneck, B.; Birss, V. *J. Electroanal. Chem*. **2002**, *538*, 153.

[58] Jhasa, A. S.; Elzanowskab, H.; Sebastiana, B.; Birss, V. *Electrochim. Acta* **2010**, *55*, 7683.

[59] Jiang, L.-C.;. Zhang, W.-D. *Biosens. Bioelectron*. **2010**, *25*, 1402.

[60] Feldheim, D. L.; Eaton, E. *ACS Nano* **2009**, *3*, 2207.

[61] Chen, J.; Cheng, F. *Acc. Chem. Res.* **2009**, *42*, 713.

[62] Cathell, M. D.; Szewczyk, J. C.; Bui, F. A.; Weber, C. A.; Wolever, J. D.; Kang, J.;

Schauer C. L. *Biomacromolecules* **2008**, *9*, 289–295.

[63] Li, X.; Zhou, Y.; Zheng, Z.; Yue, X.; Dai, Z.; Liu, S.; Tang, Z. *Langmuir* **2009**, *25*, 6580.

[64] Chen, L. Y.; Zhang, L.; Fujita, T.; Chen, M. C. *J. Phys. Chem. C* **2009**, *113*, 14195.

[65] Muñiz, A. E.; Merkoçi, A. *Expert Opin. Med. Diagn.* **2010**, *4*, 21.

[66] Ren, L.; Xian, X.; Yan, K.; Fu, L.; Liu, L.; Chen, S.; Liu, Z. *Adv. Funct. Mater.* **2010**, *20*, 1209.

[67] Zhang, Y.; Hongkun, H.; Gao, C.; Wu, J. *Langmuir* **2009**, *25*, 5814.

[68] Crespilho, F. N.; Silva, W. C.; Zucolotto, V. in Catalysis and Photochemistry in Heterogeneous Media, Research Signpost, Kerala, India, 1st edn, 2007, ch. 3, pp. 59–73.

[69] Ariga, K.; Hill, J. P.; Ji, Q. *Phys. Chem. Chem. Phys.* **2007**, *9*, 2319.

[70] Lehn, J. M. *Chem. Soc. Rev.* **2007**, *36*, 151.

[71] Lehn, J. M. *Rep. Prog. Phys.* **2004**, *67*, 249.

[72] Schmidt, D. J.; Cebeci, F. C.; Kalcioglu, Z. I.; Wyman, S. G.; Ortiz, C.; Vliet, J. V. *ACS Nano* **2009**, *I*, 2207.

[73] Lundgren, C. A.; Murray, R. W. *Inorg. Chem.* **1988**, *27*, 933.

[74] Taguchi, M.; Yagi, I.; Nakagawa, M.; Iyoda, T.; Einaga, Y. *J. Am. Chem. Soc.* **2006**, *128*, 10978.

[75] Razmi, H.; Habibi, E. *Anal. Biochem.* **2009**, *392*, 126.

[76] Li, J.; Qiu, J. D.; Xu, J. J.; Chen, H. Y.; Xia, X. H. *Adv. Funct. Mater*. **2007**, *17*, 1574.

[77] Song, Y. Y.; Jia, W. Z.; Li, W. Z. Y.; Xia, X. H.; Wang, Q. J.; Zhao, J. W. *Adv. Funct. Mater.* **2007**, *17*, 2808.

[78] Zhao, W.; Xu, J. J.; Shi, C. G.; Chen, H. Y. *Langmuir* **2005**, *21*, 9630.

[79] Cederquist, K. B.; Golightly, R. S.; Keating, C. D. *Langmuir* **2008**, *24*, 9162.

[80] Kumar, S. S.; Joseph, J.; Phani, K. L. *Chem. Mater.* **2007**, *19*, 4722.

[81] Qiu, J. D.; Peng, H. Z.; Liang, R. P.; Li, J.; Xia, X. H. *Langmuir* **2007**, *23*, 2133.

[82] Laurent, D.; Schlenoff, J. B. *Langmuir* **1997**, *13*, 1552.

[83] Gu, B. X.; Xu, C. X.; Zhu, G. P.; Liu, S. Q.; Chen, L. Y.; Li, X. S. *J. Phys. Chem. B* **2009**, *113*, 377.

[84] Wang, Y.; Hasebe, Y. *J. Environ. Sci.* **2009**, *21*, S100.

[85] Lee, Y. J.; Lyu, Y. K.; Choi, H. N.; Lee, W. Y. *Electroanalysis* **2007**, *19* ,1048.

CHAPTER 4

LAB-ON-A-CHIP PLATFORMS

Related Publications

"In-chip magnetic and electrokinetic manipulations for bead based immunosensing applications" Adriano Ambrosi, Maria Guix and Arben Merkoçi. *Electrophoresis* **2010**, *32*, 1-9.

4.1. Introduction

The introduction of the concept of micro-total analysis systems, or mTAS,[1] started the development of multiple technologies for the realization of fluidic microsystems. This is due to the advantages deriving by the use of microfluidic chips when compared with the classical analytical systems: (i) the possibility of using small quantities of sample and reagents (down to picoliters), (ii) fast reaction times when molecular diffusion lengths are of the order of the microchannel dimension, and (iii) a large surface-to-volume ratio, offering an intrinsic compatibility between the use of a microfluidic system and surface-based assays.[2,3,4,5]

In heterogenous assays, reactions occur both in a solution and in a solid phase, offering the advantage of easy separation of chemical complexes from reactants. Bead based materials are ideal reagent delivery vehicles providing large reactive surface areas for chemical binding. They can be easily recovered from a dispersion, reversibly redispersed, and are omnipresent in biomedical applications.[6,7]

Biomolecule immobilization on a solid phase (i.e. microparticles or nanoparticles) evidently results in a small volume and localized assay.[8] With respect to open microchannels, microfluidic structures with packed beds of functionalized beads or containing bead suspensions, take profit from an even larger surface-to-volume ratio, with an enhanced interaction of reactive surfaces with passing fluids. This reduces diffusion times during the microfluidic procedures and also having a higher density of binding sites, and improves the detection sensitivity. In addition, such an assay allows for a rapid regeneration and exchange of the solid support when needed.[9]

Magnetic nanoparticles and microparticles offer an additional advantage: having embedded magnetic entities, they can be easily manipulated using permanent magnets or electromagnets, independently of normal microfluidic or biological processes.[10] This extra degree of freedom is the basis of a still improved exposure of the functionalized bead surface to the surrounding liquid and of higher sample preconcentration efficiencies, due to the increased relative motion of the bead with respect to the fluid.[11]

Paramagnetic beads have been extensively used as solid support for the preparation, separation, and detection of biomolecules such as DNA[12] and protein[13,14] mostly because of their efficiency, simplicity, mild operation conditions, and low cost.[15,16,17,18]

Several applications of magnetic particles with microfluidic systems have been demonstrated for DNA hybridization and recognition,[19,20,21] immunoassays[22,23,24] cell capture/detection,[25,26] and environmental[27,28] and food control.[29]

These studies describe the manufacturing and assembling of analytical tools for different applications where magnetic particles are precisely handled in either on-channel or off-channel formats by means of permanent magnets or built-in electromagnets. Optical detection (LIF, Chemiluminescence) represents the most adopted technology for the signal transduction with excellent results in terms of limit of detection and sensitivity. Extremely low detection limits have been achieved also by means of electrochemical (EC) detection.[27,29] Fluids and magnetic particle pumping inside the microchannels is mostly accomplished by physical systems such as syringe or peristaltic pumps. However, most successful microfluidic system devices consist of microchannel networks in which the solutions are pumped using applied electric fields.[30,31] The mechanism underlying this pumping principle is electro-osmosis, a bulk flow which originates at the surface of charged substrates such as glass, and requires no pumps, valves, or other moving parts.[32] An additional advantage of using electric fields is that species may also be separated electrophoretically as a function of their different charge-to-mass ratios.[30,32,33]

High-voltage power supply (HVPS) systems used to apply the electric field are built in much reduced dimensions, and therefore promoting miniaturization of the device for portable applications. EC detection is also ideally suited to miniaturized analytical systems and is an attractive alternative mode for microchip CE devices.[34,35,36] The sensitivity and selectivity of EC detection are comparable to those of LIF detection.

There are several advantages of EC detection over other detection modes, including the ability to miniaturize both the detector and the control instrumentation and the fact that many compounds can be detected without derivatization.[37]

4.2. Bead-based protein analysis

The combination of electrophoretic and magnetic manipulations with electrochemical detection for a versatile microfluidic and bead-based biosensing application permits the use of magnetic particles as solid support for bioassays with an end-channel EC detection. EC detection is used as extremely sensitive technique to quantify the electroactive enzyme product generated within the channel. Widely used enzyme-linked immunoassay (ELISA) for the quantification of protein is based on the optical measurement of the product of the reaction between an enzyme detecting label and a specific substrate.

An alternative detection format is proposed, performing the heterogeneous immunoassay onto paramagnetic particles, and detecting the enzyme product by means of amperometric technique. The proposed analytical tool showed promising performances carefully compared with optical detecting systems and offered additional interesting features, such as the possibility for multianalysis setup, miniaturization, automation, and also a high grade of versatility since the detecting scheme could be easily adopted for protein analysis as well as for DNA analysis, cell counting, and environmental control.

The experimental setup consist on a glass microchip, where the detection system will be placed a the waste reservoir (at the channel outlet side) and consisted of a platinum wire counter, an Ag/AgCl reference, and a gold working electrode (Figure 1). These wire (reference and counter) electrodes were inserted through holes drilled in Plexiglas holder. The working electrode, housed in the plastic screw, was placed opposite to the channel outlet. Additionally, platinum wires are inserted into the individual reservoirs, serving as contacts to the high-voltage power supply.

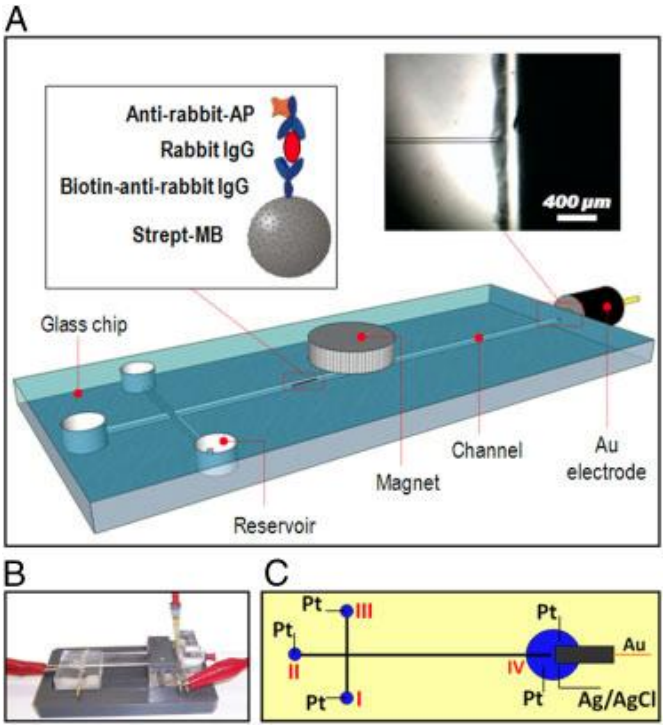

Figure 1. (A) Schematic representation of the glass microchip device components. (B) Photograph of the device setup. (C) Schematic representation of the chip design with the endchannel EC cell.

The preparation of the biotinylated alkaline phosphatase coated magnetic beads (AP-coated MBs) and the formation of the sandwich-type immunocomplex for rabbit IgG detection was held off-chip (see more details at annexes). The MB sandwich immunocomplex prepared was analyzed spectrophotometrically in order to quantify the rabbit IgG model antigen, where the specific reaction between AP and p-NPP produced a yellow-colored solution whose intensity is proportional to the concentration of rabbit IgG used during the immunoassay procedure.

Schematic representation of the EC detection principle is shown in Figure 2. Phenyl phosphate is a specific substrate for the enzyme AP, which produces phenol by hydrolysis reaction. While phenyl phosphate is electro inactive, phenol can be oxidized electrochemically. The concentration of phenol produced by the enzyme is directly proportional to the amount of enzyme itself, which is then directly related to the amount of antigen in exam. The EC detector set at the channel outlet can monitor the amount of phenol produced by the enzyme linked to the magnetic particles by the sandwich immunoassay. Antigen protein under investigation related to the amount of signaling enzyme can therefore be quantified.

Figure 2. Schematic illustration of the EC detection principle. Hydrolysis of phenyl phosphate by AP generates phenol which is then electrochemically detected.

The microchannels of the glass chip were treated before use by rinsing with 0.1M NaOH for 10 min and deionized water for another 10 min. The introduction of MBs inside the longitudinal channel is performed by injecting a small volume of suspended MBs by micropipette with the optimized number, through the buffer reservoir (II in Figure 1C) and then by means of a permanent magnet, the particles are quantitatively dragged inside the channel until the desired position is reached. In order to achieve reproducible and quantitative loading, it is crucial to have the chip channel perfectly clean and free from any small residual particles or solid impurities which could cause clogging. Once the particles have reached the desired position, they are kept in location with the magnet. At this point, the application of a low-pumping voltage (1000 V) to the buffer reservoir and then alternatively to the sample reservoirs (all filled with running buffer), while leaving the detection reservoir grounded, helps in pushing any particles eventually lost during the dragging operation. In this way, the buffer and sample reservoirs/channels are cleaned and also all the particles introduced are settled in the reaction zone, controlled by the magnet. The two sample reservoirs (I and III) are then filled with phenyl phosphate and phenol, respectively, while keeping PBS running buffer in reservoir II. At this point, in order to stabilize the EC detecting signal, the running buffer is pumped along the separation channel with a voltage of 1500 V, while simultaneously recording the EC signal at fixed potential. When the current reaches a steady state, the device is ready for measurements.

In order to achieve the best conditions for the EC detection of phenol by the hydrolysis of phenyl phosphate by AP enzyme linked to the MBs, several parameters have been optimized. Hydrodynamic study has been carried out in order to select the

best detecting potential. The graph (Figures 3A) shows the signal recorded versus potential applied, fixing injection time (10 s), injection voltage (1500 V), and pumping voltage (1500 V). As shown in the figure, by increasing the detection potential from 0.6 to 1.2 V (versus Ag/AgCl), the EC phenol oxidation signal was increased. A detecting potential of 1.1 V was chosen as optimal, also taking into account the background signal, which was significantly high at a potential of 1.2 V.

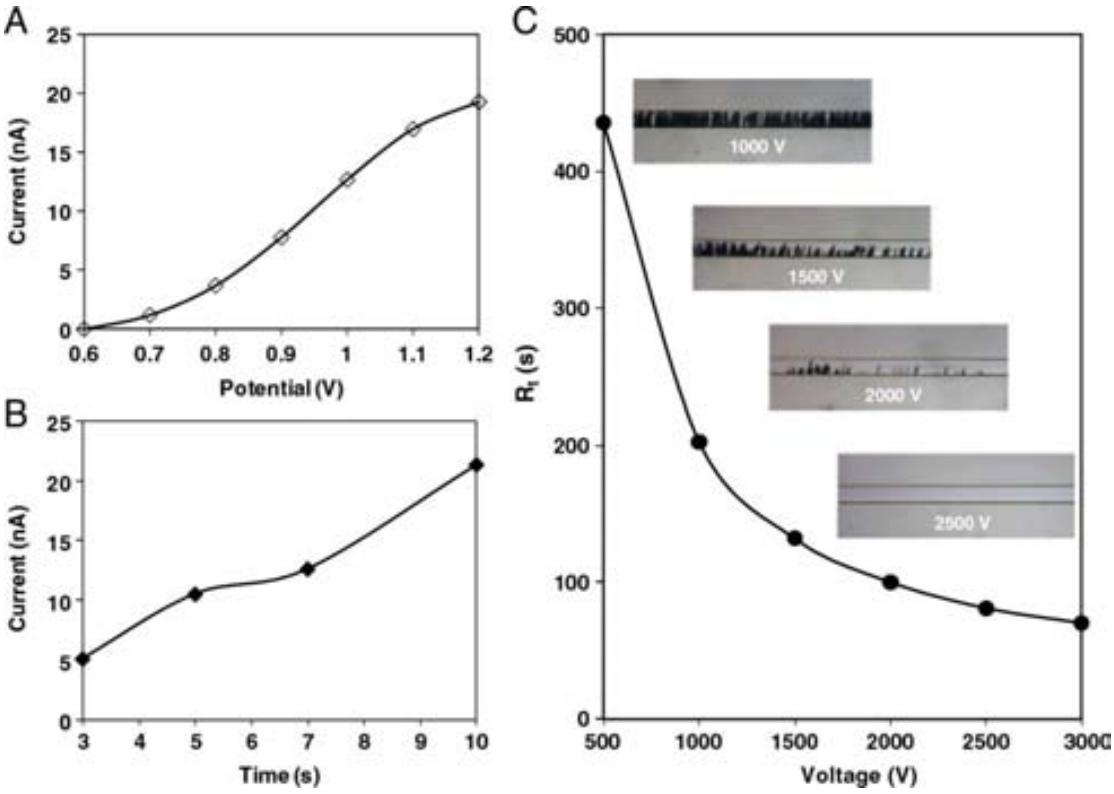

Figure 3. (A) Hydrodynamic study for the detection potential optimization. (B) Optimization of injection time. (C) Optimization of pumping voltage with retention times measured at different pumping voltages with photographs of the channel section with retained MBs. General conditions: Phenol concentration, 200 mM; electro-osmotic flow voltage, 1.5 kV; injection voltage, 1.5 kV; injection time, 10 s; detection potential, 1.1 V; detection potential, 1.1 V; running buffer, 10mM phosphate at pH 8.

Fixing the detection potential at 1.1 V and pumping voltage at 1500 V, injection time was investigated. Figure 3B shows the signal recorded for phenol detection, varying the injection time from 3 to 10 s. Increasing the injection time increases the amount of phenol introduced in the channel and therefore as expected higher signals were recorded with the highest obtained using 10 s injection. For injection times longer than 10 s, the broadening effect of the peaks (results not shown) started to be significant and therefore no optimal for the application.

Pumping voltage for this type of device is a very important parameter because not only regulates the flow at which substrate passes through the retained magnetic particles (MB bed) and the flow at which the product reaches the detector, but also has a profound effect on the stability of the MB bed. Separation voltages that are too low could generate broad peaks and with long retention times, whereas separation voltages that are too high could generate a flow, able to remove and wash away all the particles trapped by the magnet. Figure 3C shows the results of two separate experiments. First of all, the effect of the applied pumping voltage on the time necessary to phenol to reach the detector at the channel outlet was evaluated. For this experiment, as expected, increasing the pumping voltage reduced phenol retention time with a big difference between 500 and 1500 V, whereas from 1500 to 3000 V the retention time reduction is less significant. A separate experiment was also carried out in order to evaluate the effect of the pumping voltage on the stability of the MB bed. To visualize this effect, photographs of an MB bed have been taken after the application of pumping voltages between 1000 and 2500 V (see photographs in Fig. 3C). It is clear that by applying voltages lower than 1000 V, all the particles remain trapped by the magnet and fill the channel entirely. Applying a pumping voltage of 1500 V, the particles still remain trapped but forced by the flow tend to fill only the portion of the channel volume closest to the magnet generating a longer but equally stable MB bed. Finally, separation voltages higher than 1500 V start to generate flows too high for the magnetic field and an increased number of particles is washed away. It can be seen that only few particles remain trapped by the magnet at applied pumping voltage of 2000 V, whereas no particle is present at 2500 V. A good combination between reasonable analysis times with high particle retention resulted to be with the applied pumping voltage of 1500 V, which was selected as the optimal.

In order to evaluate the applicability of the method, preliminary tests have been carried out using AP-modified MBs. One of the advantages of using magnetic particles as in-chip solid support for immunoreactions is that by the manipulation of magnetic field together with the application of the electro-osmotic flow, the bioreaction surface can be easily renewed. Multianalysis procedures could be performed on the same device by following these steps: (i) particle loading, (ii) immunoreactions on trapped particles, (3) detection of the enzyme product, and (iv) washing/releasing of particles (see more details at annexes).

Additionally, the size and number of loading particles was also optimized. Figure 4 shows the signal recorded when different numbers of particles of 1 and 2.8 μm diameter size were loaded. It has to be pointed out that according to the manufacturer' specifications, the binding capacity of streptavidin magnetic particles for biotinylated protein is slightly higher for the particle of 1 mm diameter despite the lower geometrical surface. Approximatively, $6x10^5$ and $8x10^5$ biotinylated AP can be bond to one streptavidin-MB of 2.8 and 1.0 μm, respectively (www.invitrogen.com). This must be due to a different distribution or density of streptavidin molecules linked to the particles. Keeping this in mind, it is clear from the graph shown in Figure 4 that for a small number of particles loaded (10^2–10^4), the signal generated resulted similar for both types of particles increasing proportionally with the number of particles. From 10^4 to 10^7 particles of 2.8 μm size, the signal recorded increased less consistently reaching saturation using 10^5 particles. For the same range, using particles of 1.0 μm diameter, the signal increased significantly reaching saturation only for 10^6 particles. This is because the section/volume of channel that can be occupied by MBs being retained steadily by a 3mm size permanent magnet is filled approximatively by 10^5 and 10^6 particles of 2.8 and 1.0 μm, respectively. In other words, the particles in excess from the values where saturation is reached start to be located at a distance from the magnet too long to be hold at the optimized pumping voltage (1500 V). Offering larger active surface and therefore more active enzyme at the given channel volume, the particles of 1.0 μm size generated higher signals and were therefore selected to carry out the rabbit IgG immunoassay. Pictures of the two types of particles inside the channel at different magnifications are also shown in Figure 4. A number of particles of 10^5 were selected as the optimal in order to be sure that all the particles introduced are trapped effectively by the magnet increasing, in this way, reproducibility of the loading operation.

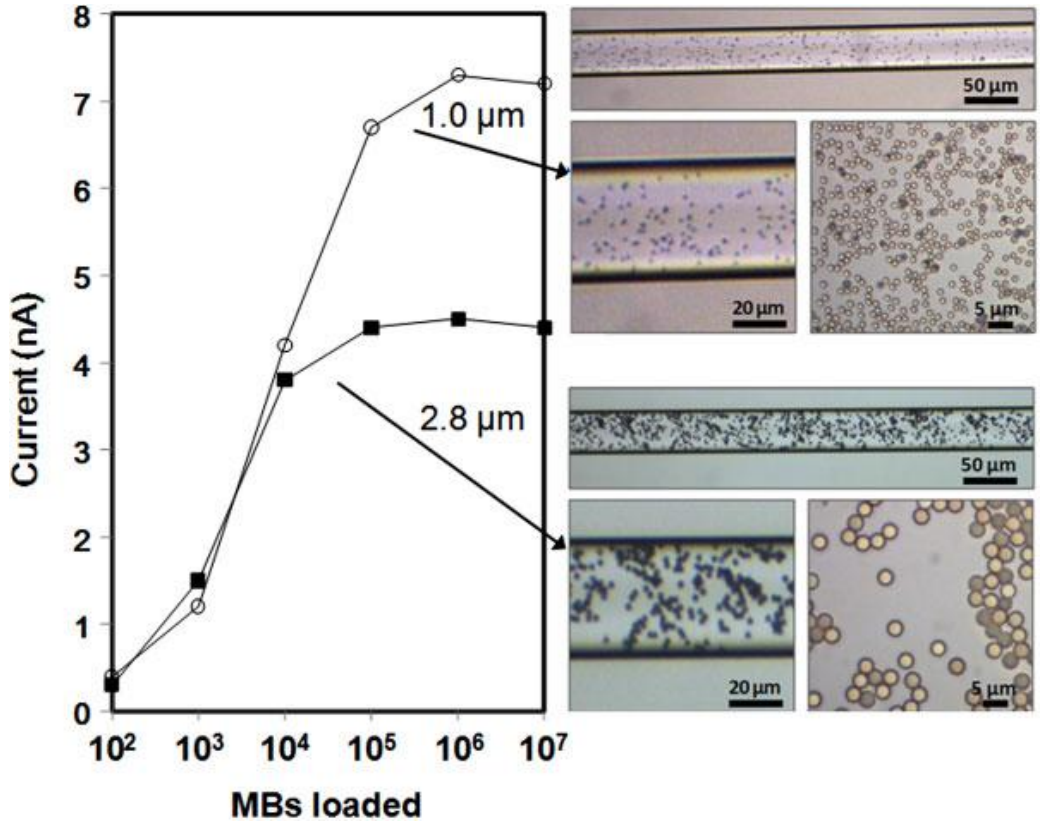

Figure 4. MB dimension study. EC phenol signals generated by MB–AP of 1 and 2.8 **µ**m diameter, loaded, and retained inside the channel by the magnet. Photographs of the beads inside the channel are also shown at different magnifications. General conditions: phenyl phosphate concentration, 500 **m**M; electro-osmotic flow voltage, 1.5 kV; injection voltage, 1.5 kV; injection time, 10 s; detection potential, 1.1 V; and running buffer, 10mM phosphate at pH 8.

Analytical utility of the microchip device loaded with paramagnetic bead was demonstrated on the detection of rabbit IgG model antigen. Two sets of MB–immunocomplexes have been prepared in parallel using standard rabbit IgG solutions at the concentration between 0.0032 and 2 µg/mL. One set of MB–immunocomplexes was used to perform the spectrophotometric analysis (Figure 5A) and the other set was used for the on-chip EC analysis. Regarding on-chip EC analysis, Phenyl phosphate (0.5 mM), introduced in reservoir I (Figure 1C) was used as a substrate to generate phenol. Figure 5B shows the EC signals recorded with MB–immunocomplexes prepared with different rabbit IgG concentrations. It appears clear that the EC detection performed using the microchip device resulted comparable to the spectrophotometric detection despite the fact that with the microchip device an extremely lower number of particles were used and also with a shorter response time. Inset in Figure 5B shows typical electropherograms recorded using different concentrations of rabbit IgG.

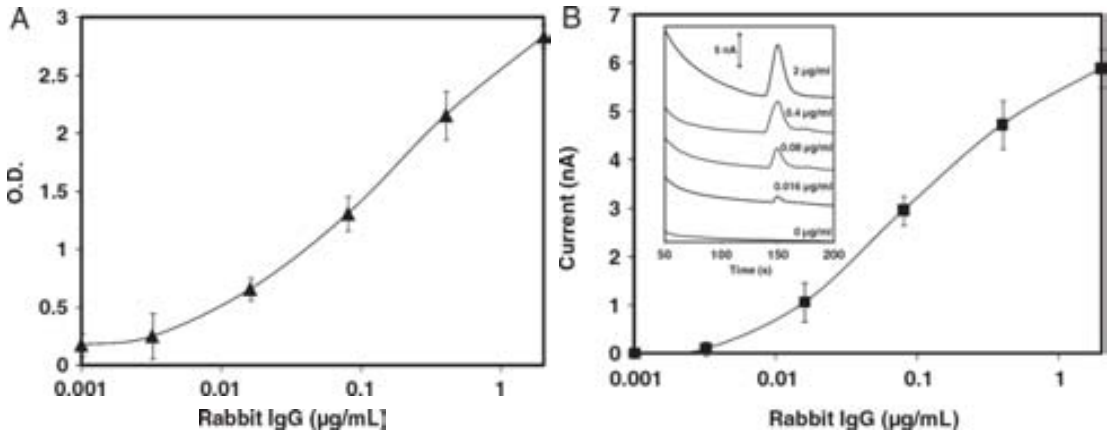

Figure 5. Off-chip spectrophotometric (A) and on-chip EC (B) detection of rabbit IgG. Inset (B) electropherograms recorded using different rabbit IgG standard solutions in the sandwich type immunoassay on MBs. General conditions for the EC detection: MBs loaded, 105; phenyl phosphate concentration, 500 **µ**M; electro-osmotic flow voltage, 1.5 kV; injection voltage, 1.5 kV; injection time, 10 s; detection potential, 1.1 V; and running buffer, 10mM phosphate at pH 8.

As a measure of the reproducibility in the preparation of the enzymatic reactor, the EC signals generated by five different MB–immunocomplexes prepared with the fixed antigen concentration of 0.08 mg/mL have been considered. The optimized amount of particles (10^5) from each of the five MB–immunocomplexes have been loaded inside the channel and the EC signals generated by passing phenyl phosphate resulted to be with a RSD lower than 10%. It should be noted that this value not only takes into account the reproducibility of the MB–immunocomplex preparation, but also includes the reproducibility of the MB loading operation inside the channel.

4.3. Conclusions and future perspectives

The combination of paramagnetic particles with microchip electrophoresis, external magnetic field manipulations, and coupled to EC detection resulted extremely promising with regard to the application to protein analysis. The use of an external permanent magnet, easy to be manipulated, allowed a reproducible loading and efficient control of magnetic particles used as solid support for immunoassay.

The experiments performed demonstrated the applicability of the device for multianalysis setup since electrophoretic and magnetic manipulations allow the renewing of the immuno-specific support. Very sensitive amperometric detection allowed quantification of the antigen rabbit IgG comparably with the

spectrophotometric method but with a number of particles and therefore immuno reactants consumed, extremely lower. In addition to the lower reagent consumption, inherent miniaturization and versatility represent the main advantages of the developed device, which in the future could be used as a universal bioanalytical tool. The total analysis procedure, entirely performed with the microchip device, including all the incubations and washing steps is presently under investigation, and this would certainly give an impressive versatility to this bioanalytical device. It could be successfully adopted not only for protein quantification, but also for DNA analysis and environmental applications.

4.4. References

[1] Manz, A.; Graber, N.; Widmer, H. M. *Sens. Actuat. B Chem.* **1990**, *1*, 244.

[2] Dodge, A.; Fluri, K.; Verpoorte, E.; de Rooij, N. F. *Anal. Chem.* **2001**, *73*, 3400.

[3] Yang, T.; Jung, S.-Y.; Mao, H.; Cremer, P. S. *Anal. Chem.* **2001**, *73*, 165.

[4] Lai, S.; Wang, S.; Luo, J.; Lee, L. J.; Yang, S.-T.; Madou, M. J. *Anal. Chem.* **2004**, *76*, 1832.

[5] Hosokawa, K.; Omata, M.; Sato, K.; Maeda, M. *Lab Chip* **2006**, *6*, 236.

[6] Kawaguchi, H. *Prog. Polym. Sci.* **2000**, *25*, 1171.

[7] Kruis, F. E.; Fissan, H.; Peled, A. *J. Aerosol. Sci.* **1998**, *29*, 511.

[8] Sato, K.; Tokeshi, M.; Odake, T.; Kimura, H.; Ooi, T.; Nakao, M.; Kitamori, T. *Anal. Chem.* **2000**, *72*, 1144.

[9] Verpoorte, E. *Lab Chip* **2003**, *3*, 60N.

[10] Pamme, N. *Lab Chip* **2006**, *6*, 24.

[11] Gijs, M. A. M. *Microfluid. Nanofluid.* **2004**, *1*, 22.

[12] Pumera, M.; Castañeda, M. T.; Pividori, M. I.; Eritja, R.; Merkoçi, A.; Alegret, S. *Langmuir* **2005**, *21*, 9625.

[13] Ambrosi, A.; Castañeda, M. T.; Killard, A. J.; Smyth, M. R.; Alegret, S.; Merkoçi, A. *Anal. Chem.* **2007**, *79*, 5232.

[14] de la Escosura-Muñiz, A.; Maltez-da Costa, M.; Merkoçi, A.,*Biosens. Bioelectron.* **2009**, *24*, 2475.

[15] Liu, G. D.; Wang, J.; Kim, J.; Jan, M. R.; Collins, G. E. *Anal. Chem.* **2004**, *76*, 7126.

[16] Wellman, A. D.; Sepaniak, M. J., *Anal. Chem.* **2006**, *78*, 4450.

[17] Fan, A. P.; Lau, C. W.; Lu, J. Z. *Anal. Chem.* **2005**, *77*, 3238.

[18] Zacco, E.; Pividori, M. I.; Alegret, S.; Galve, R.; Marco, M. P. *Anal. Chem.* **2006**, *78*, 1780.

[19] Jiang, G. F.; Harrison, D. J. *Analyst* **2000**, *125*, 2176.

[20] Kwakye, S.; Baeumner, A. *Anal. Bioanal. Chem.* **2003**, *376*, 1062.

[21] Huang, C.-J.; Lin, H.-I.; Shiesh, S.-C.; Lee, G.-W. *Biosens. Bioelectron.* **2010**, *25*, 1761.

[22] Choi, J. W.,; Oh, K. W.; Thomas, J. H.; Heineman, W. R.; Halsall, H. B.; Nevin, J. H.,; Helmicki, A. J.; Henderson, H. T.; Ahn, C. H. *Lab Chip* **2002**, *2*, 27.

[23] Liu, Y.-J.; Guo, S.-S.; Zhang, Z.-L.; Huang, W.-H.,; Baigl, D.; Chen, Y.; Pang, D.-W. *J. Appl. Phys.* **2007**, *102*, 084911.

[24] Leea, Y.-F.; Lienb, K.-Y.; Lei, H.-Y.; Leea, G.-B. *Biosens. Bioelectron.* **2009**, *25*, 745.

[25] Furdui, V. I.; Harrison, D. J. *Lab Chip* **2004**, *4*, 614.

[26] Sivagnanam, V.; Song, B.; Vandevyver, C.; Bünzli, J.-C.G.; Gijs, M. A. M. *Langmuir* **2010**, *26*, 6091.

[27] Llopis, X.,; Pumera, M.; Alegret, S.; Merkoçi, A. *Lab Chip* **2009**, *9*, 213.

[28] Martinez, N. A.; Schneider, R. J.; Messina, G. A.; Raba, J. *Biosens. Bioelectron.* **2010**, *25*, 1376.

[29] Hervás, M.; López, M. A.; Escarpa, A. *Analyst* **2009**, *134*, 2405.

[30] Harrison, D. J.; Fluri, K.; Seiler, K.; Fan, Z. H.; Effenhauser, C. S.; Manz, A. *Science* **1993**, *261*, 895.

[31] Effenhauser, C. S.; Manz, A.; Widmer, H. M. *Anal. Chem.* **1993**, *65*, 2637.

[32] Manz, A.; Effenhauser, C. S.; Burggraf, N.; Harrison, D. J.; Seiler, K.; Fluri, K., J. *Micromech. Microeng*. **1994**, *4*, 257..

[33] Jakeway, S. C.; de Mello, A. J.; Russell, E. L. *Fresenius J. Anal. Chem.* **2000**, *366*, 525.

[34] Lacher, N. A.; Lunte, S. M.; Martin, R. S. *Anal. Chem.* **2004**, *76*, 2482.

[35] Tanyanyiwa, J.; Leuthardt, S.; Hauser, P. C. *Electrophoresis* **2002**, *23*, 3659.

[36] Wang, J.; Pumera, M. *Anal. Chem.* **2002**, *74*, 5919.

[37] Vandaveer, W. R.; Pasas-Farmer, S. A.; Fischer, D. J.; Frankenfeld, C. N.; Lunte, S. M. *Electrophoresis* **2004**, *25*, 3528.

CHAPTER 5

MICROMOTORS

Related Publications

"Superhydrophobic Alkanethiol-Coated Microsubmarines for Effective Removal of Oil" Maria Guix, Jahir Orozco, Miguel García, Wei Gao, Sirilak Sattayasamitsathit, Arben Merkoçi, Alberto Escarpa and Joseph Wang. *ACS Nano* **2012**, *5*, 4445-4451.

5.1. Introduction

Self-propelled catalytic nanomotors, capable of converting energy into movement and forces,[1,2,3,4,5,6] have shown considerable promise for diverse practical applications. Particularly attractive are tubular microengines owing to their efficient bubble-induced propulsion in complex biological media and high ionic-strength environments.[4,7,8] Such chemically powered nanomotors have been commonly prepared by top-down photolithography, e-beam evaporation, and stress-assisted rolling of functional nanomembranes into conical microtubes.[5] Alternatively, a simplified membrane-template electrodeposition protocol can be used for mass production of high-performance catalytic microtubular engines.[9,10] The resulting microengines are smaller in size (~8 μm long), require low fuel concentrations (down to 0.2% hydrogen peroxide (H_2O_2)), and move at an ultrafast speed (over 1400 body lengths/s).

These template-fabricated microtubes commonly consist of a polymer/Pt bilayer and require additional Ni and Au layers for their magnetic guidance and facile functionalization (e.g., with receptors), respectively. A judicious modification of the outer Au surface by molecular bioreceptors, e.g., DNA probes,[11] aptamers,[12] antibodies,[13] or lectins,[14] has thus been shown useful for diverse target-isolation sensing applications. Considerable efforts have also been devoted toward the use of catalytic nanomotors for targeted drug delivery.[15]

Concerning environmental remediation issues, oil is a major source of ocean pollution and groundwater contamination. The presence of oils in wastewaters as a product of various manufacturing processes is common in different industries. Furthermore, episodes of major water pollution, caused by oil spillage, result in the release of millions of tons each year. For example, the 1989 Exxon Valdez and 2010 Deepwater Horizon incidents spilled millons of gallons of crude oil.[16,17] The removal of oils and organic solvents from contaminated water is thus of considerable importance for minimizing the environmental impact of these pollutants. Substantial efforts have thus been devoted to develop effective tools toward the remediation and clean up of oil spills. Although oils in wastewater plants are mostly removed by a mechanical separation, other methods have been proposed to address related pollution

episodes.[18,19] However, most of these methods lack the desired selectivity and efficiency and are not cost-effective or environmentally friendly. Accordingly, the development of new highly effective oil-water separation methods is highly desired.

5.2. Superhydrophobic alkanethiol-coated micromotors

Different synthetic and natural materials have been proposed as possible sorbents for oil removal. Surfaces with superhydrophobic properties have recently attracted particular interest for oil-water separation owing to their high efficiency and selectivity,[18,19,20,21,22] although their high cost, complex preparation processes, and scalability issues have hindered their practical applications.[16] These hydrophobic surfaces tend to repel water while strongly interact with nonpolar or oily liquids, which firmly adhere to textured interfaces.[21] Both the micronano-hierarchical texture and the chemical composition are essential for promoting the superhydrophobic character necessary for effective oil removal. The surface polarity and roughness are thus expected to influence the extent of the oil-surface interaction.[23,24] Self-assembled monolayers (SAMs), formed by the spontaneous and strong chemisorption of alkanethiols at gold or silver surfaces, have been particularly useful for transforming these surfaces into superhydrophobic interfaces.[24] Guo *et al.*[25] reported that ZnO hydrophilic surfaces become superhydrophobic after exposure to an octadecanethiol solution.

Tailoring the length of the alkanethiol chain has allowed the control of the surface polarity and hence tuning the partition of hydrophobic drugs.[26] The choice of the ending functional group is also vital for tailoring the polarity of the SAMs. For example, water contact angle studies reveal that methyl-terminated SAMs lead to hydrophobic surfaces, while hydroxyl-terminated ones provide wettable surfaces.[27] However, there are no reports of integrating these oil-sorption properties into self-propelled microengines and using such superhydrophobic nanomotors to facilitate the capture, transport, and separation of oil droplets. Autonomously moving synthetic nanomotors have recently been employed for the pick-up and transport of diverse payloads, ranging from cancer cells to drug-loaded polymeric spheres,[12,14] but not in connection to the isolation of oily contaminants.

The method herein presented is based on the creation of a SAM-modified microtubular engine able to strongly interact with oily liquids via adhesion and permeation onto its long alkanethiol coating. The new catalytic microsubmarine is template-prepared by electroplating poly(3,4-ethylenedioxythiophene) (PEDOT)/Pt bilayer followed by e-beam deposition of Ni/Au and subsequent functionalization with the SAM. In particular, it is illustrated the deliberate modification of the rough outer surface of microengines with highly hydrophobic long-chain self-assembled alkanethiol monolayers, which offers considerable promise for the capture, transport, and removal of oil droplets from water samples. The influence of the alkanethiol chain length upon the oil-nanomotor interaction and the collection efficiency has been examined using SAMs of different chain lengths, i.e., hexanethiol (C6), dodecanethiol (C12), and octadecanethiol (C18), in addition to its loading capacity in terms of oil droplets cargo.

5.2.1. Chain length effect of the *n*-alkanethiol coating

The fabrication of the oil-sorption hydrophobic microsubmarines, depicted in Figure 1, involves a template-based electrodeposition of a PEDOT/Pt bilayer microtube and e-beam vapor deposition of the Ni and Au outer layers, essential for the magnetic navigation control and surface functionalization, respectively. As illustrated in Figure 1A(d), such functionalization involves the formation of a superhydrophobic layer by self-assembly of long alkanethiol chains on the rough outer gold surface. A SEM image of the unmodified microengine (Figure 1B) indicates a rough surface, characteristic of nitrate-doped PEDOT films.[10]

The template fabrication process results in 8 μm long microtubes that are substantially smaller than common rolled-up tubular microengines.[28] The relatively similar dimensions of microsubmarine and oil droplets (which range from ~1 to ~100 μm, depending on the emulsion composition) permit convenient real time optical visualization of the oil-microengine interaction. Similar to recently developed PANI/Pt microengines,[9] the new template-prepared PEDOT/Pt microtubes were propelled efficiently in different media *via* the expulsion of oxygen bubbles generated from the catalytic oxidation of hydrogen peroxide fuel at their inner Pt layer.[10] Several factors, such as additional Ni and Au layers, influence the microengine speed.

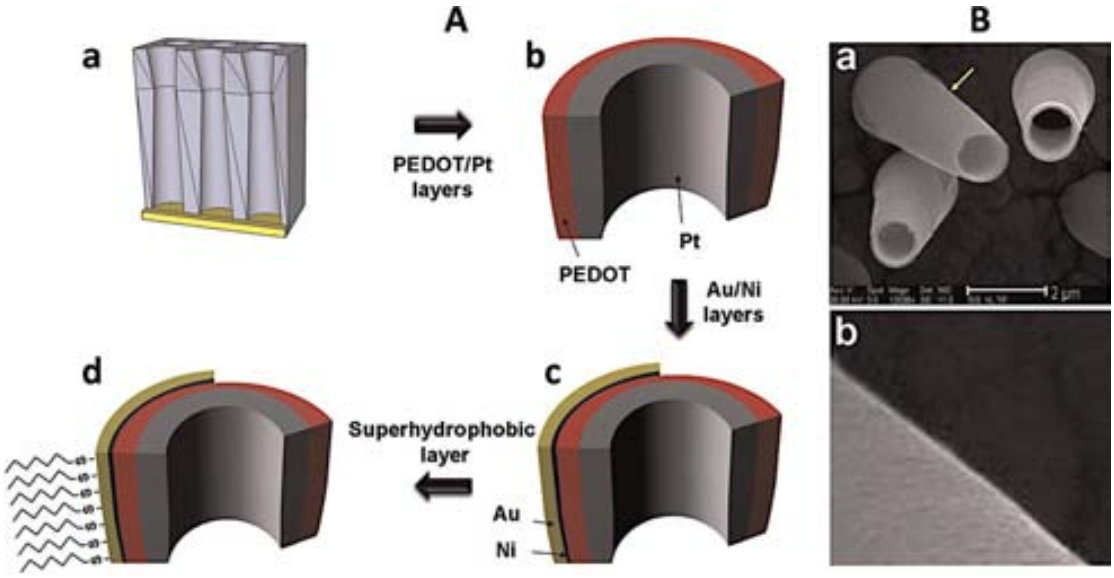

Figure 1. Fabrication and modification of the SAM-Au/Ni/PEDOT/Pt micromotors for environmental remediation. (A) A Cyclopore polycarbonate membrane is used as a template (a), PEDOT and Pt layers are electroplated into the template (b), Au and Ni layers are sputtered by e-beam (c), and a superhydrophobic layer is formed on the microsubmarine surface by incubation in a 0.5 mM **n**-dodecanethiol ethanolic solution (d). (B) SEM image of the resulting PEDOT/Pt microsubmarine (a) with a zoom-in of the zone highlighted with a yellow arrow (b).

As to create the superhydrophobic outer surface, Au/Ni/PEDOT/Pt microsubmarines were immersed in a 0.5 mM dodecanethiol ethanolic solution for 30min to form the hydrophobic monolayers on the outer gold surface, as illustrated in Figure 1D (see annexes for additional details). Such surface modification of the Au/Ni/PEDOT/Pt microsubmarine resulted in an additional 50% speed reduction, reflecting the partial blocking of the inner Pt catalytic layer.[29] However, the reduced speed is sufficient for transporting large cargoes in a manner analogous to our previously reported Au/Ni/PANI/Pt microengines.[14] Table 1 summarizes the changes in the microsubmarines' speed due to each different step involved in the fabrication process.

Table 1. Average speed of the micromotors upon each step involved in the fabrication process and pickup of oil droplets.

Micromotor step	Speed, μm/s
PEDOT/Pt	420
Au/Ni/PEDOT/Pt	200
Au/Ni/PEDOT/Pt	105

Figure 2A show the Au/Ni/PEDOT/Pt micromotor approaching, contacting, and spinning around a stained olive oil drop firmly attached to a glass slide (see additional

details and related videos in annexes). The strong interaction between the SAM-modified microsubmarine and an oil droplet results in a continuous spinning of the modified engine around the droplet with an accelerated speed ranging up to 200 μm/s. It should be pointed out that such continuous high-speed spinning is observed even after a prolonged 20min period. These data also confirm that the hydrogen peroxide fuel and the sodium cholate (NaCh) surfactant, essential for the micromotor movement, do not compromise its interaction with the oil droplet or the integrity of the SAM. In contrast, no such interaction is observed using an unmodified micromotor (Figure 2B). This bare Au/Ni/PEDOT/Pt micromotor moves rapidly, while approaching, contacting, and bypassing the droplet.

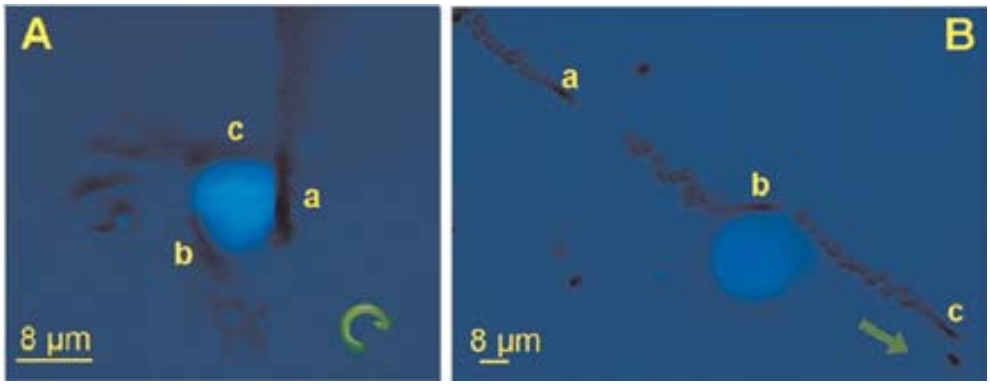

Figure 2. SAM-modified (A) and unmodified (B) microsubmarines in the presence of a stained olive oil droplet (attached to a glass slide). Images show (in a single overlaid image) the following sequential steps: approaching, contacting, and spinning around (A, a_c) the droplet and approaching, contacting, and leaving (B, a_c) the oil droplet, respectively. Fuel conditions (final concentration): 0.4% NaCh and 10% H2O2. Arrows indicate the micromotor trajectory.

Particularly attractive is the ability to tailor the polarity of the microsubmarine surface via a judicious choice of the chain length of the n-alkanethiol coating and hence their capture and transport properties. Chain length, head groups, preparation time, and other conditions (e.g., temperature) give rise to different SAM packing densities, configurations, and polarity.[30] The influence of the alkanethiol chain length on the oil-nanomotor interaction was thus examined by modifying the microengine with SAMs of different alkanethiol lengths (C6,C12, and C18). A considerable difference in the microsubmarine-oil droplet interaction was observed using C6 and C12 SAM-coated microsubmarines. Notice, for example, the strong microsubmarine-oil interaction of the C12-modified microengine spinning around a large olive oil droplet (Figure 2B) compared to the weaker interaction experienced by the C6-modified motor, where no spinning around the droplet is observed (see Supporting Figure 1A, in annexes). Similarly, a higher number of captured oil droplets are observed by using the C12

SAM modification, compared to the lower number of droplets attached to the C6-modified motor or to the absence of captured droplets by using the unmodified microsubmarine. These results are consistent with the different surface wettability properties observed in contact angle studies of *n*-alkanethiols of different lengths.[30,31] On the basis of the higher hydrophobic character of long-chain thiols, C18 SAM-coated microsubmarines are expected to offer higher oil-adsorption capabilities. However, such C18 SAM-modified microsubmarines hardly move owing to greater blocking of the inner Pt catalytic layer expected in the presence of longer alkanethiols.[29] Selective modification using alkane isonitriles[32] may be used to minimize the Pt blocking by the alkanethiol SAM, thus retaining microengine speed.

The influence of the SAM headgroup and hence surface polarity on the microsubmarines-oil interaction was examined by comparing the behavior of microengines coated with C6 SAM containing methyl and hydroxyl terminal groups using different time scales. Figure 3A(a-c), which illustrates small droplets attached to the hexanethiol-modified microsubmarine upon navigating in the sample. In contrast, and as expected from wettability measurements using hydroxyl-terminated SAM,[27] the mercaptohexanol-modified microsubmarines do not interact with the large or small olive oil droplets upon rapidly contacting them (Figure 3B, a-c). It is remarkable that even prolonged navigation of the mercaptohexanol-modified microsubmarines does not lead to any capture of the oil droplets. Clearly, and as expected,[27] the polarity of the head functional group strongly influences the interaction between the modified microsubmarines and the oil droplets and represents another key consideration (besides the chain length) when modifying the outer microengine surface.

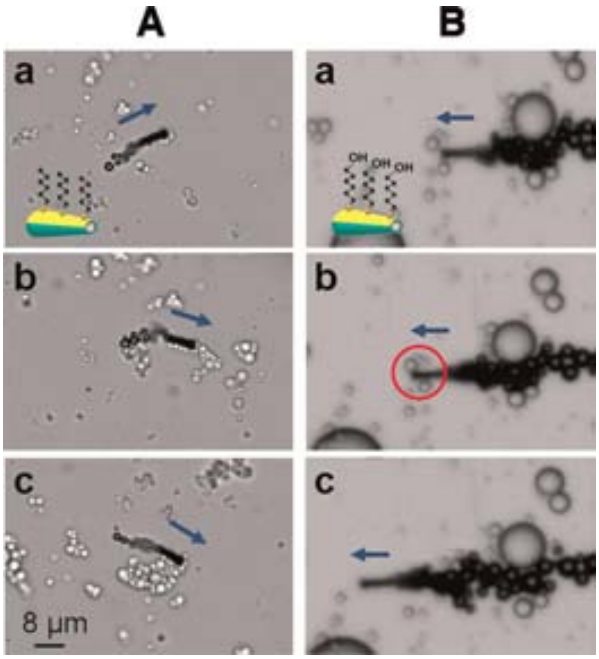

Figure 3. C6-SAM-modified microsubmotors with different head functional groups interacting with small olive oil droplets. Hexanethiol-modified micromotors are able to confine a payload of multiple oil droplets (A) (a, b, and c, time-lapse images at different navigation times: 11, 50, and 73 s (for A) and 6.57, 6.66, and 6.71 s (for B)). The corresponding mercaptohexanol-modified counterparts (B) are not able to pick up such droplets (a, b, and c images correspond to approaching, contacting, and leaving the droplets). A(a) and B(a) insets: cartoons of the respective SAM-modified microsubmarines. Arrows indicate the direction of the microsubmarine movement.

5.2.2. Loading capacity

Efficient capture and transport of oil droplets has been observed when the modified micromotor navigates in contaminated water samples containing small "free-floating" oil droplets. Figure 4 illustrates the capture and transport of multiple small olive oil droplets by the dodecanethiol SAM-modified microsubmarine. The longer the navigation time, the more oil droplets are collected and confined onto the surface of the self-propelled micromotor. While around 5 droplets (1.7 ± 0.4 μm size) are captured and transported in Figure 4A after a 12 s navigation, around 40 droplets are attached to the motor surface following 80 s (Figure 4A(d)). These observations demonstrate that these SAM-modified microengines provide high towing force for transporting efficiently approximately 10-fold their volume and indicate considerable potential for oil removal applications. As expected from the increased drag force (Stokes's law),[33] the speed of the micromachine decreases upon increasing the cargo size (i.e., number of captured droplets). This is illustrated in Figure 4B, which displays the dependence of the micromotor's speed on the number of transported oil droplets. The speed rapidly decreases from 26 to 12 μm/s upon increasing the number

of droplets from 7 to 30 and then more slowly to 11 μm/s for 43 droplets. As common for nanomotor-based cargo pickup, the optimal motor speed will provide a trade-off between sufficient contact time and large contact rate.[34,35]

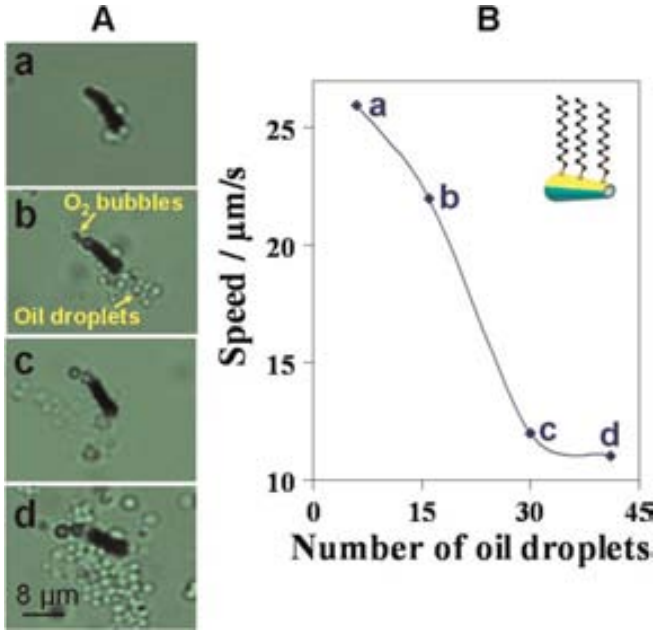

Figure 4. Dodecanethiol (C12-SAM)-modified micromotor carrying floating olive oil droplets. (A) Images a_d were taken after navigating in the water-oil (10% fuel) solution for 5, 12, 66, and 80 s, respectively (conditions, as in Figure 2). (B) Dependence of the micromotor speed upon the number of cargos (olive oil droplets). Inset: Cartoon of the dodecanethiol-modified micromotor.

Toward a practical utility of this new microsubmarine approach, we examined the ability of the dodecanethiol-modified microsubmarine to collect and transport motor oil in an oil-contaminated water sample. Figure 5 clearly illustrate that the SAM-coated microsubmarines display an "on the fly" capture upon contacting the small droplets of motor oil that are floating in the contaminated water sample. These results demonstrate the potential of the superhydrophobic-modified microsubmarines for facile, rapid, and highly efficient collection of oils in oil-contaminated water samples.

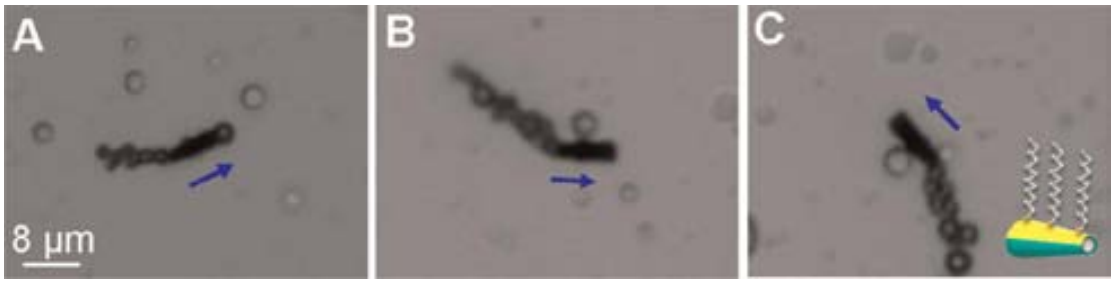

Figure 5. SAM-modified micromotor carrying floating droplets of motor oil in a fuel-enhanced oil-contaminated water sample. Images taken after 78 s navigation in the fuel-enhanced solution (conditions, as in Figure 2). (A, B, C) Time-lapse images showing the microsubmarine approaching, contacting, and carrying the droplets, respectively. Inset: Cartoon of the dodecanethiol-modified micromotor. Arrows indicate the direction of the micromotor movement.

5.3. Conclusions and future perspectives

The first example of using artificial nano/microscale machines for environmental remediation applications and specifically the tailoring of the surface of such self-propelled machines to interact strongly with oily liquids has been presented. The new SAM-Au/Ni/PEDOT/Pt micromotors thus offer a facile, rapid, and highly efficient collection and transport of oil droplets in aqueous environments through the interaction with the hydrophobic alkanethiol monolayer coating.

Comparison of different alkanethiol modifiers indicates that the dodecanethiol (C12-SAM)-modified microsubmarines offer the most favorable performance in terms of oil recovery and propulsion. Such high oil-adsorption ability indicates considerable promise for the cleanup of contaminated water samples. The extent of the micromotor-oil interaction and the collection efficiency can be tuned by controlling the surface hydrophobicity through the use of different chain lengths and head functional groups. The new micromotor capability was demonstrated either by a strong interaction between the modified nanomotor and large oil droplets (attached to a glass slide) or by the collection and transport of multiple free-floating small olive oil and motor oil droplets present in a contaminated water sample. These micromotor-oil interactions can be exploited in the suitable final disposition of oily wastes (or other organic solvents) by collecting them in a controlled fashion within a certain spatially separated zone. Simultaneous parallel movement of multiple SAM-modified micromotors holds promise for improving the efficiency of oil-removal processes. Practical large-scale oil cleaning operations would require the use of motors propelled by their own natural environment[36,37] or driven by an external (magnetic or electrical) control.[38,39]

The new superhydrophobic micromotors offer also considerable promise for the isolation of hydrophobic molecules, e.g., drugs, or for transferring target analytes between liquid-liquid immiscible interfaces, and hence great potential for diverse analytical microsystems. Multifunctional coatings of mixed (or multi) layers, coupling the preferential partition of hydrophobic compounds into the SAMs with additional functions (e.g., biocatalysis), could lead to additional advantages toward on-the-fly “capture and destroy” operations.

5.5. References

[1] Paxton,W. F.; Kistler, K. C.; Olmeda, C. C.; Sen, A., St.; Angelo, S. K.; Cao, Y.; Mallouk, T. E.; Lammert, P. E.; Crespi, V. H. *J. Am. Chem. Soc*. **2004**, *126*, 13424.

[2] Ozin, G. A.; Manners, I.; Fournier-Bidoz, S.; Arsenault, A. *Adv. Mater.* **2005**, *17*, 3011**.**

[3] Fournier-Bidoz, S.; Arsenault, A. C.; Manners, I.; Ozin, G. A. *Chem. Commun.* **2005**, *41*, 441.

[4] Wang, J. *ACS Nano* **2009**, *3*, 4.

[5] Pumera, M. *Nanoscale* **2010**, *2*, 1643.

[6] Campuzano, S.; Kagan, D.; Orozco, J.; Wang, J. *Analyst* **2011**, *136*, 4621.

[7] Mei, Y.; Solovev, A. A.; Sanchez, S.; Schmidt, O. G. *Chem. Soc. Rev.* **2011**, *40*, 2109.

[8] Huang, G.; Wang, J.; Mei, Y. *J. Mater. Chem.* **2012**, *22*, 6519.

[9] Gao, W.; Sattayasamitsathit, S.; Orozco, J.; Wang, J. *J. Am. Chem. Soc.* **2011**, *133*, 11862.

[10] Gao, W.; Sattayasamitsathit, S.; Uygun, A.; Pei, A.; Ponedal, A.; Wang, J. *Nanoscale* **2012**, 4, 2447.

[11] Kagan, D.; Campuzano, S.; Balasubramanian, S; Kuralay, F; Flechsig, G.; Wang, J. *Nano Lett.* **2011**, *11*, 2083.

[12] Orozco, J.; Campuzano, S.; Kagan, D.; Zhou, M.; Gao, W.; Wang, J. *Anal. Chem.* **2011**, *83*, 7962.

[13] Balasubramanian, S.; Kagan, D.; Hu, C. J.; Campuzano, S.; Lobo-Casta~no, M. J.; Lim, N.; Kang, D. Y.; Zimmerman, M.; Zhang, L.; Wang, J. *Angew. Chem. Int. Ed.* **2011**, *50*, 4161.

[14] Campuzano, S.; Orozco, J.; Kagan, D.; Guix, M.; Gao, W.; Sattayasamitsathit, S.; Claussen, J. C.; Merkoçi, A.; Wang, J. *Nano Lett.* **2012**, *12*, 396..

[15] Kagan, D.; Laocharoensuk, R.; Zimmerman, M.; Clawson, C.; Balasubramanian, S.; Kang, D.; Bishop, D.; Sattayasamitsathit, S.; Zhang, L.; Wang, J. *Small* **2010**, *6*, 2741.

[16] Biswas, S.; Chaudhari, S. K.; Mukherji, S. *J. Chem. Technol. Biotechnol.* **2005**, *80*, 587.

[17] Machlis, G. E.; McNutt, M. K. *Science* **2010**, *329*, 1018.

[18] Zhu, Q.; Pan, Q.; Liu, F. *J. Phys. Chem. C* **2011**, *115*, 17464.

[19] Cheng, M.; Gao, Y.; Guo, X.; Shi, Z.; Chen, J. F.; Shi, F. A. *Langmuir* **2011**, *27*, 7371**.**

[20] Yao, X.; Song, Y.; Jiang, L. *Adv. Mater.* **2011**, *23*, 719.

[21] McHale, G.; Shirtcliffe, N. J.; Aqil, S.; Perry, C. C.; Newton, M. I. *Phys. Rev. Lett.* **2004**, *93*, 036102.

[22] Zhang, J.; Pu, G.; Severtson, S. J. *ACS Appl. Mater. Interfaces* **2010**, *2*, 2880.

[23] Shirtciffe, N.; McHale, G.; Newton, M. I.; Chabrol, G.; Perry, C. C. *Adv. Mater.* **2004**, *16*, 1929.

[24] Fragoso, A.; Laboria, N.; Latta, D.; Sullivan, C. K. O. *Anal. Chem.* **2008**, *80*, 2556.

[25] Guo, M.; Diao, P.; Cai, S. *Thin Solid Films* **2007**, *515*, 7162.

[26] Wang, J.; Wu, H.; Angnes, L. *Anal. Chem.* **1993**, *65*, 1893.

[27] Faucheux, N.; Schweiss, R.; Lutzow, K.; Werner, C.; Groth, T. *Biomaterials* **2004**, *25*, 2721.

[28] Sanchez, S.; Solovev, A. A.; Schulze, S.; Schmidt, O. G. *Chem. Commun.* **2011**, *47*, 698.

[29] Floridia, M. A.; Rubert, A. A.; Benítez, G. A.; Fonticelli, M. H.; Carrasco, J.; Carro, P.; Salvarezza, R. C. *J. Phys. Chem. C* **2011**, *115*, 17788**.**

[30] Mendoza, S. M.; Arfaoui, I.; Zanarini, S.; Paolucci, F.; Rudolf, P. *Langmuir* **2007**, *23*, 582.

[31] Offord, D. A.; John, C. M.; Linford, M. R.; Griffin, J. H. *Langmuir* **1994**, *10*, 883.

[32] Lee, T. R.; Laibinis, P. E.; Folkers, J. P.; Whitesides, G. M. *Pure Appl. Chem.* **1991**, *63*, 821.

[33] Wang, J. *Lab Chip* **2012**, DOI: 10.1039/C2LC00003B.

[34] Katira, P.; Hess, H. *Nano Lett.* **2010**, *10*, 567.

[35] Agarwal, A.; Katira, P.; Hess, H. *Nano Lett.* **2009**, *9*, 1170.

[36] Gao, W.; Uygun, A.; Wang, J. *J. Am. Chem. Soc.* **2012**, *134*, 897.

[37] Zhao, G.; Seah, T. H.; Pumera, M. *Chem. Eur. J.* **2011**, *17*, 12020.

[38] Zhang, L.; Abbott, J. J.; Dong, L.; Peyer, K. E.; Kratochvil, B. E.; Zhang, H.; Bergeles, C.; Nelson, B. J. *Nano Lett.* **2009**, *9*, 3663.

[39] Loget, G.; Kuhn, A. *Nat. Commun.* **2011**, *2*, 535.

CHAPTER 6

CONCLUSIONS AND FUTURE PERSPECTIVES

6.1. General conclusions

Considering the objectives previously described in Chapter 2, along with the obtained results presented from the chapter 3 to the chapter 5, the following concluding remarks on this PhD thesis can be given:

The design and characterization of novel miniaturized (bio)sensing platforms and devices modified with different nanomaterials, such as carbon nanotubes or nanowires, have been achieved. These platforms and devices have been applied in the detection of various analytes (e.g. phenol, glucose, oil droplets), in some cases closely related to the previously immobilization of biological entities that confer selectivity and sensitivity to the analytical platform, being this the principal conclusion of the PhD thesis.

More in detail, the conclusions that can be extracted by following the entire working objectives and strategies are:

1. Novel modified carbon nanotubes screen-printed electrodes have been prepared and characterized:
    - Carbon nanotubes have been processed and successfully dispersed in tetrahydrofuran. The physico-chemical properties of the nanotubes have been tunned, leading to the partial oxidation of CNTs that produced functional oxygenated groups at the open ends and defects along the sidewall.
    - Carbon nanotubes were integrated onto the working electrode of the SPE, whose distribution and morphology was studied by SEM and Confocal Scanning Laser Microscopy (CSLM) revealing a homogenous distribution over the entire surface and a sponge-like structure with a higher surface-to-area ratio compared to its non-modified counterpart.

2. Three different approaches for Tyrosinase (Tyr) enzyme connection with CNT and SPE, along with the full characterization of the enzyme distribution throughout the entire CNT-based working electrode surface,

have been achieved, evaluating the sensibility, sensitivity and stability for each case.

- Tyrosinase has been successfully immobilized by physical adsorption in CNTs matrix in SPE, statistically studying its distribution by CSLM, and showing a good response towards phenol detection in a batch system. Comparing the frame scanned for the bare and the modified SPE a quantity of the immobilized tyrosinase enzyme 1.96 times higher in the case of the MWCNTs modified SPE is found.
- Second approach, achieved by the previous immobilization of tyrosinase enzyme by physical absorption and a creation of a glutaraldehyde film, showed a higher stability and was further implemented in a flow system.
- The last tyrosinase enzyme immobilization approach was based on the electrodeposition of a tissue onto SPE surface or CNT modified SPE, with the aid of Bi^{3+} precursor that interacts with the tissue and got reduced onto the transducer surface. Bismuth film was shown to be an alternative to the traditional film electrode and with a good response towards phenol detection in synthetically prepared wastewater samples.

3. Integration of the SPE/MWCNT/Tyr/Glu biosensor (fabricated by the second approach) in a flow injection analytical (FIA) system is achieved.
    - Several parameters such as the working potential, pH of the measuring solution, biosensor response time, detection limit, linear range of response and sensitivity were determined, showing a detection limit almost 500 times lower than the allowed levels of phenols in water as given by the EPA.
    - The biosensor keeps its activity during continuous FIA measurements at room temperature, showing a stable response (RSD 5%) within a two weeks working period at room temperature.

4. Nonenzymatic electrochemical glucose sensor, based on measuring the current response during the direct glucose oxidation on the electrode surface by chronoimpedance technique (CIT) is developed.
    - The low detection range obtained by this glucose sensor, in addition to its high repeatability and sensitivity, may allow applications to non-invasive detection of glucose in other biological fluids (saliva, sweat and urine) where glucose should be present at very low concentrations.

5. Novel assembled nanoplatform taking advantage of alternate layer depositions from Prussian blue (PB) - cyclodextrin (CD) nanoparticles (NPs) with polyallylamine (PAH) was designed.
    - The obtained hybrid PB based material is successfully characterized by SEM and TEM studies, showing a microcubic supramolecular like organization.
    - Electrochemical characterization of the PB based hybrid platform revealed that the cathodic and anodic peak currents increased with the number of bilayers, indicating that PB nanoparticles are electrically connected within multilayers.

6. The combination of paramagnetic particles with microchip electrophoresis, external magnetic field manipulations, and coupled to EC detection permitted the detection of phenol (as indicator for immunodetection) by using low reagent consumption, in addition to the inherent miniaturization and versatility of such miniaturized system.
    - Phenol detection was achieved by following the hydrolysis of phenyl phosphate by alkaline phosphatase (AP) enzyme linked to the magnetic beads (MBs).
    - Electrophoretic and magnetic manipulations allow the renewing of the immuno-specific support.

7. The development of artificial nano/microscale machines for environmental remediation applications based on the creation of a superhydrophobic outer surface to strongly interact and capture oily liquids has been achieved,.

- The extent of the micromotor-oil interaction and the collection efficiency can be tuned by controlling the surface hydrophobicity through the use of different chain lengths and head functional groups.
- Dodecanethiol (C12-SAM)-modified microsubmarines offered the most favorable performance in terms of oil recovery and propulsion.

6.2. Perspectives and future work

The results obtained during this PhD thesis period open the door to interesting application in the sensing and biosensing fields, not only in the efficiency and robustness of analytical platforms by the integration of nano/micromaterials, but also for the different platforms available, being of special interest the recent micromotor's technology, which is specially versatile and adequate for different environmental or health related applications.

The carbon nanotubes modified screen-printed electrode, apart from presenting the advantages of being a low-cost and versatile technology, have shown a great potential due to the easy immobilization of enzyme into its matrix and its electrochemical behaviour. Its high surface-to-ratio matrix and the stability that it confers to the immobilized biological entities have been quantitatively demonstrated during this thesis, being envisioned as a potential analytical platform for other kind of health or environmental related analysis.

Additionally, screen-printed electrodes have been also applied in non-enzymatic analytical platforms for glucose detection by using impedancimetric studies. Such platforms are of special interest for its stability and the possibility to work at high temperatures and other aggressive environments. Therefore, the study presented, where the nanomaterial in absence of any biological entity is performing the entire detection event, opens the door to work with many different nanomaterials coupled to other easier-to-handle miniaturized platforms, like screen-printed electrodes. Parallely, hybrid platforms developed are expected to have interesting applications in the sensing and biosensing fields, where highly conductive and tunable 'on-demand' platforms combined with biorecognition reactions are desirable.

The lab-on-a-chip related experiments demonstrated the applicability of the device for multianalysis setup since electrophoretic and magnetic manipulations allow the renewing of the immuno-specific support. Such technology and the use of alternative nano/micromaterials could be successfully adopted not only for protein quantification, but also for DNA analysis and environmental applications.

Finally, superhydrophobic micromotors offer a considerable promise for the isolation of hydrophobic molecules, like drugs, or for transferring target analytes between liquid-liquid immiscible interfaces, and hence great potential for diverse analytical microsystems. Alternative funcionalization of the outer surface, as well as the versatility of the materials involved on its fabrication by template-based deposition, could bring additional functions (e.g., biocatalysis), could lead to additional advantages toward on-the-fly “capture and destroy” operations but also playing a key role in other biosensing platforms by working as transporters or dynamic analytical platforms.

The implementation of micro/nanomaterials in different platforms, with results that opens the door to new and improved technologies, has been the aim of this PhD thesis, which has tried not only to merely integrate and characterize several analytical platforms, but to fully understand their electrochemical behaviour to project its application for useful and challenging health and environmental issues. This philosophy encourages the creation of new analytical platforms which takes advantages of the nowadays science and in particular of nanotechnologies.

PUBLICATIONS

ANNEX A. ARTICLES

ACCEPTED BY THE PhD COMISSION

Nanomaterials for Electroanalysis

Arben Merkoçi, Adriano Ambrosi, Alfredo de la Escosura-Muñiz, Briza Pérez-López, Maria Guix, Marisa Maltez, Sergio Marin

Nanobioelectronics and Biosensors Group, Institut Català de Nanotecnologia (ICN), Campus de la UAB, Bellaterra (Barcelona), Spain

The emergence of nanotechnology and nanomaterials has opened up new horizons for the development of improved analytical devices. New synthesis, fabrication, and characterization methods offer the possibility to control the size, shape, and composition of nanometric-scale materials, thereby allowing exquisite control of their properties. The ability to carefully tailor the physical properties of nanomaterials is probably the major achievement of nanoscience and represents an essential element for their application in analytical systems.

Among the numerous detecting strategies, electrochemical sensing techniques play a growing role in various fields in which an accurate, low-cost, fast, and online analytical measuring system is required. Besides the relatively low cost compared with optical instrumentation, advantages such as the possibility of miniaturization as well as in-field applications make electrochemical sensing devices very attractive.

The properties of nanostructured materials, such as high surface/volume ratio, their ability to be functionalized, favorable electronic and thermal features, and electrocatalytic effect attracted considerable attention for the assembling of novel electrochemical sensing systems. Nanomaterials such as nanoparticles (NPs), nanotubes, nanowires, nanocomposites, and nanochannels of various sizes and compositions have been applied in electroanalysis to improve the immobilization of enzymes, antigens, and nucleic acids on electrochemical transducer surfaces, to promote the direct electron-transfer reactions, and to amplify and orient the analytic signal of biorecognition events. In this article, a general description of the properties of the nanomaterials most commonly used in electroanalysis, along with their integration into electrochemical analytical tools, is given. The analytical performances and the impact such nanomaterial-based devices are expected to have upon clinical diagnostics, environmental monitoring, security surveillance, and food safety are also discussed.

1 INTRODUCTION: NANOTECHNOLOGY AND NANOMATERIALS

Nanotechnology is the term used to describe the creation and exploitation of materials with structural features in between those of atoms and bulk materials, with at least one dimension in the nanometer range ($1\,\text{nm} = 10^{-9}\,\text{m}$). The properties of materials with nanometric dimensions are significantly different from those of atoms or bulk materials. Suitable control of the properties of nanometer-scale structures can lead to new science as well as new products, devices, and technologies.[1]

There has been explosive growth of nanoscience and technology in the last decade, primarily because of the availability of new methods of synthesizing nanomaterials, as well as tools for characterization and manipulation. Several innovative methods for the synthesis of NPs and nanotubes, and their assemblies, are now available. In addition, there is a better understanding of the size-dependent electrical, optical, and magnetic properties of individual nanostructures of semiconductors, metals, and other materials.[2]

Besides the established techniques of electron microscopy, crystallography, and spectroscopy, scanning probe microscopies have provided powerful tools for the study of nanostructures. Novel methods of fabricating patterned nanostructures, as well as new device

Encyclopedia of Analytical Chemistry R.A. Meyers (Ed.)

and fabrication concepts, are constantly being discovered.

The immediate goals of the science and technology of nanomaterials must be to fully master the synthesis of isolated nanostructures (building blocks) and their ensembles and assemblies with the desired properties, to explore and establish nanodevice concepts and systems architecture, to generate new classes of high-performance materials, including biologically inspired systems, to connect nanoscience to molecular electronics and biology, and to improve known investigative methods while discovering better tools for the characterization of nanostructures.[3]

Table 1 lists typical nanomaterials of different dimensionalities commonly used in electroanalysis. Nanotubes, NPs, nanowires, and nanocomposite and nanostructurated materials have already been used to fabricate a large number of electrochemical devices, ranging from chemical sensors and enzyme-based biosensors to DNA sensors, exhibiting higher sensitivity, stability, and selectivity due to the presence of functionalized nanomaterials used as catalytic tools, as immobilization platforms, or as labels for the sensitive recognition events.[4]

Various nanostructures have been investigated to determine their properties and possible applications in electroanalysis. NPs, quantum dots (QDs), carbon nanotubes (CNTs), nanowires, and nanochannels of different sizes and materials have been applied and integrated to electrochemical platforms with functions depending on the specific features of the nanomaterials. They have been applied to improve immobilization of (bio)molecules onto electrode surfaces, to catalyze reactions, to record higher transducing signals, to enhance specificity of reactions, to miniaturize analytical systems, and speed up processes.

A detailed description of the most commonly used nanomaterials in electrochemical detecting tools, their general properties, and their most successful applications in electrochemical analysis are given in the following sections.

2 NANOPARTICLES, QUANTUM DOTS

2.1 General Properties

Metal and semiconductor NPs are certainly the most studied and applied in electrochemical analysis.[5] Owing to their small size (normally in the range of 1–100 nm), NPs exhibit unique chemical, physical, and electronic properties that are different from those of bulk materials, and can be used to construct novel and improved sensing devices; in particular, electrochemical sensors and biosensors. Such properties strongly depend on the number and kind of atoms that make up the particle. The properties of the particles generally depend on their size, shape, distribution, and stabilizing agents, which are controlled by the preparation conditions.[6] Metal NPs can be prepared by physical and chemical methods. The physical methods consist of using a low-pressure evaporation of the metal, followed by a controlled condensation in a stream of inert gas. Chemical procedures consist of the chemical reduction of metal ions to metal atoms in the presence of a stabilizer (capping agent such as citrate or thiol) that binds to their surface to impart high stability and rich linking chemistry and provide the desired charge and solubility properties. The latter preparative method is more suitable to obtain small and uniform NPs than the former; moreover, the size and uniformity of the NPs depend on the kind and amount of the reducing agent employed.[7]

NPs from metallic materials such as gold,[8] silver,[9] cobalt,[10] and platinum[11] can be synthesized. The surface plasmon absorption band can provide information of the development of the band structure in metals[12,13] and has led to a plethora of studies on the size-dependent optical properties of metal particles, particularly those of silver and gold.[14,15] The optical response of these metal NPs is both size- and shape dependent and locally variable.[16] This sensitivity to morphology makes precise control over the growth of these NPs and knowledge of their external and internal structures essential.

Table 1 Typical nanomaterials used in electroanalysis

	Size	Materials
Nanoparticles, quantum dots	1–100 nm	Metals, semiconductors, magnetic materials, ceramic oxides
Nanotubes, nanocomposites	Diameter 1–100 nm; length 1 nm – 15 μm	Metals, semiconductors, oxides, sulfides, nitrides, carbon
Nanowires	Diameter 1–100 nm; length 2 nm – 20 μm	Metals, semiconductors, oxides, sulfides, nitrides, carbon
Nanochannels, nanopores	Several square nanometers to square micrometers	Metals, oxides, carbon

Plasmonic metal NPs also show potential for biosensing[17] and cancer therapy.[18] Nanoscale shells of gold surrounding a silica core can be selectively tuned to convert near-infrared photo energy into thermal energy – nanofurnace that efficiently targets and destroys cells.[19] While some bulk metals have similar properties, only those with nanodimensions offer such tunable, and deliverable, possibilities.

During recent years, the electrochemical properties of gold NPs have been of interest for the applications to biosensing systems. The direct or indirect detection of gold NPs can be performed[20] and therefore they are used as an electrochemical label in DNA analysis[21,22] and immunoassays.[23]

QDs, also known as *semiconductor nanoparticles*, are crystalline clusters with size of few nanometers.[24] They can be synthesized from semiconductor materials such as cadmium sulfide,[25] cadmium selenide,[26] cadmium telluride,[27] gallium arsenide,[28] or indium phosphide.[29]

QDs are emerging as a new class of fluorescent labels for molecular, cellular, and in vivo imaging applications, due to their special optical properties[30,31] such as a narrow and size-tunable emission spectra,[32] broad absorption profiles, superior photostability,[33] and excellent resistance to chemical degradation or photodegradation compared to fluorescent dyes. QDs are also interesting for their electrochemical properties. They can be detected electrochemically either by dissolving with HNO_3 and liberating the metal ions[34] or by a direct detection of the QDs.[35] QDs loaded with distinguishable electrochemical properties, can be used as a ''barcode'' DNA[34] and proteins.[36]

Different kinds of techniques can be used to characterize the NPs depending on the kind of the application. Table 2 shows several characterization techniques and the parameters that can be obtained from each.

Many types of NPs of different sizes and compositions are now available, which facilitate their application in electroanalysis, bringing important advantages: (i) their immobilization on electrode surfaces generates a roughened conductive high surface area interface that enables the sensitive electrochemical detection of molecular and biomolecular analytes; (ii) NPs act as effective labels for the amplified electrochemical analysis of the respective analytes; (iii) the conductivity properties of metal NPs enable the design of biomaterial architectures with predesigned and controlled electrochemical functions.

2.2 Applications

Several applications of NPs ranging from their use for biomolecule labeling, modification of electrode surfaces, enhancement of electron-transfer, and catalysis with interest for electroanalysis are described in the following sections.

Table 2 Techniques used for nanoparticles characterization

Techniques	Characterization
Transmission electron microscopy (TEM)	Size and shape (>10 nm) Crystalline structure (poor)
High-resolution transmission electron microscopy (HRTEM)	Size and shape (>0.1 nm) Crystalline structure (poor) Crystalline lattice Microanalysis (poor)
Atomic force microscopy (AFM)	Size and shape (>0.01 nm) Size distribution
Confocal fluorescence microscopy (CLSM)	Size and shape (>100 nm) Fluorescence properties
X-ray diffraction (XRD)	Crystalline structure (exact)
Z-potential	Electrical charge Size (poor)
Electrochemical	Concentration Redox potential

2.2.1 *Labeling of Biomolecules*

The labeling of biomolecules, such as antigen, antibody, and DNA with NPs plays an increasingly important role in developing sensitive electrochemical biosensors.

Biomolecules labeled with NPs can retain their bioactivity and interact with their counterparts, and based on the electrochemical detection of those NPs, the amount or concentration of analytes can be determined.

The use of biomolecules labeled with NPs offers novel opportunities for (bio) detection systems.[37] The electrochemical detection of NPs offers highly sensitive detection alternatives besides being the easiest and cheapest technique comparing to optical detections such as fluorescence spectroscopy among others. The use of NPs as detecting labels is applied to improve the DNA and protein analysis.

2.2.1.1 DNA Analysis DNA biosensors represent a very important type of affinity biosensors in which the biorecognition molecules are oligonucleotides of known sequence and the recognition event is the hybridization with the complementary sequences.

Among the various types of DNA sensors, the electrochemical sensor has some advantage such as the use of very simple equipment to perform measurements, low cost, and possibility of miniaturization in order to obtain high-density arrays.

DNA biosensors based on DNA hybridization are playing an increasing role in DNA analysis. Some examples of DNA biosensors based on labeling with NPs are described in the following sections.

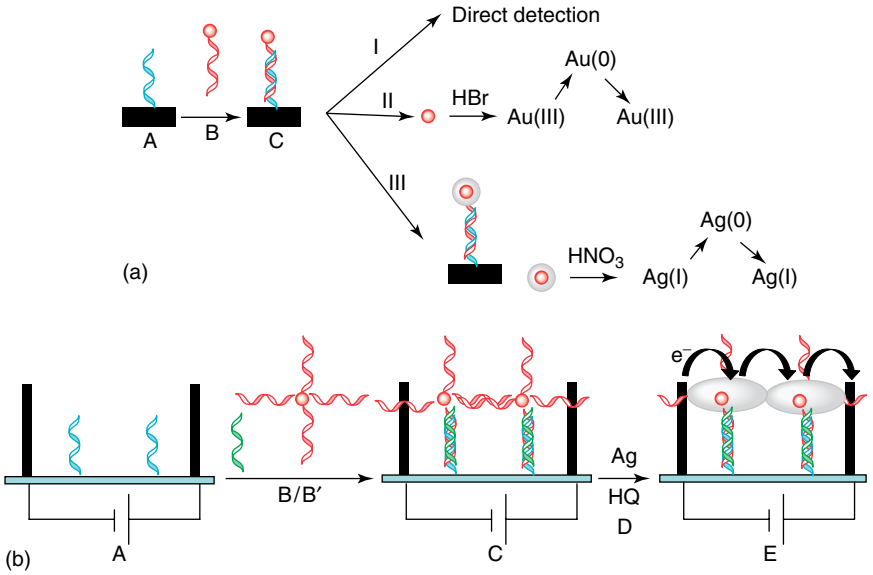

Figure 1 Detection strategies of gold nanoparticles. (a) Potentiometric/voltammetric stripping assay. The hybridization event occurs between DNA strand (A) and gold-tagged DNA (B). The gold-labeled duplex (C) formed is then detected according to each strategy: (I) direct detection of the nanoparticles onto the bare electrode without the need for tag dissolution; (II) the gold nanoparticles are dissolved with HBr/Br_2 treatment and then detected by stripping techniques; and (III) the gold nanoparticles are first covered with Ag by a deposition treatment and then detected by stripping techniques via silver enhanced signal. (b). Conductivity assay. Probe DNA immobilized in a small gap between two electrodes (A) is hybridized with DNA target (B) and then with gold-modified DNA probes (B′). Gold is accumulated in the gap (C). Silver enhancement (D) is performed in the presence of hydroquinone (HQ). The silver precipitated onto the gold nanoparticles (E) improves the sensitivity of the assay by lowering the resistance across the electrode gap.

Gold Nanoparticles Colloidal gold NPs have been used as hybridization signals in various DNA-detection assays. Both potentiometric and voltammetric stripping analysis have been used to detect gold nanoparticles following different assay alternatives (see Figure 1a).

According to the first strategy, direct detection of the nanoparticle on the bare electrode without the need of nanoparticle dissolving is performed. A DNA biosensor based on a pencil-graphite electrode and modified with the DNA target was developed following this direct detection strategy.[38] To achieve their objective, the authors covalently bound polymerase chain reaction (PCR) amplicons to a pencil-graphite electrode using carbodiimide/*N*-hydroxysuccinimide, and hybridized oligonucleotide–nanoparticle conjugates to these electrode-bound targets. Direct electrochemical oxidation of the particles was observed at a stripping potential of approximately +1.2 V.

According to the second strategy, the intrinsic electrochemical signal of the nanoparticle can be observed after dissolving it with HBr/Br_2.[39] Gold(III) ions obtained were preconcentrated by electrochemical reduction onto an electrode and subsequently determined by anodic-stripping voltammetry.

As ''tracer amplification'', silver deposition on the gold NPs after hybridization is also used and an enhanced electrochemical signal attributable to silver is obtained.[40,41] This represents the third strategy. Stripping detection is used for gold NPs/silver enhancement-related strategy.

Nevertheless, besides electrochemical-stripping techniques, other interesting methods have been reported (Figure 1b). Mirkin et al. have exploited the silver-deposition technique to construct a sensor based on conductivity measurements. In their approach, a small array of microelectrodes with gaps (20 μm) between the electrodes leads is constructed, and probe sequences are immobilized on the substrate between the gaps. Using a three-component sandwich approach, a hybridized DNA target is used to recruit gold nanoparticle-tagged reporter probes between the electrode leads. The nanoparticle labels are then developed in the silver-enhancer solution leading to a sharp drop in the resistance of the circuit.[42]

QDs and Other Nanoparticles A detection method of DNA hybridization based on labeling with CdS QD tracers followed by the electrochemical-stripping measurements of the cadmium, has been developed.[43] Nanoparticle-promoted cadmium precipitation, using a fresh cadmium solution hydroquinone, is used to enlarge the nanoparticle tag and amplify the stripping DNA hybridization signal. In addition to measurements of the

dissolved cadmium, it was demonstrated in direct "solid-state" measurements following a "magnetic" collection of a "magnetic bead/DNA hybrid/CdS tracer" assembly onto a thick-film electrode transducer. The low detection limit (100 fmol) is coupled to good reproducibility (relative standard deviation (RSD) = 6%).

Besides QDs, gold-coated iron NPs have also been used in DNA-detection assays.[44] After hybridization, the captured gold–iron NPs are dissolved and the released iron is quantified by cathodic stripping voltammetry in the presence of the 1-nitroso- 2-naphthol ligand and a bromate catalyst. The DNA-labeling mode developed offers high sensitivity, well-defined dependence on concentration, and minimal contributions from noncomplementary nucleic acids.

Electrochemical impedance spectroscopy (EIS) measurements based on CdS–oligonucleotides have been also possible, besides stripping techniques.[45] EIS was used to detect the change of interfacial electron-transfer resistance (R_{et}) of a redox marker ($Fe(CN_6)^{4^-/3^-}$) from solution to transducer surface where the DNA hybridization occurs. It was observed that, when target ssDNA-CdS nanoconjugates hybridized with a DNA probe, the R_{et} value recorded increased markedly.

Nanoparticle Carriers Polymeric microbeads carrying numerous gold-nanoparticle tags have also been used as labels for DNA in electrochemical detection procedures. The gold-tagged beads were prepared by binding biotinylated NPs to streptavidin-coated polystyrene spheres. Such carrier-sphere amplification platforms are combined with catalytic enlargement of the multiple gold tags and with the sensitive electrochemical-stripping detection of the dissolved gold tags (Figure 2a), allowing the determination of DNA targets down to the 300-amol level.[46]

SWCNTs carrying a large number of CdS QDs are used as labels for DNA detection.[47] A schematic view of the analytical protocol involving a dual hybridization event is shown in Figure 2(b).

Nanoparticles as Encoded Electrochemical Hosts The potential of current DNA-microarray technology has some limitations. Both the fabrication and readout of DNA arrays must be miniaturized to fit thousands of tests onto a single substrate. In addition, arrays must be selective enough to eliminate false-sequence calls and sensitive enough to detect few copies of a target.

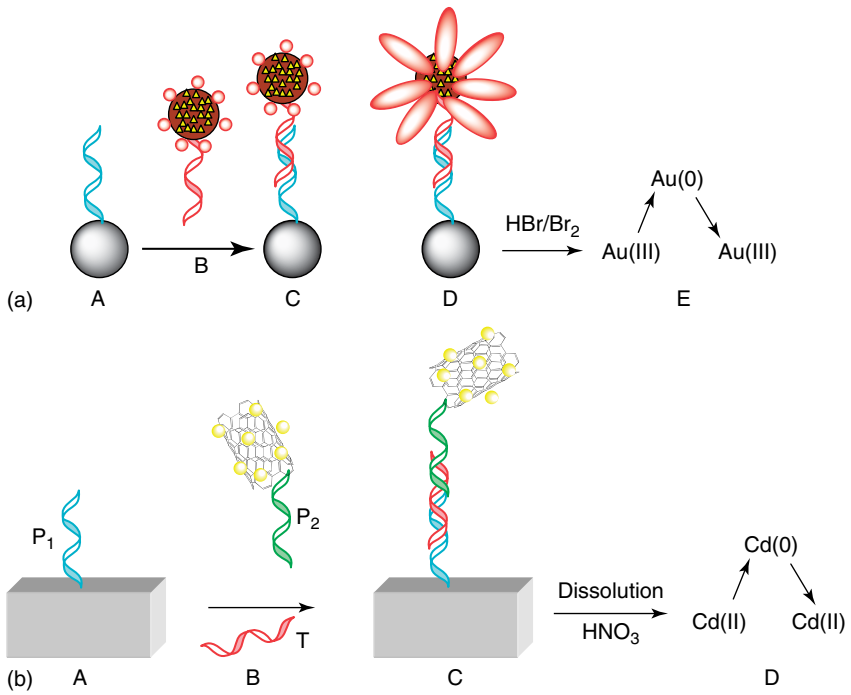

Figure 2 (a) Microparticles as nanoparticle carriers. The DNA target immobilized onto magnetic beads (A) hybridizes with the nucleic acid functionalized with Au-nanoparticle-carrier polystyrene beads (B) forming the Au-labeled hybrid (C), the tags of which are than enlarged (D), followed by magnetic separation and a dissolution process with HBr/Br_2 and then detected by stripping voltammetry (E). (b) Carbon nanotubes as carriers of QDs. The DNA probe P_1 is first immobilized onto the well of a streptavidin-assay plate (A). The DNA target (T) and the single-wall carbon nanotube (SWCNT)-CdS-labeled probe (P_2) were then added, followed by a dual hybridization event (B) forming the final CdS-tagged sandwich (C). The QDs are dissolved with 1 M HNO_3 and then detected by stripping voltammetry using a mercury-coated glassy carbon electrode (D).

NPs hold particular promise as the next generation of barcodes for multiplexing experiments. Genomic and proteomic research demand greater information from single experiments. Conventional experiments use multiple organic fluorophores to barcode different analytes in a single experiment, but positive identification is difficult because of the cross-talking signals between fluorophores.

The labeling of probes bearing different DNA sequences with different NPs enables the simultaneous detection of more than one target in a sample, as shown in Figure 3. The number of targets that can be readily detected simultaneously (without using high-level multiplexing) is controlled by the number of voltammetrically distinguishable nanoparticle markers. A multitarget sandwich hybridization assay involving a dual hybridization event, with probes linked to three tagged inorganic crystals and to magnetic beads has been reported.[34] The DNA-connected QDs yielded well-defined and resolved stripping peaks at −1.12 V (Zn), −0.68 V (Cd), and −0.53 V (Pb) at the mercury-coated glassy carbon (GC) electrode (vs the Ag/AgCl reference electrode).

Other attractive nanocrystal tracers for creating a pool of nonoverlapping electrical tags for such bioassays are ZnS, PbS, CdS, InAs, and GaAs semiconductor particles, in view of the attractive stripping behavior of their metal ions. In Table 3, the most representative examples of genosensors based on nanoparticle labels are summarized.

2.2.1.2 Protein Analysis Immunosensors and immunoanalysis are affinity ligand-based analytical tools that use antibodies as the biospecific sensing element with the immunochemical reaction coupled to a transducer. These biosensors are based on the ability of an antibody to form complexes with the corresponding antigen.[48,49]

Immunoassays are among the most specific of the analytical techniques. They provide extremely low detection limits and can be used for a wide range of substances. As research moves into the era of proteomic, such assays become extremely useful for identifying and quantifying proteins.

Immunosensors are based on immunological reactions involving the shape recognition of the antigen (AG) by the antibody (AB)-binding site to form the AB/AG stable complex:

$$AB + AG \leftrightarrow AB/AG \qquad (1)$$

Immunoassays, based on the specific reaction of ABs with the target substances (AGs) to be detected, have been widely used for the measurement of targets at low concentration in clinical samples such as urine and blood and the detection of the trace amounts of drugs and chemicals such as pesticides in biological and environmental samples.

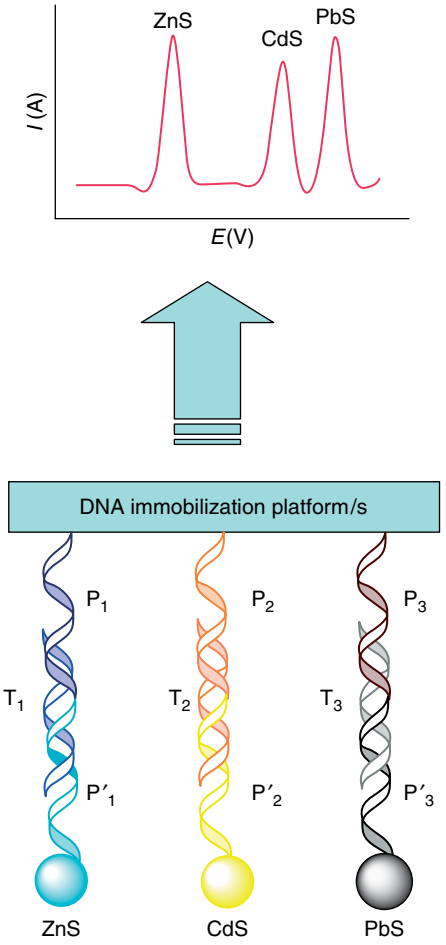

Figure 3 Schematic of multiple detection of DNA. DNA probes (P'_1, P'_2 and P'_3) bearing different DNA sequences with different nanoparticles (ZnS, CdS, and PbS, respectively) that enable the simultaneous detection of three DNA targets (T_1, T_2, and T_3) hybridized with corresponding DNA-capturing probes (P_1, P_2, and P_3) immobilized onto a direct or an indirect (magnetic particles) transducing platform.

Metalloimmunoassay (immunoassay involving metals) has been developed and extended later on to the use of a variety of other metal-based labels such as colloidal metal particles.[50] One of the first electroanalytical procedures adopted in NP-based immunosensors, consisted of the dissolution of the NP labels – mostly metal and semiconductor NPs – and the measurement of the dissolved ions with stripping voltammetry, which already represents a very powerful electrochemical technique for trace-metal analysis.[51]

For example, Limoges et al.[52] reported a sensitive electrochemical immunoassay for goat immunoglobulin G (IgG) based on a AuNP label. The primary donkey antigoat IgG was immobilized on a microwell surface and

Table 3 Details on some genosensors based on nanoparticles used as labels

Nanoparticle label	Label connection with DNA	Detection technique	Hybridization separate from detection	DNA-detection limit	RSD	Reference
Au	Au-SH-DNA	DPV at pencil graphite electrode	No	0.78 fmol ml^{-1}	≈8%	38
Au	Au-SH-DNA	PSA and silver catalytic enhancement at screen-printed electrodes	Yes	150 pg ml^{-1}	7%	40,41
Au	Au-SH-DNA	Conductivity at microelectrodes	No	500 fM		42
Au carried into PVC beads	PVC(Au) streptavidin–biotin-DNA	PSA and silver catalytic enhancement at screen-printed electrodes	Yes	40 pg ml^{-1}	13%	46
CdS QDs	CdS NH-DNA	EIS with gold electrode	No	1.43×10^{-10} M		45
CNTs loaded with CdS QDs	CNT-CdS-streptavidin–biotin-DNA	DPV at Hg-film electrode	Yes	40 pg ml^{-1}	6.4%	47
Au–Fe (core/shell)	Fe–Au-SH-DNA	DPV at Hg-film electrode	Yes	50 ng ml^{-1}	6.3%	44
CdS QDs	CdS-SH-DNA	PSA and catalytic enhancement with Cd at screen-printed electrodes	Yes	20 ng ml^{-1}	6%	43
CdS QDs	CdS-SH-DNA	Simultaneous detection with SWV at Hg-film electrode	Yes	5 ng ml^{-1}	9.4%	34
PbS QDs	PbS-SH-DNA	–	–	–	–	–
ZnS QDs	ZnS-SH-DNA	–	–	–	–	

PSA, potentiometric stripping analysis; DPV, differential pulse voltammetry; SWV, square wave voltammetry; EIS, electrochemical impedance spectroscopy.

interacted with the goat IgG to be determined, and then AuNP-labeled donkey antigoat IgG was added to the conjugate. The immunocomplex was treated with acidic bromine–bromide solution resulting in the oxidative dissolution of the AuNPs. The solubilized gold ions were then electrochemically reduced and accumulated on the electrode and subsequently detected by anodic-stripping voltammetry using carbon-based screen-printed electrodes (SPEs). The combination of the sensitive detection of Au ions with anodic-stripping voltammetry and the release of a large number of Au ions upon the dissolution of AuNPs associated with a single recognition event provides an amplification path that allowed the detection of the goat IgG at a concentration of 3 pM.

As an alternative to AuNPs, inorganic nanocrystals have been used with the advantage of having an electrodiverse population of electrical tags as needed for designing electronic coding. A multitarget electronic detection of proteins was demonstrated by Liu et al.[36] using different inorganic nanocrystal tracers. Three encoding NPs (zinc sulfide, cadmium sulfide, and lead sulfide) were used to differentiate the signals of three protein targets in connection with a sandwich immunoassay and stripping voltammetry of the corresponding metals (Figure 4). Each binding thus yielded a distinct voltammetric peak, whose position and size reflected the identity and level of the corresponding antigen, respectively.

Libraries of electrical codes have been created by encapsulating different predetermined levels of multiple inorganic nanocrystals into polymeric carrier beads or depositing various metal tracers onto the pores of a host membrane. The resulting voltammetric signatures reflect the predetermined proportions of the corresponding metals in such ''identification'' nanomaterials.[53]

Since the sensitivity of such electrical (stripping-based) bioassays depends on the size of the metallic tag, a dramatic amplification of the signals is expected using larger tracers. For example, a substantial sensitivity enhancement can be achieved by using the metal nanosphere tags as catalytic labels for subsequent enlargement and further amplification. A catalytic enlargement of an AuNP tracer was achieved by the precipitation of metal gold promoted by the NP itself[54] or by the precipitation of metal silver induced by hydroquinone.[55] Combining such enlargement of the metal particle tracers with stripping voltammetry paved the way to subpicomolar detection limits. A triple-amplification bioassay, using polymeric spheres (PS) (loaded with numerous

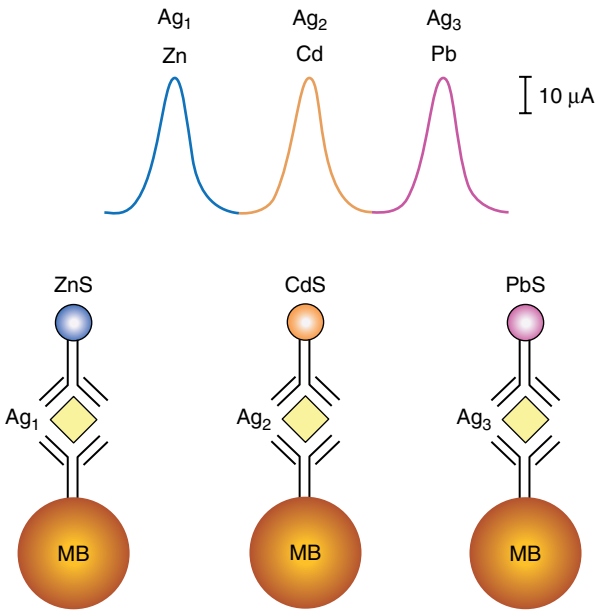

Figure 4 Multiantigen immunoassay based on different inorganic nanocrystal tracers. Each binding yields a distinct voltammetric peak, whose position and amplitude reflects the identity and concentration of the corresponding antigen. (Adapted from Ref. 53. © American Chemical Society, 2003.)

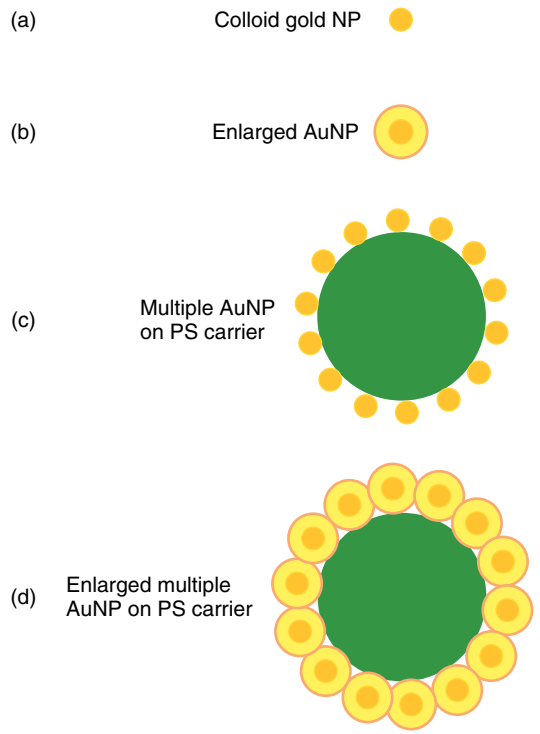

Figure 5 Generations of amplification platforms for bioelectronic detection based on AuNP tracers: (a) a single NP tag; (b) catalytic enlargement of the NP tag; (c) polymeric carrier sphere (PS) loaded with numerous AuNP tags; (d) catalytic enlargement of multiple tags on the carrier sphere. (Adapted from Ref. 56. © Wiley-VCH, 2004.)

AuNP tags) has also been demonstrated.[56] Such an enlargement of numerous gold nanoparticle tags (on a supporting sphere carrier) represents the fourth generation of amplification (Figure 5), starting with the early use of single AuNP tags.

The use of metal NP labels coupled with electroanalytical stripping analysis has resulted in several advantages for immunoassays. However, the need to dissolve the metallic labels by means of acidic bromine–bromide solution, or concentrated acidic solution, represents a distinct disadvantage. These solutions are toxic, dangerous, and difficult to handle and hence limit the use of these systems.

Direct detection of NPs consists of a so-called solid-state analysis, where the metals forming the NPs are detected electrochemically without any preliminary dissolution step to liberate the metal ions in solution. However, this type of detection needs a direct contact between the electrode surface and the metal itself and excludes from detection a large portion of nontouching particles. Despite the loss of sensitivity that could result from this phenomenon, in comparison with techniques exploiting the total NPs dissolution and all metal ions detected, direct detections achieve more rapid responses and still considerable limit of detections.

Solid-state detection of NPs has been applied in numerous immunoassays analysis exploiting the intrinsic electrochemical properties of the metal NPs used as tracers. Ambrosi et al. recently used magnetic particles as platform to perform the immunological interactions. After the specific interaction with the secondary NP-labeled antibody, these magnetic particles were collected onto the electrode surface by means of a permanent magnet inserted inside the electrode body. Differential pulse voltammetry (DPV) analyses were performed to quantify the metal NPs collected through the biospecific interaction and that are related to the target analyte concentration (protein). Very low limits of detection were achieved using this magnetic particle collection, reaching the lowest value of 260 pg mL^{-1} human IgG protein.[57]

The catalytic features of metal NPs that enable the electroless deposition of metals on the NP clusters allows the enlargement of the particles to conductive interparticle-connected entities. The formation of conductive domains as a result of biorecognition events provides an alternative path for the electrical transduction of biorecognition events. This was exemplified by the design of a miniaturized immunosensor based on AuNPs and their catalytic properties (Figure 6). Latex particles that were stabilized by an anionic protective layer were attracted to a gap between micron-sized Au electrodes upon the application of a nonuniform alternating electric field between the electrodes (dielectrophoresis). Removal of

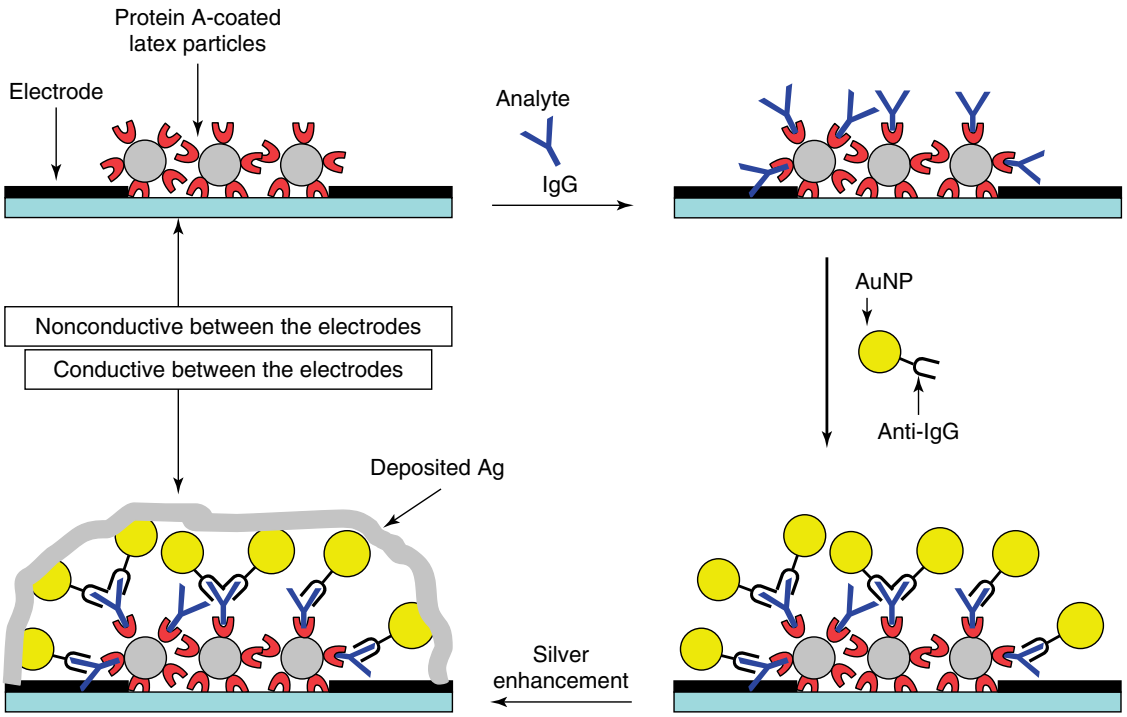

Figure 6 Immunosensing at microsized Au electrodes by the change of conductivity between the Au strips upon the binding of AuNPs and the deposition of silver. (Adapted from Ref. 58. © American Chemical Society, 1999.)

the protective layer from the latex particles by an oppositely charged polyelectrolyte resulted in the aggregation of the latex particles and their fixation in the gap domain. Adsorption of protein A on the latex surface yielded a sensing interface for the specific association of the human IgG antigen. The association of human IgG on the surface was probed by the binding of the secondary AuNP-labeled antihuman IgG antibodies to the surface, followed by the catalytic deposition of a layer of Ag on the AuNPs. The Ag layer bridged the gap between the two microelectrodes to result in a conductive "wire". Typical resistances between the microelectrodes were 50–70 Ω, whereas control experiments conducted without the specific catalytic enlargement of the domain by the AuNP–antibody conjugate yielded resistances $>10^3$ Ω. The method enabled the analysis of human IgG with a detection limit of about 0.2 pM.[58]

Normally, electrochemical immunosensors or immunoassays exploiting NP labels are based on the final detection of the NP itself. Therefore, the preparation and application of "special" NP labels is of great importance. Composite NPs with special components, for example, a core-shell NP with a shell suitable for labeling and a core containing special materials that can be sensitively detected with electrochemical methods, may play an important role in developing novel ultrasensitive methods.

2.2.2 *Modification of Electrode Surfaces*

Owing to their large specific surface area and high surface-free energy, NPs can adsorb biomolecules strongly and once introduced onto the surface of a proper transducer would play an important role in the immobilization of biomolecules and consequently improve the biosensor performance. Generally, the adsorption of biomolecules directly onto naked surfaces of bulk materials may frequently result in their denaturation and loss of bioactivity. However, the adsorption of such biomolecules onto the surfaces of NPs can retain their bioactivity. Having comparable dimensions, biomolecules conjugated to NPs maintain the natural conformation/structure and hence the functionality.

Figure 7 is a schematic that show three different mechanisms that can be used to functionalize NPs with biomolecules:

1. electrostatic adsorption
2. chemisorption of thiol derivatives
3. specific affinity interactions.

Different alternatives used for coupling NPs with antibodies, enzymes, and oligonucleotides are reviewed in the following sections.

2.2.2.1 Immobilization of Antibodies AuNPs are certainly the most exploited for enhancing the

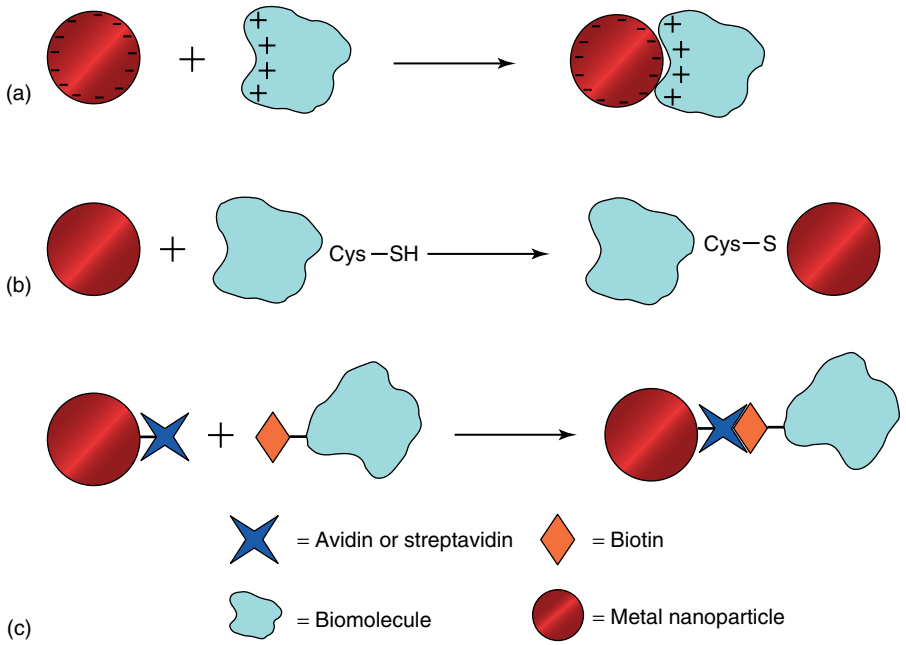

Figure 7 Schematic of different strategies used to couple NPs with biomolecules. (a) Electrostatic interaction of biomolecules with metal nanoparticles; (b) covalent interaction of biomolecules through thiol groups with metal nanoparticles; (c) bioconjugation of metal nanoparticles by the use of bioaffinity interactions upon (strept)avidin–biotin binding.

immobilization of antibodies or antigens in proximity to the electrode surface with, in most of the cases, improvement in stability. One approach consists of assembling a monolayer of AuNPs on the electrode surface, where antibodies can be electrostatically attached without loss of activity.

An amperometric immunosensor for *Schistosoma japonicum* antigen (SjAg) assay based on nanosize particulate gold (nano-Au) monolayer as a sensing platform was proposed by Lei et al.[59] The nano-Au monolayer was obtained through a chitosan-entrapped carbon paste electrode (CCPE). The high affinity of chitosan for nano-Au associated with its amino groups facilitated the formation of a nano-Au monolayer on the surface of the CCPE. A sequential competitive immunoassay format was performed on the CCPE-supported nano-Au monolayer using *S.japonicum* antibody (SjAb) and SjAg as a model system. The assay consisted of first loading SjAb on the nano-Au monolayer, then blocking with a bovine serum solution (BSA), followed by a competitive incubation in the buffer containing the SjAg (analyte) and SjAg labeled with horseradish peroxidase (HRP), and finally amperometric detection with hydroquinone as an enzymatic substrate. The dynamic concentration range for SjAg assay was 0.11–22.4 $\mu g\,ml^{-1}$ with a detection limit of 0.06 $\mu g\,ml^{-1}$. The feasibility of regenerating the nano-Au monolayer for consecutive assays was demonstrated by a simple chemical treatment after each determination. The simple construction of the nano-Au monolayer and the improved sensitivity were main features of the proposed immunosensing method.

A similar approach was followed by Li et al.,[60] who have recently developed a reusable capacitive immunosensor based on 1,6-hexanedithiol (HDT) and colloidal gold layers. The organic monolayer film was first formed by the spontaneous assembly of HDT from solution onto a gold electrode. When these thiol-rich surfaces were exposed to gold colloid, the sulfides formed strong bonds with AuNPs, anchoring the clusters to the electrode substrate. After the assembly of the AuNPs layer, the antibody could be immobilized through electrostatic adsorption between nano-Au and the antibody proteins. After use, the formed immunocomplex layer could be rinsed out via a saline solution with extreme pH. The use of AuNPs in these types of immunosensor developments has certainly brought advantages with respect to classical immunoassays employing covalent immobilization of the antibodies. However, the need for regenerating the sensing surface after each measurement still represents the main drawback for a practical analytical application of this type of immunosensor. The assay procedure consists of complex operations that require specialized operators.

Another approach was based on using membranes[61,62] or solgel composites[63,64] to entrap AuNPs and biomaterials. In all these systems, the presence of AuNPs improved the conductivity of the composite and enhanced the stability and sensitivity of the sensor owing to a higher

attachment surface availability for the biomolecules. Silica NPs do not possess conductive properties. However, due to the porosity of the material, they exhibit a very high surface area and therefore they are usually used to immobilize biomolecules. A higher number of biological molecules can be attached with a very stable interaction resulting in enhanced sensor performance.[65]

2.2.2.2 Immobilization of Enzymes In the early 1990s, Crumbliss et al. immobilized several kinds of enzymes with gold NPs and further fabricated different enzyme electrodes with retained enzymatic activity.[66] Chen et al. first attached gold NPs to gold electrodes modified with cysteamine monolayer, and then successfully immobilized horseradish peroxidase on these NPs.[67] They also studied the effect of nanoparticle size on the performance of the prepared biosensors. NPs with smaller size were found to be more suitable for enzyme immobilization.

Many similar studies have been reported for the construction of biosensors based on the immobilization of different enzymes such as horseradish peroxidase,[68,69] microperoxidase-11,[70] tyrosinase,[71] and hemoglobin[72] with gold NPs. SiO_2 NPs are also excellent matrices for enzyme immobilization because of their good biocompatibility and easy preparation. Hu et al. immobilized several heme proteins with SiO_2 NPs through the layer-by-layer assembly,[73] and investigated the driving forces for the assembly procedure.[74] Other NPs, such as Pt, Ag,[75] TiO_2, ZrO_2 NPs, and so on, can also be used for the immobilization of enzymes.

The electrostatic deposition of biomolecules, particularly proteins or enzymes, can also be extended to multilayer-level assemblies.[76] Proteins that are electrostatically attracted to the charged NPs can provide an interface for the further deposition of an oppositely charged polyelectrolyte polymer, which again allows the deposition of a secondary protein layer. Multilayer films of glucosidase,[77] glucose oxidase (GOX),[78] urease,[79] and HRP[80] have been assembled on polystyrene NPs by the alternate deposition of the proteins and an oppositely charged synthetic polyelectrolyte as a linker, e.g. positively charged poly(diallyldimethylammonium) chloride or negatively charged poly(sodium 4-styrenesulfonate). The protein/polymer multilayer shell could be varied from several to hundreds of nanometers in thickness. This strategy permits the preparation of functional films on NPs with a high density of enzyme molecules.

Chemisorption of proteins onto AuNP surface can originate from the binding of thiol groups from cysteine residues that exist in the proteins to the Au surface. If no thiolated residues are available in the native proteins, thiol groups can be incorporated by chemical means; for example, with 2-iminothiolane[81] or through genetic engineering.[82] For example, the immobilization of endoglucanase enzyme onto AuNPs through the covalent bonds formed between the Au atoms and the cysteine residues of the protein has been reported.[83]

2.2.2.3 Immobilization of Oligonucleotides The chemistry of biomolecules attached to NPs has a significant impact on their use in the analytical detection scheme. NPs functionalized in different ways have, for example in the case of their use in DNA detection, different oligonucleotide surface densities, different availability for hybridization to targets, and different tendencies to bind nonspecifically to surfaces.[7]

In order to immobilize oligonucleotides onto the surfaces of NPs, the DNA strands are often modified with special functional groups that can interact strongly with certain NPs. Fang and coworkers immobilized the oligonucleotide with a mercaptohexyl group at the 5′-phosphate end onto the 16-nm diameter gold NPs, which were self-assembled on a cysteamine-modified gold electrode and discovered that the saturated immobilization quantities of single-strand DNA on the modified electrode were about 10 times larger than that on a bare gold electrode.[84]

Thiol-functionalized oligonucleotides stick strongly to gold surfaces. The attachment via thiol linkage to nanocrystals is much stronger and more efficient than nonspecific adsorption. Unfortunately, the number of oligonucleotides attached per nanoparticle cannot be directly controlled. However, gold nanocrystals with a controlled number of attached oligonucleotides can be isolated using gel electrophoresis. In addition, the gold NPs can be connected selectively with one oligonucleotide. Nanogold maleimide was used in that case and connected with a thiolated DNA.[85]

AgNPs were also used to immobilize mercapto oligonucleotides to a thiol-containing solgel network-modified electrode.[86] The immobilization of DNA with silica NPs was also studied, obtaining enhanced analytical performances.[87]

2.2.3 Nanoparticles as Enhancers of Electron Transfer

The electrical contacting of redox enzymes with electrodes is a key process in the design of enzyme electrodes for bioelectronic applications such as biosensors,[88] or biofuel cell elements.[89] Enzymes usually lack direct electrical communication with electrodes due to the fact that their active centers are surrounded by considerably thick insulating protein shells, which, therefore, block the direct electron transfer. The conductive properties of NPs – mostly metal NPs at nanoscale dimensions – make them suitable for enhancing the electron transfer between

the enzyme active centers and electrodes, thus acting as ''mediators'' or ''electrical wires''.

Biocatalytic electrodes for biosensor applications have been prepared by the codeposition of redox enzymes/proteins and AuNPs on electrode supports.[90,91] In one example, direct electron transfer between hemoglobin and a GC electrode was facilitated by lipid-protected AuNPs. The biocatalytic electrodes were reported to operate without electron-transfer mediators. However, the random and nonoptimized positioning of the redox proteins on the conductive NPs did not allow efficient electron transfer between the active sites of the enzyme and the electrode support. Highly efficient electrical contacting of the redox enzyme GOX through a single AuNP was demonstrated by Willner et al.[92] They reconstituted the apo-flavoenzyme, apo-glucose oxidase (apo-GOX), on a 1.4-nm AuNP that was functionalized with N^6-(2-aminoethyl)flavin adenine dinucleotide (FAD cofactor, amine derivative). The resulting conjugate was assembled on a thiolated monolayer by using different dithiols as linkers. Alternatively, the FAD-functionalized AuNP could be assembled on a thiolated monolayer associated with an electrode, and apo-GOX was subsequently reconstituted on the functional NPs. The enzyme electrodes prepared by these two routes revealed similar surface coverages of about 1×10^{-12} mol cm^{-2} of the protein. The NP-reconstituted GOX layer was found to be electrically contacted with the electrode without any additional mediators, and the enzyme assembly stimulated the bioelectrocatalyzed oxidation of glucose. The resulting NP-reconstituted enzyme electrodes revealed unprecedented electrical communication efficiency with the electrode showing an electron-transfer turnover rate of about 5000 s^{-1}, nearly 7 times faster than that between GOX and its natural substrate, oxygen.

The electron transfer between other redox proteins and electrodes has also been revealed with the help of AuNPs. For example, Wang et al. self-assembled AuNPs onto a three-dimensional silica gel network-modified gold electrode, and obtained the direct electrochemistry of cytochrome c. These AuNPs acted as a bridge to transfer electrons between protein and electrode.[93] AgNPs, as well as AuNPs, have good conductivity, and they can also be used to enhance the electron transfer between enzymes and electrodes. Li et al. assembled AgNPs onto pyrolytic graphite electrodes, and then immobilized cytochrome c on these NPs. It was reported that AgNPs act as the electrical bridge that ''wires'' the electron transfer between cytochrome c and the electrode, and the electron-transfer rate constant was about 15.8 s^{-1}.[94] Some nonmetal NPs, such as oxide NPs and semiconductor NPs, can also enhance the electron transfer between enzymes and electrodes in certain systems. For instance, HRP was mixed with TiO_2 NPs and immobilized onto pyrolytic graphite electrodes, which resulted in direct electron transfer.[95] Hemoglobin, immobilized with ZrO_2 NPs, also exhibited direct electrochemistry at pyrolytic graphite electrodes and could be used for constructing mediator-free biosensors.[96] Other oxide NPs such as Fe_3O_4[97] and MnO_2[98] NPs have also been used to immobilize enzymes and enhance their direct electrochemistry. Recently, the application of semiconductor NPs for the enhancement of electron transfer between redox proteins and electrode surfaces has been reported. Hemoglobin and CdS NPs were mixed and immobilized onto pyrolytic graphite electrodes, and the immobilized hemoglobin exhibited direct electrochemistry. In fact, the effective enhancement of electron transfer was dependent not only on the conductivity of NPs but also on the arrangement between NPs and biomolecules.[99] It is believed that creating defined and ordered arrangements of NPs using nanotechnology is a promising approach to the construction of biosensors with greatly enhanced electron-transfer properties.

3 CARBON NANOTUBES

3.1 General Properties

The discovery in 1985 of buckminsterfullerene opened a new era for the chemistry of carbon and for novel materials. Sumi Ijima, the Japanese physicist, discovered nanotubes in 1991.[100] The CNTs have generated great interest for various applications based on their field emission and electronic transport properties, their high mechanical strength, and their chemical properties.[100] From this arises an increasing potential for use as field-emission devices,[101] nanoscale transistors,[102] tips for scanning microscopy,[103] or components for composite materials.[104]

In this context, CNT are particular nanomaterials that have generated a considerable interest owing to their unique structure-dependent electronic and mechanical properties.[105]

CNTs can be divided into single-wall carbon nanotubes (SWCNT) and multiwall carbon nanotubes (MWCNT)[106] (Figure 8). SWCNT (Figure 8a) possess a cylindrical nanostructure formed by rolling up a single graphite sheet into a tube. SWCNT can thus be viewed as molecular wires with every atom on the surface. MWCNT (Figure 8b) comprise of an array of such nanotubes that are concentrically nested like rings of a tree trunk.[107]

CNTs are one of the most commonly used building blocks of nanotechnology. With 100 times the tensile strength of steel, thermal conductivity better than all but

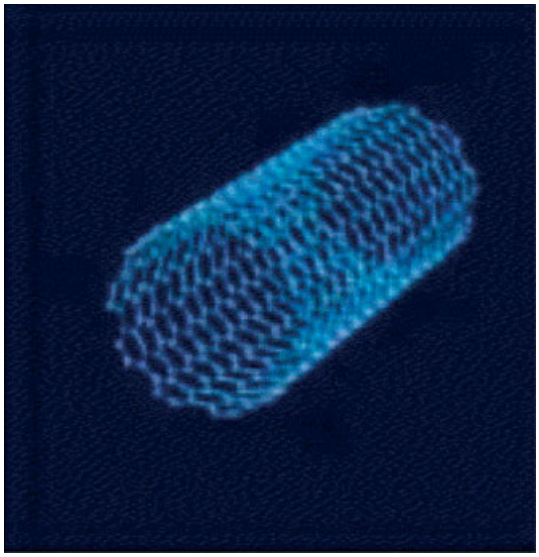

(a)

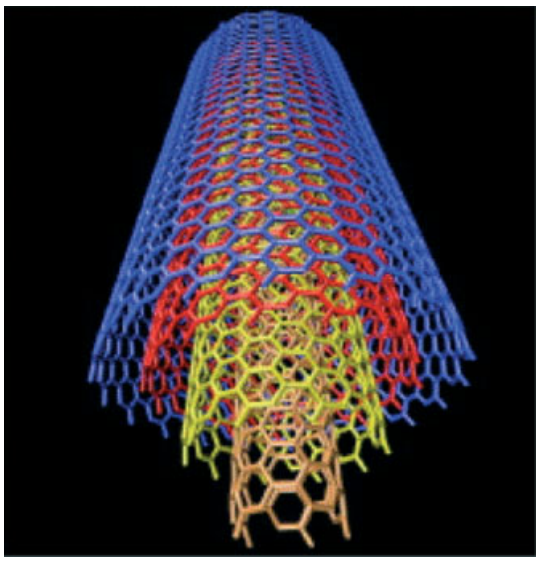

(b)

Figure 8 Schematics of an individual (a) SWCNT and (b) MWCNT. (Adapted from Ref. 106. © Elsevier, 2005.)

the purest diamond, and electrical conductivity similar to copper, but with the ability to carry much higher currents, CNTs seem to be a wonder material.

3.1.1 Production of Carbon Nanotubes

There are several methods to form CNTs: arc method, laser methods, chemical vapor deposition (CVD), etc. However, in order to use CNTs in novel devices, it is necessary to produce these materials with a high crystallinity on a large scale economically. In this context, the catalytic CVD method is considered to be the optimum for producing large amounts of CNTs, particularly with the use of a floating-catalyst method.[108] This technique is more controllable and cost efficient when compared with arc-discharge and other methods.

3.1.2 Purification of Carbon Nanotubes

Extensive research has been dedicated to the purification of CNTs in order to remove foreign NPs that modify the physicochemical properties of CNTs.

Chemical methods have been applied for purifying CNTs. SWNT purification developed by Smalley and coworkers[109] consists of refluxing as-grown SWNTs in nitric acid solutions. Subsequently, more-effective purification techniques have been developed with minor physical damage of the tubes.[110–112] The other method was reported by Martinez et al.[113] and consists in a technique of high-temperature air oxidation in conjunction with microwave acid treatments, for removing a high portion of metal particles in relatively short periods of time. The most effective methods for MWNTs purification are high-temperature treatments in an inert atmosphere (graphitization or annealing) and removing structural defects (heptagons and heptagon–pentagon pairs) or impurities such as metallic compounds.[114]

3.1.3 Dispersion of Carbon Nanotubes

Before certain applications CNTs must be transformed to a ''soluble'' product. The preparation of homogeneous dispersions of CNTs, suitable for their use in thin films or for other applications, is of a great importance. Various methods can be used for this purpose. End[115] and/or sidewall[116] functionalization, use of surfactants with sonication,[117] polymer wrapping of nanotubes,[118–120] and protonation by superacids[121] have been reported. Although these methods are quite successful, they often indicate cutting the CNTs into smaller pieces (sonication and/or functionalization), thus partly losing the high aspect ratio of SWCNTs.

Kim et al.[122] provided an example of CNT solubilization. They developed a simple, efficient process for solubilizing CNTs with amylose in dimethyl sulfoxide–H_2O (DMSO–H_2O) mixture as well as in pure water. This process requires two important conditions, presonication of CNTs in water and subsequent treatment of the fine CNT dispersion with amylose in a specified DMSO–H_2O mixture, followed by a postsonication. The best solvent composition was found to be 10–20% DMSO, in which amylose assumes an interrupted loose helix. The resulting colloidal solution was stable and exhibited no precipitation over several weeks.

CNT solubilization by covalent modification was reported by Luong et al.[123] MWCNTs were solubilized in

a mixture of 3-aminopropyltriethoxysilane (APTES) and Nafion-perfluorinated ion-exchange resin and ethanol. Uniformly dispersed MWCNTs were obtained after 20 min sonication and used for sensor applications.

3.2 Applications

CNTs have a wide range of properties that we are still in process of discovering with an ambitious variety of applications. In this case, we focus on the application of CNT-modified electrodes in bioelectroanalysis, which mainly includes electrochemical studies on neurotransmitters, proteins, nucleic acids, and other molecules.

In recent years, CNT-modified electrodes show the properties of electrocatalytic activity due to its unique electronic properties and CNTs can promote electron-transfer reactions,[124] which can be applied for the detection of analytes in a low concentration or in the complex matrix. The CNT-modified electrodes usually include CNT paste electrode,[125] CNT coating electrode,[126] or CNT embedded in a polymeric matrix.[127] Generally, CNT-modified electrodes contain an electrochemical analysis and biosensor applications.[128,129]

3.2.1 *Modifications of Electrodes Surfaces*

The derivatization of carbon surfaces allows electrochemists to design tailor-made electrodes, which offer distinct advantages for catalysis, analysis and biological applications, and the area of electrochemistry has attracted considerable attention over the last few years,[130] it has aroused great interest in modifying electrode surfaces, for example Pérez et al. integrated CNTs onto a GC electrode and use this for reduced nicotinamide adenine dinucleotide (NADH) detection. The use of polyvinyl chloride (PVC) as a matrix for CNTs dispersion aimed to ensure better mechanical/robustness properties of the sensor membrane compared to an unmodified GC electrode. Additionally, with the use of glutaraldehyde (GA) as a matrix linker, their design offer future alternatives for biosensors applications due to the ability of the developed design to aid in covalent binding of biological molecules[127] (Figure 9).

3.2.2 *Carbon Nanotubes as "Carriers/Amplifiers"*

A strategy for dramatically amplifying enzyme-linked electrical detection of proteins and DNA using CNTs as carrying enzymes has been developed by Wang et al.,[131] amplifying electrical detection and producing an ultrasensitive bioelectronic detection of DNA hybridization. First, the alkaline phosphatase (ALP) enzyme tracer was immobilized on CNTs using 1-ethyl-3-(3-dimethyl aminopropyl) carbodiimide as linker. Following this, they realize a capture of the ALP-loaded CNT tags to the streptavidin-modified magnetic beads by a sandwich DNA hybridization or antibody–antigen–antibody (Ab–Ag–Ab) interaction (Figure 10).

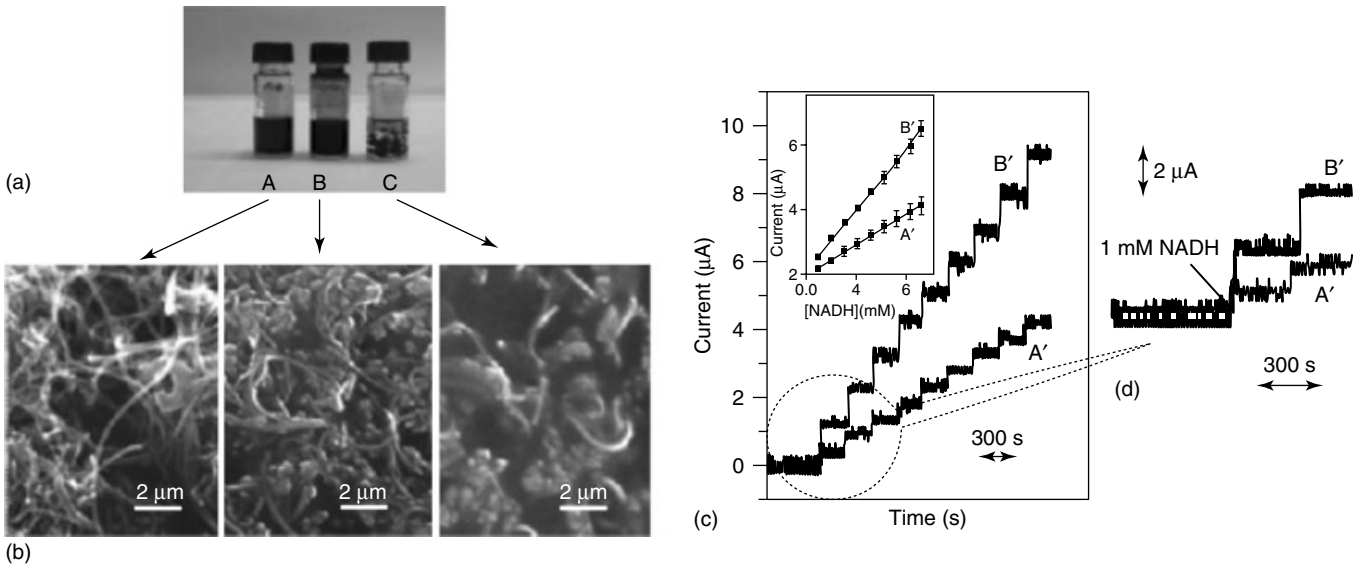

Figure 9 (a) Images of the MWCNTs in tetrahydrofuran (THF) (A), THF+PVC (B), and in THF+PVC+GA solution (C). (b) Scanning electron microscope (SEM) images of the same solutions as in the upper images. (c) Current – time recordings including (as inset) the corresponding calibration plots obtained from amperometric experiments at unmodified (A′) and at modified (B′) GC electrode for successive additions of 1 mM NADH in 0.1 M phosphate buffer pH 7. Working potential: +0.7 V. (d) The stability of the response (as zoom of the recordings in (c)) is shown for each electrode used. (Adapted from Ref. 127. © Wiley-VCH, 2008.)

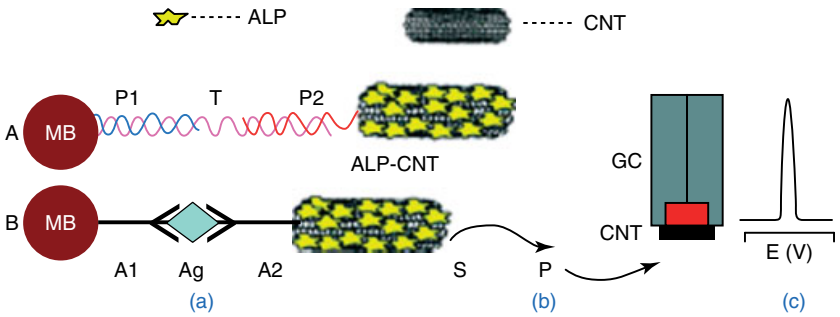

Figure 10 Schematic representation of the dramatic signal enhancement associated with the CNT-based dual amplification route for DNA hybridization (A) and Ag–Ab (B) bioassays (a); (b) enzymatic reaction; (c) electrochemical detection of the product of the enzymatic reaction at the CNT-modified glassy carbon electrode. (Adapted from Ref. 131. © American Chemical Society, 2004.)

Such coupling of several CNT-derived amplification processes results in highly sensitive detection of proteins and DNA and hence indicates great promise for PCR-free DNA assays and for assembling controllable nanoscale systems.

The loading of multiple peroxidase enzyme tracers onto CNTs "carriers" has recently been exploited by Rusling's team for highly sensitive immunodetection of cancer biomarkers in serum and tissue lysates.[132]

3.2.3 *Carbon Nanotube-based Composites*

Nanocomposites represent the first major commercial application of the MWCNTs. CNTs can be mixed with a wide range of polymeric matrices. By mixing CNTs with poly(methyl methacrylate) (PMMA), a nanocomposite PMMA/CNT with improved mechanical properties is obtained.[133] In case of working with doped polyaniline/MWCNT composites, conductivities arise 60–70% compared to the polymer nonmodified with MWCNT.[134]

Carbon nanotube epoxy-composite (CNTEC) electrode has been fabricated and characterized by our group.[135] CNTEC electrodes have been produced by loading the epoxy resin, before curing, with MWCNTs of different lengths. On the basis of the electrochemical reversibility and sensitivity studies, it was found that the electrodes containing 20% (w/w) CNT represent the optimal composition. The behavior of CNTEC electrodes has been compared with that of conventional graphite epoxy-composite (GEC) electrode. It was found that long-MWCNT (0.5–200 μm)-based epoxy-composite electrodes show strong electrocatalytic activity toward NADH and hydrogen peroxide while short-MWCNT (0.5–2 μm)-based epoxy composites show similar oxidation potential as GEC electrode for both NADH and H_2O_2. In both cases, CNTEC electrodes provide better reversibility, peak shape, sensitivity, and stability when compared to GEC electrode. The CNTEC material is more robust in terms of mechanical strength compared to CNT paste or Teflon composite reported previously. The new CNT composite indicates that it may become a new class of smart material with unique properties and applications. The resulting CNTEC electrode may offer great promise for biosensing by incorporating biomolecules, such as enzymes, antibodies, or DNA in the CNT/epoxy composite. Research in this direction is in progress in our laboratory.

3.2.4 *Use of a Single Carbon Nanotube*

Characteristics and different properties related to the structure of SWCNT are decisive for their applications in (bio)sensors. First, depending on the direction, the graphite sheet is rolled to form the CNT – a metallic or semiconducting character of the SWCNT will dominate. Impurities and defects in SWCNT are other important aspects closely related to its electrochemical activation that have to be considered.

High aspect ratio and large surface area of SWCNT are generally associated with its application in the performance of more sensitive sensors. Sensitivity of SWCNT to dopants and other substances cause dramatic changes in the electrical resistance of the semiconducting SWCNT.

The ammonia sensor[136] represents an interesting application of SWCNT via its use in a chemiresistor design. SWCNTs were chemically functionalized with poly-(*m*-aminobenzene sulfonic acid) (PABS) showing the possibility of having a very sensitive and reversible sensor. The reversibility is controlled by doping/dedoping PABS at room temperature.

4 NANOWIRES

4.1 General Properties

Nanowires are attractive materials because of their small size, high surface-to-volume ratios, and/or electronic,

optical, and magnetic properties, which can differ markedly from those observed for bulk or thin film materials as the nanowire cross-sectional diameter decreases. Because of the high surface-to-volume ratio and novel electron transport properties of these nanostructures, their electronic conductance is strongly influenced by minor surface perturbations (such as those associated with the binding of macromolecules). Such 1D materials thus offer the prospect of rapid (real-time) and sensitive label-free bioelectronic detection, and massive redundancy in nanosensor arrays. Metal and conducting polymer nanowires can be readily prepared by a template-directed electrochemical synthesis involving electrodeposition into the pores of a membrane template.[137]

Nanowires show promise in a number of different sensing strategies, including optical,[138] electrical,[139] electrochemical,[4] and mass-based[140] approaches.

Recent results suggest the possibility of incorporating large numbers of nanowires into large-scale arrays and complex hierarchical structures for high-density biosensors, electronics, and optoelectronics.[141]

4.2 Application of Nanowires to Field-effect Transistors

Semiconductor nanowire-based field-effect transistors (FETs) are an exciting new route to ultrasensitive electrical detection of biomolecular interactions.[142] In these devices, conductance is monitored to detect binding events occurring on the nanowire surface. Figure 11 shows a peptide nucleic acid (PNA) receptor-modified nanowire FET, in which uncharged PNA probes provide selective binding to detect charged DNA targets.[143] The small diameter of nanowire FETs provides extremely high sensitivity because the binding of target molecules causes accumulation/depletion of carriers throughout the wire cross section, and have been used to detect ions, DNA sequences, proteins, and viruses.[144,145] Because FETs respond to changes in surface charge, attention must be paid to the buffer solution in which measurements are performed. Physiologically reasonable ionic strength negatively impacts sensitivity by compressing the electrical double layer around the wires. This has been overcome by desalting samples before analysis to increase Debye length and with it the distance from the wire surface at which changes in charge can be detected.[146]

Recently, Heath and coworkers used electrostatically adsorbed DNA probes on functionalized silicon nanowires (SiNWs) to demonstrate DNA detection in 150-mM salt despite the short Debye length at this ionic strength.[147] There are two complementary strategies to fabricate nanowire FETs, top-down and bottom-up. In top-down strategies, the wires themselves, as well as the chip and electronic circuitry, are all fabricated from a bulk silicon wafer using advanced microelectronics technologies (i.e. lithography, etching, and deposition). These technologies are mature and reliable; however, the incorporation of biological probe molecules is limited by harsh conditions (high temperature, solvents, or reactive-ion etching (RIE)) commonly

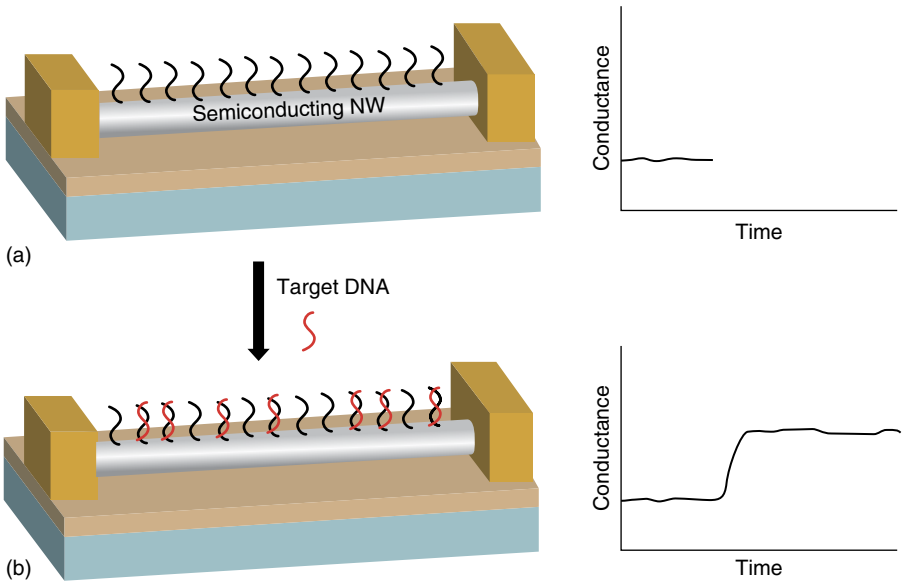

Figure 11 Semiconductor nanowire-based field-effect transistors for biomolecule detection. (a) The surface of a p-type silicon nanowire is modified with peptide nucleic acid (PNA) probe molecules. (b) The binding of DNA target molecules with a net negative charge leads to an accumulation of carriers in the nanowire and a corresponding increase in nanowire conductance. (Adapted from Ref. 143. © American Chemical Society, 2004.)

used in fabrication. In bottom-up strategies, nanowire building blocks are synthesized before assembly onto the chip surface, which provides much greater flexibility in nanowire material properties and surface functionalization but does not yet offer the fabrication reliability of top-down approaches. In top-down strategies, Stern et al. reported a complementary metal oxide semiconductor (CMOS) FET compatible technology to detect antibodies with 100-fM concentration.[148] An anisotropic wet etch was used instead of RIE, which can degrade device performance.[34] The resulting SiNWs had trapezoidal cross sections with nanometer-scale width and height. This approach enables the integration of signals from the nanowire sensors and real-time detection of biomolecules. The Lieber's group has pioneered bottom-up strategies to fabricate SiNW FETs.[142] Notably, they have demonstrated the versatility of SiNW FETs by the detection of several classes of targets including ions, small molecules, proteins, nucleic acids, and viruses with high selectivity and sensitivity. These authors also demonstrated the highest level of multiplexing, to date, for nanowire FET sensors in a simultaneous assay for three cancer markers with a detection of 0.9 pg mL^{-1} in desalted but undiluted serum samples.[146] Monoclonal antibodies, specific for each of the targets, were spotted onto different nanowire FETs; sample solutions were delivered through microfluidic channels, and the electrical signal from each FET was monitored in real time during exposure to each of the targets. Semiconductor nanowire FETs offer ultrasensitive, label-free, real-time electrical detection of biomolecules. To date, most efforts have focused on the fabrication and characterization of the FET devices, with less attention on biological multiplexing, at a current maximum of three targets at a time. New methods are needed to enable the controlled placement and integration of large numbers of functional nanowire bioFETs with different probe antibodies or nucleic acid sequences by top-down, bottom-up, or hybrid strategies.

5 NANOPORES/NANOCHANNELS

5.1 General Properties

5.1.1 Natural Ion Channels

There is increasing interest in measuring and investigating transport and electrochemical phenomena in membrane samples that contain a single pore of nanoscopic diameter. Selective transport in nanopores (protein-based ion channels) is used in living systems for electrical signaling in nerves and muscles. This natural behavior is being approached for the application of nanopores as sensing elements in biosensors.

Most membrane proteins are expected to consist of β-barrels or bundles of α-helices,[149] so attempts to engineer membrane channels and pores have focused on these two structural forms: β-barrel of trimeric porin OmpF and α-helix bundle of potassium channel KcsA (Figure 12).

The nanopore most often used is the α-hemolysin protein channel, and the typical sensor consists of a single channel embedded within a lipid bilayer membrane. An ionic current is passed through the channel, and analyte species are detected in this current as transient blocks associated with translocation of the analyte through channel-stochastic sensing.

The sensing fundament is based on the fact that by measuring the ionic current through a voltage-biased nanopore, molecules that enter the channel can be detected. When a molecule enters the channel, it displaces its own volume of solution; thereby, it modifies the channel electrical impedance and a change in the ionic current can be recorded. In Figure 13 the process that occurs in natural ion channels[150] is shown.

It is a schematic representation of a pore in a lipid bilayer, where the natural ionic current flows through, and this ionic current can be recorded. When an analyte is bound to a specific region of the pore, a change in the measurement is observed, and this can be related to the analyte and its concentration. Specifically, the intensity of the signal is related to the concentration of analyte, and the amplitude of the signal is characteristic of each analyte.

There is, however, a key impediment to developing practical sensors based on the biological nanopore. This problem concerns the fragility of the supported bilayer

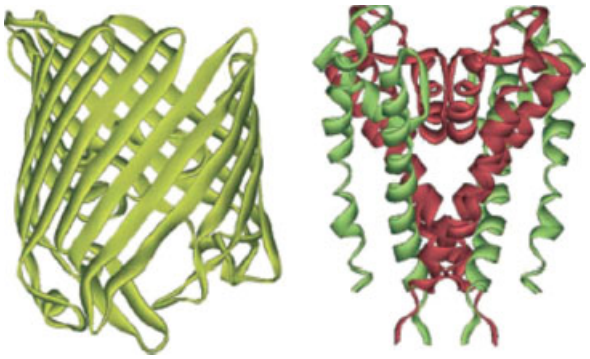

Figure 12 The two major structural forms of membrane channels and pores illustrated with X-ray structures: (a) β-barrel: one subunit of the trimeric porin OmpF; (b) α-helix bundle: the potassium channel KcsA. The channel contains four subunits: two are shown in green (pale) and two in red (dark). (Adapted with permission from Ref. 149. © Informa Healthcare, 2004.)

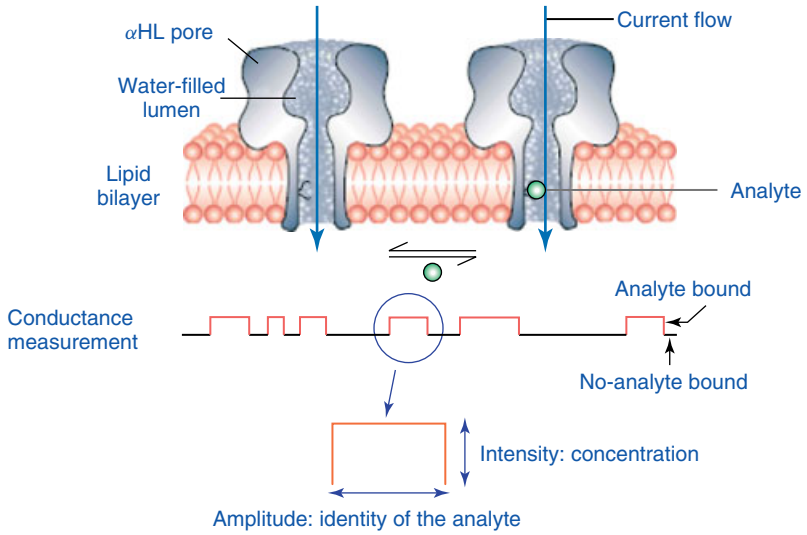

Figure 13 Schematic representation of a pore in a lipid bilayer. (Adapted from Ref. 150. © American Association for the Advancement of Science, 2004.)

membrane that houses the nanopore. Such membranes typically survive for periods of only a few hours before rupture,[151,152] which is much too short to make a practical sensing device. One approach for solving this problem consists in replacing the biological nanopore, and bilayer membrane, with an artificial nanopore embedded in a mechanically and chemically robust synthetic membrane. So, currently, research in this area is focused on the use of synthetic nanopores simulating this behavior for sensing applications.

5.1.2 *Production and Characterization of Nanoporous Materials*

The basic methods of preparing porous materials consist in (i) aggregation of particles, (ii) subtraction of a component from a compact body, and structural changes like (iii) crystallization, and (iv) inflation of a structure, for example, by swelling. There are also some special methods such as (i) compaction of powder, (ii) chemical reaction and precipitation, (iii) crystallization, and (iv) thermal treatment.

Related to the production of engineered nanopores for electrochemical analysis, the method most used is the track-etch method. It consists in bombarding a solid material (i.e. polycarbonate or silicon nitride/oxide films) with a collimated beam of high-energy nuclear fission fragments to create parallel damage tracks in the film.[153] The damage tracks are then etched into monodisperse pores by exposing the tracked film to a solution of aqueous base. The diameter of the pores is determined by the etch time and the etch-solution temperature. The pore density is determined by the exposure time to the fission fragment beam. Membranes with single nanopores down to 30 nm are obtained using this method. Conically shaped pores can also be obtained,[154] taking advantage of a dramatic enhancement in the rate of transport through the membrane, relative to analogous cylindrical pore.

In order to characterize these nanomaterials, fundamental nanofluidic parameters like ion transport numbers, membrane diffusion permeability, and specific chemical capacity have been studied. For this purpose, several techniques, such as conductance/cyclic voltammetric, nuclear magnetic resonance of ^{2}H, ^{31}P, and ^{1}H, infrared adsorption spectroscopy, X-ray diffraction, and electron–positron annihilation have been applied.

5.2 Applications in Electroanalysis

Nanopores are used as resistive-pulse sensors for molecular and macromolecule analytes in synthetic as well as biological membranes. The resistive-pulse method, which, when applied to such analytes, is sometimes called *stochastic sensing*, entails mounting the membrane containing the nanopore between two electrolyte solutions, applying a transmembrane potential difference, and measuring the resulting ion current flowing through the electrolyte-filled nanopore. In simplest terms, when the analyte enters and translocates the nanopore, it transiently blocks the ion current, resulting in a downward current pulse. The current-pulse frequency is proportional to the concentration of the analyte, and the identity of the analyte is encoded in the current-pulse signature, as defined by the average magnitude and duration of the current pulses.

In Figure 14, three examples of the use of nanopores for the detection of a variety of analytes, including biological ones, are shown.

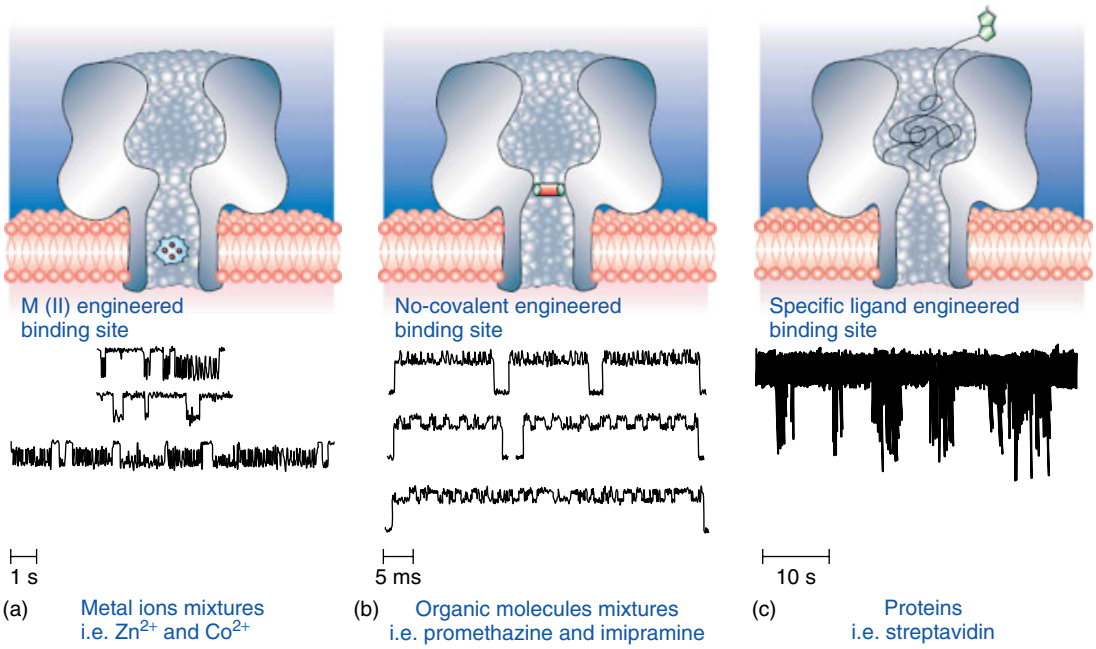

Figure 14 Scheme of the detection of a variety of analytes by stochastic sensing. (Adapted from Ref. 150. © American Association for the Advancement of Science, 2004.)

In the first case (a), the nanopore is engineered with a divalent metal-binding site. Each metal ion binds with different kinetics, so this allows to detect metal ion mixtures, for example, of zinc and cobalt. In the second case (b), the pore contains a noncovalent engineered binding site. This allows to detect organic molecule mixtures, like promethazine and imipramine. Finally, the specific detection of proteins, for example, streptavidin (c), is shown. For this purpose, the pore is engineered with a specific ligand that binds the streptavidin molecule.

The most reported application of nanopores/nanochannels for electrochemical analysis is focused on the DNA sensing. Single-stranded RNA or DNA molecules can pass through the wild type α-hemolysin pore in an elongated conformation and the transit time and extent of the current reveal information about the length of the nucleic acid and its base composition.[155,156] On the other hand, the magnitude of the conductance changes communicates additional details such as the presence of mismatches in DNA sequences. Furthermore, when single-stranded oligonucleotides are covalently attached within the large cavity of the pore, sequence-specific duplex formation can be detected. On the basis of the same fundament, cylindrical nanopores generated in polymeric membranes can be applied for DNA sequencing.[157–160] Furthermore, the inherent advantages of the conically shaped nanopores generated in polymeric membranes are also used for the electrochemical sensing of proteins[161–163] and DNA.[164]

Gold substrates are also useful substrates to build nanopores/nanochannels for electroanalysis. For example, gold nanotubes embedded within polymeric membranes can be used for proteins[165] and DNA[151] sensing, which are detected as a change in the current pulses or as a permanent blockage of the ion current.

Suitable substrates for DNA sensing are also nanoporous alumina filters. Aluminum anodized oxide disks have a high pore density ($1 \times 10^9\ cm^{-2}$) and small pore diameters, that results in a substrate with high surface area that can be easily functionalized. These filters modified with covalently linked DNA have been used to detect target DNA by monitoring the increase in impedance at the electrode upon DNA hybridization, which results from blocking the pores to ionic flow.[166,167]

Micromolding is an alternative technique that can be used to embed a nanoscale pore in polydimethysiloxane (PDMS), allowing to construct artificial nanopores for DNA molecules sensing.[168] This technique is extremely flexible and allows a variety of single-molecule detection applications.

Finally, the main advantages of the nanopore-based electrochemical sensing systems can be summarized as follows: (i) highl sensitivity; (ii) rapid and reversible response (allowing real-time monitoring); (iii) wide dynamic range; (iv) the possibility of several analytes being quantified concurrently by a single sensing element; (v) high selectivity of the sensing element not a condition, as each analyte produces a characteristic signature;

(vi) fouling of the sensing element cannot give a false reading, as the signal would not be characteristic of an analyte; (vii) potential for nanoscale miniaturization. All this makes this field a very promising research area that should bring wonderful scientific discoveries, with tremendous potential applications.

6 CONCLUSIONS AND FUTURE PERSPECTIVES

Nanomaterials ranging from NPs, QDs, CNTs, nanowires, and nanochannels or nanopores are proving to be very interesting alternatives to conventional materials in a broad range of electrochemical sensing and biosensing systems. Their integration into electrochemical platforms depends on their different sizes, forms, and constituting materials.

NPs have been applied to improve immobilization of (bio)molecules onto electrode surfaces, to catalyze reactions, and to enhance transducing signals. In addition, owing to their small size and electrochemical properties (i.e heavy metal-based QDs or even gold NPs), these are showing to be excellent labeling tags as alternative to conventional ones like dyes, enzymes, etc.

Gold NPs are the most reported labels. The low detection limits (few femtomoles) obtained for gold nanoparticle-based assays have been obtained by the combination of the gold tracing with silver enhancement. Enhancement has also been reported for QDs leading to improved detection limits. Nevertheless, the use of QD carriers such as polystyrene beads or CNTs has significantly improved (up to 500 fold) the limits of detection.

Although most of the electrochemical strategies for DNA analysis reported to date suffered from the fact that the hybridization event is still separated from the detection, there is a lot of ongoing effort is to integrate the whole electrochemical assay in a classical biosensor model with real applications for the future. The electrochemical properties of NPs make them extremely easy to detect (in both direct and indirect detection modes) by using simple instrumentation. The developed electrochemical coding technology (based on CdS, PbS, and ZnS) could be adapted to other multianalyte biological assays, particularly immunoassays. The electrochemical coding technology is thus expected to open new opportunities for DNA diagnostics, and for bioanalysis, in general, with a special interest for in-field low-cost applications.

There are various advantages that CNTs bring in the electrochemical analysis. CNTs composites seem to be an attractive alternative material in electrochemical sensors. The developed biosensors based on this kind of materials are showing clear advantages in terms of sensor operability (sensitivity, detection limit, stability, etc.) due, overall, to an improvement of electron transfer that leads to a lowering of working potential and consequently a significant remove of interferences during a real sample analysis.

Although the number of reports on CNTs applications in electrochemical sensors has increased, more efforts are required to figure out the role of CNTs in the improvement of the electrochemical properties of sensors and avoid precipitated conclusions in attributing electrocatalytic properties to nanotubes without conducting the appropriate control experiments. Further electrochemical study should be recommended for the future to understand better all the phenomena related with CNTs implementation in electrochemical sensors including the possible tuning of their electrochemical properties by modifications using doping agents as well as other materials.

Nanowires, nanochannels, and nanopores represent a novel trend in designing electrochemical (bio)sensors. Efforts are shown in their use in nanodevices with interest for both chemical sensing (i.e. nanowires) as well as biosensing (nanochannels and nanopores). While integration of nanowires into electrochemical platforms is relatively simple (i.e. by growing nanowires onto a transducing platform) the integration of nanochannels and nanopores still seems to be far from robust setups with interest for mass production. Nevertheless, the application of these nanomaterials shows special advantages for single DNA-strand analysis with future interest in genetic studies and diagnostics.

The application of the above-mentioned nanomaterials in relation to electroanalysis is already a consolidated research field not only for electroanalysis but also for the current nanoscience and nanotechnology. The experiences acquired so far in the field of electrochemistry are successfully coupled with the knowledge of new nanomaterials. This synergy is already offering interesting alternatives for several important analytical chemistry applications in fields like clinical analysis, environmental industry, safety as well as other industries.

ACKNOWLEDGMENTS

The authors acknowledge assistance from MEC (Madrid) under the projects MAT2008-03079/NAN, CSD2006-00012 ''NANOBIOMED'' (Consolider-Ingenio 2010) and Juan de la Cierva scholarship (Alfredo de la Escosura-Muñiz). Arben Merkoçi thanks all his previous collaborators (professors, doctors, and students) for their significant contributions in some of the mentioned works of this review article.

ABBREVIATIONS AND ACRONYMS

AB	Antibody
AG	Antigen
ALP	Alkaline Phosphatase
apo-GOX	Apo-glucose Oxidase
APTES	3-aminopropyltriethoxysilane
BSA	Bovine Serum Solution
CCPE	Chitosan-entrapped Carbon Paste Electrode
CMOS	Complementary Metal Oxide Semiconductor
CNTEC	Carbon Nanotube Epoxy-composite
CNTs	Carbon Nanotubes
CVD	Chemical Vapor Deposition
DMSO	Dimethyl Sulfoxide
DPV	Differential Pulse Voltammetry
EIS	Electrochemical Impedance Spectroscopy
FAD	Flavin Adenine Dinucleotide
FETs	Field-effect Transistors
GA	Glutaraldehyde
GC	Glassy Carbon
GEC	Graphite Epoxy-composite
GOX	Glucose Oxidase
HDT	1,6-hexanedithiol
HQ	Hydroquinone
HRP	Horseradish Peroxidase
IgG	Immunoglobulin G
MWCNT	Multiwall Carbon Nanotubes
NADH	Nicotinamide Adenine Dinucleotide
NPs	Nanoparticles
PABS	Poly-(*m*-aminobenzene Sulfonic Acid
PCR	Polymerase Chain Reaction
PDMS	Polydimethysiloxane
PMMA	Poly(methyl Methacrylate)
PNA	Peptide Nucleic Acid
PSA	Potentiometric Stripping Analysis
PS	Polymeric Spheres
PVC	Polyvinyl Chloride
QDs	Quantum Dots
RIE	Reactive-ion Etching
RSD	Relative Standard Deviation
SEM	Scanning Electron Microscope
SiNWs	Silicon Nanowires
SPEs	Screen-printed Electrodes
SWCNT	Single-wall Carbon Nanotubes
SWV	Square Wave Voltammetry
THF	tetrahydrofuran

RELATED ARTICLES

Biomolecules Analysis: Introduction
Biosensor Design and Fabrication
Clinical Chemistry: Introduction
DNA Arrays: Preparation and Application
Electroanalysis and Biosensors in Clinical Chemistry
Electroanalytical Chemistry in Clinical Analysis
Electroanalytical Methods: Introduction
Microbalance, Electrochemical Quartz Crystal
Nucleic Acid Analysis in Clinical Chemistry
Pulse Voltammetry
Scanning Tunneling Microscopy, In Situ, Electrochemical
Selective Electrode Coatings for Electroanalysis
Self-assembled Monolayers on Electrodes
Single Molecule Detection, Analysis, and Manipulation
Ultrafast Electrochemical Techniques
Voltammetry In Vivo for Chemical Analysis of the Living Brain
Voltammetry In Vivo for Chemical Analysis of the Nervous System

REFERENCES

1. M. Ratner, D. Ratner, *Nanotechnology: A Gentle Introduction to the Next Big Idea*, 1st edition, Prentice Hall PTR, New Jersey, USA, 2003.
2. C.N.R. Rao, A.K. Cheetham, 'Science and Technology of Nanomaterials: Current Status and Future Prospects', *J. Mater. Chem.*, **11**, 2887 (2001).
3. R. Coontz, P. Szuromi, 'Taking the Initiative', *Science*, **290**, 1523 (2000).
4. J. Wang, 'Nanomaterial-Based Electrochemical Biosensors', *Analyst*, **130**, 421 (2005).
5. S.G. Penn, L. He, M.J. Natan, 'Nanoparticles for Bioanalysis', *Curr. Opin. Chem. Biol.*, **7**, 609 (2003).
6. H. Bonnemann, F.J.M. Richards, 'Nanoscopic Metal Particles - Synthetic Methods and Potential Applications', *Eur. J. Inorg. Chem.*, **2001**, 2455 (2001).
7. C.M. Niemeyer, 'Nanoparticles, Proteins, and Nucleic Acids: Biotechnology Meets Materials Science', *Angew. Chem., Int. Ed. Engl.*, **40**, 4128 (2001).
8. M. Brust, J. Fink, D. Bethell, D.J. Schiffrin, C. Kiely, 'Synthesis and Reactions of Functionalised Gold Nanoparticles', *J. Chem. Soc., Chem. Commun.*, **117**, 1655 (1995).
9. L. Quaroni, G. Chumanov, 'Preparation of Polymer-Coated Functionalized Silver Nanoparticles', *J. Am. Chem. Soc.*, **121**, 10642 (1999).
10. B.G. Ershov, N.L. Sukhov, E. Janata, 'Formation, Absorption Spectrum, and Chemical Reactions of Nanosized Colloidal Cobalt in Aqueous Solution', *J. Phys. Chem. B*, **104**, 6138 (2000).

11. F.J. Vidal-Iglesias, J. Solla-Gullon, P. Rodriguez, E. Herrero, V. Montiel, J.M. Feliu, A. Aldaz, 'Shape-Dependent Electrocatalysis: Ammonia Oxidation on Platinum Nanoparticles with Preferential (1 0 0) Surfaces', *Electrochem. Commun.*, **6**, 1080 (2004).
12. A.B. Scott., W.A. Smith, M.A. Thompson, 'Alkali Halides Colored by Colloidal Metal', *J. Phys. Chem.*, **57**, 757 (1953).
13. W.T. Doyle, 'Absorption of Light by Colloids in Alkali Halide Crystals', *Phys. Rev.*, **111**, 1067 (1958).
14. K.S. Lee, M.A. El-Sayed, 'Gold and Silver Nanoparticles in Sensing and Imaging: Sensitivity of Plasmon Response to Size, Shape, and Metal Composition', *J. Phys. Chem. B*, **110**, 19220 (2006).
15. M. Hanauer, S. Pierrat, I. Zins, A. Lotz, C. Snnichsen, 'Separation of Nanoparticles by Gel Electrophoresis According to Size and Shape', *Nano Lett.*, **7**, 2881 (2007).
16. J. Nelayah, M. Kociak, O. Sthéphan, F.J. García, M. Tencé, L. Henrard, D. Taverna, I. Pastoriza-Santos, L.M. Liz-Marzán, C. Colliex, 'Mapping Surface Plasmons on a Single Metallic Nanoparticle', *Nat. Phys.*, **3**, 348 (2007).
17. K.A. Willets, R.P. Van Duyne, 'Localized Surface Plasmon Resonance Spectroscopy and Sensing', *Annu. Rev. Phys. Chem.*, **58**, 267 (2007).
18. P.K. Jain, I.H. El-Sayed, M.A. El-Sayed, 'Au Nanoparticles Target Cancer', *Nano Today*, **2**, 18 (2007).
19. L.R. Hirsch, R.J. Stafford, J.A. Bankson, S.R. Sershen, B. Rivera, R.E. Price, J.D. Hazle, N.J. Halas, J.L. West, 'Nanoshell-Mediated Near-Infrared Thermal Therapy of Tumors Under Magnetic Resonance Guidance', *Proc. Natl. Acad. Sci. U.S.A.*, **100**, 13549 (2003).
20. M. Pumera, M. Aldavert, C. Mills, A. Merkoçi, S. Alegret, 'Direct Voltammetric Determination of Gold Nanoparticles Using Graphite-Epoxy Composite Electrode', *Electrochim. Acta*, **50**, 3702 (2005).
21. M. Pumera, M.T. Castañeda, M.I. Pividori, R. Eritja, A. Merkoçi, S. Alegret, 'Magnetically Trigged Direct Electrochemical Detection of DNA Hybridization Using Au67 Quantum Dot as Electrical Tracer', *Langmuir*, **21**, 9625 (2005).
22. M.T. Castañeda, A. Merkoçi, M. Pumera, S. Alegret, 'Electrochemical Genosensors for Biomedical Applications Based on Gold Nanoparticles', *Biosens. Bioelectron.*, **22**, 1961 (2007).
23. A. de la Escosura-Muñiz, A. Ambrosi, A. Merkoçi, 'Electrochemical Analysis with Nanoparticle-Based Biosystems', *Trends Anal. Chem.*, **27**, 568 (2008).
24. C.J. Murphy, 'Optical Sensing with Quantum Dots', *Anal. Chem.*, **74**, 520 (2002).
25. A. Merkoçi, S. Marín, M.T. Castañeda, M. Pumera, J. Ros, S. Alegret, 'Crystal and Electrochemical Properties of Water Dispersed CdS Nanocrystals Obtained Via Reverse Micelles and Arrested Precipitation', *Nanotechnology*, **17**, 2553 (2006).
26. M.L. Steigerwald, L.E. Brus, 'Semiconductor Crystallites: A Class of Large Molecules', *Acc. Chem. Res.*, **23**, 183 (1990).
27. A. Eychmüller, A.L. Rogach, 'Chemistry and Photophysics of Thiol-Stabilized II-VI Semiconductor Nanocrystals', *Pure Appl. Chem.*, **72**, 179 (2000).
28. M.A. Olshavsky, A.N. Goldstein, A.P. Alivisatos, 'Organometallic Synthesis of Gallium-Arsenide Crystallites, Exhibiting Quantum Confinement', *J. Am. Chem. Soc.*, **112**, 9438 (1990).
29. A.A. Guzelian, J.E.B. Katari, A.V. Kadavanich, U. Banin, K. Hamad, E. Juban, A.P. Alivisatos, R.H. Wolters, C.C. Arnold, J.R. Heath, 'Synthesis of Size-Selected, Surface-Passivated InP Nanocrystals', *J. Phys. Chem.*, **100**, 7212 (1996).
30. S. Empedocles, M. Bawendi, 'Spectroscopy of Single CdSe Nanocrystallites', *Acc. Chem. Res.*, **32**, 389 (1999).
31. M. Kuno, J.K. Lee, B.O. Dabbosi, F.V. Mikulec, M.G. Bawendi, 'The Band Edge Luminescence of Surface Modified CdSe Nanocrystallites: Probing the Luminescing State', *J. Chem. Phys.*, **106**, 9869 (1997).
32. D.J. Norris, A. Sacra, C.B. Murray, M.G. Bawendi, 'Measurements of the Size Dependent Hole Spectrum in CdSe Quantum Dots', *Phys. Rev. Lett.*, **72**, 2612 (1994).
33. C.B. Murray, D.J. Norris, M.G. Bawendi, 'Synthesis and Characterization of Nearly Monodisperse CdE (E = Sulfur, Selenium, Tellurium) Semiconductor Nanocrystallites', *J. Am. Chem. Soc.*, **115**, 8706 (1993).
34. J. Wang, G. Liu, A. Merkoçi, 'Electrochemical Coding Technology for Simultaneous Detection of Multiple DNA Targets', *J. Am. Chem. Soc.*, **125**, 3214 (2003).
35. A. Merkoçi, L.H. Marcolino-Junior, S. Marín, O. Fatibello-Filho, S. Alegret, 'Detection of Cadmium Sulphide Nanoparticles by Using Screen-Printed Electrodes and a Handheld Device', *Nanotechnology*, **18**, 035502 (2007).
36. G. Liu, J. Wang, J. Kim, M.R. Jan, 'Electrochemical Coding for Multiplexed Immunoassays of Proteins', *Anal. Chem.*, **76**, 7126 (2004).
37. L. Murphy, 'Biosensors and Bioelectrochemistry', *Curr. Opin. Chem. Biol.*, **10**, 177 (2006).
38. M. Ozsoz, A. Erdem, K. Kerman, D. Ozkan, B. Tugrul, N. Topcuoglu, H. Ekren, M. Taylan, 'Electrochemical Genosensor Based on Colloidal Gold Nanoparticles for the Detection of Factor V Leiden Mutation Using Disposable Pencil Graphite Electrodes', *Anal. Chem.*, **75**, 2181 (2003).
39. J. Wang, D.A. Xu, N. Kawde, R. Polsky, 'Metal Nanoparticle-Based Electrochemical Stripping Potentiometric Detection of DNA Hybridization', *Anal. Chem.*, **73**, 5576 (2001).

40. J. Wang, R. Polsky, D. Xu, 'Silver-Enhanced Colloidal Gold Electrochemical Stripping Detection of DNA Hybridization', *Langmuir*, **17**, 5739 (2001).
41. J. Wang, D. Xu, R. Polsky, 'Magnetically-Induced Solid-State Electrochemical Detection of DNA Hybridization', *J. Am. Chem. Soc.*, **124**, 4208 (2002).
42. S.J. Park, T.A. Taton, C.A. Mirkin, 'Array-Based Electrical Detection of DNA with Nanoparticle Probes', *Science*, **295**, 1503 (2002).
43. J. Wang, G. Liu, R. Polsky, A. Merkoçi, 'Electrochemical Stripping Detection of DNA Hybridization Based on Cadmium Sulfide Nanoparticle Tags', *Electrochem. Commun.*, **4**, 722 (2002).
44. J. Wang, G. Liu, A. Merkoçi, 'Particle-Based Detection of DNA Hybridization Using Electrochemical Stripping Measurements of an Iron Tracer', *Anal. Chim. Acta*, **482**, 149 (2003).
45. Y. Xu, H. Cai, P.G. He, Y.Z. Fang, 'Probing DNA Hybridization by Impedance Measurement Based on CdS-Oligonucleotide Nanoconjugates', *Electroanalysis*, **16**, 150 (2004).
46. A.N. Kawde, J. Wang, 'Amplified Electrical Transduction of DNA Hybridization Based on Polymeric Beads Loaded with Multiple Gold Nanoparticle Tags', *Electroanalysis*, **16**, 101 (2004).
47. J. Wang, G. Liu, R.M. Jan, Q. Zhu, 'Electrochemical Detection of DNA Hybridization Based on Carbon-Nanotubes Loaded with CdS Tags', *Electrochem. Commun.*, **5**, 1000 (2003).
48. P.B. Luppa, L.J. Sokoll, D.W. Chan, 'Immunosensors-Principles and Applications to Clinical Chemistry', *Clin. Chim. Acta*, **314**, 1 (2001).
49. D.R. Shankaran, K.V. Gobi, N. Miura, 'Recent Advancements in Surface Plasmon Resonance Immunosensors for Detection of Small Molecules of Biomedical, Food and Environmental Interest', *Sens. Actuators, B*, **121**, 158 (2007).
50. X. Chu, X. Fu, K. Chen, G.L. Shen, R.Q. Yu, 'An Electrochemical Stripping Metalloimmunoassay Based on Silver-Enhanced Gold Nanoparticle Label', *Biosens. Bioelectron.*, **20**, 1805 (2005).
51. E. Katz, I. Willner, J. Wang, 'Electroanalytical and Bioelectroanalytical Systems Based on Metal and Semiconductor Nanoparticles', *Electroanalysis*, **16**, 19 (2004).
52. M. Dequaire, C. Degrand, B. Limoges, 'An Electrochemical Metalloimmunoassay Based on a Colloidal Gold Label', *Anal. Chem.*, **72**, 5521 (2000).
53. J. Wang, G. Liu, G. Rivas, 'Encoded Beads for Electrochemical Identification', *Anal. Chem.*, **75**, 4667 (2003).
54. J. Wang, D. Xu, A. Kawde, R. Polsky, 'Metal Nanoparticle-Based Electrochemical Stripping Potentiometric Detection of DNA Hybridization', *Anal. Chem.*, **73**, 5576 (2001).
55. J. Wang, R. Polsky, X. Danke, 'Silver-Enhanced Colloidal Gold Electrochemical Stripping Detection of DNA Hybridization', *Langmuir*, **17**, 5739 (2001).
56. A. Kawde, J. Wang, 'Amplified Electrical Transduction of DNA Hybridization Based on Polymeric Beads Loaded with Multiple Gold Nanoparticle Tags', *Electroanalysis*, **16**, 101 (2004).
57. A. Ambrosi, M.T. Castañeda, A.J. Killard, M.R. Smyth, S. Alegret, A. Merkoçi, 'Double- Codified Gold Nanolabels for Enhanced Immunoanalysis', *Anal. Chem.*, **79**, 5232 (2007).
58. O.D. Velev, E.W. Kaler, 'In Situ Assembly of Colloidal Particles Into Miniaturized Biosensors', *Langmuir*, **15**, 3693 (1999).
59. C.X. Lei, F.C. Gong, G.L. Shen, R.Q. Yu, 'Amperometric Immunosensor for *Schistosoma Japonicum* Antigen Using Antibodies Loaded on a Nano-Au monolayer Modified Chitosan-Entrapped Carbon Paste Electrode', *Sens. Actuators, B*, **96**, 582 (2003).
60. J. Li, Z. Wu, H. Wang, G. Shen, R. Yu, 'A Reusable Capacitive Immunosensor with a Novel Immobilization Procedure Based on 1,6-Hexanedithiol and Nano-Au Self-Assembled Layers', *Sens. Actuators, B*, **110**, 327 (2005).
61. S.Q. Hu, J.W. Xie, Q.H. Xu, K.T. Rong, G.L. Shen, R.Q. Yu, 'A Label-Free Electrochemical Immunosensor Based on Gold Nanoparticles for Detection of Paraoxon', *Talanta*, **61**, 769 (2003).
62. D.P. Tang, R. Yuan, Y.Q. Chai, X. Zhong, Y. Liu, J.Y. Dai, L.Y. Zhang, 'Novel Potentiometric Immunosensor for Hepatitis B Surface Antigen Using a Gold Nanoparticle-Based Biomolecular Immobilization Method', *Anal. Biochem.*, **333**, 345 (2004).
63. T. Yin, W. Wei, L. Yang, X. Gao, Y. Gao, 'A Novel Capacitive Immunosensor for Transferrin Detection Based on Ultrathin Alumina Sol–Gel-Derived Films and Gold Nanoparticles', *Sens. Actuators, B*, **117**, 286 (2006).
64. J. Chen, J. Tang, F. Yan, H. Ju, 'A Gold Nanoparticles/Sol–Gel Composite Architecture for Encapsulation of Immunoconjugate for Reagentless Electrochemical Immunoassay', *Biomaterials*, **27**, 2313 (2006).
65. D. Tang, R. Yuan, Y. Chai, Y. Fu, 'Study on Electrochemical Behavior of a Diphtheria Immunosensor Based on Silica/Silver/Gold Nanoparticles and Polyvinyl Butyral as Matrices', *Electrochem. Commun.*, **7**, 177 (2005).
66. A.L. Crumbliss, S.C. Perine, J. Stonehuerner, K.R. Tubergen, J. Zhao, R.W. Henkens, 'Colloidal Gold As

a Biocompatible Immobilization Matrix Suitable for the Fabrication of Enzyme Electrodes by Electrodeposition', *Biotechnol. Bioeng.*, **40**, 483 (1992).

67. Y. Xiao, H.X. Ju, H.Y. Chen, 'Hydrogen Peroxide Sensor Based on Horseradish Peroxidase-Labeled Au Colloids Immobilized on Gold Electrode Surface by Cysteamine Monolayer', *Anal. Chim. Acta*, **391**, 73 (1999).
68. J.B. Jia, B.Q. Wang, A.G. Wu, G.J. Cheng, Z. Li, S.J. Dong, 'A Method to Construct a Third-Generation Horseradish Peroxidase Biosensor: Self-Assembling Gold Nanoparticles to Three-Dimensional Sol-Gel Network', *Anal. Chem.*, **74**, 2217 (2002).
69. X.L. Luo, J.J. Xu, Q. Zhang, G.J. Yang, H.Y. Chen, 'Electrochemically Deposited Chitosan Hydrogel for Horseradish Peroxidase Immobilization Through Gold Nanoparticles Self-Assembly', *Biosens. Bioelectron.*, **21**, 190 (2005).
70. F. Patolsky, T. Gabriel, I. Willner, 'Controlled Electrocatalysis by Microperoxidase-11 and Au-Nanoparticle Superstructures on Conductive Supports', *J. Electroanal. Chem.*, **479**, 69 (1999).
71. Z.M. Liu, H. Wang, Y. Yang, H.F. Yang, S.Q. Hu, G.L. Shen, R.Q. Yu, 'Amperometric Tyrosinase Biosensor Using Enzyme-Labeled Au Colloids Immobilized on Cystamine/Chitosan Modified Gold Surface', *Anal. Lett.*, **37**, 1079 (2004).
72. H.Y. Gu, A.M. Yu, H.Y. Chen, 'Direct Electron Transfer and Characterization of Hemoglobin Immobilized on a Au Colloid–Cysteamine-Modified Gold Electrode', *J. Electroanal. Chem.*, **516**, 119 (2001).
73. P.L. He, N.F. Hu, 'Electrocatalytic Properties of Heme Proteins in Layer-by-Layer Films Assembled with SiO_2 Nanoparticles', *Electroanalysis*, **16**, 1122 (2004).
74. P.L. He, N.F. Hu, J.F. Rusling, 'Driving Forces for Layer-by-Layer Self-Assembly of Films of SiO_2 Nanoparticles and Heme Proteins', *Langmuir*, **20**, 722 (2004).
75. I.D.G. MacDonald, W.E. Smith, 'Orientation of Cytochrome *c* Adsorbed on a Citrate-Reduced Silver Colloid Surface', *Langmuir*, **12**, 706 (1996).
76. F. Caruso, 'Nanoengineering of Particle Surfaces Advanced Materials', *Adv. Mater.*, **13**, 11 (2001).
77. F. Caruso, H. Fiedler, K. Haage, 'Assembly of β-Glucosidase Multilayers on Spherical Colloidal Particles and their Use as Active Catalysts', *Colloids Surf., A*, **169**, 287 (2000).
78. C. Schüler, F. Caruso, 'Preparation of Enzyme Multilayers on Colloids for Biocatalysis', *Macromol. Rapid Commun.*, **21**, 750 (2000).
79. Y. Lvov, F. Caruso, 'Biocolloids with Ordered Urease Multilayer Shells as Enzymatic Reactors', *Anal. Chem.*, **73**, 4212 (2001).
80. F. Caruso, C. Schüler, 'Enzyme Multilayers on Colloid Particles: Assembly, Stability, and Enzymatic Activity', *Langmuir*, **16**, 9595 (2000).
81. E. Droz, M. Taborelli, P. Descouts, T.N.C. Wells, R.C. Werlen, 'Covalent Immobilization of Immunoglobulins G and Fab Fragments on Gold Substrates for Scanning Force Microscopy Imaging in Liquids', *J. Vac. Sci. Technol., B*, **14**, 1422 (1996).
82. S. Kanno, Y. Yanagida, T. Haruyama, E. Kobatake, M. Aizawa, 'Assembling of Engineered IgG-Binding Protein on Gold Surface for Highly Oriented Antibody Immobilization', *J. Biotechnol.*, **76**, 207 (2000).
83. A. Gole, S. Vyas, S. Phadtare, A. Lachke, M. Sastry, 'Studies on the Formation of Bioconjugate of Endoglucanase with Colloidal Gold', *Colloids Surf., B: Biointerf.*, **25**, 129 (2002).
84. H. Cai, C. Xu, P. He, Y. Fang, 'Colloid Au-Enhanced DNA Immobilization for the Electrochemical Detection of Sequence-Specific DNA', *J. Electroanal. Chem.*, **510**, 78 (2001).
85. B.G. Torre, J.C. Morales, A. Aviño, D. Iacopino, A. Ongaro, D. Fitzmaurice, D. Murphy, H. Doyle, G. Redmond, R. Eritja, 'Synthesis of Oligonucleotides Carrying Anchoring Groups and their Use in the Preparation of Oligonucleotide - Gold Conjugates', *Helv. Chim. Acta*, **85**, 2594 (2002).
86. Y.Z. Fang, R. Yuan, L. Xu, Y.Q. Chai, Y. Liu, D.P. Tang, Y. Zhang, 'Electrochemical Impedance Behavior of DNA Biosensor Based on Colloidal Ag and Bilayer Two-Dimensional Sol–Gel as Matrices', *J. Biochem. Biophys. Methods*, **62**, 163 (2005).
87. D. Zhang, Y. Chen, H.Y. Chen, X.H. Xia, 'Silica-Nanoparticle-Based Interface for the Enhanced Immobilization and Sequence-Specific Detection of DNA', *Anal. Bioanal. Chem.*, **379**, 1025 (2004).
88. F.A. Armstrong, G.S. Wilson, 'Recent Developments in Faradaic Bioelectrochemistry', *Electrochim. Acta*, **45**, 2623 (2000).
89. I. Willner, G. Arad, E. Katz, 'A Biofuel Cell Based on Pyrroloquinoline Quinone and Microperoxidase-11 Monolayer-Functionalized Electrodes', *Bioelectrochem. Bioenerg.*, **44**, 209 (1998).
90. X. Han, W. Cheng, Z. Zhang, S. Dong, E. Wang, 'Direct Electron Transfer Between Hemoglobin and a Glassy Carbon Electrode Facilitated by Lipid-Protected Gold Nanoparticles', *Biochim. Biophys. Acta*, **1556**, 273 (2002).
91. S. Liu, Z. Dai, H. Chen, H. Ju, 'Immobilization of Hemoglobin on Zirconium Dioxide Nanoparticles for Preparation of a Novel Hydrogen Peroxide Biosensor', *Biosens. Bioelectron.*, **19**, 963 (2004).
92. Y. Xiao, F. Patolsky, E. Katz, J.F. Hainfeld, I. Willner, '"Plugging into Enzymes": Nanowiring of Redox

Enzymes by a Gold Nanoparticle', *Science*, **299**, 1877 (2003).

93. L. Wang, E.K. Wang, 'Direct Electron Transfer Between Cytochrome c and a Gold Nanoparticles Modified Electrode', *Electrochem. Commun.*, **6**, 49 (2004).
94. T. Liu, J. Zhong, X. Gan, C. Fan, G. Li, N. Matsuda, 'Wiring Electrons of Cytochrome c with Silver Nanoparticles in Layered Films', *Chemphyschem*, **4**, 1364 (2003).
95. Y. Zhang, P.L. He, N.F. Hu, 'Horseradish Peroxidase Immobilized in TiO_2 Nanoparticle Films on Pyrolytic Graphite Electrodes: Direct Electrochemistry and Bioelectrocatalysis', *Electrochim. Acta*, **49**, 1981 (2004).
96. S.Q. Liu, Z.H. Dai, H.Y. Chen, H.X. Ju, 'Immobilization of Hemoglobin on Zirconium Dioxide Nanoparticles for Preparation of a Novel Hydrogen Peroxide Biosensor', *Biosens. Bioelectron.*, **19**, 963 (2004).
97. D.F. Dao, P.L. He, N.F. Hu, 'Electrochemical Biosensors Utilising Electron Transfer in Heme Proteins Immobilised on Fe_3O_4 Nanoparticles', *Analyst*, **128**, 1268 (2003).
98. Y. Lvov, B. Munge, O. Giraldo, I. Ichinnose, S.L. Suib, J.F. Rusling, 'Films of Manganese Oxide Nanoparticles with Polycations or Myoglobin from Alternate-Layer Adsorption', *Langmuir*, **16**, 8850 (2000).
99. H. Zhou, X. Gan, T. Liu, Q.L. Yang, G.X. Li, 'Effect of Nano-Cadmium Sulphide on the Electron Transfer Reactivity and Peroxidase Activity of Haemoglobin', *J. Biochem. Biophys. Methods*, **64**, 38 (2005).
100. S. Iijima, 'Helical Microtubules of Graphitic Carbon', *Nature*, **56**, 354 (1991).
101. W.B. Choi, D.S. Chung, J.H. Kang, H.Y. Kim, Y.W. Jin, I.T. Han, Y.H. Lee, J.E. Jung, N.S. Lee, G.S. Park, J.M. Kim, 'Fully Sealed, High-Brightness Carbon-Nanotube Field-Emission Display', *Appl. Phys. Lett.*, **75**, 3129 (1999).
102. S.J. Tans, A.R.M. Verschueren, C. Dekker, 'Room-Temperature Transistor Based on a Single Carbon Nanotube', *Nature*, **393**, 49 (1998).
103. H. Dai, J.H. Hafner, A.G. Rinzler, D.T. Colbert, R.E. Smalley, 'Nanotubes as Nanoprobes in Scanning Probe Microscopy', *Nature*, **384**, 147 (1996).
104. M.S. Shaffer, X. Fan, A.-H. Windle, 'Dispersion and Packing of Carbon Nanotubes', *Carbon*, **36**, 1603 (1998).
105. Y. De Gani, A. Heller, 'Direct Electrical Communication Between Chemically Modified Enzymes and Metal Electrodes. I. Electron Transfer from Glucose Oxidase to Metal Electrodes Via Electron Relays, Bound Covalently to the Enzyme', *J. Phys. Chem.*, **91**, 1285 (1987).
106. A. Merkoçi, M. Pumera, X. Llopis, B. Pérez, M. del Valle, S. Alegret, 'New Materials for Electrochemical Sensing VI: Carbon Nanotubes', *Trends Anal. Chem.*, **24**, 826 (2005).
107. A. Heller, 'Electrical Connection of Enzyme Redox Centers to Electrodes', *J. Phys. Chem. Res.*, **96**, 3579 (1992).
108. M. Endo, T. Hayashi, Y.A. Kim, M. Terrones, M.S. Dresselhaus, 'Applications of Carbon Nanotubes in the Twenty–First Century', *Philos. Trans. R. Soc. London, Ser. A*, **362**, 2223 (2004).
109. J. Liu, A.G. Rinzler, H. Dai, J.H. Hafner, R.K. Bradley, P.J. Boul, A. Lu, T. Iverson, K. Shelimov, C.B. Huffman, F. Rodriguez-Macias, Y.S. Shon, T.R. Lee, D.T. Colbert, R.E. Smalley, 'Fullerene pipes', *Science*, **280**, 1253 (1998).
110. S. Bandow, A.M. Rao, A. Thess, R.E. Smalley, 'Purification of Single-Wall Carbon Nanotubes by Microfiltration', *J. Phys. Chem. B*, **101**, 8839 (1997).
111. A.G. Rinzler, J. Liu, H. Dai, P. Nikolaev, C.B. Huffman, F.J. Rodriguez-Marcias, 'Large-Scale Purification of Single-Wall Carbon Nanotubes: Process, Product, and Characterization', *Appl. Phys. A*, **67**, 29 (1998).
112. A.C. Dillon, T. Gennett, K.M. Jones, J.L. Alleman, P.A. Parilla, M.J. Heben, 'A Simple and Complete Purification of Single-Walled Carbon Nanotube Materials', *Adv. Mater.*, **11**, 1354 (1999).
113. M.T. Martinez, M.A. Callejas, A.M. Benito, W.K. Maser, M. Cochet, J.M. Andres, J. Schreiber, O. Chauvet, J.L. Fierro, 'Microwave Single Walled Carbon Nanotubes Purification', *Chem. Commun.*, **9**, 1000 (2002).
114. R. Andrews, D. Jacques, D. Qian, E.C. Dickey, 'Purification and Structural Annealing of Multiwalled Carbon Nanotubes at Graphitization Temperatures', *Carbon*, **39**, 1681 (2001).
115. J. Chen, M.A. Hamon, H. Hu, Y. Chen, A.M. Rao, P.C. Eklund, R.C. Haddon, 'Solution Properties of Single-Walled Carbon Nanotubes', *Science*, **282**, 95 (1998).
116. D. Tasis, N. Tagmatarchis, V. Georgakilas, M. Prato, 'Soluble Carbon Nanotubes', *Chem. – Eur. J.*, **9**, 4000 (2003).
117. M.F. Islam, E. Rojas, D.M. Bergey, A.T. Johnson, A.G. Yodh, 'High Weight Fraction Surfactant Solubilization of Single-Wall Carbon Nanotubes in Water', *Nano Lett.*, **3**, 269 (2003).
118. A. Star, J.F. Stoddart, D. Steuerman, M. Diehl, A. Boukai, E.W. Wong, X. Yang, S.W. Chung, H. Choi, J.R. Heath, 'Preparation and Properties of Polymer-Wrapped Single-Walled Carbon Nanotubes', *Angew. Chem., Int. Ed. Engl.*, **40**, 1721 (2001).
119. M.J. O'Connell, P. Boul, L.M. Ericson, C. Huffman, Y. Wang, E. Haroz, C. Kuper, J. Tour, K.D. Ausman, R.E. Smalley, 'Reversible Water-Solubilization of Single-Walled Carbon Nanotubes by Polymer Wrapping', *Chem. Phys. Lett.*, **342**, 265 (2001).

120. J. Chen, H. Liu, W.A. Weimer, M.D. Halls, M.D.H. Waldeck, G.C. Walker, 'Noncovalent Engineering of Carbon Nanotube Surfaces by Rigid, Functional Conjugated Polymers', *J. Am. Chem. Soc.*, **124**, 9034 (2002).

121. S. Ramesh, L.M. Ericson, V.A. Davis, R.K. Saini, C. Kittrell, M. Pasquali, W.E. Billups, W. Adams, R.H. Hauge, R.E. Smalley, 'Dissolution of Pristine Single Walled Carbon Nanotubes in Superacids by Direct Protonation', *J. Phys. Chem. B*, **108**, 8794 (2004).

122. O.K. Kim, J. Je, J.W. Baldwin, S. Kooi, P.E. Pehrsson, L.J. Buckley, 'Solubilization of Single-Wall Carbon Nanotubes by Supramolecular Encapsulation of Helical Amylase', *J. Am. Chem. Soc.*, **125**, 4426 (2003).

123. J.H.T. Luong, S. Hrapovic, D. Wang, F. Bensebaa, B. Simard, 'Solubilization of Multiwall Carbon Nanotubes by 3-Aminopropyltriethoxysilane Towards the Fabrication of Electrochemical Biosensors with Promoted Electron Transfer', *Electroanalysis*, **16**, 132 (2004).

124. W. Yue-Rong, H. Ping, L. Qiong-Lin, L. Guo-An, W. Yi-Ming, 'Application of Carbon Nanotube Modified Electrode in Bioelectroanalysis', *Chin. J. Anal. Chem.*, **36**, 1011 (2008).

125. P.J. Britto, K.S.V. Santhanam, P.M. Ajayan, 'Carbon Nanotube Electrode for Oxidation of Dopamine', *Bioelectrochem. Bioenerg.*, **41**, 121 (1996).

126. Z.H. Wang, J. Liu, Q.L. Liang, Y.M. Wang, G.A. Luo, 'Carbon Nanotube-Modified Electrodes for the Simultaneous Determination of Dopamine and Ascorbic Acid', *Analyst*, **127**, 653 (2000).

127. B. Pérez López, J. Sola, S. Alegret, A. Merkoçi, 'A Carbon Nanotube PVC Based Matrix Modified with Glutaraldehyde Suitable for Biosensor Applications', *Electroanalysis*, **20**, 603 (2008).

128. B. Pérez, M. Pumera, M. del Valle, A. Merkoçi, S. Alegret, 'Glucose Biosensor Based on Carbon Nanotube Epoxy Composites', *J. Nanosci. Nanotechnol.*, **5**, 1694 (2005).

129. B. Pérez López, A. Merkoçi, 'Improvement of the Electrochemical Detection of Catechol by the Use of a Carbon Nanotube Based Biosensor', *Analyst*, **134**, 60 (2009).

130. M. Pandurangappa, N.S. Lawrence, L. Jiang, T.G.J. Jones, R.G. Compton, 'Physical Adsorption of N,N-diphenyl-p-phenylenediamine Onto Carbon Particles: Application to the Detection of Sulphide', *Analyst*, **128**, 473 (2003).

131. J. Wang, G. Liu, M.R. Jan, 'Ultrasensitive Electrical Biosensing of Proteins and DNA: Carbon-Nanotube Derived Amplification of the Recognition and Transduction Events', *J. Am. Chem. Soc.*, **126**, 3010 (2004).

132. X. Yu, B. Munge, V. Patel, G. Jensen, A. Bhirde, J.D. Gong, S.N. Kim, J. Gillespie, J.S. Gutkind, F. Papadimitrakopoulos, J.F. Rusling, 'Carbon Nanotube Amplification Strategies for Highly Sensitive Immunodetection of Cancer Biomarkers', *J. Am. Chem. Soc.*, **128**, 11199 (2006).

133. Z. Jia, Z. Wang, C. Xu, J. Liang, B. Wei, D. Wu, S. Zhu, 'Study on Poly(methyl methacrylate)/carbon Nanotube Composites', *Mater. Sci. Eng., A*, **271**, 395 (1999).

134. T.M. Wu., Y.W. Lin, 'Doped Polyaniline/Multi-Walled Carbon Nanotube Composites: Preparation, Characterization and Properties', *Polymer*, **47**, 3576 (2006).

135. M. Pumera, A. Merkoçi, S. Alegret, 'Carbon Nanotube-Epoxy Composites for Electrochemical Sensing', *Sens. Actuators, B*, **113**, 617 (2006).

136. E. Bekyarova, M. Davis, T. Burch, M.E. Itkis, B. Zhao, S. Sunshine, R.C. Haddon, 'Chemically Functionalized Single-Walled Carbon Nanotubes as Ammonia Sensors', *J. Phys. Chem. B*, **108**, 19717 (2004).

137. C.R. Martin, 'Template Synthesis of Electronically Conductive Polymer Nanostructures', *Acc. Chem. Res.*, **28**, 61 (1995).

138. S.E. Brunker, K.B. Cederquist, C.D. Keating, 'Metallic Barcodes for Multiplexed Bioassays', *Nanomedicine*, **2**, 695 (2007).

139. F. Patolsky, B.P. Timko, G. Zheng, C.M. Lieber, 'Nanowire-Based Nanoelectric Devices in the Life Sciences', *MRS Bull.*, **32**, 142 (2007).

140. L.G. Carrascosa, M. Moreno, M. Alvarez, L.M. Lechuga, 'Nanomechanical Biosensors: A New Sensing Tool', *Trends Anal. Chem.*, **25**, 196 (2006).

141. C.M. Lieber, Z.L. Wang, 'Functional Nanowires', *MRS Bull.*, **32**, 99 (2007).

142. F. Patolsky, G. Zheng, C.M. Lieber, 'Nanowire-Based Biosensors', *Anal. Chem.*, **78**, 4260 (2006).

143. J.I. Hahm, C.M. Lieber, 'Direct Ultrasensitive Electrical Detection of DNA and DNA Sequence Variations Using Nanowire Nanosensors', *Nano Lett.*, **4**, 51 (2004).

144. Y. Cui, Q. Wei, H. Park, C.M. Lieber, 'Nanowire Nanosensors for Highly Sensitive and Selective Detection of Biological and Chemical Species', *Science*, **293**, 1289 (2001).

145. F. Patolsky, G. Zheng, C.M. Lieber, 'Fabrication of Silicon Nanowire Devices for Ultrasensitive, Label-Free, Real-Time Detection of Biological and Chemical Species', *Nat. Protoc.*, **1**, 1711 (2006).

146. G. Zheng, F. Patolsky, Y. Cui, W.U. Wang, C.M. Lieber, 'Multiplexed Electrical Detection of Cancer Markers with Nanowire Sensor Arrays', *Nat. Biotechnol.*, **23**, 1294 (2005).

147. Y.L. Bunimovich, Y.S. Shin, W.S. Yeo, M. Amori, G. Kwong, J.R. Heath, 'Quantitative Real-Time

Measurements of DNA Hybridization with Alkylated Nonoxidized Silicon Nanowires in Electrolyte Solution', *J. Am. Chem. Soc.*, **128**, 16323 (2006).

148. E. Stern, J.F. Klemic, D.A. Routenberg, P.N. Wyrembak, D.B. Turner-Evans, A.D. Hamilton, D.A. LaVan, T.M. Fahmy, M.A. Reed, 'Label Free Immunodetection with CMOS-Compatible Semiconducting Nanowires', *Nature*, **445**, 519 (2007).
149. H. Bayley, L. Jayasinghe, 'Functional Engineered Channels and Pores', *Mol. Membr. Biol.*, **21**, 209 (2004).
150. H. Bayley, P.S. Cremer, 'Stochastic Sensors Inspired by Biology', *Nature*, **413**, 226 (2001).
151. P. Kohli, C.C. Harrell, Z. Cao, R. Gasparac, W. Tan, C.R. Martin, 'DNA-Functionalized Nanotube Membranes with Single-Base Mismatch Selectivity', *Science*, **305**, 984 (2004).
152. J. Schmidt, 'Stochastic Sensors', *Mater. Chem.*, **15**, 831 (2005).
153. M.Y. Wu, D. Krapf, M. Zandbergen, H. Zandbergen, P.E. Batson, 'Formation of Nanopores in a SiN/SiO2 Membrane with an Electron Beam', *Appl. Phys. Lett.*, **87**, 113106–113101 (2005).
154. N. Li, S. Yu, C.C. Harrell, C.R. Martin, 'Conical Nanopore Membranes: Preparation and Transport Properties', *Anal. Chem.*, **76**, 2025 (2004).
155. N. Ashkenasy, J. Sánchez-Quesada, H. Bayley, M.R. Ghadiri, 'Recognizing a Single Base in an Individual DNA Strand: A Step Toward DNA Sequencing in Nanopores', *Angew. Chem., Int. Ed. Engl.*, **44**, 2 (2005).
156. J. Nakane, M. Wiggin, A. Marziali, 'A Nanosensor for Transmembrane Capture and Identification of Single Nucleic Acid Molecules', *Biophys. J.*, **87**, 615 (2004).
157. H. Chang, F. Kosari, G. Andreadakis, M.A. Alam, G. Vasmatzis, R. Bashir, 'DNA-Mediated Fluctuations in Ionic Current Through Silicon Oxide Nanopore Channels', *Nano Lett.*, **4**, 1551 (2004).
158. P. Chen, J. Gu, E. Brandin, Y.R. Kim, Q. Wang, D. Branton, 'Probing Single DNA Molecule Transport Using Fabricated Nanopores', *Nano Lett.*, **4**, 2293 (2004).
159. A.J. Storm, J.H. Chen, H.W. Zandbergen, C. Dekker, 'Translocation of Double-Strand DNA Through a Silicon Oxide Nanopore', *Phys. Rev. E*, **71**, 051903–051901 (2005).
160. A.J. Storm, C. Storm, J. Chen, H. Zandbergen, J.F. Joanny, C. Dekker, 'Fast DNA Translocation Through a Solid-State Nanopore', *Nano Lett.*, **5**, 1193 (2005).
161. J.E. Wharton, P. Jin, L.T. Sexton, L.P. Horne, S.A. Sherrill, W.K. Mino, C.R. Martin, 'A Method for Reproducibly Preparing Synthetic Nanopores for Resistive-Pulse Biosensors', *Small*, **8**, 1424 (2007).
162. M. Ali, B. Yameen, R. Neumann, W. Ensinger, W. Knoll, O. Azzaroni, 'Biosensing and Supramolecular Bioconjugation in Single Conical Polymer Nanochannels, Facile Incorporation of Biorecognition Elements into Nanoconfined Geometries', *J. Am. Chem. Soc.*, **130**, 16351 (2008).
163. E.A. Heins, Z.S. Siwy, L.A. Baker, C.R. Martin, 'Detecting Single Porphyrin Molecules in a Conically Shaped Synthetic Nanopore', *Nano Lett.*, **5**, 1824 (2005).
164. C.C. Harrell, Y. Choi, L.P. Horne, L.A. Baker, Z.S. Siwy, C.R. Martin, 'Resistive-Pulse DNA Detection with a Conical Nanopore Sensor', *Langmuir*, **22**, 10837 (2006).
165. Z. Siwy, L. Trofin, P. Kohli, L.A. Baker, C. Trautmann, C.R. Martin, 'Protein Biosensors Based on Biofunctionalized Conical Gold Nanotubes', *J. Am. Chem Soc.*, **127**, 5000 (2005).
166. I. Vlassiouk, P. Takmakov, S. Smirnov, 'Sensing DNA Hybridization Via Ionic Conductance Through a Nanoporous Electrode', *Langmuir*, **21**, 4776 (2005).
167. P. Takmakov, I. Vlassiouk, S. Smirnov, 'Hydrothermally Shrunk Alumina Nanopores and their Application to DNA Sensing', *Analyst*, **131**, 1248 (2006).
168. O.A. Saleh, L.L. Sohn, 'An artificial Nanopore for Molecular Sensing', *Nano Lett.*, **3**, 37 (2003).

Structural characterization by confocal laser scanning microscopy and electrochemical study of multi-walled carbon nanotube tyrosinase matrix for phenol detection†

Maria Guix,[ab] Briza Pérez-López,[a] Melike Sahin,[ac] Mònica Roldán,[d] Adriano Ambrosi[a] and Arben Merkoçi*[ae]

Received 14th January 2010, Accepted 13th May 2010
DOI: 10.1039/c000929f

A novel visualization methodology based on the use of immunofluorescence and Confocal Laser Scanning Microscopy (CLSM) was used to quantify and visualize tyrosinase enzyme within a MWCNTs matrix immobilized onto carbon based screen-printed electrodes. CLSM was shown to be an extremely powerful technique which allowed a clear visualization of the distribution of the enzyme within both the MWCNTs and carbon based layers and provided additional and useful morphological data for a better understanding of the interaction between biomolecules and electrode materials. Transmission Electron Microscopy (TEM) and Scanning Electron Microscopy (SEM) were also employed to fully characterize the system components. The proposed MWCNT/Tyrosinase matrix was applied to the detection of phenol, as an alternative biosensor material. Electrochemical analytical performances of the biosensor were investigated in order to determine the optimal fabrication design along with the enzyme stability. The biosensor based on the developed biomaterial matrix proved promising results in terms of cost, simplicity and analytical performance. A detection limit of 1.35 μM and a sensitivity of 47.4 μA mM^{-1} within a linear response range of 2.5 to 75 μM phenol were obtained. The biosensor performed well as a disposable device and could be stored in a refrigerator (−18 °C) without loss of activity for up to 2 months.

Introduction

Phenolic compounds are on the priority pollutants list of the European Community and the environmental Protection Agency of the United States because of their toxicity and persistency in the environment. They are commonly used in resin manufacture, and polymer and pharmaceutical products.[1] As they are compounds of particular environmental significance, it is important to be able to quantify and monitor them on-site.

Phenolic compounds are classically determined by gas chromatography and spectrophotometric analyses,[2] but these techniques are expensive, time-consuming and difficult to apply *in situ*. Electrochemical biosensors represent a promising alternative to the mentioned technique due to the extremely high sensitivity achievable, the simplicity of their use, very low cost and the fact that biosensors can be easily combined with miniaturized devices. Amperometric biosensors based on tyrosinase enzyme show high selectivity for phenol detection. Different matrixes such as carbon paste,[3] graphite epoxy composite,[4] sol–gel composite,[5] graphite-teflon electrodes,[6] glassy carbon electrodes[7] and screen-printed electrodes (SPEs)[8] have been reported. Screen-printing is a well-established microfabrication technology for the mass production of thick film electrodes and it is widely applied to build biological or chemical sensors,[9] which can be used without complicated sample pretreatment and therefore are suitable for on-site monitoring.[10]

Immobilization of the enzyme represents the crucial point in obtaining adequate sensitivities and overall stability of the biosensor. Different approaches, based on adsorption, covalent binding[11] or entrapment in polymers,[12] have been performed to achieve better immobilization of the enzyme. Nanostructured materials can be used to improve the incorporation of the enzyme into the sensing matrix and avoid its leaking. Better responses in terms of the biosensor performance are related to the intrinsic properties of the nanostructured materials used. Carbon nanotubes (CNTs) have unique structure-dependent electronic and mechanical properties[13] that when coupled with the specific recognition properties of enzymes provide important improvements in biosensors. Their advantages in electrochemical biosensing applications are mostly related to their capacity to mediate electron transfer reactions between electroactive species[14] and transducers thanks to their excellent electrical conductivity. Other exceptional properties of CNTs such as their mechanical strength and large surface area, which make them a potential linking bridge to attach biomolecules to the biosensor transducer, have been reported.[15,16]

[a]*Nanobioelectronics and Biosensors Group, Catalan Institute of Nanotechnology, UAB Campus, 08193 Bellaterra, Spain. E-mail: arben.merkoci.icn@uab.es; Fax: +34 935868020; Tel: +34 935868014*
[b]*Autonomous University of Barcelona, UAB Campus, 08193 Bellaterra, Spain*
[c]*Akdeniz University, Dumlupinar Boulevard, 07058 Campus Antalya, Turkey*
[d]*Microscopy Service, Autonomous University of Barcelona, UAB Campus, 08193 Bellaterra, Spain*
[e]*ICREA, Spain*

† Electronic supplementary information (ESI) available: Operational conditions in confocal studies, evaluation of possible autofluorescence of the materials and supplementary figures S1–S5. See DOI: 10.1039/c000929f

Incorporating carbon nanotubes into sensing devices generally requires the dispersion of CNTs in certain solvents so they can be processed into thin films or other applications.[17] To control the properties of the CNTs it is necessary to remove foreign nanoparticles that modify the physico-chemical properties of carbon nanotubes. CNTs processing permit the elimination of non-nanotube material, dispersion of individual nanotubes and chemical functionalization.[18] Purification of CNTs by sonication can induce sidewall[19] or end[20] functionalization, which is of interest for facilitating their manipulations.[21]

An accurate and extensive characterization of the CNTs based matrix is very important for understanding the improved response mechanisms and consequently a correct interpretation of the device responses. Although CNTs are usually characterized prior to application by electron microscopy (SEM and TEM), Raman spectroscopy, thermal analysis and absorption spectroscopy (UV-Vis-NIR), it is also important to evaluate their properties once they have been applied/integrated into a matrix where biological molecules (*i.e.* enzymes) will be included. Careful testing with these techniques provides important information on the morphology, distribution and possible linkages of CNTs that can lead to significant improvements in CNTs based biosensors. In addition to the above mentioned techniques, confocal laser scanning microscopy (CLSM) is emerging as an indispensable tool that can provide valuable information related to the distribution of the incorporated enzyme within the sensing matrix layer.[22]

CLSM can be useful for characterizing not only the outer layer of the biosensing surface but also its interior, and provide at the same time a relative quantification of the enzyme. These studies aim to obtain a better understanding and control of the structure, shape and composition of the CNTs based biosensing materials and could be of interest for further investigations including biofuel cells,[23] drug delivery[24] or biomarkers analysis,[25] between others. Step by step CLSM characterisations of the carbon nanotube and tyrosinase based sensor along the preparation and use in order to further relate its structural characteristics to the electrochemical behaviour are presented. The study has not been limited to the 3D visualization of the matrix, but also an extensively CLSM statistical study to evaluate material roughness and its effect on enzyme distribution has been performed. Enzyme distribution and aggregation effects considered of crucial importance on the electrochemical process have also been studied.

Experimental

Materials and equipment

The following materials were obtained from the respective suppliers and used as received, except where indicated: CNTs powders (Aldrich, Germany, 95% purity), tetrahydrofuran (Fluka, Spain), phenol (SigmaUltra, Spain, > 99.5%), tyrosinase from mushroom (Sigma; *BioChemika*, Spain, lyophilized, ≥ 2000 units/mg 93898), mouse anti-tyrosinase (Invitrogen, United States, unconjugated monoclonal antibody specific to human tyrosinase. Concentration: 100μg/200μl.), Alexa Fluor ® 488 (Invitrogen, Molecular Probes, United States), TWEEN 20© (Sigma, Spain).

Potassium phosphate buffer (PBS) of pH 6.5 was prepared with potassium phophate monobasic (Fluka), potassium phosphate dibasic anhydrous and potassium chloride in MilliQ water. TWEEN buffer was prepared with TWEEN 20© (Aldrich).

Electrochemical experiments were performed using a model CHI 660A electrochemical workstation from CH Instrument Inc., Austin, TX. All electrochemical experiments were performed in a system composed of an electrochemical cell with the introduced SPE that contains working, auxiliary and reference electrodes in a single strip. SPE were fabricated in a semi-automatic screen-printing machine DEK 248 (DEK International, Switzerland), and the materials used were polyester sheets (Autostat HT5 from McDermid Autotype), Acheson carbon ink (Electrodag PF407C), Acheson silver/silver chloride ink (Electrodag 6037SS), and Minico 7000 Blue insulating ink (Acheson Industries, The Netherlands). Scanning electron microscopic images (SEM) of SPE were obtained using a Hitachi S-570 (Hitachi Ltd, Japan). Observations were carried out using a Leica TCS SP2 AOBS confocal microscope (Leica Microsystems, Germany) for the roughness experiments, a Leica TCS SP5 AOBS confocal microscope (Leica Microsystems, Germany) for the 3D images and to evaluate the enzyme distribution, and an Olympus FluoView FV1000 (Olympus, Tokyo, Japan) confocal microscope to compare the fluorescence intensity of different electrode formulations under the same conditions (for more information on the working conditions of the confocal studies see the ESI†). Samples were observed on Mat-Teck culture dishes (Mat Teck Corp., United States).

Preparation and characterization of SPE and their modification with CNTs

Screen-printed microfabrication is based on the sequential deposition of a graphite ink, Ag/AgCl ink and an insulating ink on a polyester substrate. After each layer is deposited a drying process is carried out, which consists on keeping the polyester substrate at 90 °C for 15 min. Previously to their dispersion, CNTs were purified by stirring them in 2 M nitric acid at 25 °C for 24 h. Multiwalled CNTs used have a purity of 95%.[26] The working surface area of a bare SPE was modified by depositing a 7 μl drop of MWCNTs suspension (1 mg MWCNTs/1 ml THF) onto the working electrode surface, followed by a drying process at room temperature for 24 h. The characterization process of the working electrode surface was performed by SEM to check if a homogeneous distribution of CNTs over the surface was achieved. SPEs characterization was performed by SEM studies of the surface and profile of the working electrode. Electrodes were mounted on adhesive carbon films and then coated with gold. Profile images were taken from electrodes that were previously immersed in liquid N_2 and immediately cut with a knife.

Immobilization of tyrosinase onto the working electrode SPE

Tyrosinase was immobilized onto the electrode surface by physical adsorption. Tyrosinase was dissolved in 0.1 M phosphate buffer (PBS) at pH 6.5 (prepared with MilliQ water). Tyrosinase solution (1 mg Tyrosinase/50 μl PBS) was stirred during 1 h and deposited onto the working electrode surface,

which was followed by a drying process at room temperature during 3 h.

Immunostaining protocol of tyrosinase

The protocol followed for immunostaining the working electrode surface was based on first incubating the primary label mouse anti-tyrosinase (30 μg/ml) during 3 h at 30 °C in a thermo shaker. The sample was cleaned with TWEEN20 at 0.05% in order to remove the primary marker not specifically attached to the enzyme. The second incubation step with the secondary antibody anti-mouse IgG conjugated to Alexa Fluor® 488 (5 μg/ml) was carried out under the same conditions used for the primary marker. The sample was washed again with TWEEN20 and left to dry for an hour. Alexa 488 labels were excited with an Ar laser (488 nm) and detected in the 495 to 520 nm range. The autofluorescence of the materials used was also studied in the spectral range of interest.

Evaluation of the roughness of the sample

Several fields of the electrode surface were evaluated. CSLM in reflection mode and three-dimensional analysis (topographic image) to assess the different parameters of roughness were used. Roughness parameters were calculated according to DIN-EN-ISO 4287 (1997).[27] Average roughness (Pa; arithmetic average of the profile ordinates within the measured section), root mean square (Pq; root mean square value of the profile ordinates within the measured section), maximum values for the valleys (Pn, depth of the greatest profile valleys) and peaks (Pp; height of the highest profile peak) are measured.

Although CLSM has less resolution than SEM, it is not limited to the surface characterization of the materials. Being a non-destructive method it can provide quantitative information on the roughness and the relative surface-to-area value of the different electrodes evaluated.

Results and discussion

CNTs dispersion

CNTs must be dispersed into a suitable solvent in order to achieve their homogeneous distribution onto the working electrode surface. Chemical oxidation (by previously stirring CNTs into 2 M nitric acid at 25 °C for 24 h) and physical treatment (applying a sonication process at room temperature during 4 h) shorten the CNTs and lead to the partial oxidation of the CNTs to produce functional oxygenated groups at the open ends and defects along the sidewall.[28] Impurities and defects in CNTs were characterized by SEM microanalysis and showed that traces of iron (Fe), nickel (Ni) and potassium (K) from 0.5%, 1.6% and 1.5% were decreased to 0.1%, 0.9% and 0.4% after treatment with nitric acid.[29] CNTs were dispersed in THF (1 mg of CNTs/1 ml THF) during four hours by sonication.

The TEM image (see Fig. S1 of the ESI†) reveals a good dispersion of the CNTs in THF. At the same time, some impurities that are probably related to the remaining metals are observed in the different TEM images taken. Defects along the tubes can also be seen in addition to the impurities.

Working electrode characterization

There are many different ways to characterize surfaces and to compare them to each other. Visual comparison of SEM images represents the most common way. In addition, various roughness parameters have been previously identified as important to quantify different materials.[30] Surface characterization in terms of roughness and CNTs distribution was evaluated by taking SEM images of the electrode surfaces for both bare and MWCNTs modified SPEs (see Fig. 1A to C). The images of different areas (considering not only the working electrode surface, but also the insulator area, reference electrode and counter electrode) have been taken. These images (not shown) didn't demonstrate any effect of THF in terms of roughness. Profile images of the working electrode surface are shown in order to study the structure and roughness of the different layers that configure the membrane of a SPE modified with CNTs (Fig. 1D).

A more sponge-like structure of the MWCNTs modified surface (C2) in comparison to bare SPE surface (B2) can be observed. The cut view of the MWCNTs (Fig. 1D) clearly shows the MWCNTs layer deposited over the previous imprinted carbon layer. The evident roughness would be with interest for biosensing application due to the increased sensing area.

A more accurate quantitative study of the sensor surface is done by calculating several statistical data that correspond to the studied sensor surfaces using CLSM (using the reflection mode previously described). The average roughness (Pa), the root mean square (Pq), maximum values for the valleys (Pn) and peaks (Pp) of both bare and CNT modified SPEs are summarized in Table 1. These values clearly indicate that quantitatively SPE modified with CNTs have a higher average roughness and a higher maximum values for the valleys and peaks compared to the carbon surface of the unmodified SPE.

The CLSM data are in agreement with SEM images and confirm once again the increase of roughness, area, maximum values of valleys and peaks of the CNTs modified *versus* bare SPE.

Coupling CLSM with the specificity of immunostaining techniques has been proved to be a good technique for evaluating the distribution of biological species in certain matrixes.[31] Tyrosinase immobilization into the CNTs matrix can be evaluated by CLSM using optical sectioning through a material up to a 100 μm depth. Maximum height section studied was *ca.* 18.14 μm (corresponding to the electrode modified with CNTs). Taking several images of successive depth planes of the material allow three dimensional (3D) imaging of the matrix.

The possible autofluorescence of the different electrode constituents (*i.e.* polyester substrate and carbon ink) before and after applying the immunostaining protocol have been studied. The control of the possible autofluorescence coming from the different materials that constitute the biosensing area are also evaluated so as to avoid false positives. The used electrode materials didn't show any autofluorescence in the spectra of interest (results not shown). Consequently, the fluorescence of the studied sensors is only due to the presence of the tyrosinase in the different studied matrixes. This protocol allows the problems usually present in immunochemistry to be avoided. First, non-specific binding is prevented by using a non-ionic detergent

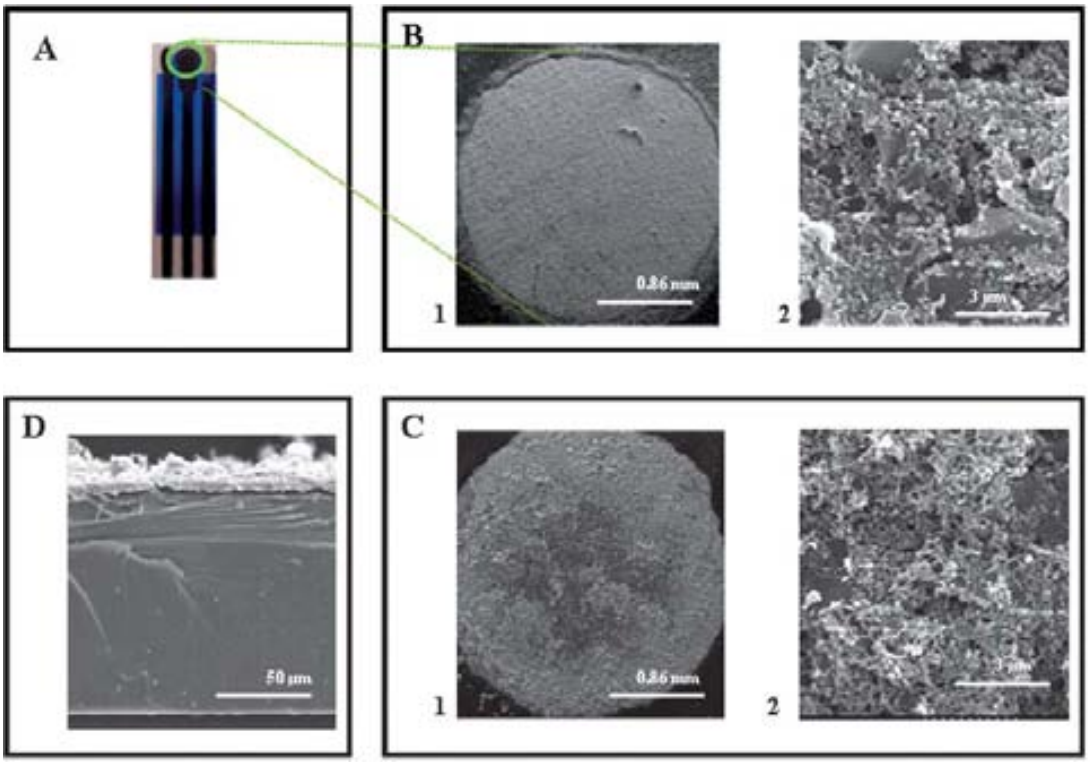

Fig. 1 Image of the SPE (A) where the working surface area evaluated by SEM is circled in green. SEM images of the working surface area of a bare (B) and MWCNTs (C) modified SPE at different resolutions: 0.86 mm (B1 and C1) and 3 μm (B2 and C2). In the case of SPE modified with MWCNTs, a suspension of 7 μl of MWCNTs dispersion (1 mg MWCNT/1 ml THF) was dropped onto the working electrode area and left to be dried at room temperature during 24 h. SEM image of the profile of SPE modified with MWCNTs (D) is also shown.

(TWEEN20) that removes the primary marker of the secondary label not specifically attached. By simultaneously combining temperature and agitation we prevented the extended incubation times, thus reducing the normal time of 48 h[31a] which can often provoke high background, to 3 h.

CLSM is suitable to study the enzyme distribution through the working electrode surface. An *in situ* 3D representation of this distribution can be seen in Fig. 2. A better distribution of tyrosinase onto the electrode surface as well as in depth is observed at the CNTs based SPE. Furthermore, it is possible to have been measured across all individual CLSM images of the stack. This value gives an idea of the sum of the total fluorescence in the frame scanned. As the fluorescence is proportional to the enzyme present in the sample, this integrated value can be related to the total enzyme adsorbed in this stack. Comparing the frame scanned for the bare and the modified SPE a quantity of the immobilized tyrosinase enzyme 1.96 times higher in the case of the MWCNTs modified SPE is found.

Additional information on the relation between the tyrosinase distribution and the roughness can be found by overlapping the signal obtained by the reflection mode and the fluorescence signal obtained in the same linear region of interest (ROI) (see Fig. 3). The graphics of the fluorescence *versus* the depth along the ROI (left Fig. 3 graphics) demonstrate that the enzyme distribution is directly affected by the roughness of the sample.

CLSM images (Fig. 2 & 3) including the corresponding 3D and ROI related graphics qualitatively demonstrate that tyrosinase is well-distributed within the surface and the depth of the CNTs based matrix.

A quantitative evaluation of the enzyme distribution through the sensor surfaces was also studied by using a Leica TCS SP5 CLSM with the AOBS (Acousto Optical Beam Splitter) yielding a 264 × 264 μm^2 field. An x–y line is drawn at increasing z depths to provide information on the evolution of the grey level intensity with z as shown in Fig. 4 (lower part). Graphs (upper part at Fig. 4) show that in both cases enzyme aggregates are formed.

Table 1 Quantitative information over the roughness of different formulations evaluated by CLSM. Formulation evaluated were bare SPE and SPE modified with CNTs. Statistical data and its standard deviation are presented and consists of the average roughness (Pa), root mean square (Pq), maximum values for the valleys (Pn) and peaks (Pp). Seven fields for each surface (bare and CNTs modified) were studied using the reflection mode evaluated by DIN-EN-ISO 4287[26]

SPE	Pa	Pq	Pn	Pp
Bare	1.51 ± 0.25	2.06 ± 0.57	14.57 ± 1.58	13.49 ± 3.14
CNTs modified	2.23 ± 0.39	3.03 ± 0.45	18.14 ± 1.62	15.52 ± 1.74

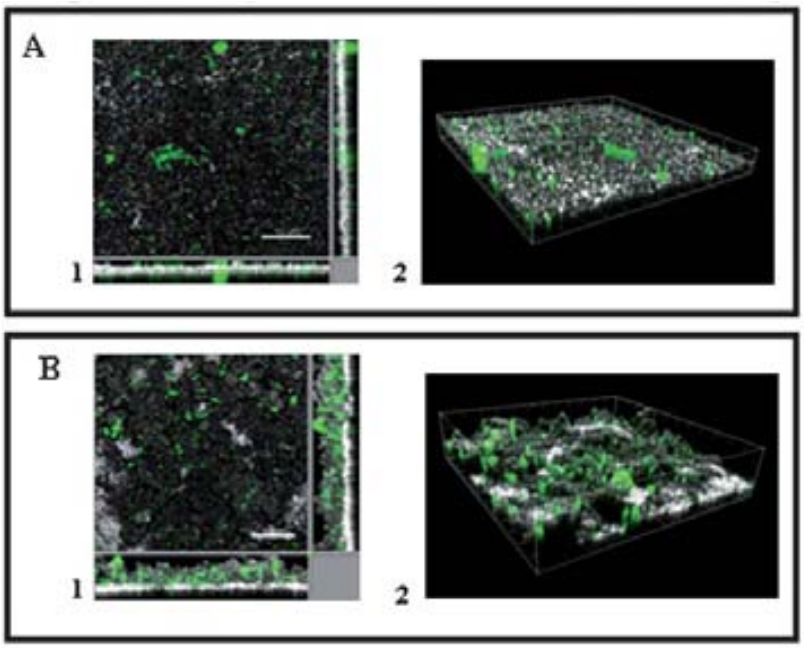

Fig. 2 CLSM images of the sensor surfaces. (A) Distribution of tyrosinase in the SPE carbon matrix (1) and its corresponding 3D confocal images (2). (B) Distribution of tyrosinase in the SPE CNTs matrix (1), and its corresponding 3D confocal images (2). Scale bar 50 μm. Experimental details as described in the text.

These aggregates are differently distributed depending on the matrix. The mentioned aggregates are related to wider and higher intensity bands observed in several *z* depths. Bigger but not homogeneously distributed aggregates can be observed in the case of the bare SPE (carbon based only) being a more homogenous distribution of the enzyme, with fewer and smaller aggregates for the CNTs matrix.

Electrochemical testing of SPE/MWCNT/Tyr

Tyrosinase has hydroxylase activity, by which phenol can be hydroxylated to catechol using molecular oxygen, and then oxidase activity that can catalyze the oxidation of catechol to o-quinone. At moderately negative potential the o-quinone product of phenol oxidation may be reduced electrochemically to

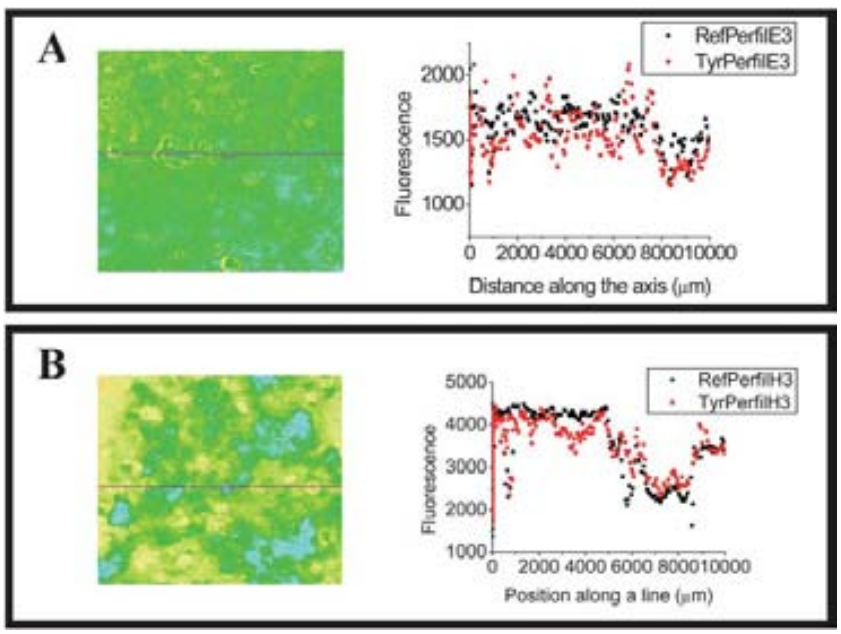

Fig. 3 Confocal micrographs of bare SPE (A) and CNTs modified SPE (B), with their corresponding graph. Fluorescence of the Alexa Fluor® 488 dye (pink) is overlapped with the signal obtained by working in the reflection mode (blue). ROI (linear region of interest) used for each surface is shown. Other experimental details as described in the text.

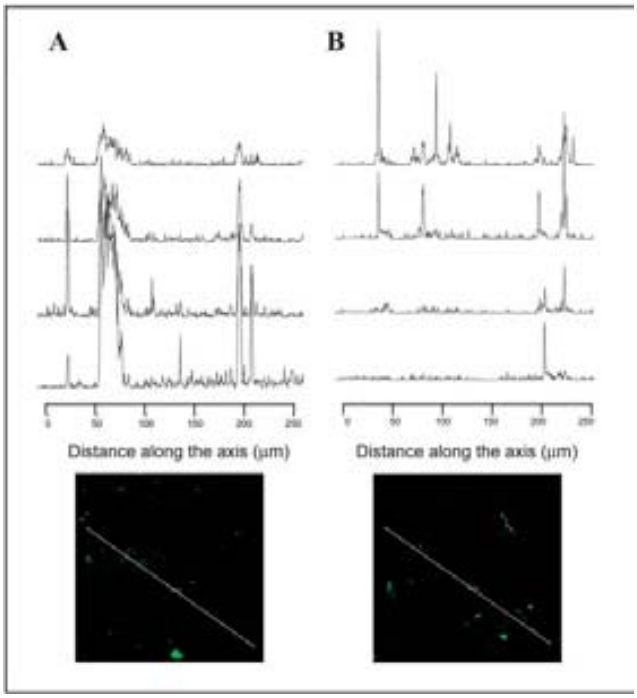

Fig. 4 Typical profiles of the grey level intensity along a given x–y line at increasing depths (step = 0.5μm) from $z = 20$ μm to $z = 60$ μm for the case of the enzyme immobilized in the bare SPE and the MWCNTs modified SPE. CLSM and other experimental conditions as explained in the text.

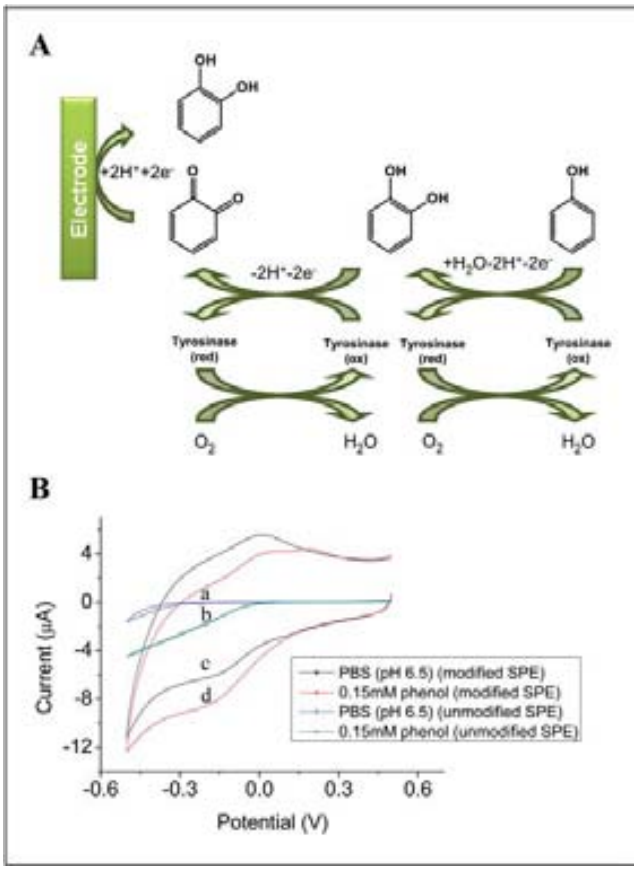

Fig. 5 Schematic diagram displaying the electrode reactions involved in the detection of phenol at the SPE surface using the tyrosinase enzyme (A). Cyclic voltammograms recorded for unmodified and modified SPE in 0.1 M PBS (pH 6.5) (B). Without (a), and with (b) 0.15 mM phenol addition with the SPE/Tyr biosensor; without (c) and with (d) 0.15mM phenol addition with the SPE/MWCNT/Tyr. Conditions used in the cyclic voltammograms: starting potential of 0.5 V; scan rate of 0.05 V/s and switching potential of −0.5 V. Reproducibility of peak potential, 11%; reproducibility of peak current, 39%.

catechol. Oxidation by the enzyme followed by reduction at the electrode may result in cycling between the catechol and o-quinone and yields a catalytically amplified current[6] (see Fig. 5A). Therefore, what is occurring at the electrode surface is the reduction of o-quinone to catechol (the working electrode acting as a cathode).

In order to understand the phenol detection mechanism using the developed MWCNT/Tyrosinase matrix cyclic voltammetry studies have been performed. The developed matrixes (SPE/Tyr and SPE/MWCNT/Tyr) are studied in the absence and presence of phenol substrate. While in the absence of phenol the SPE/Tyr did not give any significant response (see Fig. 5B, curve a) in the presence of phenol (Fig. 5B, curve b) a narrow shape CV characterized by a reduction peak (starting at −300 mV that goes toward more negative values) without reaching a plateau has been observed. A similar response to phenols at less negative potentials has also been previously reported.[6] SPE/MWCNT/Tyr displays a CV (Fig. 5B, curve c) with a broad shape and a peak at less negative potential (at −150 mV) in comparison to SPE/Tyr. In the presence of 0.15 mM of phenol an increase of the anodic current for SPE/MWCNT/Tyr (Fig. 5B, curve d) can be observed.

The working potential as well as enzyme loading have been studied. The working potential is a crucial parameter for the good operation of the biosensor. The optimum working potential is determined by two different methods. According to the first method, which is also the most reported, a hydrodynamic voltammogram is used to find the working potential (see Fig. S2 in the ESI†). This method consists in measuring the current obtained at different applied potentials for the same substrate concentration. A single addition of phenol is carried out before starting the experiment in stirring conditions. The variation of current *vs.* working potential is obtained and the optimal potential is determined according to the criteria of achieving a compromise between the highest current and the signal to noise ratio. According to the second method different chronoamperograms (current *vs.* phenol concentration for different working potential values) have been performed so as to better localize the working potential by also considering the phenol concentration level (see Fig. S3 in the ESI†).

The first method provides clear information on the best formulation according to the signal to noise criteria. The SPE/MWCNT/Tyr tyrosinase shows a higher current and a stable and practically without noise signal. The graphic of signal/noise *vs.* potential shows that the response to phenol for this matrix starts at −0.2 V. Taking into consideration the signal to noise ratio as well as the objective of working at the lowest potential value, a −0.2 V for SPE/MWCNT/Tyr was chosen as the optimal value for this first study.

Enzyme immobilization requires dissolving the tyrosinase enzyme. Enzyme was always solubilised in 0.1 M phosphate

buffer solution (PBS) pH 6.5, and the tyrosinase concentration used was 1 mg tyrosinase in 50 μl buffer. The responses to phenol detection were studied for two different concentration ranges of phenol: 2.5 μM to 25 μM and 25 μM to 250 μM. The first range is of special environmental interest. In the phenol concentration range of 25 to 250 μM the SPE/Tyr does not show any response while for the SPE/MWCNT formulation significantly enhances the current response (see Fig. S4 in the ESI†). The SPE modified with MWCNTs shows a stable and fast response for the first three additions, and starts to show saturation of the signal at the fourth addition due to the fouling of the electrode (Fig. 6). This fouling effect is mainly caused by the coupling reactions of o-quinone produced during phenol detection. This matrix is especially interesting for low phenol concentration detection, the high stability of the signal and the rapid response of the biosensor at the working range. Moreover, phenol concentrations over 2.5 and 25 μM are of special interest in the field of environmental analysis.

A stability study was carried out in order to evaluate the performance of the electrodes after being used (see Fig. 7). It can be observed that electrochemical activity of the electrode decreases from the first to the second day, probably due to the leaching of the enzyme from the surface of the SPE to the bulk of the solution. This would be due to the inefficiency of the immobilization method. Although the current tends to decrease after the second day, a considerable response was observed up to the seventh day. For the sake of comparability, the same conditions and stacks using an Olympus FluoView FV1000 microscope were considered (for more details see the ESI†). It is important to take into account that after electrochemical testing of the two matrixes (SPE with and without modification with CNTs), more aggregates were present in the SPE without CNTs (see Fig. 7).

SPEs modified with CNTs and tyrosinase with a concentration of 1 mg tyrosinase/50 μl buffer immobilized by physical adsorption were found to be the best conditions for phenol determination in batch. A range of phenol concentrations from 2.5 to 250 μM was studied. The analytical parameters related to our electrode formulation were a detection limit of 1.35 μM and a sensitivity of 47.4 μA mM^{-1} within a linear response range of 2.5 to 75 μM phenol (see Fig. 6). The limit of quantification, calculated as 10 times the concentration corresponding to noise level current, was found to be 4.51 μM; standard deviation of slope, 0.005 μM/μA; standard deviation of intercept, 0.008 μA. A shelf lifetime study (see Fig. S5 in the ESI†) was also performed and showed very promising results, with a shelf lifetime of 68 days while being stored in the refrigerator. This study consists in determining the lifetime during which the biosensor retains its quality under a certain set of storage conditions. This study was performed by keeping the SPEs modified with MWCNTs and tyrosinase in a refrigerator. The analytical performance of the electrodes was evaluated after 68 days and compared with the results obtained for the SPE checked on the first day of preparation. The analytical response of the electrodes after 68 days is practically the same as that of the preparation day.

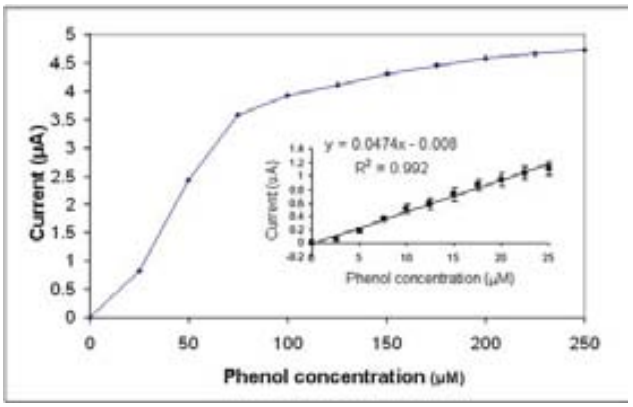

Fig. 6 Calibration plot corresponding to successive additions of 5 μl of a 2.5×10^{-5} M phenol solution into a 20 ml 0.1 M PBS (pH 6.5) during stirring conditions with a Tyr/MWCNT/SPE biosensor with tyrosinase concentration of 1 mg tyrosinase/50μl buffer. **Inset**: Calibration plot under the same conditions at the 2.5 to 25 μM range is shown.

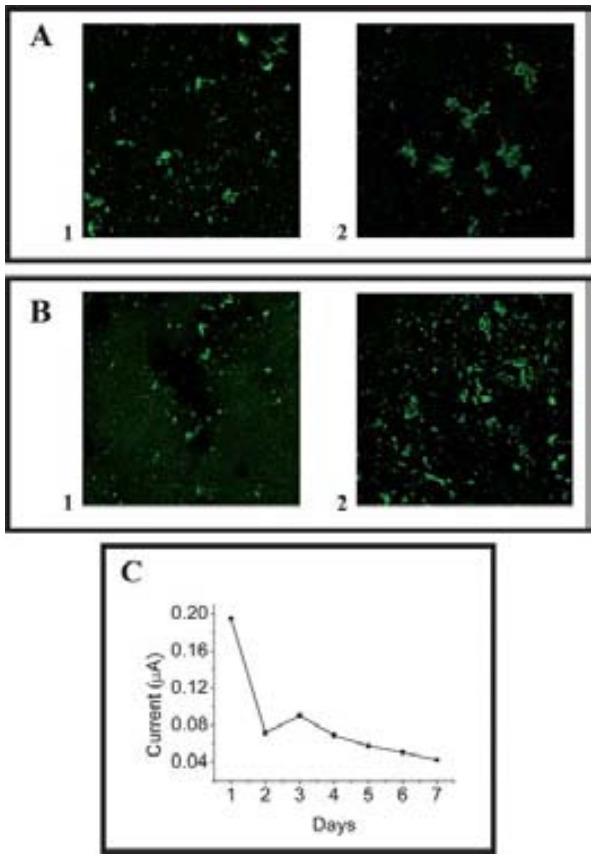

Fig. 7 *z*-projection of 20 stacks, separated by 0.5 μm, from bare SPE (A) and modified SPE with CNTs (B), both with the tyrosinase immobilized. Images A1 and B1 correspond to fresh electrodes not used for electrochemical measurements, and images A2 and B2 correspond to electrodes electrochemically tested after 7 days. Stability of the SPE/MWCNT with tyrosinase concentration of 1 mg tyrosinase/50 μl buffer toward a phenol solution obtained by adding 10 μl of a 5×10^{-6} M phenol solution into a 20 ml 0.1 M PBS (pH 6.5) during stirring conditions (C).

Conclusions

A promising MWCNTs and tyrosinase matrix (MWCNT/Tyr) applied onto the surface of a carbon based screen-printed

electrode (SPE) with interest to be used as phenol biosensor is developed. This matrix and the corresponding biosensor (SPE/MWCNT/Tyr) have advantages in terms of cost, simplicity, analytical performances while being used in phenol detection. SEM, TEM and Confocal Laser Scanning Mircroscopy (CLSM) studies had enabled a better understanding of the tyrosinase distribution within the MWCNTs based matrix. SPE without MWCNTs was compared to the SPE/MWCNT evaluating their roughness and how it interferes with the enzyme distribution by considering the enzyme distribution onto the surface as well as the depth of the carbon or MWCNTs matrix. Roughness has been qualitatively and quantitatively studied using SEM and CSLM. 3D images of CSLM demonstrate a better distribution of the enzyme onto the MWCNTs matrix while higher aggregate formation in the case of the bare SPE electrode have been visualized. The formation of aggregates is also observed after a certain period of use and is related to a loss of electrochemical activity.

In terms of electrochemical behaviour, the electrode presents a detection limit of 1.35 μM and a sensitivity of 47.4 μA mM^{-1} within a linear response range of 2.5 to 75 μM phenol was obtained. The developed biosensors performed well as disposable devices and could be saved in a freezer (−18 °C) for up to 2 months.

The obtained detection limit of the developed biosensor should be useful for monitoring phenol contamination in the case of accidental pollution, industrial effluents *etc*. The application of this biosensor in drinking water monitoring would need further improvements so as to achieve the European drinking water limits.

Acknowledgements

The financial support from the Spanish Ministry of Science and Innovation through project MAT2008-03079/NAN and predoctoral fellowship (BES-2009-023939 given to M. G.) are acknowledged.

Notes and references

1 S. E. Manahan, *Environmental Chemistry*; Lewis Publishers, Chelsea, MI, 1991.
2 V. Janda and K. Krijt, *J. Chromatogr., A*, 1984, **283**, 309–314.
3 (*a*) M. P. Byfield and R. A. Abuknestra, *Biosens. Bioelectron.*, 1994, **9**, 373–399; (*b*) L. Gorton, *Electroanalysis*, 1995, **7**, 23–45; (*c*) K. Kalcher, J. M. Kauffmann, J. Wang, I. Svancara, K. Vytras, C. Neuhold and Z. Yang, *Electroanalysis*, 1995, **7**, 5–22; (*d*) K. R. Rogers, J. Y. Becker and J. Cembrano, *Electrochim. Acta*, 2000, **45**, 4373–4379.
4 (*a*) B. Pérez and A. Merkoçi, *Analyst*, 2009, **134**, 60–64; (*b*) B. Serra, E. Mateo, M. Pedrero, A. J. Reviejo and J. M. Pingarrón, *Analusis*, 1999, **27**, 592–299.
5 (*a*) B. Wang and S. Dong, *J. Electroanal. Chem.*, 2000, **487**, 45–50; (*b*) Rajesh, W. Takashima and K. Kaneto, *React. Funct. Polym.*, 2004, **59**, 163–169; (*c*) J. Kochana, A. Gala, A. Parczewski and J. Adamski, *Anal. Bioanal. Chem.*, 2008, **391**, 1275–1281.
6 (*a*) B. Serra, E. Mateo, M. Pedrero, A. J. Reviejo and J. M. Pingarrón, *Analusis*, 1999, **27**, 592–299; (*b*) B. Serra, S. Jiménez, M. L. Mena, A. J. Reviejo and J. M. Pingarrón, *Biosens. Bioelectron.*, 2002, **17**, 217–226; (*c*) V. Carralero, M. L. Mena, A. Gonzalez-Cortés, P. Yáñez-Sedeño and J. M. Pingarrón, *Biosens. Bioelectron.*, 2006, **22**, 730–736.
7 (*a*) D. Shan, C. Mousty, S. Cosnier and S. Mu, *Electroanalysis*, 2003, **15**, 1506–1512; (*b*) M. A. Kim and W. Y. Lee, *Anal. Chim. Acta*, 2003, **479**, 143–150; (*c*) T. Zhang, B. Tian, J. Kong, P. Yang and B. Liu, *Anal. Chim. Acta*, 2003, **489**, 199–206.
8 (*a*) R. Solná and P. Skládal, *Electroanalysis*, 2005, **17**, 2137–2146; (*b*) M. R. Montereali, W. Vastarella, L. Seta and R. Pilloton, *Int. J. Environ. Anal. Chem.*, 2005, **85**, 795–806.
9 P. Fanjul-Bolado, D. Hernández-Santos and P. J. Lamas-Ardisana, *Electrochim. Acta*, 2008, **53**, 3635–3642.
10 (*a*) C. D. Chriswell, R. C. Chang and J. S. Fritz, *Anal. Chem.*, 1975, **47**, 1325–1329; (*b*) J. Poerschmann, A. Zhang, F. D. Kopinke and T. Pawliszyn, *Anal. Chem.*, 1997, **69**, 597–600.
11 M. R. Montereali, W. Vastarella, L. Seta and R. Pilloton, *Int. J. Environ. Anal. Chem.*, 2005, **85**, 795–806.
12 S. Sánchez, M. Roldán, S. Pérez and E. Fabregas, *Anal. Chem.*, 2008, **80**, 6508–6514.
13 Y. Degani and A. Heller, *J. Phys. Chem.*, 1987, **91**, 1285–1289.
14 X. Zhang, H. Ju and J. Wang, *Electrochemical Sensors, Biosensors and Their Biomedical Applications*, Elsevier, Amsterdam, 2007.
15 Y. P. Sun, L. F. Fu, Y. Lin and W. J. Huang, *Acc. Chem. Res.*, 2002, **35**, 1096–1104.
16 M. Meyyappan, *Carbon Nanotubes: Science and Applications*, CRC Press, Boca Raton, 2005.
17 (*a*) H. Luo, Z. Shi, L. Nangiang, G. Zhennan and Q. Zhuang, *Anal. Chem.*, 2001, **73**, 915–920; (*b*) J. Wang and M. Musameh, *Analyst*, 2004, **129**, 1–2.
18 U. Yogeswaran and S. M. Chen, *Anal. Lett.*, 2008, **41**, 210–243.
19 D. Tasis, N. Tagmatarchis, V. Georgakilas and M. Prato, *Chem.–Eur. J.*, 2003, **9**, 4001–4008.
20 J. Chen, M. A. Hamon, H. Hu, Y. Chen, A. M. Rao, P. C. Eklund and R. C. Haddon, *Science*, 1998, **282**, 95–98.
21 K. Gong, Y. Yan, M. Zhang, L. Su, S. Xiong and L. Mao, *Anal. Sci.*, 2005, **21**, 1383–1393.
22 J. Li, Z. Jiang, H. Wu, L. Zhang, L. Long and Y. Jiang, *Soft Matter*, 2010, **6**, 542–550.
23 (*a*) S. C. Wang, F. Yang, M. Silva, A. Zarow, Y. Wang and Z. Iqbal, *Electrochem. Commun.*, 2009, **11**, 34–37; (*b*) X. Li, H. Zhou, P. Yu, L. Su, T. Ohsaka and L. Mao, *Electrochem. Commun.*, 2008, **10**, 851–854; (*c*) Y. Yan, W. Zheng, L. Su and L. Mao, *Adv. Mater.*, 2006, **18**, 2639–2643.
24 (*a*) A. Bianco, K. Kostarelos and M. Prato, *Curr. Opin. Chem. Biol.*, 2005, **9**, 674–679; (*b*) K. Kostarelos, A. Bianco and M. Prato, *Nat. Nanotechnol.*, 2009, **4**, 627–633; (*c*) Z. Liu, A. C. Fan, K. Rakhra, S. Sherlock, A. Goodwin, X. Chen, Q. Yang, D. W. Felsher and H. Dai, *Angew. Chem., Int. Ed.*, 2009, **48**, 7668–7672; (*d*) W. Wu, R. Li, X. Bian, Z. Zhu, D. Ding, X. Li, Z. Jia, X. Jiang and Y. Hu, *ACS Nano*, 2009, **3**, 2740–2750.
25 X. Yu, B. Munge, V. Patel, G. Jensen, A. Bhirde, J. D. Gong, S. N. Kim, J. Gillespie, J. S. Gutking, F. Papadimitrakopoulos and J. F. Rusling, *J. Am. Chem. Soc.*, 2006, **128**, 11199–11205.
26 B. Pérez, M. Pumera, M. Valle, A. Merkoçi and S. Alegret, *J. Nanosci. Nanotechnol.*, 2005, **5**, 1694–1698.
27 ISO 4287. *Geometrical product specifications (GPS)-surface texture: profile method-terms, definitions and surface texture parameters, International Organization for Standardization*, Switzerland, 1997.
28 N. W. S. Kam, T. C. Jessop, P. A. Wender and H. Dai, *J. Am. Chem. Soc.*, 2004, **126**, 6850–6851.
29 G. Alarcón-Angeles, B. Pérez-López, M. Palomar-Pardave and M. T. Ramírez-Silva, *Carbon*, 2008, **46**, 898–906.
30 (*a*) M. Pohl and J. Stella, *Wear*, 2002, **252**, 501–511; (*b*) F. V. Antunes, A. Ramalho and J. M. Ferreira, *Int. J. Fatigue*, 2000, **22**, 781–788; (*c*) B. Işık, *Int. J. Adv. Manuf. Technol.*, 2008, **37**, 42–48.
31 (*a*) H. Liu and W. W. Y. Kao, *Mol. Vis.*, 2009, **15**, 505–517; (*b*) M. Chalal, F. Ehrburger-Dolle, I. Morfin, J. C. Vial, M. R. Aguilar, J. San-Roman, N. Bölgen, E. Piskin, O. Ziane and R. Casalegno, *Macromolecules*, 2009, **42**, 2749–2755.

Supplementary Material (ESI) for Analyst

Structural characterization by confocal laser scanning microscopy and electrochemical study of multi-walled carbon nanotube tyrosinase matrix for phenol detection

Maria Guix,[a,b] Briza Pérez[a], Melike Sahin[a,c], Mònica Roldán[d], Adriano Ambrosi[a] and Arben Merkoçi[a,e*]

Supporting information

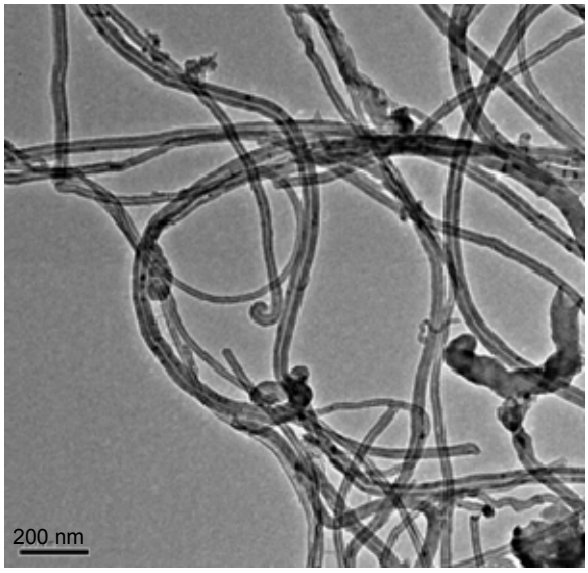

Figure S1. TEM image of the MWCNT purified and dispersed in THF (1mg of MWCNT/ 1ml THF).

- **Operational conditions in Confocal studies**

Roughness experiments were carried out using a Leica TCS SP2 AOBS confocal microscope (Leica Microsystems, Germany) equipped with a Plan Apo 20x (NA 0.4, dry). Stacks of 40 sections every 2µm were acquired along the z axis using the Leica Confocal Software. The profile roughness parameters were the average roughness (Pa) and the maximum profile peak height (Pp) and can be calculated according to DIN EN ISO 4287. The mean roughness, Pa, is the arithmetic average of the profile ordinates within the measured section (average height).

Leica TCS SP5 AOBS confocal laser scanning microscope (Leica Microsystems, Germany) was used to take 3D the images using a Plan Apo 63x (NA 1.4, oil HC x PL

APO lambda blue) objective. To determine the 3D structure, a series of horizontal (x-y) optical sections were collected at 0.5µ intervals along the material thickness. The projections of the series obtained were generated with Imaris v. 6.1.0. Software (Bitplane; Zürich, Switzerland). Profile analysis of fluorescence intensity was measured using Leica LAS AF software to determine the fluorescence intensity (FI) along the line segment.

To compare the fluorescence intensity, samples were observed under Olympus FluoView FV1000 microscope equited with a 60x/1.42 (oil PL APO) objective. The fluorescence intensity was measured at the same laser excitation and photomultiplier gain setting from SPE. Argon lasers were emitted at 488nm, at an intensity of 60%, a contrast of 1% and a sensibility of 800. To construct the fluorescent image, 20 sections separated by 0.5µm were taken. Images are presented as a *z*-projection of the 20 stacks acquired. Integrated fluorescene intensity of Anti-tyrosinase was quantified using the Metamorph software package (Universal Imaging Corporation Downington, PA). The data sets were exported into Microsoft Excel for analysis. The intensity of each pixel had a value ranging from 0 to 4095 level of gray.

- **Evaluation of possible autofluorescence of the materials**

Every layer that constitutes the electrodes studies (bare SPE and SPE modified with MWCNT) is studied in order to evaluate if they present auto fluorescence. Consequently, different materials were studied. First of all, support polystyrene sheet for both electrode configurations was evaluated for all the wavelengths, and specially for the range where our fluorophore (Alexa Fluor® 488) emits (the maximum adsorption is at 495nm and the maximum emission is on 519). In this case, polystyrene sheet only shows auto fluorescence in the blue spectral range. Therefore, polystyrene sheet doesn't represent any interference when the final experiments are held with Alexa Fluor® 488.

We did the control of the autofluorescence from the different components (Carbon, carbon nanotubes) including that of the tyrosinase without and with primary label alone and didn't found any fluorescence. Consequently the obtained signal, using the

secondary label (Alexa Fluor® 488), at the green spectra range, is only due to the presence of Tyrosinase marked with the primary and the secondary label.

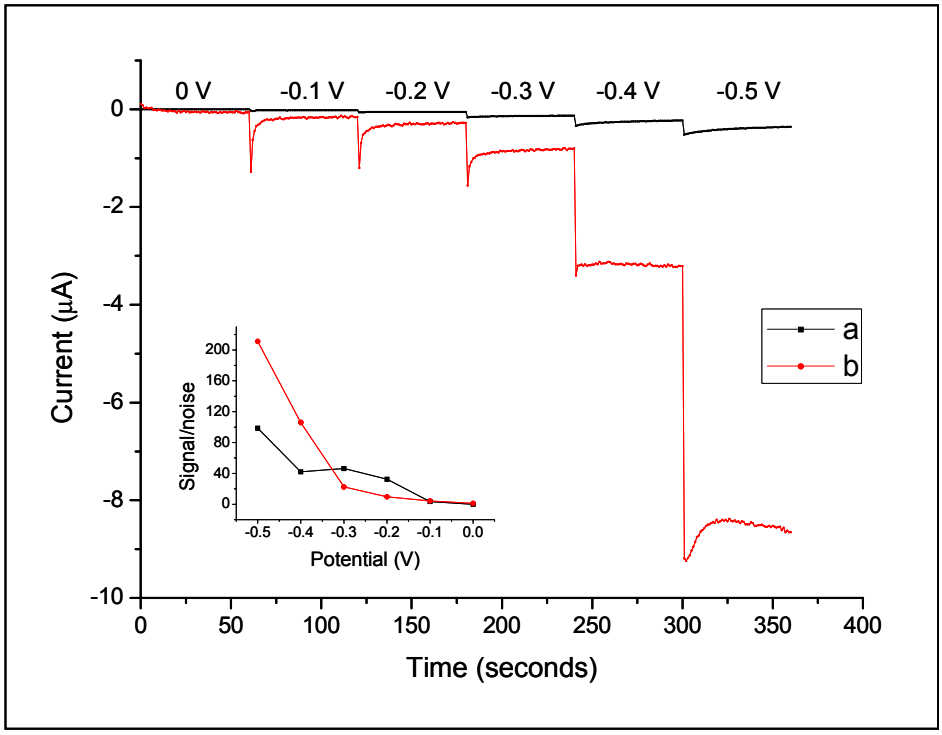

Figure S2. Hydrodynamic voltammograms for Tyr/SPE (a) and Tyr/MWCNT/SPE (b). Measurements are taken for a phenol concentration of 2.5 x 10-6 M into a 20 ml electrolytic cell containing 0.1M PBS (pH 6.5) under stirring conditions. **Inset**: corresponding graphic of signal/noise vs. potential for each formulation.

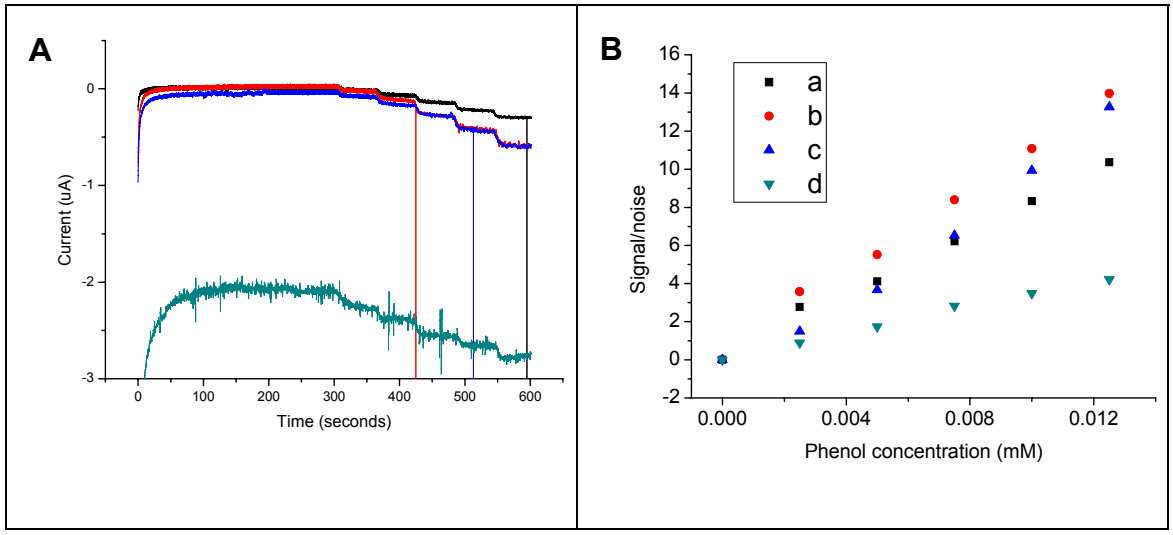

Figure S3. (**A**) Amperometric responses to a 2.5 x 10^{-6} M phenol solution successively added in 5µl (stock phenol solution: 0.01M) into a 20 ml electrolytic cell containing 0.1M PBS (pH 6.5) under stirring conditions. Tyr/MWCNT/SPE biosensors with tyrosinase concentration of (1mg tyrosinase/50µl buffer)

at different working potentials are evaluated: 0V (a), -0.1V (b), -0.2V (c) and -0.4V(d). (**B**) Corresponding calibration for the electrodes described in Figure 7**A**.

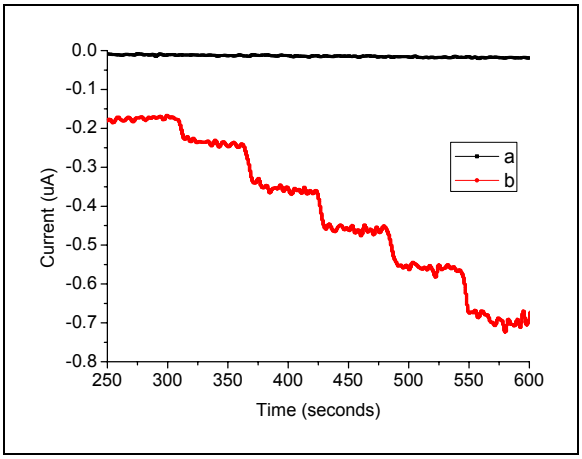

Figure S4. Amperometric responses for successive addition of 5µl of 2.5 x 10^{-6} M phenol solution into a 20 ml electrolytic cell containing 0.1M PBS (pH 6.5) under stirring conditions at a working potential of -0.2V for Tyr/SPE biosensor with tyrosinase concentration of 1mg tyrosinase/50µl buffer (a) and Tyr/MWCNT/SPE biosensor with tyrosinase concentration of 1mg tyrosinase/50µl buffer (b).

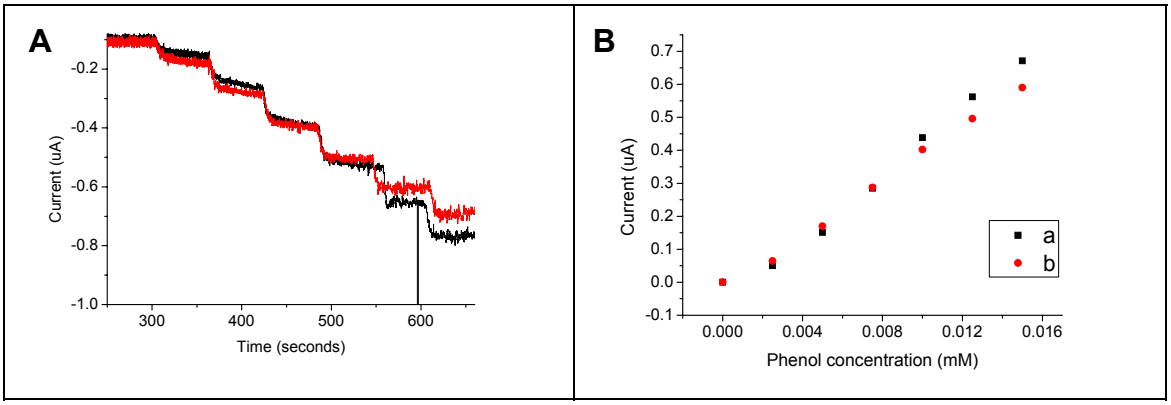

Figure S5. Shelf lifetime study. (**A**) Amperometric responses for successive additions of 25µl. of 5 x 10^{-6} M phenol solution successively added into a 20 ml 0.1M PBS (pH 6.5) under stirring conditions for a Tyr/MWCNT/SPE biosensor with tyrosinase concentration of 1mg tyrosinase/50µl buffer tested on the preparation day (24.11.08) (b) and after 68 days of being prepared (30.01.09). (**B**) Corresponding calibration plots

Stable and sensitive flow-through monitoring of phenol using a carbon nanotube based screen printed biosensor

2010 Nanotechnology 21 245502

(http://iopscience.iop.org/0957-4484/21/24/245502)

Nanotechnology **21** (2010) 245502 (9pp) doi:10.1088/0957-4484/21/24/245502

Stable and sensitive flow-through monitoring of phenol using a carbon nanotube based screen printed biosensor

G Alarcón[1,2], M Guix[1,3], A Ambrosi[1], M T Ramirez Silva[4], M E Palomar Pardave[2] and A Merkoçi[1,5,6]

[1] Nanobioelectronics and Biosensors Group, Catalan Institute of Nanotechnology, Campus UAB, 08193 Bellaterra, Barcelona, Catalonia, Spain
[2] Departamento de Materiales, Universidad Autónoma Metropolitana, Azcapotzalco, 02200 México Distrito Federal, Mexico
[3] Chemistry Department, Autonomous University of Barcelona, Campus UAB, 08193 Bellaterra, Barcelona, Catalonia, Spain
[4] Departamento de Química, Universidad Autónoma Metropolitana Iztapalapa, 09340 México Distrito Federal, Mexico
[5] ICREA, Barcelona, Catalonia, Spain

E-mail: arben.merkoci.icn@uab.es

Received 7 January 2010, in final form 21 April 2010
Published 25 May 2010
Online at stacks.iop.org/Nano/21/245502

Abstract

A stable and sensitive biosensor for phenol detection based on a screen printed electrode modified with tyrosinase, multiwall carbon nanotubes and glutaraldehyde is designed and applied in a flow injection analytical system.

The proposed carbon nanotube matrix is easy to prepare and ensures a very good entrapment environment for the enzyme, being simpler and cheaper than other reported strategies. In addition, the proposed matrix allows for a very fast operation of the enzyme, that leads to a response time of 15 s.

Several parameters such as the working potential, pH of the measuring solution, biosensor response time, detection limit, linear range of response and sensitivity are studied. The obtained detection limit for phenol was 0.14×10^{-6} M. The biosensor keeps its activity during continuous FIA measurements at room temperature, showing a stable response (RSD 5%) within a two week working period at room temperature.

The developed biosensor is being applied for phenol detection in seawater samples and seems to be a promising alternative for automatic control of seawater contamination. The developed detection system can be extended to other enzyme biosensors with interest for several other applications.

S Online supplementary data available from stacks.iop.org/Nano/21/245502/mmedia

1. Introduction

Phenolic compounds are important contaminants of ground and surface waters, causing problems for the living environment and showing adverse effects on animals and plants. Many analytical techniques, such as the optical method (Huili *et al* 2007), gas chromatography (Regueiro *et al* 2009), liquid chromatography (Zgoła-Grześkowiak *et al* 2009) and capillary electrophoresis (Li *et al* 2009) have been used for monitoring phenols. Therefore, the sensitive, rapid, and precise determination of phenols and its derivatives are of growing interest in environmental control and protection.

Electrochemical biosensors are considered to be the most attractive techniques for such applications. The use of electrochemical devices offers many advantages in comparison

6 Address for correspondence: Centre d'Investigació en Nanociència i Nanotecnologia Escola Tècnica, Superior d'Enginyeria (ETSE) Campus de la UAB-Edifici Q-2ªplanta, 08193 Bellaterra, Spain.

for example to optical methods. Electrochemical sensors can operate in turbid media and are more amenable to miniaturization, which is of crucial importance for monitoring purposes. In addition, the excellent compatibility of electrochemical sensors with flow injection analytical systems (FIA) increases the potential for assay automation, to which more and more attention has been paid in many fields including food analysis (Mizutani *et al* 1998) and environmental monitoring (Vazquez *et al* 2006).

One of the biggest challenges in designing a new enzyme-based biosensor is to find the optimal balance between stability and activity of the enzyme. Immobilization methods, such as cross-linking bonding (Jung and Paradiso 2009), covalent attachment (Drevon *et al* 2002), polymer inclusion (Umran and Memet 2009) and simple adsorption, have different effectiveness with regard to the stability of the signal generated, due to the fact that a higher or lower percentage of enzyme immobilized is lost during the measurement. On the other hand, better stability is generally obtained, paying the price of the loss of signal intensity related to a lower enzyme catalytic activity. A good combination of support material and immobilization method is of fundamental importance to achieve the desired performances from the sensing system.

With regard to the fabrication of enzyme-based phenol biosensors, many examples can be found in the literature, where various sources of tyrosinase and a wide variety of matrixes including graphite (Nistor *et al* 1999), carbon paste (Caruso *et al* 1999, Merkoçi *et al* 2005), conducting polymers (Adeyoju *et al* 1996, Christophe *et al* 2003), biopolymers (Aihua *et al* 2005), Nafion membrane (Furbee *et al* 1993), nanoparticles (Li *et al* 2006), silica sol–gel composite films (Li *et al* 1998) and hydrogel (Nistor *et al* 1999) have been used, with different combinations of stability and sensitivity, depending on the application.

The use of enzymatic electrodes is an inherently sensitive alternative for the detection of enzyme substrate. Many biosensors for phenol determination have been developed in the past using the catalytic activity of the redox enzymes such as tyrosinase, peroxidase, laccase (Duran and Esposito 2000) etc using different electrode materials, flow systems and sample pre-treatment techniques.

Some of these fabrication methods are relatively complicated and require the use of several reagents, and often the biosensor presents stability problems with usage and sometimes has a short lifetime (Dornelles and Tatsuo 2002). Currently, there is an increasing interest for the design of functional membranes for biosensing application because of their possible use for analytical applications (Liu *et al* 2005).

Biosensors based on carbon nanotubes (CNTs) have shown great potential in several fields. From the first application of CNTs as a modifier of glassy carbon electrodes for NADH detection (Wang *et al* 2002), several other interesting applications have been reported by our and other groups. The use of CNTs has become relevant due to their excellent conductivity, including the improvement of electron transfer between enzymes and electrode surfaces (Merkoçi 2006), and at the same time provides a very good matrix for enzyme immobilization (Pérez *et al* 2008). On the other hand, biosensors based on nanostructured compounds (Pérez *et al* 2005, Pumera *et al* 2006) have been demonstrated to be simple in preparation and offer great promise for developing amperometric biosensors.

In this work we propose a novel CNT based matrix for the fabrication of a stable biosensor for multiple and continuous monitoring of phenol content in seawater samples. In combination with an especially in-house-designed flow injection system, the sensing device offered excellent sensitivity with very low detection limits and also offers a concrete possibility of its implementation in automatic control systems.

2. Experimental details

2.1. Reagents

Tyrosinase (TYR, EC232-653-4, 5370 unit mg^{-1} from mushroom), phenol and glutaraldehyde (25%) were purchased from Sigma Co. (USA), and all other chemicals were analytical grade, and used without further purifications. Standard solutions of phenolic compounds were prepared by dissolving each reagent in water.

Multiwalled carbon nanotube (MWCNT) powders used were purchased from Aldrich (Stenheim, Germany) with a 95% purity, tetrahydrofuran (THF).

Potassium phosphate buffer solution (PBS) of pH 6.5 was prepared with potassium phosphate monobasic (Fluka), potassium phosphate dibasic anhydrous and potassium chloride in MilliQ water.

2.2. Preparation of the biosensor

2.2.1. Preparation of screen printed electrode (SPE). Screen printed microfabrication is based on the sequential deposition of a graphite ink, Ag/AgCl ink and insulating ink on a polyester substrate. After each layer is deposited a drying process is carried out, which consists in keeping the polyester substrate at 90 °C for 15 min.

2.2.2. MWCNT treatment. Previous chemical oxidation and thermal treatment in order to functionalize MWNCTs, and subsequently shorten and partially oxidize them, is performed as reported earlier (Pérez *et al* 2005). The chemical oxidation process consists in stirring MWCNTs in 2 M nitric acid (PanReac, Spain) at 25 °C for 24 h. The multiwalled CNTs used have a purity of 95%. After their purification, the CNT dispersion is held by sonicating a MWCNT suspension (1 mg MWCNT/1 ml THF) for 4 h. Some works have reported good CNT stability, and it has already been reported that chemical processing can improve the morphology and thermal stability of MWCNTs (Yang *et al* 2008). In addition, other works demonstrate CNT stability when they are treated with nitric acid, showing that the concentration in the dispersion after 30 days is 85% of the initial value (Peng *et al* 2009).

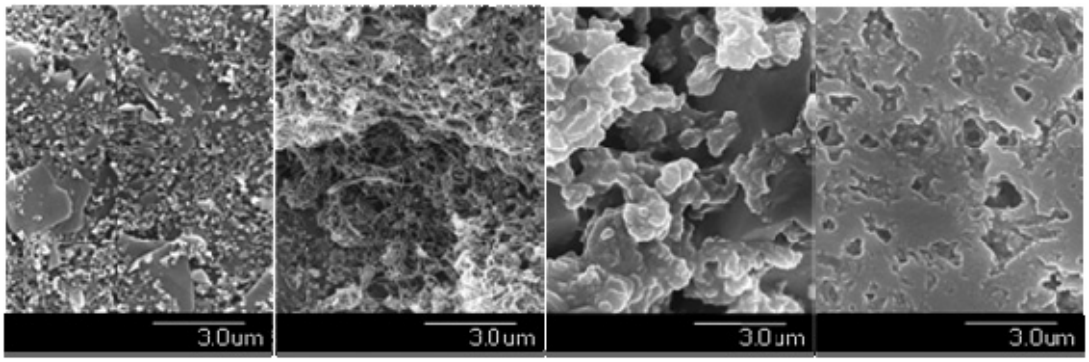

Figure 1. SEM images of the working surface area of (A) bare SPE, (B) SPE modified with MWCNTs, (C) SPE modified with MWCNT/Tyr and (D) SPE modified with MWCNT/Tyr/Glu. Images are taken at a resolution of 3 μm and an acceleration voltage of 15 kV.

2.2.3. Modification of SPE with CNT. The working surface area of a bare SPE was modified by depositing a 7 μl drop of MWCNT suspension (1 mg MWCNT/1 ml THF) onto the working electrode surface, followed by a drying process at room temperature for 24 h. The characterization process of the working electrode surface was performed by SEM to check if a homogeneous distribution of CNT over the surface was achieved.

2.2.4. Immobilization of the enzyme. 1 mg of tyrosinase (Tyr) enzyme was dissolved in 50 μl of 0.1 M phosphate buffer (PBS) at pH 6.5 (prepared with ultra-pure water from a Millipore-MilliQ system). A 7 μl drop of Tyr solution was deposited onto the working SPE/MWCNT electrode surface and allowed to dry at room temperature for 3 h. Finally, 7 μl of glutaraldehyde (Glu) solution at 5% were cast onto the SPE/MWCNT/Tyr electrode surface and left to dry at room temperature for 4 h. The prepared SPE/MWCNT/Tyr/Glu biosensor was kept at room temperature for stability study measurements or stored, if not in use, in the refrigerator at 5 °C.

2.3. Surface characterization

SPE characterization of the surface and the profile of the working electrode were performed by scanning electron microscope (SEM). Electrodes were mounted on adhesive carbon films and then coated with gold. SEM images were recorded with an S-570 SEM (Hitachi Ltd Japan) at an accelerating voltage of 15 kV.

2.4. Electrochemical measurement procedures

An FIA setup (see figure S1 in the supporting information available at stacks.iop.org/Nano/21/245502/mmedia) that uses a home-made flow-through cell of 20 μl was built and housed the SPE/MWCNT/Tyr/Glu biosensor, ensuring a stable operational analysis. In a typical measurement a 0.1 M buffer solution of pH 6.5 was introduced for 5 min at a flow rate of 3 ml min^{-1} by using a peristaltic pump (Perimax16/3). Volumes of phenol standard solutions from 0.5 to 25 μl were injected by using an automatic injector (Hamilton 36781). The injected phenol is passed through the electrochemical flow-through cell with the integrated SPE/MWCNT/Tyr/Glu biosensor. The measurements were performed under a flow-through regime. A working potential of −100 mV was applied and chronoamperometric measurements were performed by using a model Ch-Instrument potentiostat 660A electrochemical workstation from CH Instruments Inc., Austin, TX.

Impedance analysis of the prepared SPE modified electrodes was performed by using an Autolab302 potentiostat/galvanostat/frequency-response analyser PGST30, controlled by GPES/FRA Version 4.9. All impedance measurements were conducted in the presence of 50 mM $[Fe(CN)_6]^{3-/4-}$ (1:1) mixture in PBS (pH 7.0) as redox probe. The tested frequency range was from 10 mHz to 100 kHz with an applied potential of 240 mV. Nyquist (imaginary impedance versus real impedance) diagrams were recorded.

3. Results and discussion

3.1. Morphological studies by scanning electron microscope (SEM)

The morphology of the modified electrodes was examined by SEM. Figure 1 displays typical images of the bare (a), MWCNT (b), MWCNT/Tyr (c) and MWCNT/Tyr/Glu (d) modified SPE electrodes. CNT distribution and glutaraldehyde film were evaluated. It is observed that MWCNTs are homogeneously distributed for all the used matrices. A more sponge-like surface is observed for CNT modified electrodes in comparison to the bare SPE (figures 1(A) and (B)). This would lead to an increase of the surface-to-area ratio due to the MWCNT incorporation into the working electrode area. Regarding the glutaraldehyde film, its presence is clearly evidenced by the more planar surface (figure 1(D)).

Chemical processing can improve the morphology and thermal stability of MWCNTs (Yang *et al* 2008). We checked the presence of CNTs in the biosensing matrix after being electrochemically tested. SEM images (see figure S2 in the supporting information available at stacks.iop.org/Nano/21/245502/mmedia) show CNTs still dispersed within the glutaraldehyde film.

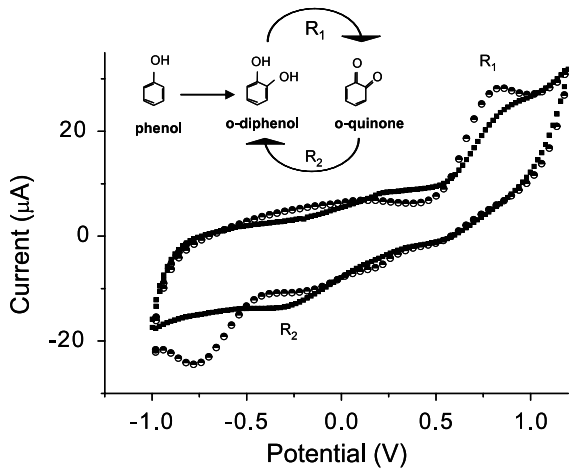

Figure 2. Cyclic voltammetry of 1 mM phenol with SPE/MWCNT (◓) and SPE/MWCNT/Tyr/Glu (■) in PBS, pH 6.5, scan rate 0.1 V s^{-1}; other experimental conditions as described in section 2 in the text.

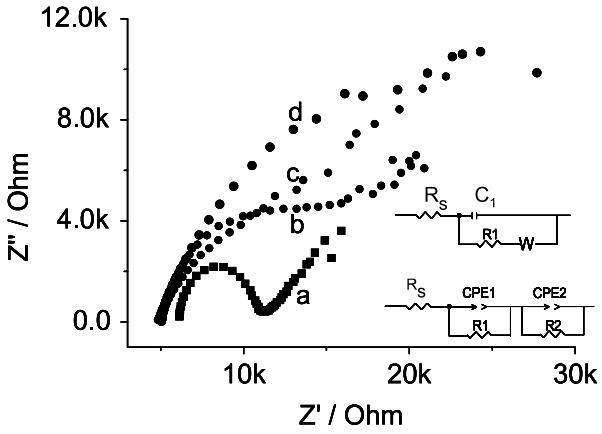

Figure 3. Typical Nyquist diagrams of electrochemical impedance analysis for (a) SPE, (b) SPE/MWCNT, (c) SPE/MWCNT/Tyr and (d) SPE/MWCNT/Tyr/Glu. A 50 mM $[Fe(CN)_6]^{3-/4-}$ (1:1) mixture in PBS (pH 7.0) is used as redox probe. The frequency range used was from 10 mHz to 100 kHz. Applied potential was 240 mV. Corresponding circuits to bare SPE (upper part) and SPE/MWCNT/TYR/Glu (lower part) are shown. R_s is the resistance of the electrolyte solution; C_1 is the double layer capacitance of the SPE surface; W is the Warburg impedance; R_1 is the electron transference resistance and R_2, CPE1 and CPE2 are the resistance and the capacitance associated with electrode films.

3.2. Biosensor's response mechanism toward phenol detection

In order to make a biosensor selective to phenol detection tyrosinase immobilization has been used in numerous ways. Tyrosinase (Tyr) is a known copper containing protein, which uses molecular oxygen to catalyse the oxidation of phenolic compounds in two steps: the orthohydroxylation of monophenols and the two-electron oxidation of *o*-diphenols to *o*-quinones (Solomon *et al* 1996) (R_1). This reaction was firstly studied by using cyclic voltammetry of the SPE/MWCNT/Tyr/Glu biosensor (SPE modified with MWCNT and Tyr and glutaraldehyde, –Glu– as explained in section 2). In figure 2, the reduction of *o*-quinone to *o*-diphenols (R_2) is already observed to start at around 0 mV. The current increases rapidly as the applied potential moves negatively from 0 to −400 mV, achieving a steady state at around −250 mV, which can be due to the increased driving force for the fast reduction of *o*-quinone at low potential.

Figure 2 also shows, for comparison purposes, the CVs of 1 mM phenol solution obtained by using an SPE/MWCNT biosensor (SPE modified with only MWCNTs as described in section 2). By comparing the responses given by SPE/MWCNT with that given by SPE/MWCNT/Tyr/Glu it can be clearly appreciated that it is difficult to see (R_2) the reduction of quinone in the case when the Tyr is missing.

(The peak at −750 mV also appears for the pH 6.5 PBS used as a blank; see figure S3 in the supporting information available at stacks.iop.org/Nano/21/245502/mmedia.)

3.3. Impedance studies

The surfaces of unmodified and modified SPEs are also investigated using electrochemical impedance spectroscopy (EIS). EIS is a well known method used to study the features of surface modified electrodes. It is employed to analyse the detailed electrochemical response of the modified electrode while using individual or mixed components. The impedance features are discussed in terms of Nyquist plots so as to analyse the contributions of different components of the cell. Figure 3 shows Nyquist plots of the impedance spectrum at different stages of SPE modifications. The electrode impedance is presented as a dependence plot between two components: the imaginary $Z''(\omega)$ versus real $Z'(\omega)$ components, that originate mainly from the capacitance and the resistance of the cell. From the shape of the impedance spectrum, the electron-transfer kinetics and diffusion characteristics can be extracted. The respective semicircles of the curves correspond to the electron-transfer resistance (R) and the double layer capacity (C) nature of the modified electrode.

The EIS presented as Nyquist plots (Z'' versus Z') for the bare, MWCNT, MWCNT/Tyr and MWCNT/Tyr/Glu modified SPE respectively are shown in figure 3. On the other hand bare SPE exhibits a semicircle at high frequencies that corresponds to the electron-transfer limited process and the linear part represents the characteristics of the diffusion limited electron-transfer process on the electrode surface. Under the same conditions the MWCNT modified SPE shows an increment in the diameter of the semicircle with an interfacial resistance. The increase of the semicircle is related to the increase of the capacitance due to the presence of carbon nanotube onto the SPE surface. The EIS of the MWCNT/Tyr and MWCNT/Tyr/Glu modified SPEs shows similar behaviours also related to their composition and morphology.

In the case of the CNT matrix the study shows an especially low electron-transfer resistance. At the same time the diffusion process is improved, due to the CNT contribution not only in enhancing surface-to-area ratio but also improving an increase in the faradaic currents, leading to an improvement in the electrochemical behaviour (reflected in the analytical parameters of the biosensor). In addition, biosensor lifetime

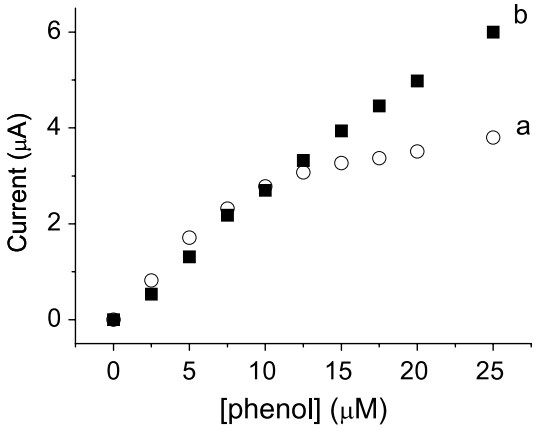

Figure 4. Effect of phenol concentration on the amperometric batch response of the biosensor: (a) SPE MWCNT/Tyr; (b) SPEMWCNT/Tyr/Glu. All measurements were made in 0.01 M phosphate buffer, pH 6.5 at 25 °C; an operating potential of −100 mV versus Ag/AgCl reference was used.

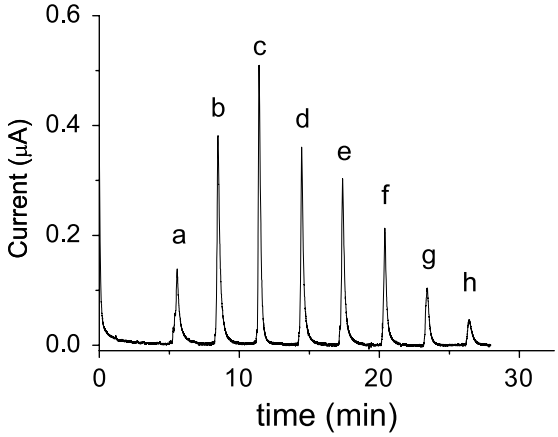

Figure 5. Amperometric responses of the SPE/MWCNT/Tyr/Glu biosensor at different pH values: (a) 4.67; (b) 5.99; (c) 6.50; (d) 7.16; (e) 7.53; (f) 8.18; (g) 8.52; (h) 8.82. Each peak corresponds to the injection of 20 μl of 10 μM of phenol solution at phosphate buffer 0.01 M, pH 6.5 at 25 °C; an operating potential of −100 mV versus Ag/AgCl was used. Other experimental conditions were as described in the text.

increases even in atmospheric conditions, making it not necessary to store them under strict environmental conditions.

The amperometric current responses of SPE/MWCNT/Tyr and SPE/MWCNT/Tyr/Glu versus phenol concentrations up to 25 μM were also studied (see figure 4) in order to find the effect of glutaraldehyde. SPE/MWCNT/Tyr (curve (a), figure 4) shows a lower sensitivity compared to SPE/MWCNT/Tyr/Glu (curve (b), figure 4). This phenomenon is probably due to the fact that the enzyme in the case of SPE/MWCNT/Tyr is directly exposed to substrate (phenol). The sites of catalytic activity of the enzyme are more accessible, compared to the case where glutaraldehyde is covering the enzyme. As seen from curve (a) of figure 4 the saturation of the enzyme for the SPE/MWCNT/Tyr biosensor seems to occur at a phenol concentration of around 10 μM. The calculated value of apparent Michaelis–Menten constant (K_M^{app}) for the SPE with free Tyr enzyme (SPE/MWCNT/Tyr) was 25 mM. This value for the enzyme covered by glutaraldehyde (SPE/MWCNT/Tyr/Glu) was 68 mM. K_M^{app} shows the affinity of an enzyme for its substrate, so if K_M^{app} is smaller this indicates a stronger substrate binding and higher catalytic activity. This effect is probably related to glutaraldehyde acting as an enzyme cross-linker. It helps a better immobilization of tyrosinase, preserving protein conformation (Quiocho and Richards 1964) and thus maintaining its biological activity (Avrameas 1969) and preventing leakage (Satish and Mohapatra 1994).

On other hand the K_M^{app} value for SPE/MWCNT/Tyr/Glu is lower compared to other reported matrixes used for Tyr immobilization like Tyr–titania sol–gel (Yu *et al* 2003), poly(allylamine)–tyrosinase–carbon fibre (PAA-Tyr-PAA/CF) (Rijiravanich *et al* 2006), graphite–Teflon (Serra *et al* 2002) and Tyr–ZnO nanorods (Chen *et al* 2007). The obtained results show that the MWCNTs connected with glutaraldehyde provide an excellent matrix for the immobilization of tyrosinase, which retains high catalytic activity for phenol oxidation.

3.4. Optimization of experimental variables

Parameters such as working potential, pH of the measuring solution, flow rate and injection time were analysed so as to find the optimum working conditions. The effect of applied potential on the phenol response of the biosensor was studied by the amperometric technique in the range of 0 to −500 mV (see figure S4 in the supporting information available at stacks.iop.org/Nano/21/245502/mmedia). The highest signal-to-noise ratio was recorded applying a working potential of −100 mV, and therefore this potential was used for the further optimizations and studies.

The enzymatic activity is greatly influenced by the medium pH; therefore, the sensor response was investigated using pH ranging from 4.6 to 8.8. Figure 5 shows the FIA responses of the biosensor for different pH values. The biosensor response increased from pH 4.6 up to 6.5. A gradually decreased response was observed at pH values above 6.5, which can be associated with a lower tyrosinase activity. The pH value of 6.5 was selected as optimal and used in all the following measurements.

Parameters related to the FIA system were also optimized. The effect of injection time from 2 to 30 s on the amperometric response of the biosensor towards phenol was studied (see figure S5 in section S1 available at stacks.iop.org/Nano/21/245502/mmedia). A stable and reproducible response at 10 s injection time was obtained. For shorter injection times (t < 10 s) the analytical response was not reproducible. A current decrease related to the short exposure time of the enzyme to the phenol substrate was observed. For longer injection times (10 s < t < 60 s) a saturation of the signal was observed. The heights of the peaks for retention times longer than 60 s remained almost constant but broadened, and therefore not adequate in terms of the time of analysis.

The study of the flow rate effect (results not shown) shows that the response time of the biosensor decreases at flow rates

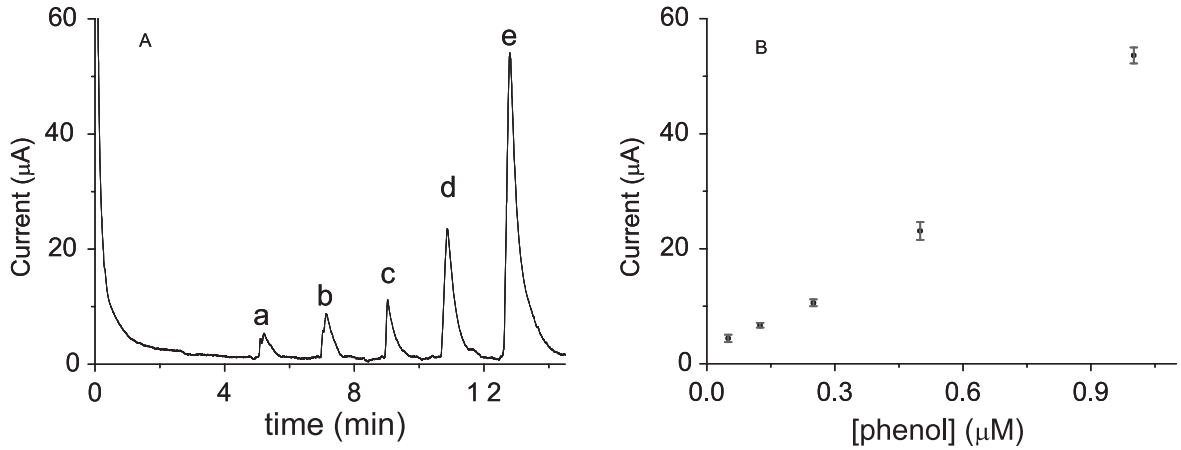

Figure 6. (A) FIA peaks obtained by chronoamperometric detection of phenol with concentrations of (a) 0.05, (b) 0.125, (c) 0.25, (d) 0.5, (e) 1 and (f) 1.25 μM. (B) Corresponding calibration curve of the current response versus phenol concentration. The error bars indicate the standard error for triplicate measurements. Conditions: temperature, 25 °C; operating potential, −100 mV versus Ag/AgCl reference; 0.01 M PBS solution at pH 6.5 is used as buffer. SPE/MWCNT/Tyr/Glu biosensor is used as detector.

lower than 2 ml min^{-1}. At higher rates the response time and the peak current increase. This is probably related to a more efficient diffusion process occurring under these conditions. This behaviour can be associated with chemical kinetics of the enzyme due to the fact that the response is better controlled by the enzymatic reaction at smaller volumes (Martinez *et al* 2008). A flow rate of 3 ml min^{-1} was chosen as the best to get a fast, stable and repeatable response.

3.5. Amperometric response of the biosensor

Electrochemical quantification of phenol using the FIA system was studied. The biosensor exhibited good response as a function of phenol concentration. The plot of the cathodic current versus phenol concentration (figure 6) in the range of 0.05–1 μM phenol shows a correlation coefficient of 0.99. The biosensor exhibits a sensitivity of 52.5 nA μM^{-1} and a detection limit of 0.14 μM phenol. The obtained detection limit is almost 500 times lower than the allowed levels of phenols in water as given by the EPA.

3.6. Stability study

The study of the analytical performance of the developed biosensor was performed in FIA conditions by following the cathodic current and using the optimal conditions obtained: applied potential (E_a) −100 mV; pH 6.5; flow rate 3 ml min^{-1}; injection time 10 s.

The typical current–time peaks were obtained for 10 μM phenol solution injections using the SPE/MWCNT/Tyr/Glu (see in figure S6 in the supporting information available at stacks.iop.org/Nano/21/245502/mmedia). Well defined peaks, virtually without any cathodic decay, were observed. A relative standard deviation (RSD) value for ten successive determinations and three replicates of 5.8% was obtained. An improved repeatability for phenol detection in comparison to other reported biosensors is obtained.

The long term stability of the biosensor (stored when not in use at room temperature in phosphate buffer 6.5) was tested for up to one month by monitoring of the cathodic current produced by injection of a 10 μM phenol solution every 3–5 days (results not shown). The biosensor shows stable response up to two weeks with an RSD of around 5%, while up to one month the RSD achieved a 25% value. The stability of this biosensor during this working period is related to the good entrapment of the enzyme within the MWCNT/Glu matrix. A remaining enzymatic activity of around 95% for a two week measuring period represents a good parameter compared to other complex matrices such as Fe_3O_4 MNPs-CNTs/Tyr (Cheng *et al* 2009) and TiO_2/CeO_2/Tyr (Njagi *et al* 2008). The storage of this biosensor at room temperature is another advantage for future technological developments and commercialization issues.

The obtained stability results probably are related to the fact that MWCNT and Glu are able to minimize surface fouling of the biosensor surface.

3.7. Phenol detection in seawater

Considering the interest for future applications of this biosensor for real seawater analysis, the recovery tests were also performed (see figure S7 in the supporting information available at stacks.iop.org/Nano/21/245502/mmedia). The recovery test in aqueous solution samples containing 5, 10 and 25 μM phenol in PBS (pH 6.5) were carried out. In addition, the recoveries of various phenol quantities added to real seawater samples (collected from the Mataro region in Barcelona, Spain, and without previous pre-treatment) were also measured.

Recovery values of around 94, 98 and 90% in PBS and 74, 99 and 98% in seawater samples respectively were obtained (see table 1 in the supporting information available at stacks.iop.org/Nano/21/245502/mmedia). The obtained results show good promise for further applications of the developed biosensor in automatic control systems with interest for the environment.

Table 1. Summary of the most relevant recent works regarding phenol detection using amperometric sensors. (GCE, glassy carbon electrode; CPE, carbon paste electrode; SPE, screen printing electrode; MWCNTs, multiwalled carbon nanotubes; SWCNTs, single-walled carbon nanotubes; PDDA, poly(dimethyldiallylammonium) chloride; PBS, phosphate buffer solution; Tyr, tyrosinase from mushroom; FIA, flow injection analysis; chit, chitosan.)

Electrode				Enzyme		Phenol detection			
Transductor	Modification	Stability	Stored	Enzyme/loading	Immobilization technique	Mode/technique	LOD (μM)	Sample	Reference
SPE/pasta carbon	No	—	—	Tyr (2590 units mg^{-1})	Cross-linking with glutaraldehyde	Batch/amperometric	0.410	Wastewater samples	Solná *et al* (2005)
GCE	No	75% after 30 days	PBS (pH 7.4) at 4 °C	Tyr mushroom (5370 units mg^{-1})	Composite MWNTs and cobalt phthalocyanine (CoPc)	Batch/amperometric	0.030	Bisphenol in plastic products	Yin *et al* (2010)
Pt	No	—	—	Tyr (4200 units mg^{-1})	Electropolymerized poly-amphiphilic pyrrole matrix or cross-linked with glutaraldehyde	Batch/amperometric	—	—	Stanca and Pospescu (2004)
CPE	SWCNTs	90% after 30 days	Dry at 4 °C	Tyr (3566 units mg^{-1})	Incorporated in the CPE	Batch/amperometric	0.020	Bisphenol	Mita *et al* (2007)
GCE	MWCNTs and TiO_2	89% after 10 days	PBS (pH 7.0). at 4 °C	Tyr (4400 unit mg^{-1})	Nafion film	Batch/amperometric	0.090	—	Lee *et al* (2007)
GCE	MWNTs–chit	93% after 10 days	PBS (pH 7.0) at 4 °C	Tyr (5370 units mg^{-1})	Glutaraldehyde	Batch/amperometric	0.005	Coliforms represented by *Escherichia coli*	Cheng *et al* (2008)
GCE	SWCNT	—	PBS (pH 7.0) at 4 °C	Tyr (3216 units mg^{-1})	Nafion film	Batch/amperometric	0.020	—	Wang (2005)
GCE	MNPs were absorbed CNTs wrapped with cationic polyelectrolyte PDDA	—	—	Tyr (5370 units mg^{-1})	Cross-linking with glutaraldehyde	FIA/amperometric	0.005	—	Cheng *et al* (2009)
ITO	No	—	4 °C	Tyr (25 000 unit, 0.3 mg)	Mixed chitosan, tyrosinase, and hydroxyl group-functionalized MWNTs	Batch/amperometric	—-	Commercial wine	Yang *et al* (2009)
SPE	3-aminopropyl	30 days	PBS (pH 7.0) at 4 °C	Tyr 2000 units mg^{-1}	Cross-linking with glutaraldehyde	FIA/amperometric	0.056	Pharmaceutical formulation	Martinez *et al* (2008)
SPE	MWCNTs	30 days 75%	Room temperature	Tyr (5370 unit mg^{-1})	Cross-linking with glutaraldehyde	FIA/amperometric	0.140	Seawater samples	Present work

4. Conclusions

A novel biosensor that uses MWCNTs and glutaraldehyde as the immobilization matrix of tyrosinase is designed and applied for phenol analysis in a FIA system. The used MWCNTs and glutaraldehyde not only immobilize the enzyme but also increase the long term stability of the biosensor.

The developed biosensor exhibited relatively fast response time (15 s) and good performance in terms of sensitivity and detection limit when the Tyr enzyme is entrapped within the MWCNT/glutaraldehyde matrix. The proposed immobilization matrix is easy to prepare and cheaper than other materials like nanorods (Gu *et al* 2009), nanoparticles, fibres (Wang and Hasebe 2009) and polymers (Lee *et al* 2007). The detection limit is comparable to other reported complex matrices (see table 1) and is below the value established by EPA criteria. The developed SPE/MWCNT/Tyr/Glu biosensor seems to be an interesting alternative for phenol detection in water including its integration into automatic control systems for pollution control in water samples.

Acknowledgments

The financial support by the Spanish Ministry of Science and Innovation through projects MAT2008-03079/NAN is acknowledged. G Alarcón thanks CONACyT for the postdoctoral fellowship (105024). M Guix thanks the *Ministerio de Ciencia e Innovación* (Madrid) for the pre-doctoral fellowship (BES-2009-023939) associated with the research project MAT2008-03079.

References

Adeyoju O, Iwuoka E J, Smyth M R and Leech D 1996 High-performance liquid chromatographic determination of phenols using a tyrosinase-based amperometric biosensor detection system *Analyst* **121** 1885–9

Aihua L, Itaru H and Haoshen Z 2005 Electrochemical investigation of the permselectivity of a novel positively-charged sol–gel silicate prepared from tetraethyloxysilane and *N*-octadecyldimethyl-[3-(trimethoxysilyl)propyl]ammonium chloride *Electrochem. Commun.* **7** 233–6

Avrameas S 1969 Coupling of enzymes to proteins with glutaraldehyde. Use of the conjugates for the detection of antigens and antibodies *Immunochemistry* **6** 43–52

Caruso C, Vieira I and Filho O 1999 Determination of epinephrine and dopamine in pharmaceutical formulations using a biosensor based on carbon paste modified with crude extract of cara root (Dioscorea bulbifera) *Anal. Lett.* **32** 39–50

Chen L Y, Gu B X, Zhu G P, Wu Y F, Liu S Q and Xu C 2007 Tyrosinase immobilization on ZnO nanorods for phenol detection *Nano Brief Rep. Rev.* **2** 281–4

Cheng Y, Liu Y, Huang J, Li K, Xian Y, Zhang W and Jin L 2009 Amperometric tyrosinase biosensor based on Fe_3O_4 nanoparticles-coated carbon nanotubes nanocomposite for rapid detection of coliforms *Electrochim. Acta* **54** 2588–94

Cheng Y X, Liu Y J, Huang J J, Xian Y Z, Zhang Z G and Jin L T 2008 Fabrication of tyrosinase biosensor based on multiwalled carbon nanotubes–chitosan composite and its application to rapid determination of coliforms *Electroanalysis* **20** 1463–9

Christophe V, Silvia F and Canh T 2003 Amperometric tyrosinase based biosensor using an electrogenerated polythiophene film as an entrapment support *Talanta* **59** 535–44

Dornelles M L and Tatsuo K L 2002 Review of the use of biosensors as analytical tools in the food and drink industries *Food Chem.* **77** 237–56

Drevon G F, Danielmeier K, Federspiel W, Stolz D B, Wicks D A, Yu P C and Russell A J 2002 High activity enzyme-polyuretane coatings *Biotechnol. Bioeng.* **79** 785–94

Duran N and Esposito E 2000 Potential applications of oxidative enzymes and phenoloxidase-like compounds in wastewater and soil treatment: a review *Appl. Catal.* B **28** 83–99

EPA: http://www.epa.gov/waterscience/criteria/phenol/index.htm

Furbee J, Thomas C, Kelly R and Malachowski M 1993 Mediated electrochemical reduction of cytochrome-c and tyrosinase at perfluorosulfonated ionomer coated electrodes *Anal. Chem.* **65** 1654–7

Gu B X, Xu C X, Zhu G P, Liu S Q, Chen L Y and Li X S 2009 Tyrosinase immobilization on ZnO nanorods for phenol detection *J. Phys. Chem.* B **113** 377–81

Huili Q, Jiagen Lv and Baoxin L 2007 Determination of phenol at ng L^{-1} level by flow-injection chemiluminescence combined with on-line solid-phase extraction *Spectrochim. Acta* A **66** 874–8

Jung D and Paradiso M 2009 Formation of cross-linked glucose oxidase aggregates in mesocellular foams *J. Mater. Sci.* **4** 6747–53

Lee Y J, Lyu Y K, Choi H N and Lee W Y 2007 Amperometric tyrosinase biosensor based on carbon nanotube–titania–nafion composite film *Electroanalysis* **19** 1048–54

Li J, Chia L S, Goh N K and Tan S N 1998 Silica sol–gel immobilized amperometric biosensor for the determination of phenolic compounds *Anal. Chim. Acta* **362** 203–11

Li T, Jia Q, Song L, Sua R, Lei Y, Zhoua W and Li H 2009 Coupling poly-(methacrylic acid-co-ethylene glycol dimethacrylate) monolith microextraction to capillary electrophoresis for the determination of phenols in water samples *Talanta* **78** 1497–1502

Li Y, Liu Z, Liu Y, Yang Y, Shen G and Yu R 2006 A mediator-free phenol biosensor based on immobilizing tyrosinase to ZnO nanoparticles *Anal. Biochem.* **349** 33–40

Liu A, Zhou H and Honma I 2005 Electrochemical investigation of the permselectivity of a novel positively-charged sol–gel silicate prepared from tetraethyloxysilane and *N*-octadecyldimethyl-[3-(trimethoxysilyl) propyl] ammonium chloride *Electrochem. Commun.* **7** 1–4

Martinez N A, Messina G A, Bertolino F A, Salinas E and Raba J 2008 Screen-printed enzymatic biosensor modified with carbon nanotube for the methimazole determination in pharmaceuticals formulations *Sensors Actuators* B **133** 256–62

Merkoçi A 2006 Carbon nanotubes: exciting new materials for microanalysis and sensing *Microchim. Acta* **152** 155–6

Merkoçi A, Pumera M, Llopis X, Perez B, Del Valle M and Alegret S 2005 New materials for electrochemical sensing VI: carbon nanotubes *Trends Anal. Chem.* **24** 826–38

Mita D G, Attanasio A, Arduini F, Diano N, Grano V, Bencivenga U, Rossi S, Amine A and Moscone D 2007 Enzymatic determination of BPA by means of tyrosinase immobilized on different carbon carriers *Biosens. Bioelectron.* **23** 60–65

Mizutani F, Sato Y, Hirata Y and Yabuki S 1998 High-throughput flow-injection analysis of glucose and glutamate in food and biological samples by using enzyme/polyion complexbilayer membrane-based electrodes as the detectors *Biosen. Bioelectron.* **13** 809–15

Nistor C, Emneuso J, Gorton L and Ciucu A 1999 Improved stability and altered selectivity of tyrosinase based graphite electrodes for detection of phenolic compounds *Anal. Chim. Acta* **387** 309–26

Njagi J, Ispas C and Andreescu S 2008 Mixed ceria-based metal oxides biosensor for operation in oxygen restrictive environments *Anal. Chem.* **80** 7266–74

Peng X, Jia J, Gong X, Luan Z and Fan B 2009 Aqueous stability of oxidized carbon nanotubes and the precipitation by salts *J. Hazard. Mater.* **15** 1239–42

Pérez B, Pumera M, Del Valle M, Merkoçi A and Alegret S 2005 Glucose biosensor based on carbon nanotube epoxy composites *J. Nanosci. Nanotechnol.* **5** 1694–8

Pérez B, Sola J, Alegret S and Merkoçi A 2008 A carbon nanotube PVC based matrix modified with glutaraldehyde suitable for biosensor applications *Electroanalysis* **20** 603–10

Pumera M, Merkoçi A and Alegret S 2006 Carbon nanotube-epoxy composites for electrochemical sensing *Sensors Actuators* B **113** 617–22

Quiocho F A and Richards F M 1964 Intermolecular cross-linking of a protein in the crystalline state: carboxypeptidase A *Proc. Natl Acad. Sci. USA* **52** 833–9

Rijiravanich P, Aoki K, Chen J, Surareungchai W and Somasundrum M 2006 Micro-cylinder biosensors for phenol and catechol based on layer-by-layer immobilization of tyrosinase on latex particles: theory and experiment *J. Electroanal. Chem.* **589** 249–58

Regueiro J, Llomparta M, Psillakis E, Garcia-Monteagudoc J C and Garcia-Jaresa C 2009 Ultrasound-assisted emulsification–microextraction of phenolic preservatives in water *Talanta* **79** 1387–97

Satish C and Mohapatra J T 1994 Time dependent behaviour of the cross-linking reaction of α-chymotrypsin with glutaraldehyde *Biotechnol. Tech.* **8** 13–6

Serra B, Jiménez S, Mena M L, Reviejo A J and Pingarrón J M 2002 Composite electrochemical biosensors: a comparison of three different electrode matrices for the construction of amperometric tyrosinase biosensors *Biosen. Bioelectron.* **17** 217–26

Solná R, Dock E, Christenson A, Winther-Nielsen M, Carlsson C, Emnéus J, Ruzgas T and Skládal P 2005 Amperometric screen-printed biosensor arrays with co-immobilised oxidoreductases and cholinesterases *Anal. Chim. Acta* **528** 9–19

Solomon E I, Sundaram U M and Machonkin T E 1996 Multicopper oxidases and oxygenases *Chem. Rev.* **96** 2563–605

Stanca S E and Pospescu I C 2004 Phenols monitoring and Hill coefficient evaluation using tyrosinase-based amperometric biosensors *Bioelectrochemistry* **64** 47–52

Umran Y and Memet V K 2009 Covalent immobilization of a-amylase onto UV-curable coating *J. Appl. Polym. Sci.* **114** 3716–22

Vazquez M D, Tascon M L and Deban L 2006 Determination of Pb(II) with a dithizone-modified carbon paste electrode *J. Environ. Sci. Health* A **41** 2735–46

Wang J 2005 Carbon-nanotube based electrochemical biosensors: a review *Electroanalysis* **17** 7–14

Wang J, Musameh M, Merkoci A and Lin Y 2002 Low-potential stable NADH detection at carbon-nanotube-modified glassy carbon electrodes *Electrochem. Commun.* **4** 743–6

Wang Y and Hasebe Y 2009 Highly sensitive flow-biosensor for toxic phenolic compounds using tyrosinase and acridine orange-adsorbed carbon felt *J. Environ. Sci.* **21** S100–4

Yang J H, Lee J C and Choi S H 2009 Tyrosinase-immobilized biosensor based on the functionalized hydroxyl group-MWNT and detection of phenolic compounds in red wines *J. Sensors* **2009** 1–9

Yang K, Gu M, Han H and Mu G 2008 Influence of chemical processing on the morphology, crystalline content and thermal stability of multi-walled carbon nanotubes *Mater. Chem. Phys.* **112** 387–92

Yin H, Zhou Y, Xu J, Ai S and Cui L 2010 Amperometric biosensor based on tyrosinase immobilized onto multiwalled carbon nanotubes-cobalt phthalocyaninesilk fibroin film and its application to determine bisphenol A *Anal. Chim. Acta* **659** 144–50

Yu J H, Liu S Q and Ju H X 2003 Mediator-free phenol sensor based on titania sol–gel encapsulation matrix for immobilization of tyrosinase by a vapor deposition method *Biosens. Bioelectron.* **19** 509–14

Zgoła-Grześkowiak A, Grzeskowiak T, Rydlichowski R and Łukaszewski Z 2009 Determination of nonylphenol and short-chained nonylphenol ethoxylates in drain water from an agricultural area *Chemosphere* **75** 513–8

Supporting Information

STABLE AND SENSITIVE FLOW THROUGH MONITORING OF PHENOL USING A CARBON NANOTUBE BASED SCREEN PRINTED BIOSENSOR

G. Alarcón[a,c], M. Guix[a,b], A. Ambrosi[a], M.T. Ramirez Silva[d], M.E. Palomar Pardave[c] , A. Merkoçi[a,f*2].

[a] *Nanobioelectronics & Biosensors Group, Catalan Institute of Nanotechnology Campus UAB, 08193 Bellaterra, Barcelona, Catalonia, Spain.*

[b] *Chemistry Department, Autonomous University of Barcelona, Campus UAB, 08193 Bellaterra, Barcelona, Catalonia, Spain.*

[c] *Departamento de Materiales, Universidad Autónoma Metropolitana Azcapotzalco, 02200 México Distrito Federal, Mexico*

[d] *Departamento de Química, Universidad Autónoma Metropolitana Iztapalapa, 09340 México Distrito Federal, Mexico*

[f] *ICREA, Barcelona, Catalonia, Spain*

*arben.merkoci.icn@uab.es

[2] Prof. Arben Merkoçi
E-mail: arben.merkoci.icn@uab.es
Tel: +34935868014
Fax: +34935868020
Centre d'Investigació en Nanociència i Nanotecnologia Escola Tècnica Superior d'Enginyeria (ETSE) Campus de la UAB -Edifici Q- 2ª planta
08193 Bellaterra, Spain

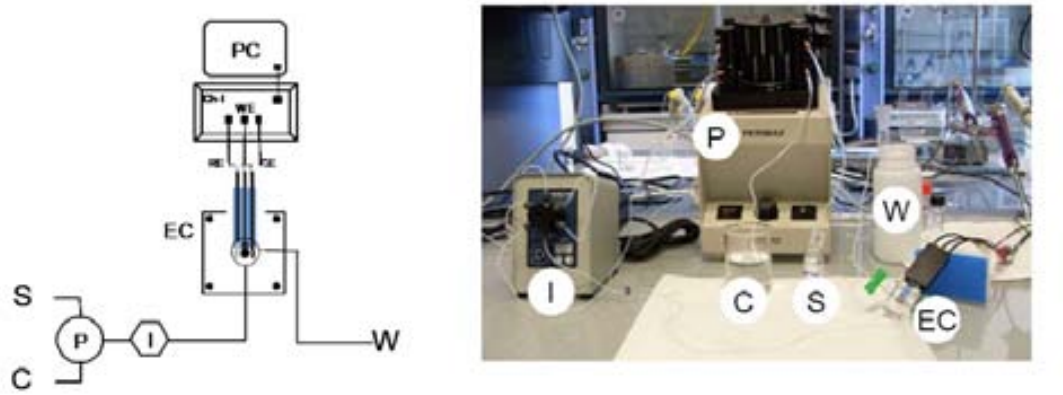

Fig. S1. Schematic representation of flow analysis system used for phenol amperometric detection. S, sample; C, carrier; P, pump; I, injector; EC, Electrochemical cell; RE, reference electrode; WE, work electrode; CE, counter electrode; PC, computer used for data collection.

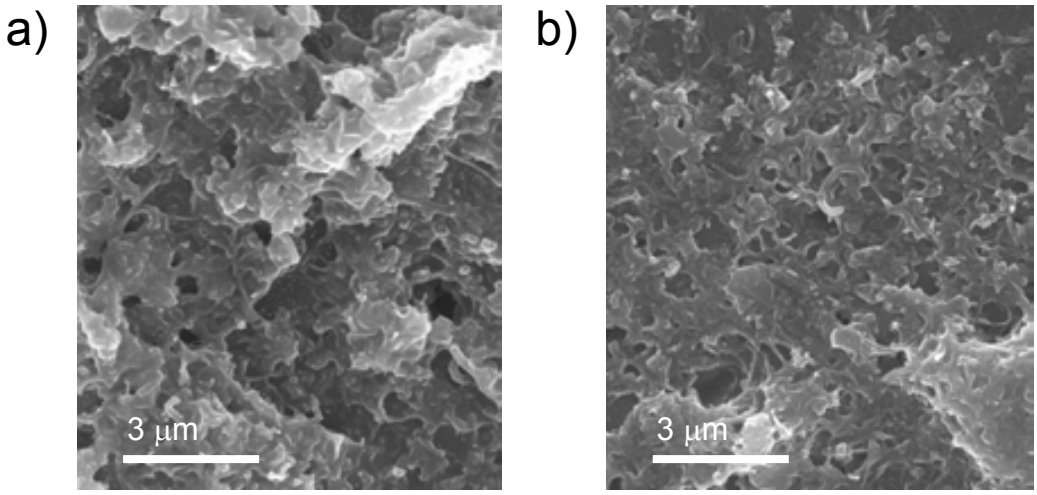

Fig. S2. SEM images of the working surface area of SPE modified with MWCNT/Tyr/Glu before (a) and after (b) being tested. Images are taken at a resolution of 3□m and a acceleration voltage of 15kV.

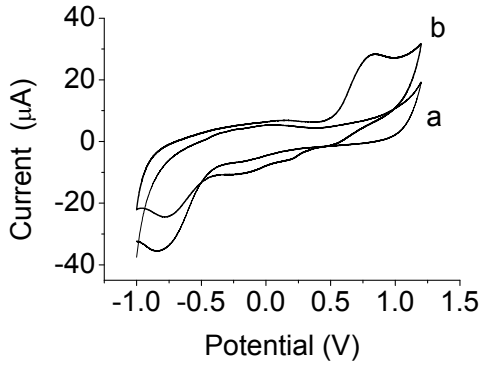

Fig. S3. CV of a) pH 6.5 PBS used as blank b) phenol 1mM in pH 6.5 PBS; working electrode: SPE/MWCNT; scan rate $0.1V \cdot s^{-1}$; Other experimental conditions as described at experimental section in the main text.

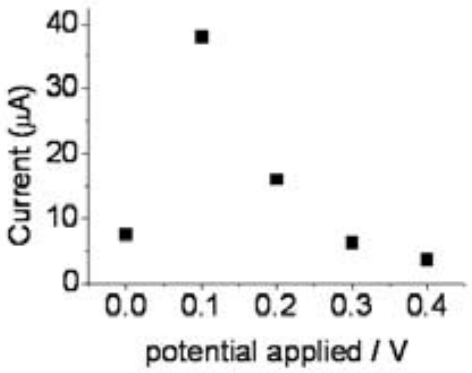

Fig. S4. Effect of working potential upon the current for a phenol solution of 10 × 10^{-6} M. Conditions: temperature, 25 °C; operating potential, -100 mV versus Ag/AgCl reference; pH 6.5 PBS 0.01M solution is used as buffer. Working electrode is the SPE/MWCNT/Tyr/Glu.

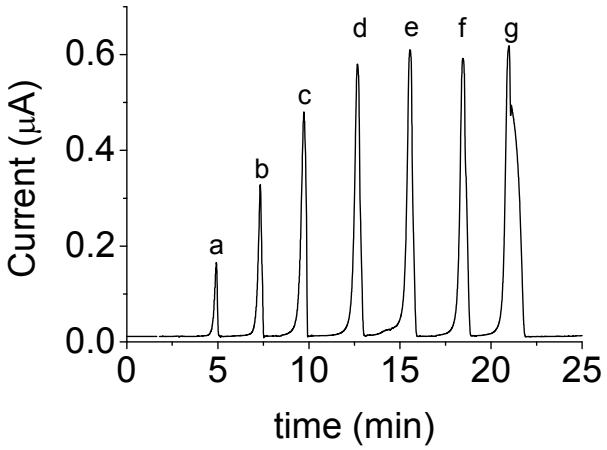

Fig. S5. Amperometric responses of SPE/MWCNT/Tyr/Glu biosensor at different injection times: (a) 2s, (b) 5s, (c) 8s, (d) 10s, (e) 15s, (f) 20s, (g) 30s, of amperometric response of the biosensor. All measurements were made for 10μM of phenol at phosphate buffer 0.01M, pH 6.5 at 25 °C; An operating potential of -100 mV versus Ag/AgCl. Other experimental conditions as described in the text.

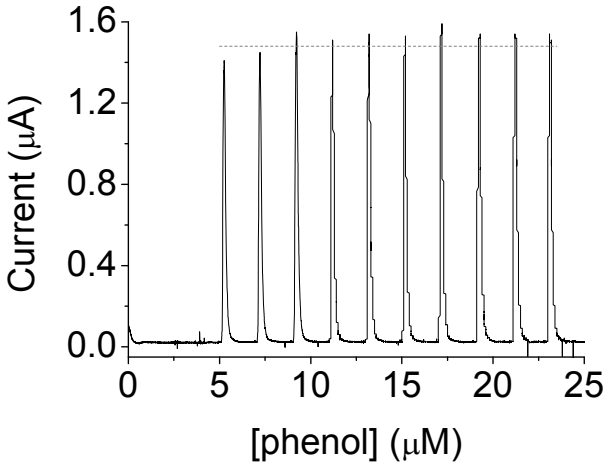

Fig. S6. Response of SPE/MWCNT/Tyr/Glu biosensor to successive injections of 10 μM phenol. Conditions: pH =6.5, temperature, 25 °C; operating potential, -100 mV versus Ag/AgCl reference. Other experimental conditions as described in the text.

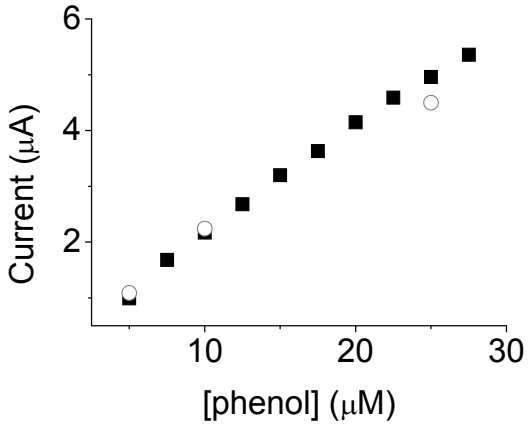

Fig. S7. Calibration curve (■) for phenol concentration from 5 to 27.5 μM. Current values (o) corresponding to 5μM, 10μM and 25 μM phenol added into a pH 6.5 PBS 0.01M solution used as buffer are also shown. Conditions: temperature, 25 °C; operating potential, -100 mV versus Ag/AgCl reference;. SPE/MWCNT/Tyr/Glu is used as working electrode. Other experimental conditions as described in the main text.

Table S1. Recoveries of phenol at synthetic sea water samples, getting from amperometric response using SPE/MWCNT/Tyr/Glu biosensor.

[phenol] of sample / μM	[phenol] found / μM	Recovery / %
5	3.73	74
10	9.94	99
25	24.50	98

Bismuth Film Combined with Screen-Printed Electrode as Biosensing Platform for Phenol Detection

Arben Merkoçi,[a,b]* *Ulku Anik*,[c]* *Serdar Çevik*,[c] *Meliha Çubukçu*,[c,d] *Maria Guix*[a,e]

[a] Nanobioelectronics and Biosensors Group, Catalan Institute of Nanotechnology (ICN), Bellaterra, Barcelona, Catalonia, Spain
tel: +34935868014; fax: +34935868020
[b] ICREA, Barcelona, Spain
[c] Mugla University, Faculty of Arts and Science, Chemistry Department, 48000 Kotekli/Mugla, Turkey
tel: +90-2522111503
[d] Ege University, Faculty of Science, Chemistry Department, 35100 Bornova, Izmir, Turkey
[e] Chemistry Department, Universidad Autónoma de Barcelona, 08193 Bellaterra, Catalonia, Spain
*e-mails: arben.merkoci.icn@uab.es; ulkuanik@yahoo.com; ulkuanik@gmail.com

Received: November 9, 2009
Accepted: March 10, 2010

Abstract
Mushroom tissue was immobilized onto plain screen printed electrode (SPE) and multiwalled carbon nanotube (MWCNT) modified SPE (SPE/MWCNT) via bismuth (Bi) deposition. By this way, SPE/Bi/Tissue and SPE/MWCNT/Bi/Tissue biosensors for phenol detection were obtained. UV-visible spectroscopy and SEM were utilized for explain the immobilization procedure. After optimizing working parameters, both biosensors were compared in terms of analytical characteristics. Linear range of response were found as 5–100 μM for SPE/Bi/Tissue and 2–200 μM for SPE/MWCNT/Bi/Tissue while detection limits were calculated as 0.48 μM and 1.17 μM for SPE/Bi/Tissue and SPE/MWCNT/Bi/Tissue respectively. Developed systems were also applied for phenol detection in synthetically prepared waste water sample and very promising results were obtained.

Keywords: Bi-film, Mushroom tissue, Phenol biosensor, Screen printed electrode, Biosensors, Bismuth

DOI: 10.1002/elan.200970002

Dedicated to a Decade of Bismuth Electrodes in Modern Electroanalysis

1. Introduction

Phenolic compounds are one of the major pollutants of industrial waste waters while the concentration of these compounds in natural water or soil may vary to some degree, but on the whole they are present at the ppb level. On the other hand, these compounds have detrimental effect on human health and for these reasons they require rapid, easy to operate and low-cost toxicity screening procedures [1, 2].

Many methods are available for the determination of phenolic compounds, including gas chromatography and spectrophotometric analyses [3, 4]. However, these methods suffer from complicated sample pretreatment and unsuitable on-site monitoring. In order to provide simplification and automation of the analysis methods, some electrochemical procedures were developed which are mainly based on biosensors [1, 5–7]. Various matrixes such as carbon paste, graphite-epoxy composite have been employed for the incorporation of the proper enzyme on the electrode surface [2, 8–17]. On the other hand, immobilization technique is very important at biosensor construction since it might directly affect simplicity, sensitivity and stability of electroanalytical procedures [18].

In this work, mushroom tissue was immobilized and accumulated via Bi^{3+} ions on carbon ink screen printed electrode (SPE) and multiwalled carbon nanotube (MWCNT) modified SPE. As a result, suitable biosensor for phenol detection was obtained.

Plant tissues provide some advantages at biosensor constructions like high stability and high level of activity resulting from the maintenance of the enzyme in its natural environment. Moreover, the availability and low price of plant tissues, the avoidance of tedious and time-consuming enzyme extraction and purification steps and the presence of the required cofactors in the same tissue make the usage of wide variety of plant tissues as bioreceptors in different biosensor formats [19].

Mushroom tissues are known to have a high polyphenol oxidase enzyme (PPO) content that recognizes a large variety of mono-and polyphenols. They also contain laccase oxidase enzyme which can be define as large potential for the determination of phenolic compounds [19]. On the other hand, bismuth film electrode (BiFE) was developed as an alternative electrode material to mercury film electrode (MFE) in 2000 by J. Wang's group [20]. BiFE was easily formed by accumulation of Bi^{3+} ions on proper electrode surface by applying suitable potential at significant period of

time BiFE has attained extensive attention for ten years and have been used for various applications including trace metal analysis [20–31] organic compounds detection [21, 27, 32, 33] and recently as biosensor transducer [34, 35].

The novelty of our work relays on the immobilization procedure. The immobilization procedure in presented work was achieved by electrodeposition of tissue onto SPE surface with the aid of Bi^{3+} precursor that interacts with the tissue and got reduced onto the transducer surface. This represents an in-situ Bi and tissue deposition/entrapment without using any other matrix like gelatin or binder glutaraldehyde. At the first part of this study, we are trying to demonstrate this Bi^{3+}-tissue interaction by using spectroscopic methods and SEM. In the second part, developed systems were tested as biosensors for phenol detection. After the optimization of experimental parameters of SPE/Bi/Tissue, analytical characteristics were examined both for SPE/Bi/Tissue and SPE/MWCNT/Bi/Tissue. Finally obtained biosensors were subjected to phenol detection in synthetically prepared waste water sample.

2. Experimental

2.1. Apparatus

Chronoamperometric experiments were carried out with the AUTOLAB PGSTAT 12 electrochemical measurement system from ECO CHEMIE Instruments B.V. (The Netherlands) driven by GPES software. UV-visible absorbance spectra were recorded on a UV-1601 spectrometer (SHIMADZU), which were equipped with a 1 cm path length quartz cell. The spectra were recorded between 200 and 800 nm. Scanning electron microscopy (SEM) images were obtained with a scanning electron microscope (Hitachi-Japan) with resolution of 1 μm, magnification of 30 k× and accelerating potential of 15 kV.

2.2. Reagents and Materials

Phenol was purchased from Prolabo ($M_A = 94.11$ g/mol, %94 pure). All other chemicals were of analytical grade. Standard stock solution of bismuth (1000 mg L^{-1}, atomic absorption standard solution) was obtained from Aldrich and diluted as required. 0.1 M sodium acetate buffer solution (acetic acid/acetate 100%, puriss (glacial) Riedel-de Haën UN 2789, pH 4.5) served as supporting electrolyte. Sodium acetate buffer solution (100 mM, pH 4.5) was utilized as the supporting electrolyte during bismuth film formation while simultaneously used as the supporting electrolyte for all measurements. On the other hand, phosphate buffer solution (KH_2PO_4, Merck/purity 99,995%, pH 7.5) was used as supporting electrolyte during cleaning process for the modified electrode. Mushrooms were purchased from a local market.

2.3. Tissue Sample

100 mg tissue was removed from internal part of the mushroom using a spatula. The removed tissue was put into the mortar, smashed and grounded until proper amount of tissue liquid was obtained. 5 μL tissue liquid was used for every biosensing platform and the rest was kept at 4 °C. Freshly prepared tissue samples were used in every two days.

2.4. Biosensor Preparation

2.4.1. Preparation of SPEs

Screen-printed microfabrication is based on the sequential deposition of a graphite ink, Ag/AgCl ink and an insulating ink on a polyester substrate. After each layer is deposited a drying process is carried out, which consists in keeping the polyester substrate at 90 °C for 15 minutes.

CNT dispersion and characterization: Previously to their dispersion, CNTs are purified by stirring them in 2 M nitric acid at 25 °C for 24 hours. MWCNT used has a purity of 95%.

Modification of SPE with CNT: The working surface area of a bare SPE was modified by depositing a 7 μL drop of MWCNT suspension (1 mg MWCNT/1 mL THF) onto the working electrode surface, followed by a drying process at room temperature for 24 hours. The characterization process of the working electrode surface was performed by SEM to check if a homogeneous distribution of CNT over the surface was achieved.

2.4.2. Bi and Tissue Deposition and Immobilization

In-situ immobilization procedure was applied for deposition of Bi-film together with mushroom tissue onto SPE (both with bare and MWCNT) by following the usual procedure, which includes introducing 50 mg L^{-1} Bi solution, and 5 μL mushroom tissue (optimized value) into a working cell containing 10 mL acetate buffer (100 mM, pH 4.5). Proper deposition potential was applied for a significant period of time without applying any deaeration procedure for accumulating Bi together with tissue on SPEs. Biosensors were freshly prepared before each measurement.

2.5. Measurements

Chronoamperometric measurements were carried out in 0.1 M acetic acid/acetate buffer (pH 4.5) medium under the operating potential of +0.8 V for both SPE/Bi/Tissue and SPE/MWCNT/Bi/Tissue biosensors while the solution was being stirred. The duration of each analysis was 150 s and the transient current decayed to a steady state value after 75 s in the presence of supporting electrolyte.

2.6. Cleaning Process

After completion of the measurement, the electrode was inserted into 0.1 M, 20 mL nitric acid and sonicated for about 10 minutes. Then same electrode was put into pure water and again sonicated for about 10 minutes. Square wave measurements were applied three times for cleaning electrode surfaces in phosphate buffer solution (pH 7.0) between -0.5 V and $+1.25$ V.

2.7. Sample Application

Artificial waste water of a highly acidic and salty nature included 50 g/L NaCl and 100 g/L phenol in 1.0 M HCl solution was prepared and diluted in the ratio of 1:10 according to the literature [36]. The last phenol concentration in the measuring vessel was 50 μM.

3. Results and Discussion

3.1. Examination of Immobilization Mechanism

The novelty of our work relays on the immobilization procedure of mushroom tissue through bismuth electrodeposition onto a SPE. The complex that is formed between Bi and mushroom tissue is accumulated onto the electrode surface by applying proper voltage. In order to explain the process, UV spectroscopy and SEM techniques were utilized. Figure 1 demonstrates the UV spectrums of 150 μL tissue (a), 150 μL Bi solution (0.1 g/100 mL) (b) and mixture of these two solutions (c). From Figure 1, it can be concluded that when Bi and tissue are mixed a complex is formed. The disappearance of peaks and the shift at the wavelength demonstrate this formation. However, the exact place of Bi linkage with tissue structure can not still be clarified. As mentioned in introduction part, mushroom tissue has a complex structure containing PPO and laccase oxidases but also other enzymes that are not specific to phenol [19]. At this acidic pH, 4.5, it is known that Bi stays in cationic form [37]. This cationic Bi^{3+} can probably link with negatively charged enzyme. A similar electroactive interaction of mushroom tyrosinase with ZnO nanorods have been studied earlier [38]. The Bi^{3+}/tissue 'complex' along with execs Bi^{3+} in our case are afterward electrochemically deposited onto the SPE/MWCNT surface. The formed SPE/MWCNT/Bi/Tissue is further studied so as to see its availability for phenol detection.

CNT distribution, as well as BiFE formation, was studied by scanning electron microscope (SEM). SEM images of the working electrode surface show a homogeneous distribution of MWCNT all over the electrode surface as well as a more sponge like surface compared to the bare SPE (Figure 2 Part 1A and 1B). This effect can be directly related to the increase on the surface-to-area ratio by the MWCNT incorporation onto the working electrode. Regarding BiFE formation, its deposition is clearly evidenced by a plainer surface and aggregates formation together with darker coverage compared to plain SPE (Figure 2, Part 2A and 2B). Introduction of tissue to the Bi film structure creates more complex structure as demonstrated in Figure 2 Part 3A and 3B. This difference between Figure 2 Part 2A, 2B and Part 3A 3B is another evidence that confirms accumulation of tissue together with Bi on electrode surface.

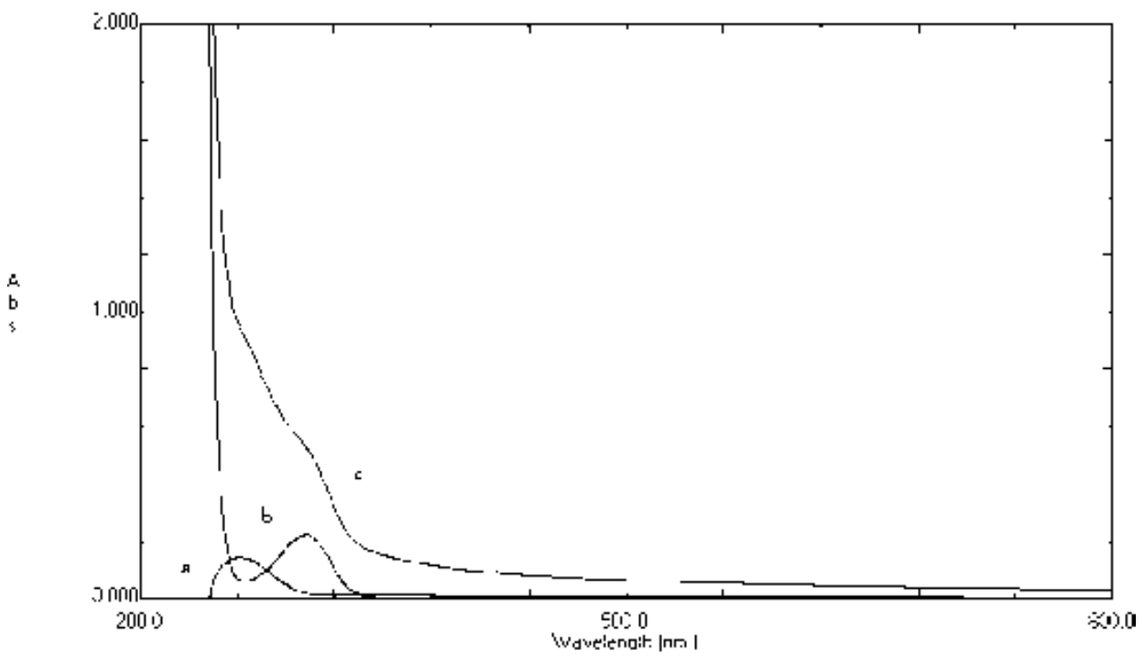

Fig. 1. UV spectra of a) tissue (20 μL) b) Bi solution (150 μL) and c) Bi (150 μL) and tissue (20 μL) solution.

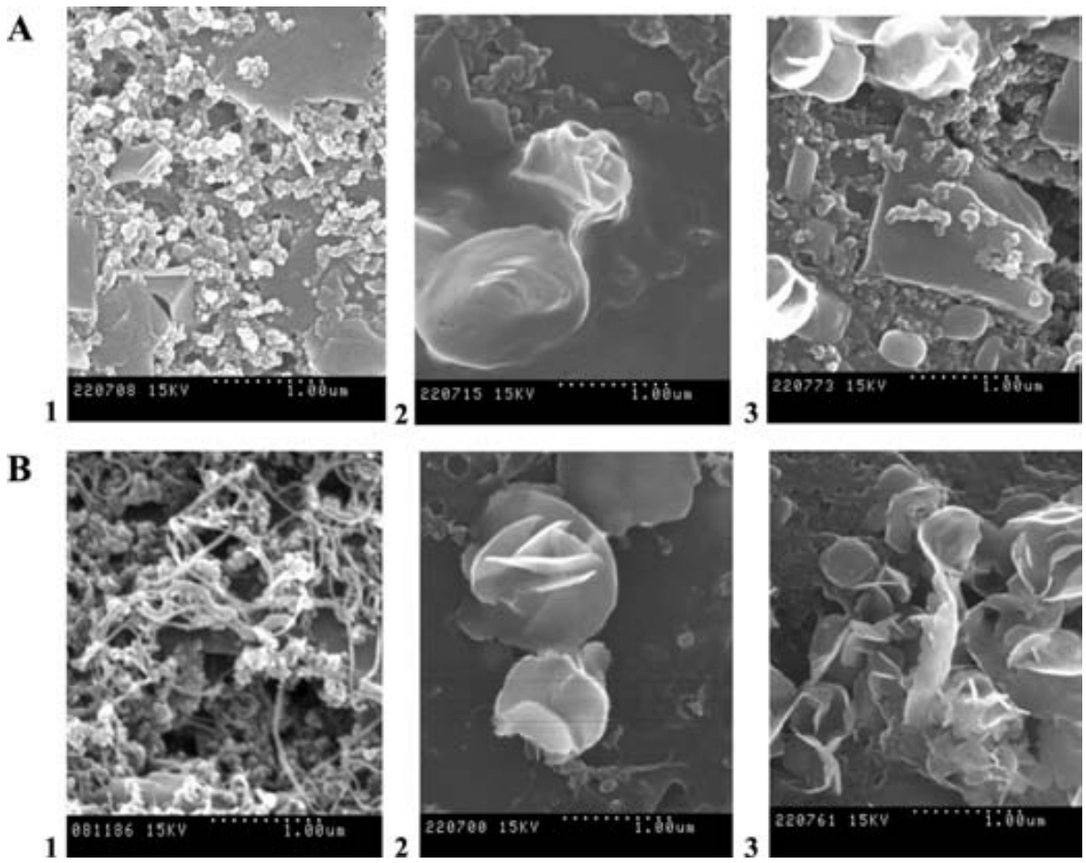

Fig. 2. SEM images of plain-SPE (1A), BiFE on SPE (2A), SPE/Bi/Tissue (3A) and SEM images of MWCNT modified SPE (1B), BiFE on MWCNT/SPE (2B), SPE/MWCNT/Bi/Tissue (3B). Resolution of 1 μm, magnification of 30 k × and accelerating potential of 15 kV have been used. Other experimental details as described in the text.

3.2. SPE/Bi/Tissue as Biosensing Platform

3.2.1. Optimization of Bi Film Formation

Effects of Bi amount, deposition time (t_d) and deposition potential (E_d) have profound effect on accumulation of Bi^{3+} onto electrode surface. For this reason, these parameters were optimized for 50 μM phenol on plain SPE in the presence of proper amount of Bi^{3+} with 10 μL tissue. The working potential was +0.8 V and results were given in Figure 3 and summarized in Table 1. As can be seen from Figure 3 and Table 1, optimized t_d and E_d were found as 4 min and −1.0 V respectively while optimum Bi amount was investigated as 50.0 mg/L.

3.2.2 Optimization of Experimental Parameters

Optimum Working Potential

Considering immobilization of tissue via Bi film onto SPE for phenol detection, optimum potential is needed to be defined for proper measurements. In order to examine this effect, the performance of the biosensor was tested between 600–900 mV with increment of 100 mV for 50 μM phenol solution (Figure 4). At 600 mV almost no current was observed and the highest current value was obtained at 800 mV. Same experiment was repeated for SPE electrode containing only Bi-film but not any tissue. No significant current values were obtained at this potential range demonstrating that obtained current values are results of enzymatic reactions provided by mushroom tissue. Considering electrocatalytic contribution of MWCNT, optimum potential study was investigated by using SPE/MWCNT/Bi/Tissue. As a result, again at 800 mV the highest current value was obtained like SPE/Bi/Tissue (data not shown). It is expected to strip off the Bi-film from the electrode surface at this potential. However as it was demonstrated with UV spectroscopy, a complex between Bi-film and mushroom tissue should have been formed. The presence of phenol during measurements resulted with more complex interactions which require the application of a cleaning process between two measurements in order to decrease the background current.

Effect of pH

The effect of pH on the electrode response was investigated at various pHs (3.5 to 6.5 with increment of 1.0) by using

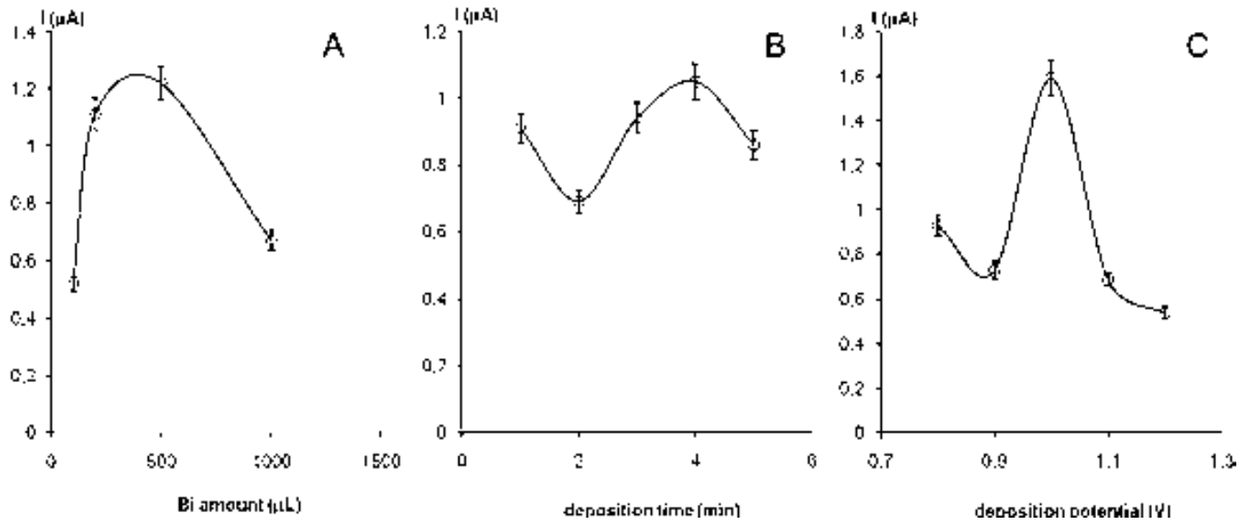

Fig. 3. The effect of (A) Bi amount, (B) deposition time and (C) deposition potential on current values for 50 μM phenol on SPE/Bi/Tissue biosensor, the obtained curve is plotted according to 5% error bars in 0.1 M, acetic acid/acetate buffer, pH 4.5, 10 μL tissue, +0.8 V as working potential. Other conditions for Bi^{3+} accumulation, (A) $E_d = -1.1$ V, $t_d = 5$ min; (B) 50.0 mg/L Bi^{3+}, $E_d = -1.1$ V; (C) 50.0 mg/L Bi^{3+}, $t_d = 4$ min.

Table 1. The optimum conditions for Bi^{3+} accumulation in 0.1 M, pH 4.5, acetic acid/acetate buffer, 10 μL tissue, +0.8 V as working potential for 50 μM phenol.

Optimum conditions	Optimum conditions
Amount of bismuth ($E_d = -1.1$ V, $t_d = 5$ min)	50.0 mg/L
Deposition time (50.0 mg/L Bi, $E_d = -1.1$ V)	4 min
Deposition potential of bismuth (50.0 mg/L Bi, $t_d = 4$ min)	−1.0 V

acetic acid/acetate buffer systems (0.1 M) for 50 μM phenol (Figure 5). As can be seen from the figure, the response current of the electrode to phenol increases significantly from pH 3.5 to 4.5, and then a sharp decrease is obtained at pH value higher than 4.5. As a result pH 4.5 was chosen as optimum pH and used for further studies. Though optimum working pH of mushroom tissue modified electrodes for phenol detection is reported at more basic pHs, between 6.5–8.0 [39], we prefer to examine this range, since optimum pH for Bi film formation is at pH 4.5 in the acetate buffer medium [20].

Tissue Amount

The effect of tissue amount (1, 2, 5, 10 and 20 μL) as enzyme source on current values for 50 μM phenol at SPE/Bi/Tissue was examined (Figure 6). Proper mushroom tissue was introduced into working cell which contains 50.0 mg/L of bismuth solution. Then −1.1 V was applied for 4 minutes and tissue was immobilized onto electrode surface. After that fresh buffer was put into working cell and chronoamperometry was applied at +0.8 V. At 75.th second chronoamperogram was recorded. From the figure, it is obvious

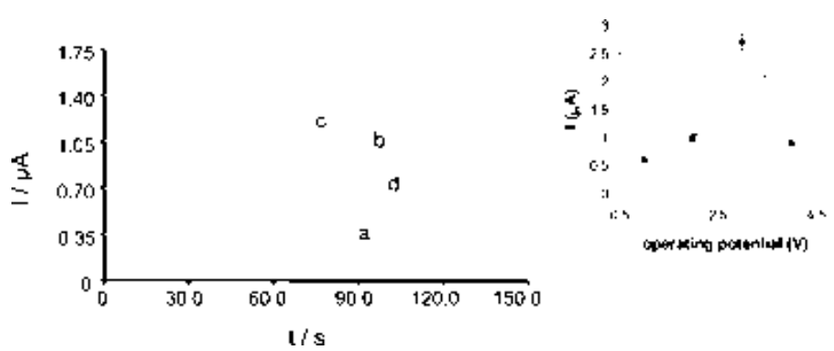

Fig. 4. The chronoamperometric curves of SPE//Bi/Tissue biosensor for 50 μM phenol showing varying operating potential effect on current values; a) 0.6 V, b) 0.7 V, c) 0.8 V, d) 0.9 V. Inset: The curve demonstrating effect of operating potential. on current values. The curve is plotted according to 5% error bars. Conditions: 0.1 M acetic acid/acetate buffer pH 4.5, 10 μL tissue. For BiFE 500 μL Bi solution, E_d −1.1 V, t_d 5 min.

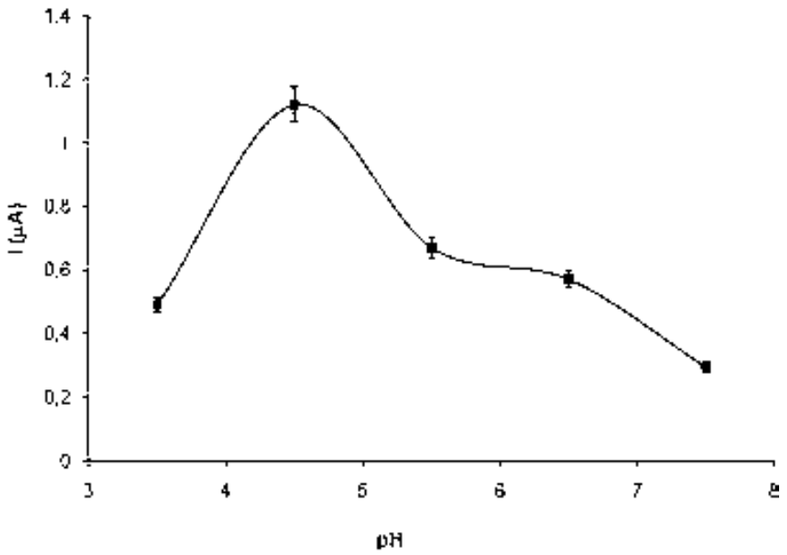

Fig. 5. The effect of pH (3.5 to 6.5) on current values for 50 μM phenol at, SPE//Bi/Tissue biosensor. Obtained curve is plotted according to 5% error bars in 0.1 M, acetic acid/acetate buffer, 5 μL tissue, 50.0 mg/L Bi^{3+}, $E_d = -1.0$ V, $t_d = 4$ min.

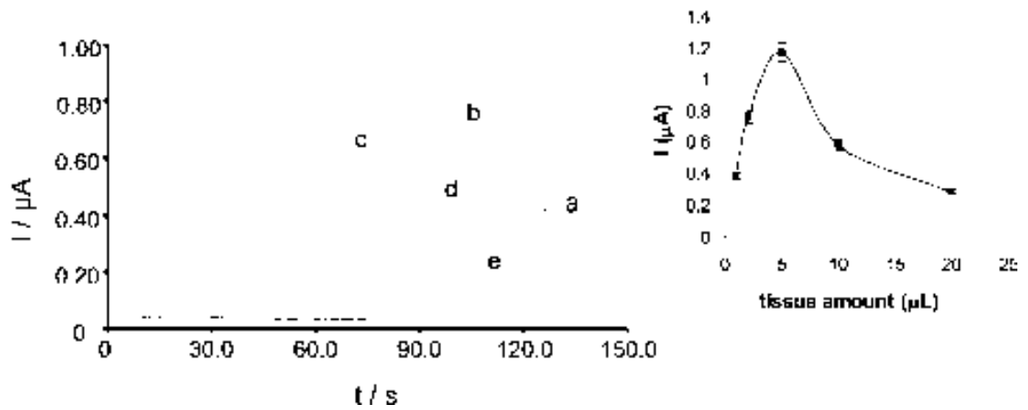

Fig. 6. The effect of tissue amount on current values for 50 μM phenol at SPE/Bi/Tissue biosensor, the obtained curve is plotted according to 5% error bars in 0.1 M, acetic acid/acetate buffer, pH 4.5, 50.0 mg/L Bi^{3+}, $E_d = -1.0$ V, $t_d = 4$ min.

that 5 μL gave the best current value. So this tissue amount was used for further experiments.

3.2.3. *Comparison of SPE/Bi/Tissue Biosensor with SPE/ MWCNT/Bi/Tissue Biosensor*

Under optimum working conditions, SPE/Bi/Tissue system was compared with SPE/MWCNT/Bi/Tissue biosensor in terms of analytical characteristics. Results were given in Table 2. Introducing MWCNT into electrode structure provides wider linear range with better RSD value. This is probably related to the diffusion process of the electroactive specie undergoing oxidation onto the SPE electrode. On the other hand, plain SPE provides slightly better *LOD* and *LOQ* values compared to MWCNT/SPE. Developed systems were also applied for phenol detection in synthetically prepared waste water sample as described in experimental part. As a result, recoveries of 95.20% (SPE/Bi/Tissue) and

Table 2. Comparison of SPE/Bi/Tissue with SPE/ MWCNT/Bi/Tissue.

Electrode	Linear range (μM)	*LOD* (μM)	*LOQ* (μM)	*RSD* (%) ($n = 3$)	Recovery (%) ($n = 3$)
BiFE-SPE	5 – 100	0.48	1.6	1.1	95.20
BiFE-MWCNT-SPE	2 – 200	1.17	3.93	0.46	95.60

95.60% (SPE/MWCNT/Bi/Tissue) were obtained with the electrodes.

4. Conclusions

In this work, for the first time, enzyme source mushroom tissue was electrochemically immobilized onto SPE or SPE/MWCNT/ surface with the aid of Bi film. This immobilization and complex formation of Bi^{3+}-ions with tissue were demonstrated with UV spectroscopy and SEM measurements. Then developed biosensor's working conditions were optimized and obtained system was subjected to phenol detection in synthetically prepared waste water sample. As a result, almost similar promising recoveries were obtained with both types of SPE.

Avoiding the usage of matrices like gelatin might be helpful to overcome diffusion problems caused by these membranes. On the other hand, stability of tissue was provided by means of Bi film that was formed during the accumulation procedure. Usage of more specific enzyme like tyrosinase or laccase might result more sensitive results for this system. On going efforts for developing BiFE based immobilization procedures continue in our labs.

As mushroom tissue has a complex structure (PPO, laccase oxidases between others) rending this material not specific to phenol it is impossible at this stage of research to propose the exact mechanism for interaction between Bi film and mushroom tissue. Besides, the response mechanism is very complex. Different types of enzymes could have affected this response. At this stage of our research although it could be difficult to predict the right response, several phenomena and the corresponding hypothesis could be considered as follows. Firstly, as there are many types of undefined enzymes in the tissue, our reaction might be product of one of them that follows their metabolic pathway; secondly, working potential (+0.8 V) is suitable to monitor hydrogen peroxide oxidation to water. In addition it is also known that, quinone could polymerize onto electrodes after oxidation of phenol. If after this polymerization a phenolic substance like dihydroanthraquinone is formed, it is possible to follow H_2O_2 by monitoring oxidation of this substance to anthraquinone; thirdly, the tissue also contains catalase enzymes that under normal conditions may oxidize phenol at +0.4 V. Considering the Bi complex formation of this substance, the shift at oxidation potential could be explained.

The use of less complex material as an enzyme source along with the application of alternative spectroscopic techniques like IR spectroscopy would probably clarify this phenomena in the future. In addition the use of less complex and more active enzyme source will probably open the way to the increase of the lifetime of the biosensor. This work is still in the process at our laboratories and will be object of future publications.

Acknowledgements

We acknowledge funding from the *MICINN* (Madrid, Spain) for the Projects MAT2008-03079/NAN and for the scholarship BES-2009-023939 given to M. Guix.

References

[1] S. Timur, N. Pazarlıoglu, R. Plilloton, A. Telefoncu, *Talanta* **2003**, *61*, 87.
[2] M. A. Kim, W. Lee, *Anal. Chim. Acta* **2003**, *479*, 143.
[3] C. D. Chriswell, R. C. Chang, J. S. Fritz, *Anal. Chem*. **1975**, *47*, 1325.
[4] J. Poerschmann, Z. Zhang, F. D. Kopinke, T. Pawliszyn, *Anal. Chem*. **1997**, *69*, 597.
[5] E. A. Cummings, S. Linquette-Mailley, P. Mailley, S. Cosnier, B. R. Eggins, E. T. McAdams, *Talanta* **2001**, *55*, 1015.
[6] H. M. Tan, S. P. Cheong, T. C. Tan, *Biosens. Bioelectron*. **1994**, *9*, 1.
[7] S. C. Chang, C. J. Mc Neil, *Biosens. Bioelectron*. **2002**, *17*, 1015.
[8] C. R. Tillyer, P. T. Gobin, *Biosens. Bioelectron*. **1991**, *6*, 560.
[9] G. F. Hall, D. J. Best, A. P. F. Turner, *Anal. Chim. Acta* **1988**, *213*, 113.
[10] D. Puig, D. Barcelo, *Trends Anal. Chem*. **1996**, *15*, 362.
[11] J. Wang, Q. Chen, *Anal. Lett*. **1995**, *28*, 1131.
[12] E. S. M. Lutz, E. Dominguez, *Electroanalysis* **1996**, *8*, 117.
[13] H. Kotte, B. Gründig, K.-D. Vorlop, B. Strehlitz, U. Stottmeister, *Anal. Chem*. **1995**, *67*, 65.
[14] J. Wang, Q. Chen. *Anal. Chim. Acta* **1995**, *312*, 39.
[15] J. Wang, F. Lu, L. David, *Analyst* **1994**, *119*, 445.
[16] P. Önnerfjord, J. Emneus, G. Marko-Varga, L. Gorton, F. Ortega, E. Dominguez, *Biosens. Bioelectron*. **1995**, *10*, 607.
[17] S. Cosnier, C. Innocent, *Bioelectrochem. Bioenerg*. **1993**, *31*, 147.
[18] V. C. Sanz, M. L. Mena, A. Gonzalez-Cortes, P. Yanez-Sedeno, J. M. Pingarron, *Anal. Chim. Acta* **2005**, *528*, 1.
[19] M. Campas, R. Carpentier, R. Rouillon, *Biotechnol. Adv.* **2008**, *26*, 370.
[20] J. Wang, J. Lu, S. B. Hočevar, P. A. M. Farias, B. Ogorevc, *Anal. Chem*. **2000**, *72*, 3218.
[21] E. A. Hutton, B. Ogorevc, S. B. Hočevar, F. Weldon, M. R. Smyth, J. Wang, *Electrochem. Commun.* **2001**, *3*, 707.
[22] J. Wang, J. Lu, Ü. Anık-Kirgöz, S. B. Hočevar, B. Ogorevc, *Anal. Chim. Acta* **2001**, *434*, 29.
[23] J. Wang, U. Anık-Kirgöz, J. Lu, *Electrochem. Commun*. **2001**, *3*, 703.
[24] G. Kefala, A. Economou, A. Voulgaropoulos, M. Sofoniou, *Talanta* **2003**, *61*, 603.
[25] A. Charalambous, A. Economou, *Anal. Chim. Acta* **2005**, *547*, 53.
[26] A. Królicka, R. Pauliukaitė, I. Švancara, R. Metelka, A. Bobrowski, E. Norkus, K. Kalcher, K. Vytřas, *Electrochem.-Commun.* **2002**, *4*, 193.
[27] G. Kefala, A. Economou, M. Sofoniou, *Talanta* **2006**, *68*, 1013.
[28] D. Demetriades, A. Economou, A. Voulgaropoulos, *Anal. Chim. Acta* **2004**, *519*, 167.
[29] S. Legeai, O. Vittori, *Anal. Chim. Acta* **2006**, *560*, 184.
[30] E. A. Hutton, S. B. Hočevar, B. Ogorevc, *Anal. Chim. Acta* **2005**, *537*, 285.
[31] S. B. Hočevar, J. Wang, R. P. Deo, B. Ogorevc, *Electroanalysis* **2002**, *14*, 112.
[32] M. Yang, Z. Zhang, Z. Hu, J. Li, *Talanta* **2006**, *69*, 1162.

[33] M. Bučková, P. Gründler, G.-U. Flechsig, *Electroanalysis* **2005**, *17*, 440.
[34] U. Anık, S. Timur, M. Çubukcu, A. Merkoçi, *Microchim Acta* **2008**, *160*, 269.
[35] S. Timur, U. Anık, *Anal. Chim. Acta* **2007**, *598*, 143.
[36] S. Timur, U. Anık, D. Odacı, L. Gorton, *Electrochem. Commun.* **2007**, *9*, 1810.
[37] R. R. Jia, C. P. Wu, Y. X. Yang, Y. R. Chen, J. R. Zhang, Y. Q. Jia, *Amino Acids* **2005**, *28*, 409.
[38] L. Chen, B. Gu, G. Zhu, Y. Wu, S. Liu, C. Xu, *J. Electroanal. Chem.* **2008**, *617*, 7.
[39] Z. Wang, Z. Zhang, Z. Fu, L. Fang, W. Luo, D. Chen, X. Zhang, *Anal. Chim. Acta* **2003**, *494*, 63.

ChemComm

Cite this: *Chem. Commun.*, 2012, **48**, 1686–1688

www.rsc.org/chemcomm

COMMUNICATION

Bimetallic nanowires as electrocatalysts for nonenzymatic real-time impedancimetric detection of glucose†

Carmen C. Mayorga-Martinez,[ab] Maria Guix,[ac] Rossana E. Madrid[b] and Arben Merkoçi*[ad]

Received 24th October 2011, Accepted 5th December 2011
DOI: 10.1039/c2cc16601a

Gold-platinum nanowires are proposed as electrocatalysts for a real-time nonenzymatic impedancimetric detection of glucose. The electrochemical behavior of the obtained platform toward electrocatalytic oxidation of glucose, including a proposal for the detection mechanism, is shown.

Development and improvement of glucose biosensors has been an important subject of interest during the last fifty years.[1] Most of the known amperometric glucose biosensors are based on glucose oxidase (GOx) or glucose dehydrogenase (GDH) immobilization.[2,3] Moreover, in some applications, it is necessary to have sensors which are stable when they are exposed to high temperatures or other aggressive environments.[4] Most of these nonenzymatic electrochemical glucose sensors rely on measuring the current response during the direct glucose oxidation on the electrode surface. The use of noble metals such as Pt and Au to develop nonenzymatic sensors has been reported.[2] However, in the presence of glucose these electrodes quickly lose their activity due to accumulation of chemisorbed intermediates, which block the electrocatalytic surface.[2]

On the other hand the chronoimpedance technique (CIT) for real-time determination of glucose concentration in first and second generation glucose oxidase/carbon paste electrodes has been implemented. This technique allows continuous and rapid time response measurements and is only limited by the transient response of the biosensor. This new method is supposed to be applicable to any other biosensor system.[5,6] It has been reported that the nanostructured electrodes possess a very large surface to area activation ratio, favoring kinetically controlled reactions like electrocatalytic oxidation of glucose more than diffusion controlled reactions expecting a high sensitivity toward glucose detection.[7] For this reason we propose the combination of both materials and consequently the use of a bimetallic platinum/gold nanowire (Au–Pt NW) as a free-enzyme electrocatalyst for glucose detection. This is achieved through Au–Pt NW integration on the working electrode of a screen printed electrode (SPE) followed by CIT measurements performed for the first time in an integrated and miniaturized three electrode system. The use of an iridium oxide (IrOx) thin layer electrodeposited onto the working electrode surface was necessary to reduce the electrode–electrolyte interface impedance (EEIZ) for CIT measurements, as previously described.[8] Au–Pt NWs were immobilized onto the SPE working electrode surface by using the IrOx thin layer and the cross-linking agent glutaraldehyde.

Morphological and structural studies of bimetallic nanowires were performed by a Transmission Electron Microscope (TEM). Highly regular and uniform average diameter Au–Pt NWs of about 140 nm (Fig. 1) can be observed. X-Ray microanalysis of nanowires was performed by TEM, showing an Au and Pt alloy at different proportions along the nanowire. Compositions in terms of Pt and Au percentages at different sections of the Au–Pt NW are given in the inset table of Fig. 1(A). A homogeneous distribution of the nanowires on the electrode surface can be observed by a Scanning Electron Microscopy (SEM) image (Fig. 1B). Fig. 1C shows the effect of glutaraldehyde as a binding matrix, showing a good entrapment of the wires within the mentioned matrix.

The electrocatalytic effect of Au–Pt NWs toward glucose detection was evaluated (see ESI† for experimental conditions). By increasing glucose concentration a current decrease was observed, indicating that Au–Pt NWs are exhibiting electrocatalytic activity toward glucose presence. For all the

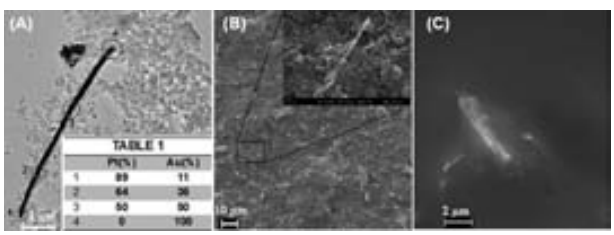

Fig. 1 TEM image of a single (Au/Pt)NW(A). SEM micrographs of modified SPE with a (Au/Pt)NW (B). Effect of glutaraldehyde as a binding matrix for NW entrapment (C).

[a] *Nanobioelectronics & Biosensors Group, Catalan Institute of Nanotechnology, Campus UAB, 08193 Bellaterra, Barcelona, Catalonia, Spain*
[b] *Laboratorio de Medios e Interfaces (LAMEIN), Departamento de Bioingeniería (DBI), (FACET), (UNT)/Instituto Superior de Investigaciones Biológicas (INSIBIO), Consejo Nacional de Investigaciones Científicas y Técnicas (CONICET), CC 327—Correo Central (4000) Tucumán, Argentina*
[c] *Autonomous University of Barcelona, UAB Campus, 08193 Bellaterra, Spain*
[d] *ICREA, Barcelona, Catalonia, Spain. E-mail: arben.merkoci.icn@uab.es; Fax: +34 935868020; Tel: +34 935868014*

† Electronic supplementary information (ESI) available: Additional characterization data for SPE/IrOX/Au–Pt NW, evaluation of the percentage normalized modulus, and experimental section. See DOI: 10.1039/c2cc16601a

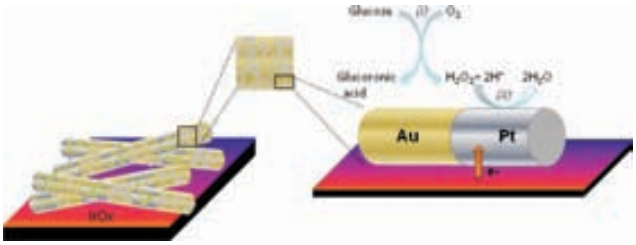

Fig. 2 Proposed mechanism for the glucose electrocatalytic detection using a Au–Pt NW. (i) Glucose is transported by convection to the gold surface, where it is oxidized to glucuronic acid by reducing O_2 to H_2O_2, (ii) H_2O_2 decomposes into H_2O on the platinum surface.

glucose concentrations the catalytic effect of NWs in the range from 0 to 0.1 V (data not shown) can be clearly observed.

A Bode diagram was obtained using electrochemical impedance spectroscopy (EIS) in absence and in the presence of 150μM of glucose. The EIS data were used to calculate the Percentage Normalized Modulus (PNM). Higher PNM values were observed at the low frequency range (0.1–10 Hz) (See Fig. S2†).

It is possible to conclude from the PMN evaluation that the most important impedancimetric response is observed at the low frequencies range, being this phenomenon similar to the one reported in the previous work.[5,6] Therefore for CIT implementation 0.4 Hz was used, because at this frequency the response obtained appreciably reflects $|Z|$ change.

In an electrode–electrolyte interface (EEI) the electric current flows due to the charge transfer occurring during the electrochemical reactions that take place between the electrode surface and the electrolyte. In our specific case, the electrochemical reaction on the SPE/IrOx/Au–Pt NW sensor surface can be described considering the different metallic surfaces present along the alloy (Fig. 2). The mentioned mechanism based on the glucose oxidation on the gold surface and H_2O_2 reduction on the platinum surface is the reason why this sensor presents such a high sensitivity and a low linear range for glucose detection. It is well known that Au nanoclusters can behave as GOx mimicking units able to catalytically oxidize glucose and produce gluconates and H_2O_2.[9,10]

This process, catalysed by AuNPs, is similar to the one performed using the natural enzyme glucose oxidase, which also catalyzes the oxidation of glucose with the co-substrate O_2.

The recent implementation of an Au NW modified sensor for nonenzymatic glucose detection also has confirmed that nanostructured gold is able to act by mimicking the GOx activity.[1] On the other hand, Pt is a widely used electrode material for H_2O_2 detection and biosensor fabrication. Most of the platinum based biosensors detect H_2O_2 at relatively high potential (around 0.6 V). However, Pt NWs and Pt nanoparticles (NPs) were recently reported for H_2O_2 detection at 0 mV.[11,12] The use of a bimetallic gold–platinum nanowire as a free-enzyme electrocatalyst for glucose detection is a very interesting application due to the non-competitive mechanism taking place on the electroactive surface.

For a better elucidation of the glucose detection mechanism further impedance measurements were carried out. Measurements were performed under different experimental conditions. The first one (Fig. 3A) is carried out using a SPE/IrOx/Au–Pt NW, while the second (Fig. 3B) and the third (Fig. 3C) case correspond

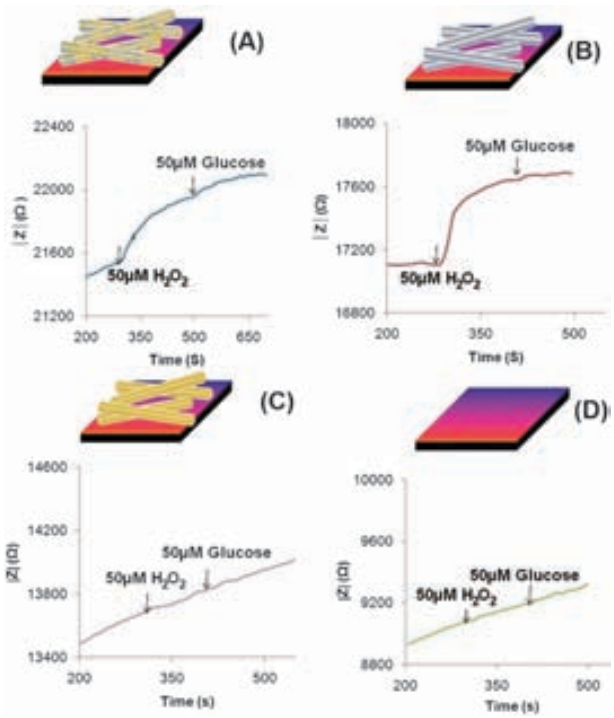

Fig. 3 Real-time impedancimetric response of the SPE/IrOx/Au–Pt NW (A), SPE/IrOx/Pt NW (B), SPE/IrOx/Au NW (C) and SPE/IrOx (D) sensors upon successive additions of 50 μM H_2O_2 and 50 μM glucose.

to SPE/IrOx sensors modified only with platinum and gold nanowires, respectively. Finally, a SPE/IrOx without NW was also checked (Fig. 3D). The impedance response ($|Z|$) of each electrode toward 50 μM H_2O_2 and 50 μM glucose additions was recorded showing an appropriate impedance response to H_2O_2 (see Fig. 3A and 3B). An increase of $|Z|$ of around 500 Ω and 300 Ω can be observed for SPE/IrOx/Pt NW and SPE/IrOx/Au–Pt NW sensors respectively. The higher SPE/IrOx/Pt NW sensor response toward peroxide is due to the fact that more platinum area is available for the reduction of H_2O_2 than the Pt–Au NW sensor. Reaction (ii) (Fig. 2) shows electron consumption, which increases the EEIZ. This impedance increase is related to hydrogen peroxide (reduced afterwards at the Pt surface) produced by oxidation of glucose in presence of dissolved oxygen.

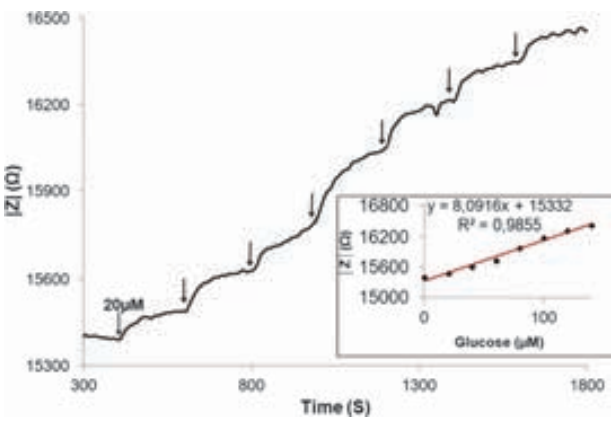

Fig. 4 (A) Real-time impedancimetric response of the SPE/IrOx/Au–Pt NW sensor. (B) Sensor calibration given as impedance magnitude *versus* glucose concentration in the 0–140 μM range.

SPE/IrOx/Au NW (Fig. 3C) and SPE/IrOx (Fig. 3D) sensors don't show any response toward either H_2O_2 or glucose. Results are consistent with the sensors composition, as in the first configuration platinum is not present to reduce H_2O_2 (product of glucose oxidation on the Au surface) and in the second configuration H_2O_2 is not catalyzed by iridium oxide at this potential value.[13,14]

The SPE/IrOx/Au–Pt NW sensor is the only one which exhibits response to glucose addition, showing an impedance change of around 150 Ω (Fig. 3A). This sensor can detect glucose because both metals (Pt and Au) are present and both reactions can be coupled, the oxidation of glucose to gluconic acid (Au surface) and reduction of hydrogen peroxide (Pt surface).

Real-time determination of impedance changes ($|Z|$) in 50 mM NaOH solution during successive addition of glucose 20 μM was carried out by using a composed signal of 100 mV DC plus a 50 mV ac of 0.4 Hz (Fig. 4). Impedance response shows a linear range up to 140 μm with 8557 Ω mM^{-1} of sensitivity, and 0.99 of correlation coefficient (inset of Fig. 4). In order to compare the repeatability of 3 sensors, the normalized impedance (relative value to zero concentration of glucose) is evaluated. The results of triplicate sets, indicated by error bars, show the repeatability and reproducibility corresponding to the measurements with a relative standard deviation (RSD) less than 5% for a glucose concentration range of 20–140 μM.

The low detection range obtained by this glucose sensor may allow applications to non-invasive detection of glucose in other biological fluids (saliva, sweat and urine) where glucose is too low. Moreover this low detection range would allow the implementation of a miniaturized system for detection of glucose in diluted blood samples using just a few μl of the sample.

It is well known that for the systems based on electrochemical detection of the produced H_2O_2 at a potential range of about 0–200 mV *vs.* Ag/AgCl there is almost no effect of interferences. Working under these conditions would bring a high selectivity along with the high sensitivity and the fast response of the developed biosensor.[15] In our case working with a dc potential of 100 mV combined with the chronoimpedance technique are the main reasons for such improvements.

Selectivity is a very important parameter to be considered for nonenzymatic glucose sensors. To evaluate the selectivity of the sensor, impedancimetric response toward uric acid (UA) and ascorbic acid (AA) was measured. These interference species are normally present in real physiological samples and are usually examined in the presence of glucose. It must be considered that the concentration of glucose studied is at least 30 times lower than the one in human blood,[16] and in addition for this experiment the glucose concentration is 20 times higher than the concentration of interference species. Citric acid (CA) is also evaluated due to its presence as a preservative in soft drinks and other foods. Fig. 5 presents experimental results obtained by adding 50 μM of glucose in 50 mM NaOH, followed by 2.5 μM UA, 2.5 μM AA and 10 μM CA. Good selectivity of the SPE/IrOx/Au–PtNW sensor is shown toward glucose oxidation, because interference species (such as UA, AA and CA) can be neglected.

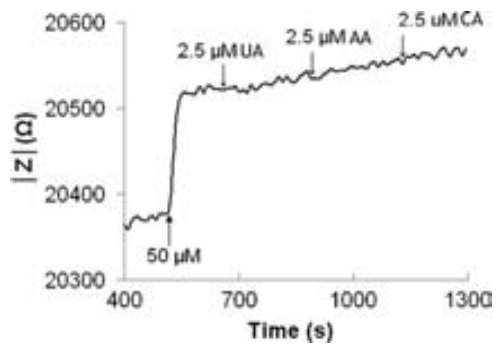

Fig. 5 Evaluation of interfering species.

Au–Pt NWs are obtained by an electrodeposition method and implemented on a glucose sensor based on SPE modified by IrOx and Au–Pt nanowires. Their electrochemical behavior toward glucose detection is evaluated by CIT. This sensor uses very low DC potential, decreasing this way the effect of interference species such as UA, AA and CA. This sensor presents high repeatability and sensitivity. A glucose detection mechanism associated to the designed sensor is also determined. The obtained results show that the use of the CIT as a novel transduction platform coupled with bimetallic nanowires can bring advantages in the design of nonenzymatic sensors achieving improved analytical performance besides the robustness and stability of the biosensing system with interest for applications in various fields.

This work was supported by grants from the Agencia Nacional de Promoción Científica y Tecnológica (ANPCyT), Consejo Nacional de Investigaciones Científicas y Técnicas (CONICET), and institutional funds from the Instituto Superior de Investigaciones Biológicas (INSIBIO) and Consejo de Investigaciones de la Universidad Nacional de Tucumán (CIUNT). The financial support from the Spanish Ministry of Science and Innovation through project MAT2008-03079/NAN and predoctoral fellowship (BES-2009-023939 given to M. G.) is acknowledged.

Notes and references

1 S. Cherevko and C.-H. Chung, *Sens. Actuators, B*, 2009, **142**, 216.
2 L. Meng, J. Jin, G. Yang, T. Lu, H. Zhang and C. Cai, *Anal. Chem.*, 2009, **81**(17), 7271.
3 J.-Y. Chiua, C.-M. Yua, M.-J. Yena and L.-C. Chena, *Biosens. Bioelectron.*, 2009, **24**, 2015.
4 X. Kang, Z. Mai, X. Zou, P. Cai and J. Mo, *Anal. Biochem.*, 2007, **363**, 143.
5 C. C. Mayorga Martinez, E. F. Treo, R. E. Madrid and C. J. Felice, *Biosens. Bioelectron.*, 2010, **26**, 1239.
6 C. C. Mayorga Martinez, E. F. Treo, R. E. Madrid and C. J. Felice, *Biosens. Bioelectron.*, 2011, **29**, 200.
7 Y.-J. Lee and J.-Y. Park, *Sens. Actuators, B*, 2011, **155**(1), 134.
8 C. C. Mayorga Martinez, R. E. Madrid and C. J. Felice, *Sens. Actuators, B*, 2008, **133**, 682.
9 W. Luo, C. Zhu, S. Su, D. Li, Y. He, Q. Huang and C. Fan, *ACS Nano*, 2010, **4**(12), 7451.
10 X. Zheng, Q. Liu, C. Jing, Y. Li, D. Li, W. Luo, Y. Wen, Y. He, Q. Huang, Y.-T. Long and C. Fan, *Angew. Chem., Int. Ed.*, 2011, **50**, 1.
11 M. Yang, F. I. Qua, Y. Lua, Y. Heb, G. Shena and R. Yua, *Biomaterials*, 2006, **27**, 5944.
12 S. Guo, D. Wen, Y. Zhai, S. Dong and E. Wang, *ACS Nano*, 2010, **4**(7), 3959.
13 E. A. Irhayem, H. Elzanowska, A. S. Jhas, B. Skrzyneck and V. Birss, *J. Electroanal. Chem.*, 2002, **538**, 153.
14 A. S. Jhasa, H. Elzanowskab, B. Sebastiana and V. Birss, *Electrochim. Acta*, 2010, **55**, 7683.
15 J. Wang, *Electroanalysis*, 2001, **13**(12), 983.
16 L.-C. Jiang and W.-D. Zhang, *Biosens. Bioelectron.*, 2010, **25**, 1402.

Electronic supplementary information (ESI)

Bimetallic Nanowires as Electrocatalyst for Nonenzymatic Real Time Impedancimetric Detection of Glucose

Carmen C. Mayorga-Martinez[a,b], Maria Guix[a,c], Rossana E. Madrid[b], and Arben Merkoçi[*a,d]

[a]Nanobioelectronics & Biosensors Group, Catalan Institute of Nanotechnology, Campus UAB, 08193 Bellaterra, Barcelona, Catalonia, Spain.
[b] Laboratorio de Medios e Interfaces (LAMEIN), Departamento de Bioingeniería (DBI), (FACET), (UNT)/Instituto Superior de Investigaciones Biológicas (INSIBIO), Consejo Nacional de Investigaciones Científicas y Técnicas (CONICET). CC 327 – Correo Central (4000) Tucumán, Argentina.
[c]Autonomous University of Barcelona, UAB Campus, 08193 Bellaterra, Spain
[d]ICREA, Barcelona, Catalonia, Spain. E-mail: arben.merkoci.icn@uab.es, Tel: +34935868014; Fax number: +34935868020.

Non-modified surfaces and IrOx or IrOx/Au-PtNWs modified SPEs were firstly evaluated in a PBS (pH=7.0) by using cyclic voltammetry (CV) and electrochemical impedance spectroscopy (EIS), so as to confirm the Au-PtNW immobilization. Fig. S1A shows CVs of the unmodified SPE, IrOx modified SPE and IrOx/Au-PtNW modified SPE. CV corresponding to the unmodified SPE does not show any peak. However, the CV of the SPE/IrOx and SPE/IrOx/Au-PtNW present characteristic peaks around 300 and 600mV.[1] When NWs are immobilized onto the electrode surface through entrapment within glutaraldehyde the obtained current slightly decreases.

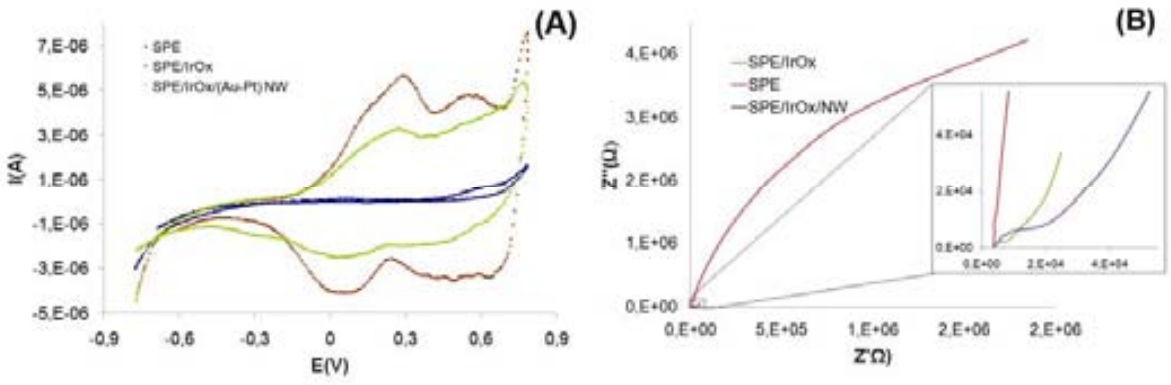

Fig. S1 Estimation of electroactive surface area by cyclic voltamperograms (CVs) at 50mV/s (A) and EIS characterization (B) of the bare, IrOX andIrOx/Au-PtNW modified SPE electrodes in phosphate buffer solution at pH 7.

EIS is a well known method used to study the surface features of modified electrodes.[2] It is employed to analyze the detailed electrochemical response of the modified electrodes by using individual or mixed components Argand diagram (Z' versus Z'') for the bare, SPE/IrOx and SPE/IrOx/Au-PtNW modified SPE, respectively shown in Fig. S1B. Bare SPE exhibits high electrode–electrolyte interface impedance (EEIZ), whereas IrOx modified electrode shows a reduction of two orders of magnitude in the EEIZ, similar to the one reported in the literature. NWs deposited through glutaraldehyde onto the electrode surface showed a slight EEIZ increase. The presence of glutaraldehyde, being an insulator, should have affected the EEIZ by increasing it.

In order to determine the working frequency, the percentage normalized modulus (PNM), defined in our previous work[7,8], was calculated by using equation inset in Fig. S2. The measured modules without ($Z_{0\mu M}$) and with 150µM of glucose ($Z_{150\mu M}$) in the range of 0.1–100 Hz are used to calculate the PNM, which indicates the rate of impedance variation per mole of glucose added to the system as a function of frequency. The PNM curve obtained (Fig. S2) presents a maximum value of 0.21%/µM, measured at 0.1 Hz. As frequency increases, the PNM curve continuously decreases down to approximately 0.03%/ µM for frequencies higher than 10 Hz.

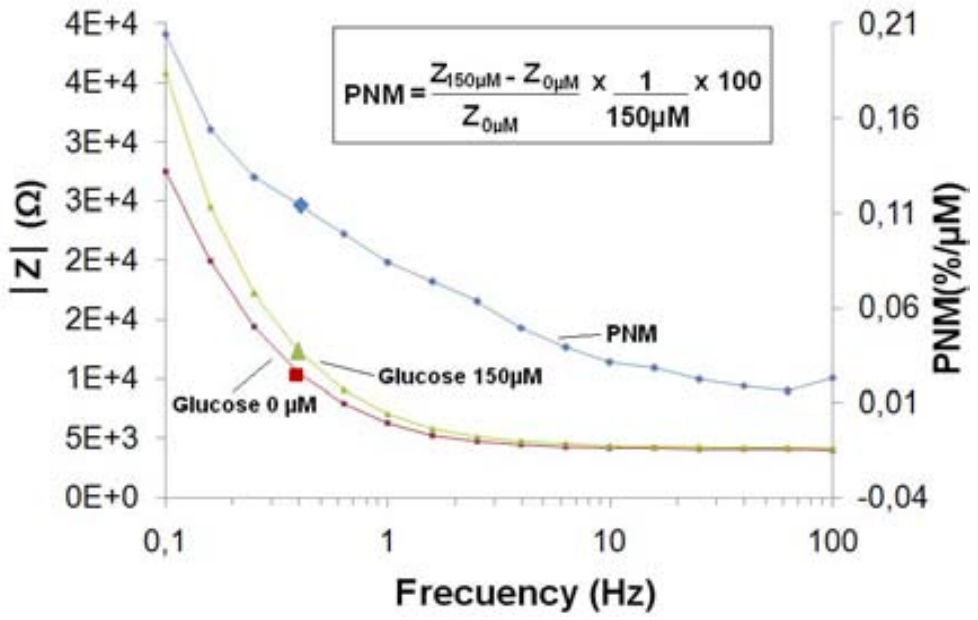

Fig. S2 Impedance magnitude in the absence and presence of 150 mM of glucose. Percentage Normalized Modulus (PNM) of the SPE/IrOx/Au–Pt NW sensor. $Z_{150\mu M}$ and $Z_{0\mu M}$ impedance modulus measured at 0 and 150 µM of glucose concentration.

MATERIALS AND METHODS

Apparatus and Reagents

Electrochemical measurements were performed with a Solartron 12508W impedance analyzer composed by a Solartron 1287 Electrochemical Analyzer and a Solartron 1250 Frequency Response Analyzer, commanded by the corresponding software provided by the manufacturer (ZPlot ®, Scribner Associates Incorporated). Magnetic stirrer was used to provide the convective transport during the impedancimetric measurements. Statistical computations were carried out by means of GraphPadPism version 3.00 Software. Scanning electron microscope (SEM) analysis was performed by using an EVO (Carl Zeiss NTS GmbH. Germany). Transmission electron microscope (TEM) images were taken with a JEM-2011 (Jeol, Ltd., Japan).

Track-etched porous aluminum oxide (0.02 μm) membranes were provided by Whatman (Anodisc 13mm, 0.02 μm). Glutaraldehyde (25%) was purchased from Sigma Aldrich. D-glucose anhydrous, potassium dihydrogen phosphate, sodium monohydrogen phosphate dehydrate and potassium chloride were purchased from Laboratories Cicarelli. All electrochemical experiments were carried out at room temperature (22ºC) in 0.07M phosphate buffer solution (PBS) pH 7 with 0.1M KCl. All solutions were prepared with single distilled water with conductivity lower than 5μS/m.

Synthesis of Platinum/Gold Nanowires (Au-Pt NW)

Pt-AuNW were prepared by using a three-step electrochemical deposition process, slightly adapted to the previously described setup.[3,4] Prior to Pt/AuNW synthesis, an ultrathin Au film was firstly sputtered by using a conventional ion sputtering method onto one side of the anodic alumina as to make the template conductive to be used as the working electrode contact. A platinum wire (0.3 mm diameter) was used as counter electrode and an Ag/AgCl wire was used as reference electrode. A cooper layer was previously electrodeposited so as to seal the aluminum oxide membrane porous.[5] Platinum had been electrodeposited at -2mA for 30

minutes and gold was electrodeposited at -0.9V for 40 minutes (see schematic of the setup, Figure S3). After electroplating, gold sputtered layer and copper layers are dissolved by mechanical polishing by using nitric acid 35%. As to release the NW from the alumina template, the membrane was dissolved by immersing it in NaOH 3M solution at room temperature for 1 hour. Then the Nanowires were centrifuged and rinsed in deionized water up to six times to remove the remaining NaOH. After template removal, NWs were resuspended and stored in acetone.

Preparation of Screen Printed Electrode (SPE) and Modification with Au-Pt NWs.

Screen printing electrodes fabrication is based on the sequential deposition of a graphite ink, Ag/AgCl ink and insulating ink on a polyester substrate. After the deposition of each layer a drying process is followed by keeping the polyester substrate at 90 ◦C for 15 min. The SPE working surface area was modified by electrodepositing an IrOx thin film, as previously reported.1,[6] A 10μL Au-PtNW solution drop was deposited onto the working SPE/IrOx electrode surface and allowed to dry at room temperature for 20min. Finally, 7 μl of glutaraldehyde (Glu) solution at 5% were cast onto the SPE/IrOx/Pt-AuNW electrode surface and let to dry at room temperature for 4 hours. The prepared SPE/IrOx/Pt-AuNW sensor was kept at room temperature.

Electrochemical Experiments

All electrochemical experiments were carried out at room temperature. The electrocatalytic detection of glucose by using SPE/IrOx/Au-PtNw was evaluated in 50mM NaOH solution in absence and in presence of different glucose concentrations (50, 100 and 150 μM). CV measurements were carried out at the potential range of -0.8 to 0.8 V vs. Ag/AgCl . In order to determine the working conditions for CIT implementation and study the characteristics of the modified electrodes surface, electrochemical impedance spectroscopy (EIS) studies were performed. The AC frequency range was 0.1 Hz to 100Hz logarithmic scale with 10 points per decade (in this frequency range it is possible to evaluate the impedance of the interface and the medium) in absence and in presence of 150μM glucose by applying 50mV of AC (optimization

of AC value is previously reported[7,8]). CTI measurement was performed by stimulating the system with a composed signal from a 100mVDC potential superimposed with a 50mV AC potential to a single frequency of 0.4 Hz.

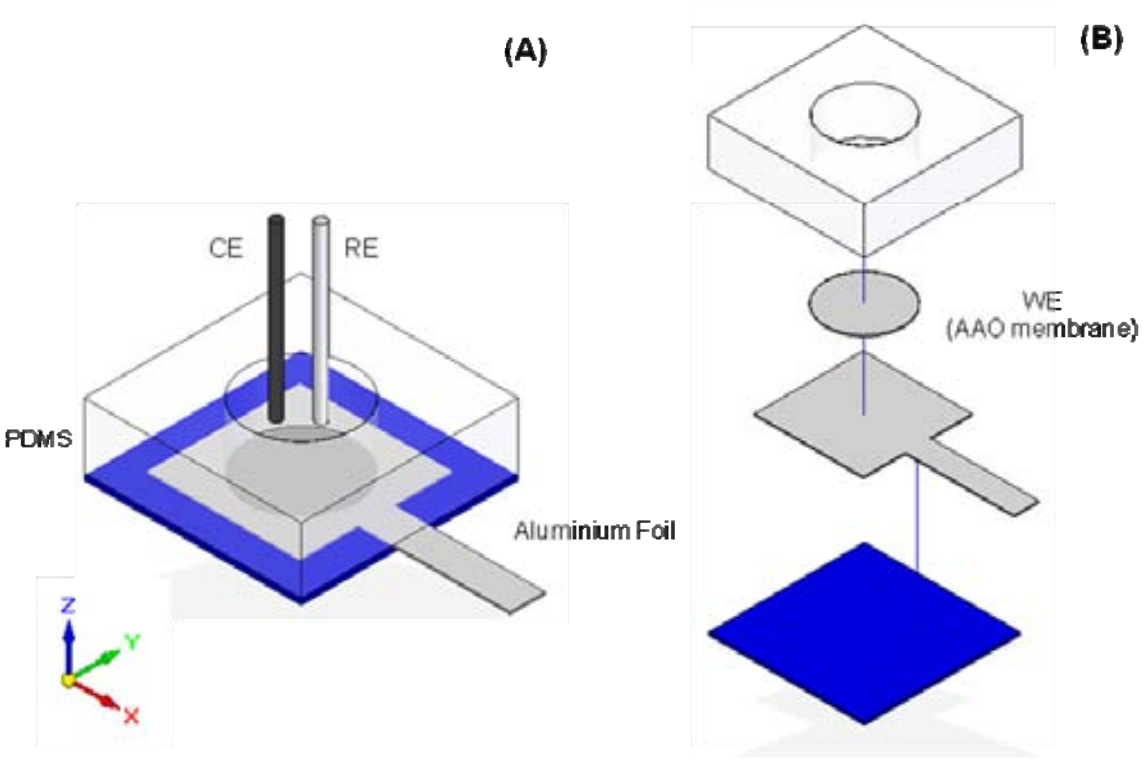

Fig. S3 Schematic of electrodeposition cell.

Notes and references

1 R. Meyer, S. Cogan, T. Nguyen, R. Rauh, *IEEE Trans. Neural. Sys. Rehabil. Eng.* **2001**, 9, 2.

2 G. Alarcón, M. Guix, A. Ambrosi, M. T. Ramirez Silva, M. E. Palomar Pardave, A. Merkoçi, *Nanotechnology* **2010**, 21, 245502 .

3 D. Kagan, P. Calvo-Marzal, S. Balasubramanian, S. Sattayasamitsathit, K. ManianManesh, G.-U. Flechsig, J. Wang, *J. Am. Chem. Soc.* **2009**, 131, 12082.

4 R. Laocharoensuk, J. Burdick, J. Wang, *ACS Nano*, **2009**, 2 (5), 1069.

5 J. Wang, J. Dai, T. Yarlagadda, *Langmuir* **2005**, 21(1), 9.

6 C. C. Mayorga Martinez, R. E.Madrid, C. J. Felice, Sens.Actuatiors B: Chem. 2008, 133, 682.

7 C. C. Mayorga Martinez; E. F. Treo, R. E. Madrid, C. J. Felice, *Biosens. Bioelectron.* **2010**, 26, 1239.

8 C. C. Mayorga Martinez, E. F. Treo, R. E. Madrid, C. J. Felice, Biosens. Bioelectron. 2011, 29, 200.

Compact microcubic structures platform based on self-assembly Prussian blue nanoparticles with highly tuneable conductivity†

Welter Cantanhêde Silva,[ab] Maria Guix,[a] Georgina Alarcón Angeles[ac] and Arben Merkoçi*[acd]

Received 23rd June 2010, Accepted 25th August 2010
DOI: 10.1039/c0cp00960a

Control of molecular and supramolecular properties is used to obtain a new advanced hybrid material based on Prussian blue nanoparticles (PB NPs). This hybrid material is obtained through a self-assembled Layer-by-Layer (LbL) approach combining the advantageous features of β-cyclodextrin (β-CD) polysaccharides, PB NPs and poly(allylamine hydrochloride) from electrostatic interaction between the deposited layers. Transmission electronic microscopy images suggested that PB NPs were protected by β-CD polysaccharides that prevent the aggregation phenomena. In addition, as confirmed by scanning electronic microscopy images, it was found that PB NPs are organized in microcubic supramolecular like structures *via* a mesoscale self-assembly process. Interestingly, the 3-bilayer {PAH/PB-CD} film exhibited a higher density of microcubic structures and a high electrochemical response with PB sites available for redox reactions at a supramolecular level. By utilizing fewer bilayers and consequently less material deposition, the formed {PAH/PB-CD} multilayer films of a tuneable conductivity can be expected to have interesting future applications for host–guest like dependent electrochemical biosensing designs.

Introduction

Advanced functional materials have been constructed based on the combination of appropriate building blocks such as inorganic compounds,[1–3] biopolymers,[4] semiconductor quantum dots,[5] metallic nanoparticles,[6,7] and carbon nanotubes.[8–10] For this purpose, layer-by-layer (LbL) and self-assembled[2,11] structures provide an excellent approach, since several hybrid supramolecular nanodevices can be built combining suitable oppositely charged components.[2,11] In the LbL method, the self-assembly process is governed by individual immobilization of positively and negatively charged polyelectrolytes, which allow for design and control of the thickness and structural morphology aspects.[2,11–14] In the context of nanoscience, constitutional dynamic chemistry (CDC) concepts[15] confer the means to interpret and control functional supramolecular entities, since dynamic character such as functional recognition and self-organization must be directly involved on the molecular level.[16]

Cyclodextrin (CD) molecules are defined as macrocyclic oligosaccharides composed of six (α), seven (β) or eight (γ) linked glucosyl units organized in a cone shape, which show a lipophilic central cavity and hydrophilic outer surface.[17–19] This unique structural characteristic of the CD molecules allows the formation of new supramolecular nanoplatforms aiming to develop functional drug delivery systems.[20] Also, Prussian blue (PB)—iron(II) hexacyanoferrate(III)—is defined as a mixed valence coordination compound[21,22] exhibiting unique electronic, electrochemical and structural features with a wide range of applications including molecular magnets,[23] sensors,[24,25] semiconductors,[26] electrochromic devices,[21,23] and biosensors.[27] In the chemical structure of PB the Fe^{3+} and Fe^{2+} ions are coordinated to the nitrogen and carbon atoms, respectively, through the bridging cyanide ligands.[21,22,28] Moreover, the charge balance in the face-centered cubic lattice[29–31] must be reached by potassium ions that confer distinct soluble—$KFe[Fe(CN)_6]$—and insoluble—$Fe_4[Fe(CN)_6)_3]$—forms. However, the two forms have been utilized on studies related to chemically modified electrodes.[31–36]

In order to obtain supramolecular structures with interest for both host–guest model and DNA probe applications,[28] PB nanoparticles protected by β-CD, designed as PB-CD NPs, have been reported that could improve the charge transfer inside the β-CD cavity producing an attractive nanocomposite.[35] To the best of our knowledge this is the first example of PB nanoparticles using β-CD polymer as a stabilizer, which opens the way to develop new supramolecular devices with interest for sensing and biosensing applications.

We report a novel assembled nanoplatform that takes advantage of alternate layer depositions from PB-CD NPs with polyallylamine (PAH). It is obtained on a tin oxide substrate by using the LbL technique, which is able to control

[a] *Institut Català de Nanotecnologia, Universitat Autônoma de Barcelona (UAB), 08193 Campus Bellaterra, Barcelona, Catalonia, Spain. E-mail: arben.merkoci.icn@uab.es; Fax: +34 935812379*
[b] *Department of Chemistry, Federal University of Piaui, 64049-550, Teresina, Piaui, Brazil. E-mail: welter@ufpi.edu.br*
[c] *Basic Sciences Department, Autonomous Metropolitan University, Unit Azcapotzalco, 02200 Mexico City, Mexico*
[d] *Institució Catalana de Recerca i Estudis Avançats, Passeig Lluís Companys, 23 08010 Barcelona, Spain*

† Electronic supplementary information (ESI) available: TEM images for PB nanoparticles using β-CD/Fe^{2+} ratio of 20 and 1.5; FTIR spectrum of PB-CD using β-CD/Fe^{2+} ratio of 10; SEM images for PAH, PB and PB-CD monolayers, and $\{PAH/PB\text{-}CD\}_n$ films; Influence of scan rate and electrochemical stability for 3-bilayers of {PAH/PB-CD} and cyclic voltammograms for 3-bilayers of PAH/PB-CD and PAH/PB. See DOI: 10.1039/c0cp00960a

the nano/micro supramolecular structure and in this way tune its conductivity. Multilayer characterization and formation of compact microcube structures at the molecular level have been evidenced by optical and electrochemical experiments. The developed platform is expected to have interesting applications in the sensing and biosensing fields, where highly conductive and tunable 'on-demand' platforms combined with biorecognition reactions are desirable.

Experimental section

Chemicals and materials

$FeCl_2{\cdot}4H_2O$, $K_3[Fe(CN)_6]$, H_2O_2 (d = 1.1 kg L^{-1}, 30%), KCl, NH_3 (30%) and acetone were acquired from Panreac, while PAH and β-CD polymers were purchased from Aldrich. KH_2PO_4 and K_2HPO_2, acquired from Fluka, were utilized to prepare 0.1 mol L^{-1} phosphate buffer solution at pH 6.2. All the other chemical reagents were of analytical grade purity and used as received. Ultra-pure water was supplied by a Milli-Q purification system and used in all experiments.

Synthesis of Prussian blue nanoparticles protected by β-cyclodextrin (PB-CD NPs)

β-cyclodextrin protected Prussian blue nanoparticles were prepared reacting $FeCl_2{\cdot}4H_2O$ and $K_3[Fe(CN)_6]$ in a 1 : 1 stoichiometric ratio using β-cyclodextrin as the matrix.[27,37] In a reaction flask, 2 mL of aqueous $K_3[Fe(CN)_6]$ (5.26 mg, 1.6×10^{-3} mol) was slowly added to an aqueous mixture (8 mL) that contained $FeCl_2{\cdot}4H_2O$ (3.18 mg, 1.6×10^{-3} mol) and β-CD (1.6×10^{-2} mol). Immediately, the formation of a dark blue product was observed. The above nanocomposite mixture was kept at 25 °C and stirred for 12 h, under nitrogen flow. 25 mL of acetone was added to the last mixture and the solvent was removed by centrifugation. The collected nanocomposite was washed with acetone at least three times in order to remove the ferrocyanide and ferric ion impurities as well as residual KCl.[38] The solid was left to be dried at room temperature for at least two hours.

Synthesis of Prussian blue nanoparticles (PB NPs)

The PB NPs were prepared as described for PB-CD NPs except for the use of β-CD polymer. The PB NPs, obtained as a solid precipitate, were purified by washing several times with acetone. Previous to the preparation of the LbL films, the PB and PB-CD NPs were characterized by UV-visible and IR spectroscopy and electrochemical techniques.[21–24,38]

Self-assembly of Layer-by-Layer {PAH/PB-CD} films

The resulting PB-CD NPs or PB NPs (18 mg) were dispersed in 2 mL water and sonicated for 10 min to achieve a well-dispersed suspension, which was used as negative polyelectrolyte in LbL method.[11] In order to clean and introduce negative charge onto the indium tin oxide (ITO; Delta Technologies Ltda, R_s = 70–100 Ω) surface, the substrates were treated with acetone at 80 °C for 10 min and washed with water, followed by sonicating in $H_2O : NH_3 : H_2O_2$ solution (5 : 1 : 1 v/v) prior to preparing the LbL films.[12–14] Self-assembly of the hybrid architectures was carried out by immersion of ITO electrodes into the cationic polyelectrolyte—PAH solution—(0.5 mg mL^{-1}) for 5 min, then rinsed with HCl solution (pH 5.0) and dried under nitrogen stream. After this step, the polymer monolayer was immersed into PB-CD NPs (or PB NPs) solution for 5 min, rinsed with HCl solution (pH 5.0) and dried with nitrogen. The above procedure was repeated to obtain the desired number of bilayers deposited onto the ITO substrate.

Characterization of PB-CD NPs and $\{PAH/PB\text{-}CD\}_n$ multilayer films

Infrared spectra of PB-CD NPs samples, prepared as KBr pellets, were run on a Perkin–Elmer FT spectrophotometer, series 2000 in the range 4000–600 cm^{-1}. Ultraviolet and visible (UV-Vis) absorption spectra were recorded with SpectraMax M2e spectrophotometer and employed to characterize the PB-CD and also follow the deposition process of the multilayer films onto the ITO substrate. Self-assembled films from 1 to 4 bilayers were characterized using cyclic voltammetry technique in an electrochemical analyzer (CH Instruments), where $\{PAH/PB\text{-}CD\}_n$ films (n = number of bilayers) deposited onto ITO acted as a working electrode. The electrochemical experiments were carried out using a conventional three-electrode cell with Pt as auxiliary electrode and Ag/AgCl (3 mol L^{-1} KCl) as reference electrode. Prior to electrochemical experiments, the cell was purged with nitrogen flow for at least 10 min at room temperature in order to remove the dissolved oxygen. Transmission electron microscopy (TEM) was performed using a JEOL JEM 2011 (Jeol Ltd Tokyo, Japan), operating at an accelerating voltage of 200 kV. A drop of each solution of PB or PB-CD NPs was cast on the copper grid, allowed to dry and imaged by TEM. The scanning electronic microscopy (SEM) images for PAH/PB-CD LbL films with 1, 2, 3 and 4 bilayers deposited onto ITO substrates were obtained using a Hitachi S-570 SEM. For comparison purposes, monolayer films were also obtained from solutions of PAH, PB NPs and PB-CD NPs utilized to prepare the LbL films.

Results and discussion

1 Formation of PB-CD NPs and multilayer growth of {PAH/PB-CD} bilayers

Initially, the influence of β-CD polysaccharide on the PB nanoparticle formation was investigated with 1.5, 10 and 20 β-CD/Fe^{2+} stoichiometry ratios. Upon mixing of the Fe^{2+} and $[Fe(CN)_6]^{3-}$ ions (with respective β-CD/Fe^{2+} stoichiometry ratios as described in the experimental section) the solutions immediately turned dark blue, suggesting the formation of PB species in the form of PB-CD NPs. The mechanism for PB/β-CD nanocomposite formation contains two steps: (1) Fe^{2+} species binds to the OH^- sites of the polymer chain, and (2) after adding $[Fe(III)(CN)_6]^{3-}$ species, coordination of Fe^{2+} species to the cyanide ligand occurs. In addition, the UV-Vis spectra exhibited a broad band with λ_{max} at 695 nm. The UV-Vis absorption spectrum of PB-CD NPs, synthesized as described in the experimental section, was attributed to the intervalence charge transfer band (IVCT) from Fe^{2+} to Fe^{3+} species in PB (ESI†).[21–24] This band is typical for PB species and its maximum

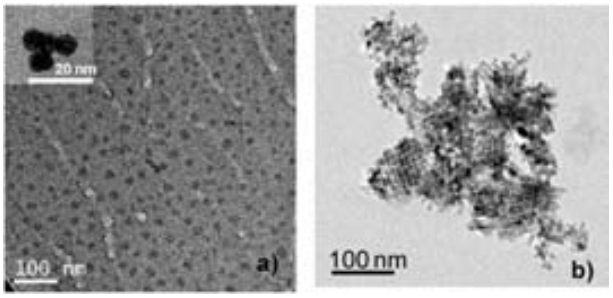

Fig. 1 TEM images for (a) PB nanoparticles protected by β-cyclodextrin and (b) PB NPs. The agglomerate formation of PB NPs in absence of β-CD can be observed.

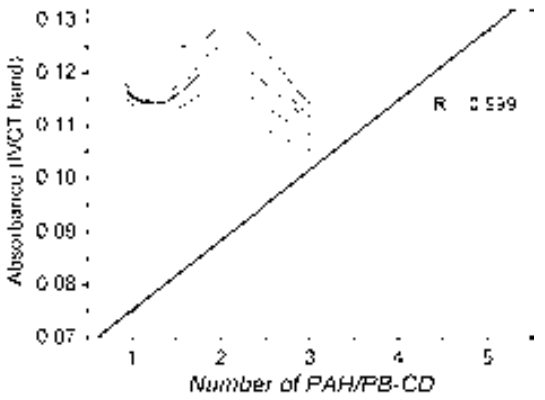

Fig. 2 Maximum absorbance at 705 nm *vs.* number of PAH/PB-CD bilayers. Inset: Electronic spectra for PAH/PB-CD films containing 1 to 5 bilayers.

of absorption can be affected by the interaction between PB and the surface protecting polymer, causing a change in the energy of electron transfer from Fe^{2+} to Fe^{3+} in the PB compound.[37–39]

We observed through the TEM images (Fig. 1a) that the formation of spherical nanoparticles without particle aggregation was favoured when the stoichiometric ratio of β-CD/$Fe(CN)_6^{3-}$ (or Fe^{2+}) species was kept at 10. Probably at this stoichiometric ratio a homogeneous distribution of β-CD species around the PB complex occurs, avoiding aggregation of PB molecules with each other. In contrast, the TEM images for PB nanoparticles (without β-CD) used as control experiments, and those with a higher quantity of β-CD (β-CD/$Fe(CN)_6^{3-}$ higher than 10), showed an aggregation phenomenon (Fig. 1b),[37,38] which is expected for PB nanocomposites formed from organic polymers such as polyvinyl pyrrolidone—PVP, polyallylamine hydrochloride—PAH, and polystyrene sulfonate—PSS. These findings indicate that PB NPs were well stabilized in the β-CD matrix and further aggregation of nanoparticles is prevented. It is important to point out that PB nanoparticle preparation was carefully investigated in terms of its reproducibility, and only when the stoichiometric ratio of β-CD/$Fe(CN)_6^{3-}$ species was equal to 10 were well dispersed PB nanoparticles produced.

The conclusion that PB nanoparticles are capped by β-CD molecules can be presumed, because of the nano-size of the PB and β-CD polysaccharide species observed in TEM images, as shown in Fig. 1. In fact, PB nanoparticles with diameters of 10–12 nm were obtained using the mentioned experimental conditions. Synthesis performed using lower (up to 1.5 fold excess) and higher (up to 20 fold excess) β-CD concentrations showed that PB NPs remained either aggregated or dispersed respectively (ESI†). The vibrational modes for PB species and β-CD appeared in the infrared spectrum of the nanocomposite (ESI†) prepared with well dispersed PB in β-CD matrix.[37–39] The broad absorption (medium intensity) in the range from 3600 to 3000 cm^{-1} and peaks found in the range from 1160 to 940 cm^{-1} were associated with the primary and secondary OH groups and C–O–C stretching, respectively, from β-CD.[39] The peak at 2073 cm^{-1} (medium intensity) was assigned to the CN stretching in the Fe^{2+}–CN–Fe^{3+} fragment. The results obtained are in accordance with previous work on several nanocomposites containing PB nanoparticles protected by organic polymers.[37,38]

The growth of the multilayer LbL films was followed by UV-Vis spectroscopy by recording spectra after each deposition step and finding the relation between the adsorption intensities for PAH/PB-CD nanostructured films and bilayer number (Fig. 2). The maximum time used for electrode immersion (5 min) in the PAH and PB-CD NPs (or PB NPs) polyelectrolytes was based on previous adsorption kinetic studies from UV-Vis and electrochemical measurements.[33,40]

As shown inset in Fig. 2, the λ_{max} for LbL films from 1 to 5 bilayers was observed at 705 nm and also attributed to the Fe^{2+}–CN–Fe^{3+} transition for PB species.[20–23,30] This peak maximum is the same as that found for LbL films containing PB NPs and β-CD. The difference in energy between the IVCT bands for LbL films and PB nanoparticles dispersed in aqueous solution (10 nm) suggests a stronger electrostatic interaction between PAH and PB-CD NPs groups. The cited supramolecular stabilization has been observed for several LbL systems and justified by salt-bridge formation at the molecular level due to the interaction resulting from ionic attraction of oppositely charged layers.[12–14,33,38] Furthermore, the peak shifted to longer wavelength for PB NPs can also be interpreted as an interaction between the surface polymer and inner PB particles.[33] It is clear that the multilayer deposition of PAH/PB-CD assemblies is reproducible with sequential steps. This is indicated by the linearity between the absorbance and bilayer number (Fig. 2).

2 Film assembly and evidence of compact microcubic structures

SEM images for PAH, PB and PB-CD monolayers and LbL films deposited onto ITO substrates were used to investigate the morphology of the PAH/PB-CD bilayer films (ESI†). A closer look at the SEM images reveals that the roughness of the $\{PAH/PB\text{-}CD\}_n$ system increases with deposition of the bilayers and formation of the microcubic structures, starting to appear from the 2-bilayers film formation. Fig. 3 displays typical SEM images for 3-bilayer PAH/PB-CD and PAH/PB films assembled onto ITO substrates. As evidenced in Fig. 3a, the average size of the microcubic structures for $\{PAH/PB\text{-}CD\}_3$ films is 200–300 nm with a higher density of microcubic structures when compared with 2 and 4-bilayer films (ESI†). On the other hand, for $\{PAH/PB\}_3$ films (without β-CD matrix) it was only observed that large pores cover the entire

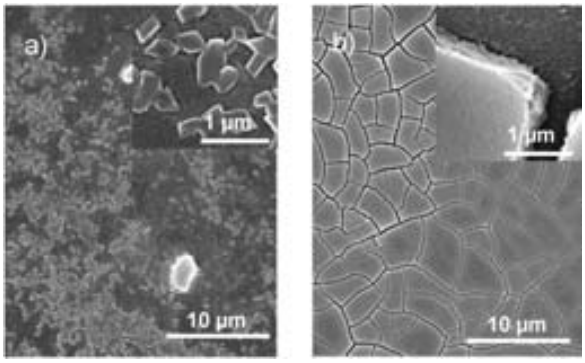

Fig. 3 SEM images of 3-bilayer films for: (a) PAH/PB-CD and (b) PAH/PB LbL systems onto ITO coated electrode.

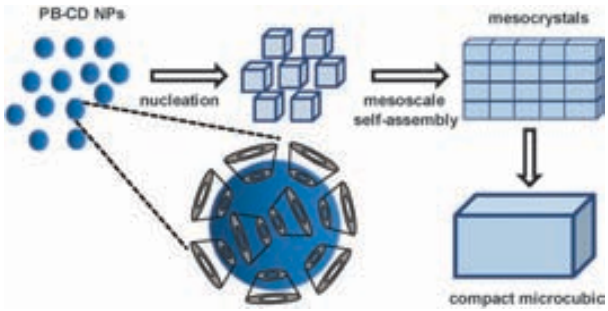

Fig. 4 Mechanism for growth of compact microcubic structure.

surface of ITO substrates (Fig. 3b). This distinct behaviour can be probably associated with the role of the β-CD molecules in avoiding aggregation phenomena of PB nanoparticles (already evidenced in TEM images) but affecting the organization of PB NPs in microcubic supramolecular-like structures.

The SEM images indicate that PB-CD microcrystals did not follow a classical crystalization process,[29] which would allow enlargement of the building blocks such as molecules or small supramolecular clusters onto the nuclei surfaces. Probably, the PB-CD microcrystals with cubic orientation are formed *via* a mesoscale self-assembly process allowing a non-covalent supramolecular interaction between PB building blocks and the β-CD polymer. Fig. 4 illustrates a possible mechanism to explain this process that might have occurred in three steps: (1) nucleation of PB-CD NPs within the LbL flask, (2) the unit cells of microcrystals support a mesoscale self-assembly process, and (3) supramolecular conversion of mesocrystals to a compact microcubic structure. Probably, the time adopted for electrode immersion in PB-CD NPs solution (LbL method) must affect the formation of microcubic structures, especially at the beginning because the assembled 1-bilayer of PAH/PB-CD did not show the mentioned process. Also, the PB NPs (without β-CD), utilized as experimental control, did not support the mesoscale self-assembly process, which indicate that β-CD molecules play fundamental role in supramolecular organization. The mesoscopic self-assembly (MESA) and molecular self-assembly concepts are well discussed in ref. 29. Furthermore, the immobilization of PAH, PB and PB-CD monolayers for 5 min from respective polyelectrolytes were also utilized to understand the formation of microcubic

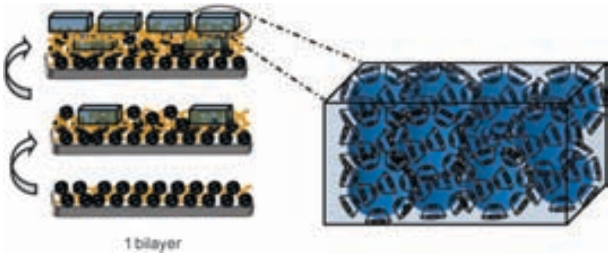

Fig. 5 Self-assembly for 1, 2 and 3-bilayers based on interaction between Prussian blue nanoparticles protected by β-cyclodextrin (blue) and PAH polymer (orange). Detail: Microcubic structure.

structures. Thus, based on this careful SEM investigation, we propose the formation of microcubic structures and supramolecular like structures for {PAH/PB-CD} LbL films (Fig. 5).

Interestingly, 3-bilayer {PAH/PB-CD} films exhibited a higher density of microcubic structures and a high electrochemical response with PB sites available for redox reactions at the supramolecular level. The formation of microcubes from PB nanoparticles has also been observed in several other conditions. For example, Zheng and co-workers[29] have proposed a nonclassical growth mechanism of PB microcubes under hydrothermal conditions by mesoscale self-assembly. In this case, the concentration of $K_3[Fe(CN)_6]$ and the reaction time seems to affect the preparation of the microcubic structure.[29,30] Using sonochemical synthesis, Wu *et al.* obtained single nanocubes with a regular square shape.[30]

3 Electrochemical behavior of LbL PAH/PB-CD modified electrodes

The layer-by-layer assembly onto ITO electrodes from PAH and PB-CD NPs was performed (up to 4 bilayers) and monitored by cyclic voltammetry (after each deposition step) over a potential range of −0.3 to 1.1 V *vs.* Ag/AgCl in 0.2 mol L^{-1} KCl. As illustrated in Fig. 6, typical *j*–*E* electrochemical responses were obtained for $\{PAH/PB\text{-}CD\}_n$ systems showing two well-defined redox couples at 125 ($E_{(1/2)1}$) and 800 mV ($E_{(1/2)2}$) attributed to the conversion of Prussian white (PW) to Prussian blue (PB) and Prussian blue (PB) to Berlin green (BG), respectively, which are similar to those of PB species immobilized in LbL films reported previously.[27,33,40] The following equations describe the steps involved in the

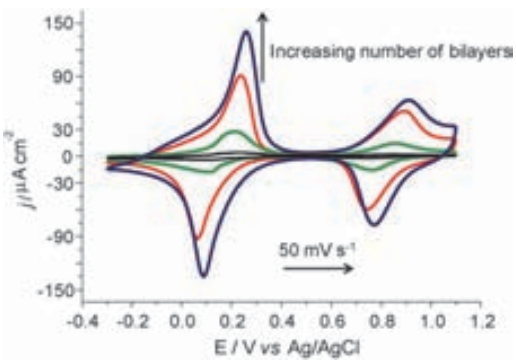

Fig. 6 Cyclic voltammograms for self-assembly {PAH/PB-CD} multilayers onto ITO electrode containing 1, 2, 3, and 4 bilayers. Scan rate: 50 mV s^{-1}. Electrolyte: KCl—0.2 mol L^{-1}, T = 25 °C.

charge transport for PB and its analogues, and the dependence on K^+:

$$K_2[Fe^{2+}Fe^{2+}(CN)_6](PW) \underset{K^+ + e^-}{\overset{-K^+ - e^-}{\rightleftharpoons}} K[Fe^{2+}Fe^{3+}(CN)_6](PB) E_{(1/2)I} \quad (1)$$

$$K[Fe^{2+}Fe^{3+}(CN)_6](PB) \underset{K^+ + e^-}{\overset{-K^+ - e^-}{\rightleftharpoons}} [Fe^{3+}Fe^{3+}(CN)_6](BG) E_{(1/2)II} \quad (2)$$

Moreover, the cathodic and anodic peak currents increased with the number of bilayers. This last behavior indicates that PB nanoparticles are electrically connected within multilayers, with the charge transport reaction proceeding through an electron hopping process,[12–14,27,33,40] as proposed initially by Laurent and Schlenoff.[41] Based on the multilayer deposition monitored by UV-Vis spectroscopy and cyclic voltammetry, we should assume that the amount of deposited PB species could be simply controlled by selecting the LbL step deposition.[27,33,40] It is necessary to point out that β-CD polysaccharides in the $\{PAH/PB\text{-}CDNP\}_n$ system showed no electroactivity in the potential range studied. We believe that the electrochemical processes from β-CD molecules are overlapped by the redox pair from PB that occurs in the selected window potential.[17]

In order to avoid the effect of the amount of deposited bilayers upon the electrochemical processes of LbL films (loss of their reversibility and sensitivity)[13,14,27] especially for LbL films from 5-bilayers,[13,14,27] we decided to work only with modified electrodes containing up to 4-bilayers of PAH/PB-CD.[27] According to previous self-assembly studies with polymers and metallophthalocyanine,[12,14] the LbL films containing more than 4-bilayers are usually thicker due to the nonconductive material deposition onto the ITO plate (*i.e.* PAH polymer and chitosan); in addition, increasing the of number of bilayers hinders the electron transfer to the electrode surface. For thin films containing up 4-bilayers a different behavior is expected due to the initial supramolecular organization of components at the molecular level.[12–14] Furthermore, for the 3-bilayer films of PAH/PB-CD and PAH/PB, prepared as described in the experimental section, no significant differences in the electrochemical behaviour of PB were observed (ESI†).

The influence of the scan rates (v) on the peak currents (I_{pa} and I_{pc}) for LbL electrodes containing PAH and PB-CD nanoparticles was investigated in the range of 10 to 200 mV s^{-1} in 0.2 mol L^{-1} KCl electrolyte (Fig. 7). The peak currents increased with scan rate up to 200 mV s^{-1} with the profiles of the voltammograms being consistent with strong PB immobilization onto the ITO surface, since redox peaks assigned to the PB and its analogues appeared.[27,33,40] Under CV conditions, the peaks associated with the redox processes from PB follow the linearity of peak current *vs.* potential up to a scan rate of 70 mV s^{-1} (ESI†). For scan rates higher than 70 mV s^{-1} a linearity in the I *versus* $v^{1/2}$ plot was observed at scan rates up to 500 mV s^{-1}, where charge transport and counterion diffusion are expected to be rate-determining.[27,35,42] These findings suggest a change of the charge transfer mechanism to a diffusion-controlled process.[27,35,42] Similar behaviour

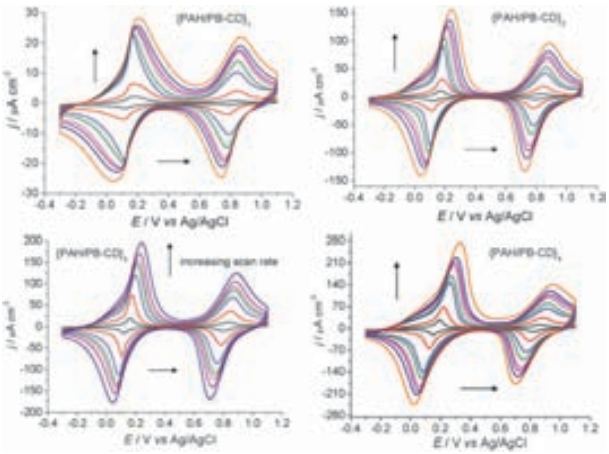

Fig. 7 Cyclic voltammograms from PAH/PB-CD LbL films containing 1, 2, 3 and 4 bilayers at scan rates: 10, 30, 50, 70, 100, 120, 150 and 200 mV s^{-1}. Electrolyte: KCl—0.2 mol L^{-1}, T = 25 °C.

was also proposed by Kumar and collaborators for electrochemical deposition of gold-PB nanocomposite film.[35] In another work, Li *et al.*[25] also evidenced that reaction kinetics affect the electrochemical response of a composite containing multi-walled carbon nanotubes, poly(vinylpyridine) and PB. A linear relationship of I_{pa} *versus* scan rate was observed at lower scan rate (between 1 and 15 mV s^{-1}), but at higher scan rates (up to 1000 mV s^{-1}) the anodic peak currents were proportional to the $v^{1/2}$.

As evidenced by Zhao and co-workers,[27] the cyclic voltammogram response for a PB modified electrode containing Glucose Oxidase (GOD) can assume a quasi-reversible electrochemical behavior due to the participation of K^+ in the redox process. Furthermore, for ITO modified electrodes with the PAH and PB-CD layers it was observed that ΔE_p increases with increasing scan rate, where E_{pa} and E_{pc} shift slightly to positive and negative regions, respectively, indicating slower kinetics.[27,35,42] This behaviour can be interpreted in terms of the resistance of LbL films, that increases as a function of the number of bilayers due to higher film thickness and amount of nonconductive PAH polymer.[27] However, the $E_{1/2}$ values are practically the same, independent of the scan rates and number of bilayers. In order to check the electrochemical stability and independence of the redox responses of the peaks from ITO-$\{PAH/PB\text{-}CD\}_3$ electrodes, their voltammetric responses were analyzed in several potential windows and cycles. As observed in Fig. 7, the cyclic voltammograms from −0.1 to 0.6 and 0.6 to 1.2 V indicate that both redox pairs are independent. However, after 10 cycles in the whole potential window (Fig. 8a), the anodic currents of the I and II peaks decrease to only 17 and 22% of their initial respective values. Conversely, for CV responses in the −0.1 to 0.6 V and 0.6 to 1.2 V regions an increase in PB stability was observed, when anodic currents decrease only 6 and 18% from the first cycle, respectively (Fig. 8b and c). Initially, the electrochemical stability study for PB modified electrodes containing 3-bilayers was performed in 0.2 mol L^{-1} KCl electrolyte and showed that faradaic currents decrease quickly (ESI†) even in the cathodic region (−0.1 to 0.6 V), where the LbL films formed from PB NPs are usually investigated.[24,27,31–36] These results indicate

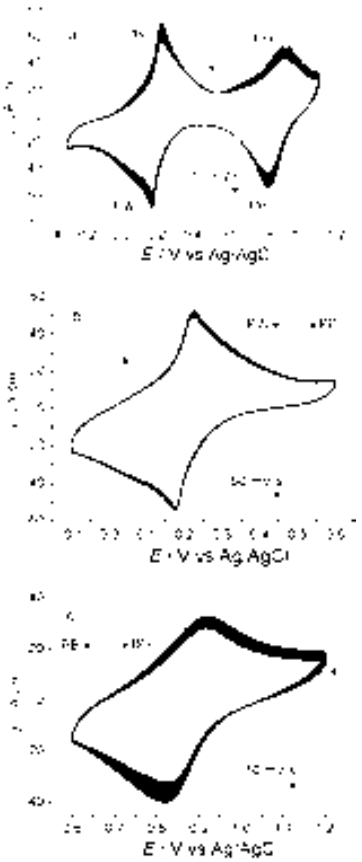

Fig. 8 Continuous cyclic voltammograms (10 cycles) for the ITO-{PAH/PB-CD}$_3$ electrode in: (a) −0.3 to 1.1 V range (b) −0.1 to 0.6 V range, and (c) 0.6 to 1.2 V range. Electrolyte 0.1 mol L^{-1} KCl + 0.1 mol L^{-1} PBS (pH 6.2). Scan rate: 50 mV s^{-1}, T = 25 °C.

that the incorporation of PBS in the supporting electrolyte containing KCl enhances the electrochemical stability of PB NPs immobilized into 3-bilayer films. It is interesting to point out that according to the common opinions also given earlier by other authors[24,27,31–36] the stability of PB modified electrodes depends on the nature of the supporting electrolyte, the number of voltammetric cycles and also the potential range. The electrochemical experiments using a nanostructured LbL PAH/PB-CD system in electrolyte solution containing both KCl and PBS has been selected for use due to the better electrochemical response and possibility of host–guest interactions, with interest for biosensor applications in a biocompatible physiological media.

It is envisaged that unique features arising from the nanostructured PAH/PB-CD LbL films and overall tuning of the conductivity upon LbL control may be exploited in several sensing and biosensing designs. The use of host–guest interaction studies with interest for biosensing applications are underway in our laboratories.

Conclusions

Combining the advantageous features of β-CD polysaccharide, Prussian blue nanoparticles and the layer-by-layer process, a new {PAH/PB-CD} platform was prepared and characterized by optical and electrochemical techniques. As also suggested by TEM and SEM images, the presence of β-CD species protected the PB NPs, avoiding aggregation phenomena and also affecting the organization of PB NPs in microcubic supramolecular like structures through a mesoscale self-assembly process. In contrast, agglomeration of PB NPs without β-CD was evidenced. The 3-bilayer {PAH/PB-CD} film showed a higher density of microcubic structures with a high electrochemical response due to PB sites available for redox reactions at the supramolecular level. Working with a LbL approach, β-CD and PB NPs and utilizing fewer bilayers was suggested as a compromise between reduced material deposition and the conductivity of the platform. The developed nano/microstructurated PB based platform is expected to have interesting applications in the design of novel sensing and biosensing systems.

Acknowledgements

The financial support from CNPq, Brazil (process number 200515/2009-8), and the financial support by the Spanish Ministry of Science and Innovation through projects MAT2008-03079/NAN, CSD2006-00012 "NANOBIOMED" (Consolider-Ingenio 2010) and a pre-doctoral fellowship (BES-2009-023939 given to M. G.) are acknowledged. G. Alarcón thanks CONACyT for the post-doctoral fellowship (105024).

Notes and references

1 D. L. Feldheim and B. E. Eaton, *ACS Nano*, 2009, **3**, 2207–2216; K. Ariga, J. Hill, M. V. Lee, A. Vinu, R. Charvet and S. Acharya, *Sci. Technol. Adv. Mater.*, 2008, **9**, 014109.
2 F. N. Crespilho, W. C. Silva and V. Zucolotto, in *Catalysis and Photochemistry in Heterogeneous Media*, Research Signpost, Kerala, India, 1st edn, 2007, ch. 3, pp. 59–73.
3 J. Chen and F. Cheng, *Acc. Chem. Res.*, 2009, **42**, 713–723.
4 M. D. Cathell, J. C. Szewczyk, F. A. Bui, C. A. Weber, J. D. Wolever, J. Kang and C. L. Schauer, *Biomacromolecules*, 2008, **9**, 289–295.
5 X. Li, Y. Zhou, Z. Zheng, X. Yue, Z. Dai, S. Liu and Z. Tang, *Langmuir*, 2009, **25**, 6580–6586.
6 L. Y. Chen, L. Zhang, T. Fujita and M. C. Chen, *J. Phys. Chem. C*, 2009, **113**, 14195–14199.
7 A. E. Muniz and A. Merkoçi, *Expert Opin. Med. Diagn.*, 2010, **4**, 21–37.
8 L. Ren, X. Xian, K. Yan, L. Fu, L. Liu, S. Chen and Z. Liu, *Adv. Funct. Mater.*, 2010, **20**, 1209–1223.
9 C. N. R. Rao, R. Voggu and A. Govindaraj, *Nanoscale*, 2009, **1**, 96–105.
10 Y. Zhang, H. Hongkun, C. Gao and J. Wu, *Langmuir*, 2009, **25**, 5814–5824.
11 G. Decher, *Science*, 1997, **277**, 1232–1237; K. Ariga, J. P. Hill and Q. Ji, *Phys. Chem. Chem. Phys.*, 2007, **9**, 2319–2340; P. Alessio, M. L. Rodriguez-Mendes, J. A. S. Saez and C. J. L. Constantino, *Phys. Chem. Chem. Phys.*, 2010, **12**, 3972–3983; N. Ferreyra, L. Coche-Guérente, J. Fatisson, M. L. Teijelo and P. Labbé, *Chem. Commun.*, 2003, 2056–2057.
12 W. S. Alencar, F. N. Crespilho, M. V. A. Martins, V. Zucolotto, O. N. Oliveira-Jr. and W. C. Silva, *Phys. Chem. Chem. Phys.*, 2009, **11**, 5086–5091.
13 W. S. Alencar, F. N. Crespilho, M. R. M. C. Santos, V. Zucolotto, O. N. Oliveira-Jr. and W. C. Silva, *J. Phys. Chem. C*, 2007, **111**, 12817–12821.
14 A. C. Santos, R. A. S. Luz, L. G. F. Ferreira, J. R. Santos-Jr., F. N. Crespilho and W. C. Silva, *Quim. Nova*, 2010, **33**, 539–546.
15 J. M. Lehn, *Chem. Soc. Rev.*, 2007, **36**, 151–160.

16 J. M. Lehn, *Rep. Prog. Phys.*, 2004, **67**, 249–265.
17 G. A. Angeles, B. P. López, M. P. Pardave, M. T. R. Silva, S. Alegret and A. Merkoçi, *Carbon*, 2008, **46**, 898–906.
18 S. Pande, S. K. Ghosh, S. Praharaj, S. Panigrahi, S. Basu, S. Jana, A. Pal, T. Tsukuda and T. Pal, *J. Phys. Chem. C*, 2007, **111**, 10806–10813.
19 T. Ogoshi, M. Hashizume, T. Yamagishi and Y. Nakamoto, *Langmuir*, 2010, **26**, 3169–3173.
20 C. A. Nijhuis, K. A. Dolatowska, B. J. Ravoo, J. Huskens and D. N. Reinhoudt, *Chem.–Eur. J.*, 2007, **13**, 69–80.
21 D. J. Schmidt, F. C. Cebeci, Z. I. Kalcioglu, S. G. Wyman, C. Ortiz, J. V. Vliet and P. T., *ACS Nano*, 2009, **3**, 2207–2216.
22 C. A. Lundgren and R. W. Murray, *Inorg. Chem.*, 1988, **27**, 933–939.
23 M. Taguchi, I. Yagi, M. Nakagawa, T. Iyoda and Y. Einaga, *J. Am. Chem. Soc.*, 2006, **128**, 10978–10982.
24 H. Razmi and E. Habibi, *Anal. Biochem.*, 2009, **392**, 126–132.
25 J. Li, J. D. Qiu, J. J. Xu, H. Y. Chen and X. H. Xia, *Adv. Funct. Mater.*, 2007, **17**, 1574–1580.
26 Y. Y. Song, W. Z. Jia, W. Z. Y. Li, X. H. Xia, Q. J. Wang and J. W. Zhao, *Adv. Funct. Mater.*, 2007, **17**, 2808–2814.
27 W. Zhao, J. J. Xu, C. G. Shi and H. Y. Chen, *Langmuir*, 2005, **21**, 9630–9634.
28 K. B. Cederquist, R. S. Golightly and C. D. Keating, *Langmuir*, 2008, **24**, 9162–9171.
29 N. Bowden, I. S. Choi, B. A. Grzybowski and G. M. Whitesides, *J. Am. Chem. Soc.*, 1999, **121**, 5373–5391; X. J. Zheng, Q. Kuang, T. Xu, Z. Y. Jiang, S. H. Zhang, Z. X. Xie, R. B. Huang and L. S. Zheng, *J. Phys. Chem. C*, 2007, **111**, 4499–4502.
30 X. Wu, M. Cao, C. Hu and X. He, *Cryst. Growth Des.*, 2006, **6**, 26–28.
31 A. Abbaspour and M. A. Kamyabi, *J. Electroanal. Chem.*, 2005, **584**, 117–123.
32 Y. Miao and J. Liu, *Sci. Technol. Adv. Mater.*, 2009, **10**, 025001.
33 J. D. Qiu, H. Z. Peng, R. P. Liang, J. Li and X. H. Xia, *Langmuir*, 2007, **23**, 2133–2137.
34 M. Orellana, L. Ballesteros, R. D. Rio, P. Grez, R. Schrebler and R. Córdova, *J. Solid State Electrochem.*, 2009, **13**, 1303–1308.
35 S. S. Kumar, J. Joseph and K. L. Phani, *Chem. Mater.*, 2007, **19**, 4722–4730.
36 Y. Shan, G. Yang, J. Gong, X. Zhang, L. Zhu and L. Qu, *Electrochim. Acta*, 2008, **53**, 7751–7755.
37 T. Uemura, M. Ohba and S. Kitagawa, *Inorg. Chem.*, 2004, **43**, 7339–7345.
38 Y. Xian, Y. Zhou, Y. Xian, L. Zhou, H. Wang and L. Jin, *Anal. Chim. Acta*, 2005, **546**, 139–146.
39 M. M. Omari, N. H. Daraghmeh, M. I. El-Barghouthi, M. B. Zughul, B. Z. Chowdhry, S. A. Leharne and A. A. Badwan, *J. Pharm. Biomed. Anal.*, 2009, **50**, 449–458.
40 P. A. Fiorito, V. R. Gonçalves, E. A. Ponzio and S. I. C. Torrresi, *Chem. Commun.*, 2005, 366–368.
41 D. Laurent and J. B. Schlenoff, *Langmuir*, 1997, **13**, 1552–1557.
42 F. N. Crespilho, V. Zucolotto, C. M. A. Brett, O. N. Oliveira-Jr. and F. C. Nart, *J. Phys. Chem. B*, 2006, **110**, 17478–17483.

Adriano Ambrosi[1]
Maria Guix[1]
Arben Merkoçi[1,2]

[1]Nanobioelectronics and Biosensors Group, Institut Català de Nanotecnologia, CIN2 (ICN-CSIC), Barcelona, Catalonia, Spain
[2]ICREA, Barcelona, Spain

Received May 14, 2010
Revised June 19, 2010
Accepted June 21, 2010

Research Article

Magnetic and electrokinetic manipulations on a microchip device for bead-based immunosensing applications

The combination of electrophoretic and magnetic manipulations with electrochemical detection for a versatile microfluidic and bead-based biosensing application is demonstrated. Amperometric detection is performed in an off-channel setup by means of a voltammetric cell built at the microchannel outlet and using a gold working electrode. Superparamagnetic particles are introduced and handled inside the channel by means of an external permanent magnet in combination with the electrogenerated flow which allows reproducible loading. The specific detection of phenol as electroactive alkaline phosphatase product is used in this study as proof of concept for a sensitive protein quantification. Characterizations and optimization of different parameters have been carried out in order to achieve the best detection signal. The applicability of the device has been finally demonstrated by the detection of rabbit IgG as model protein after an immunoassay performed on magnetic particles as immobilization platform. A comparison between the electrochemical detection using the developed device and the optical standard detection revealed similar performances with, however, extremely lower amount of reagent used and shorter analysis time. The developed electrophoretic- and magnetic-based chip may open the way to several other biosensing applications with interest not only for other proteins but also for DNA analysis, cell counting, and environmental control.

Keywords:
Amperometric detection / Immunoassay / Magnetic beads / Microchip capillary electrophoresis / Miniaturization
DOI 10.1002/elps.201000268

1 Introduction

The introduction of the concept of micro-total analysis systems, or μTAS [1], started the development of multiple technologies for the realization of fluidic microsystems. This is due to the advantages deriving by the use of microfluidic chips when compared with the classical analytical systems: (i) the possibility of using small quantities of sample and reagents (down to picoliters), (ii) fast reaction times when molecular diffusion lengths are of the order of the microchannel dimension, and (iii) a large surface-to-volume ratio, offering an intrinsic compatibility between the use of a microfluidic system and surface-based assays [2–5].

In heterogenous assays, reactions occur both in a solution and in a solid phase, offering the advantage of easy separation of chemical complexes from reactants. Bead-based materials are ideal reagent delivery vehicles providing large reactive surface areas for chemical binding. They can be easily recovered from a dispersion, reversibly redispersed, and are omnipresent in biomedical applications [6, 7].

Biomolecule immobilization on a solid phase (i.e. microparticles or nanoparticles) evidently results in a small volume and localized assay [8]. With respect to open microchannels, microfluidic structures with packed beds of functionalized beads or containing bead suspensions, profit from an even larger surface-to-volume ratio, with an enhanced interaction of reactive surfaces with passing fluids. This reduces diffusion times during the microfluidic procedures and also having a higher density of binding sites, and improves the detection sensitivity. In addition, such an

Correspondence: Professor Arben Merkoçi, Institut Català de Nanotecnologia, CIN2 (ICN-CSIC), Campus de la UAB, Edifici Q (ETSE), 2ª planta, 08193 Bellaterra (Barcelona), Spain
E-mail: arben.merkoci.icn@uab.es
Fax: +34935812379

Abbreviations: **AP,** alkaline phosphatase; **EC,** electrochemical; **MB,** magnetic bead; **p-NPP,** *p*-nitrophenyl phosphate

Colour Online: See the articles online to view Figs. 1, 2 and 4 in colour.

assay allows for a rapid regeneration and exchange of the solid support when needed [9].

Magnetic nanoparticles and microparticles offer an additional advantage: having embedded magnetic entities, they can be easily manipulated using permanent magnets or electromagnets, independently of normal microfluidic or biological processes [10]. This extra degree of freedom is the basis of a still improved exposure of the functionalized bead surface to the surrounding liquid and of higher sample preconcentration efficiencies, due to the increased relative motion of the bead with respect to the fluid [11].

Paramagnetic beads have been extensively used as solid support for the preparation, separation, and detection of biomolecules such as DNA [12] and protein [13, 14] mostly because of their efficiency, simplicity, mild operation conditions, and low cost [15–18].

Several applications of magnetic particles with microfluidic systems have been demonstrated for DNA hybridization and recognition [19–22], immunoassays [23–27] cell capture/detection [28, 29], and environmental [30, 31] and food control [32].

These studies describe the manufacturing and assembling of analytical tools for different applications where magnetic particles are precisely handled in either on-channel or off-channel formats by means of permanent magnets or built-in electromagnets. Optical detection (LIF, Chemiluminescence) represents the most adopted technology for the signal transduction with excellent results in terms of limit of detection and sensitivity. Extremely low detection limits have been achieved also by means of electrochemical (EC) detection [30, 32]. Fluids and magnetic particle pumping inside the microchannels is mostly accomplished by physical systems such as syringe or peristaltic pumps. However, most successful microfluidic system devices consist of microchannel networks in which the solutions are pumped using applied electric fields [33, 34]. The mechanism underlying this pumping principle is electro-osmosis, a bulk flow which originates at the surface of charged substrates such as glass, and requires no pumps, valves, or other moving parts [35]. An additional advantage of using electric fields is that species may also be separated electrophoretically as a function of their different charge-to-mass ratios [33–36].

High-voltage power supply (HVPS) systems used to apply the electric field are built in much reduced dimensions, and therefore promoting miniaturization of the device for portable applications.

EC detection is also ideally suited to miniaturized analytical systems and is an attractive alternative mode for microchip CE devices [37–39]. The sensitivity and selectivity of EC detection are comparable to those of LIF detection. There are several advantages of EC detection over other detection modes, including the ability to miniaturize both the detector and the control instrumentation and the fact that many compounds can be detected without derivatization [40].

In this study, we propose the combination of electrokinetic pumping and magnetic manipulation in a microfluidic device, employing magnetic particles as solid support for bioassays with an end-channel EC detection. EC detection is used as extremely sensitive technique to quantify the electroactive enzyme product generated within the channel. Widely used enzyme-linked immunoassay (ELISA) for the quantification of protein is based on the optical measurement of the product of the reaction between an enzyme detecting label and a specific substrate. We propose an alternative detection format, performing the heterogeneous immunoassay onto paramagnetic particles, and detecting the enzyme product by means of amperometric technique. The proposed analytical tool showed promising performances carefully compared with optical detecting systems and offered additional interesting features, such as the possibility for multianalysis setup, miniaturization, automation, and also a high grade of versatility since the detecting scheme could be easily adopted for protein analysis as well as for DNA analysis, cell counting, and environmental control.

2 Materials and methods

2.1 Reagents

Streptavidin-coated paramagnetic beads (MB) of diameter of 2.8 μm (M-280) and 1.0 μm (MyOne) were purchased from Invitrogen Dynal AS (Oslo, Norway). Biotin conjugate anti-rabbit IgG (B5283, developed in goat and γ-chain specific), rabbit IgG from serum, anti-rabbit IgG-alkaline phosphatase (AP) conjugate (A7539, developed in goat and whole molecule), *p*-nitrophenyl phosphate (p-NPP), phenol, sodium phenyl phosphate, and BSA were purchased from Sigma-Aldrich. Biotin conjugate AP was purchased from Cultek S. L.U. (Madrid, Spain). All buffer reagents and other inorganic chemicals were supplied by Sigma, Aldrich, or Fluka, unless otherwise stated. All chemicals were used as received, and all aqueous solutions were prepared in doubly distillated water. The running buffer for the electrophoretic experiments consisted of 10 mM phosphate-buffered solution (pH 8.0).

The phosphate buffer solution used for the immunoassay procedure consisted of 0.01 M PBS, 0.137 M NaCl, and 0.003 M KCl (pH 7.4). Blocking buffer solution consisted of a PBS solution with added 5% w/v BSA (pH 7.4). The washing buffer consisted of a PBS solution with added 0.05% v/v Tween-20 (pH 7.4).

2.2 Apparatus

The glass microchip was obtained from Micralyne (Edmonton, Canada). The 88 mm × 16 mm chip consisted of four-way injection cross, with 74 mm long separation channel, and 5 mm side arms. The original waste reservoir was cut off, leaving the channel outlet at the end of the chip, and thus facilitating the end-channel amperometric detection

(Fig. 1A). The channels had dimensions of 50×20 μm (width × height). Plexiglas holder was fabricated for holding the separation chips and housing the detector and reservoirs (Fig. 1B) [41]. A short pipette tip was inserted into each of three holes on the glass chip and corresponding reservoirs for the solution contact between the channel on the chip and the corresponding reservoir on the chip holder. (for larger photograph, see Supporting Information Fig. S1).

A Neodymium-iron-boron permanent magnet (diameter 3 mm, height 1.5 mm, Halde Gac Sdad, Barcelona, Spain) was used to handle the MBs inside the microchip channels.

Pictures and videos were recorded using a digital microscope connected to a personal computer and using Motic Images Plus software (Motic, Spain).

The detection system was placed in the waste reservoir (at the channel outlet side) and consisted of a platinum wire counter, an Ag/AgCl reference, and a gold working electrode. These wire (reference and counter) electrodes were inserted through holes drilled in Plexiglas holder. The working electrode, housed in the plastic screw, was placed opposite to the channel outlet, at a distance of 50 μm controlled under microscope. Prior to its use, the working electrode was polished 5 min with 0.05 μm alumina on polishing strips (Orion, Spain). Platinum wires, inserted into the individual reservoirs served as contacts to the high-voltage power supply. The home-made high-voltage power supply had an adjustable voltage output between 0 and +4000 V. Amperometric detection was performed with an EC analyzer CHI630B (CH Instruments, Austin, TX, USA)

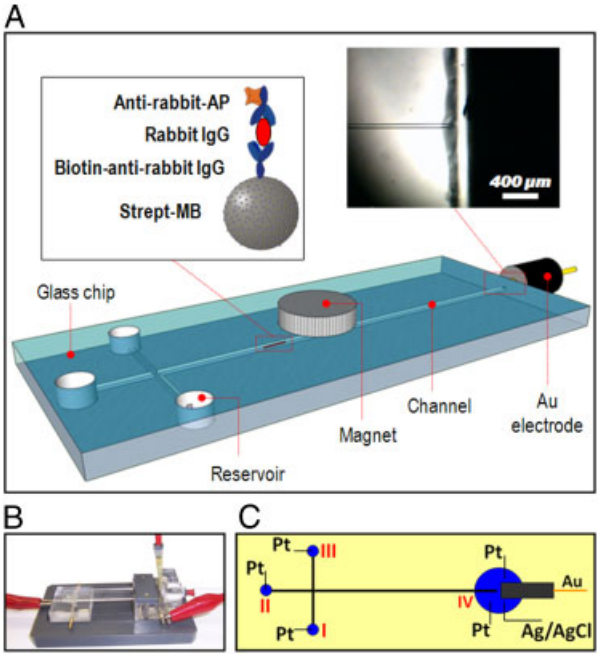

Figure 1. (A) Schematic representation of the glass microchip device components. (B) Photograph of the device setup. (C) Schematic representation of the chip design with the end-channel EC cell.

connected to a personal computer. The electropherograms were recorded with a time resolution of 0.1 s while applying the detection potential. Substrate injections were performed after stabilization of baseline. Spectrophotometric measurements were performed using a Gemini SpectraMax M2^e Multi-Mode Microplate Reader (Molecular Devices, CA, USA).

2.3 Preparation of AP-coated MBs

Biotinylated AP was linked to streptavidin-coated MB of 2.8 and 1 μm of diameter, using a slightly modified procedure recommended by Dynal. Briefly, 100 μg (10 μL from the stock solution) of streptavidin-coated paramagnetic beads was transferred into a 0.5 mL Eppendorf tube. The MBs were washed twice with 150 μL of washing buffer. The MBs were then resuspended in 100 μL of a buffered solution of biotinylated AP at a concentration of 80 μg/mL which is up to fourfold excess with respect to the stated binding capacity of the MBs. This is to ensure maximum loading of AP to the MBs. The resulting MB and AP solution was incubated for 30 min at 25°C with gentle mixing in a TS-100 ThermoShaker. The formed MB–AP complex was then separated from the incubation solution using a magnetic separator DynaMag (Dynal), washed three times with 150 μL of washing buffer, and resuspended in 100 μL of PBS.

2.4 Off-chip preparation of MB immunocomplex

Preparation of the sandwich-type immunocomplex for rabbit IgG detection was carried out as follows: 150 μg (15 μL from the stock solution) of streptavidin-coated MBs (diameter, 1 μm) were transferred into a 0.5-mL Eppendorf tube. After washing twice with washing buffer, the MBs were resuspended in 100 μL of 80 μg/mL buffered solution of biotinylated anti-rabbit IgG and incubated for 30 min at 25°C with gentle mixing. The formed MB/anti-rabbit IgG complex was then separated from the incubation solution and washed three times with 150 μL of washing buffer. The preparation process was followed by the resuspension of the MB/anti-rabbit IgG in 150 μL of blocking buffer (PBS-BSA, 5%) to block any remaining active surface of MBs, and the mixture was incubated at 25°C for 20 min. After the washing steps with washing buffer, the MB/anti-human IgG was incubated at 25°C for 30 min with 150 μL of rabbit IgG antigen at different concentrations forming, by this way, the immunocomplex MB/anti-rabbit IgG/rabbit IgG. Finally, after the washing steps, the MB/anti-rabbit IgG/rabbit IgG immunocomplexes were resuspended and incubated at 25°C for 30 min with 150 μL of anti-rabbit-AP (80 μg/mL). After the washing procedure with washing buffer, the immunocomplex MB/anti-rabbit IgG/rabbit IgG/anti-rabbit-AP was resuspended in 100 μL PBS buffer solution.

2.5 Spectrophotometric analysis

The MB sandwich immunocomplex prepared was analyzed spectrophotometrically in order to quantify the rabbit IgG model antigen. The analysis procedure is shown in Supporting Information Fig. S4. The MB sandwich-type immunocomplex purified magnetically as described previously was resuspended in the Eppendorf tube with 150 μL of a ready-to-use p-NPP solution. After the optimized time of 5 min (data not shown), the specific reaction between AP and p-NPP produced a yellow-colored solution whose intensity is proportional to the concentration of rabbit IgG used during the immunoassay procedure. The reaction was arrested by adding 50 μL of 3 M HCl to ensure the same reaction time in all the tubes. Using an external magnet, the MBs were then separated from the solution, which was subsequently transferred to a 96-well plastic plate for the spectrophotometric analysis performed by measuring the absorbance at 405 nm.

2.6 EC analysis

Schematic representation of the EC detection principle is shown in Fig. 2. Phenyl phosphate is a specific substrate for the enzyme AP which produces phenol by hydrolysis reaction. While phenyl phosphate is electro inactive, phenol can be oxidized electrochemically. The concentration of phenol produced by the enzyme is directly proportional to the amount of enzyme itself which is then directly related to the amount of antigen in exam. The EC detector set at the channel outlet can monitor the amount of phenol produced by the enzyme linked to the magnetic particles by the sandwich immunoassay. Antigen protein under investigation related to the amount of signaling enzyme can therefore be quantified.

2.7 Magnetic and electrokinetic manipulations

The microchannels of the glass chip were treated before use by rinsing with 0.1 M NaOH for 10 min and deionized water for another 10 min. The introduction of MBs inside the longitudinal channel is performed by injecting a small volume of suspended MBs by micropipette with the optimized number, through the buffer reservoir (II in Fig. 1C) and then by means of a permanent magnet, the particles are quantitatively dragged inside the channel until the desired position is reached. In order to achieve reproducible and quantitative loading, it is crucial to have the chip channel perfectly clean and free from any small residual particles or solid impurities which could cause clogging. Once the particles have reached the desired position, they are kept in location with the magnet. At this point, the application of a low-pumping voltage (1000 V) to the buffer reservoir and then alternatively to the sample reservoirs (all filled with running buffer), while leaving the detection reservoir grounded, helps in pushing any particles eventually lost during the dragging operation. In this way, the buffer and sample reservoirs/channels are cleaned and also all the particles introduced are settled in the reaction zone, controlled by the magnet. The two sample reservoirs (I and III) are then filled with phenyl phosphate and phenol, respectively, while keeping PBS running buffer in reservoir II. At this point, in order to stabilize the EC detecting signal, the running buffer is pumped along the separation channel with a voltage of 1500 V, while simultaneously recording the EC signal at fixed potential. When the current reaches a steady state, the device is ready for measurements. Photographs of the loading operations are shown in Supporting Information Fig. S2.

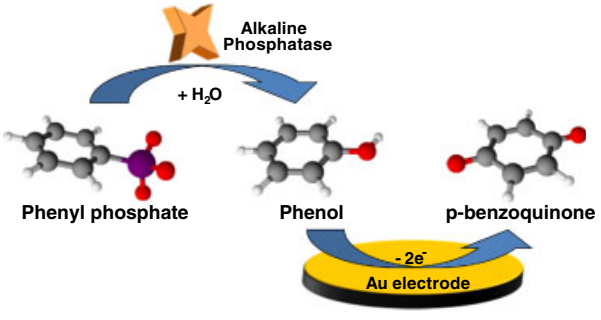

Figure 2. Schematic illustration of the EC detection principle. Hydrolysis of phenyl phosphate by AP generates phenol which is then electrochemically detected.

2.8 Safety considerations

The high-voltage supply should be handled with extreme care in order to avoid electric shock.

3 Results and discussion

3.1 Chip operation optimizations

As shown in Fig. 2, the device is based on the principle of detecting phenol produced by the hydrolysis of phenyl phosphate by AP enzyme linked to the MBs. In order to achieve the best conditions for the EC detection of phenol, several parameters have been optimized. This study has been carried out (see also Fig. 1), introducing a 200 μM buffered solution of phenol inside the sample reservoir I. Both reservoirs II and III were filled with running PBS buffer (pH 8.0).

Using this setup first, a hydrodynamic study has been carried out in order to select the best detecting potential. The graph (Fig. 3A) shows the signal recorded versus potential applied, fixing injection time (10 s), injection voltage (1500 V), and pumping voltage (1500 V). As shown in the figure, by increasing the detection potential from 0.6 to 1.2 V (versus Ag/AgCl), the EC phenol oxidation signal was

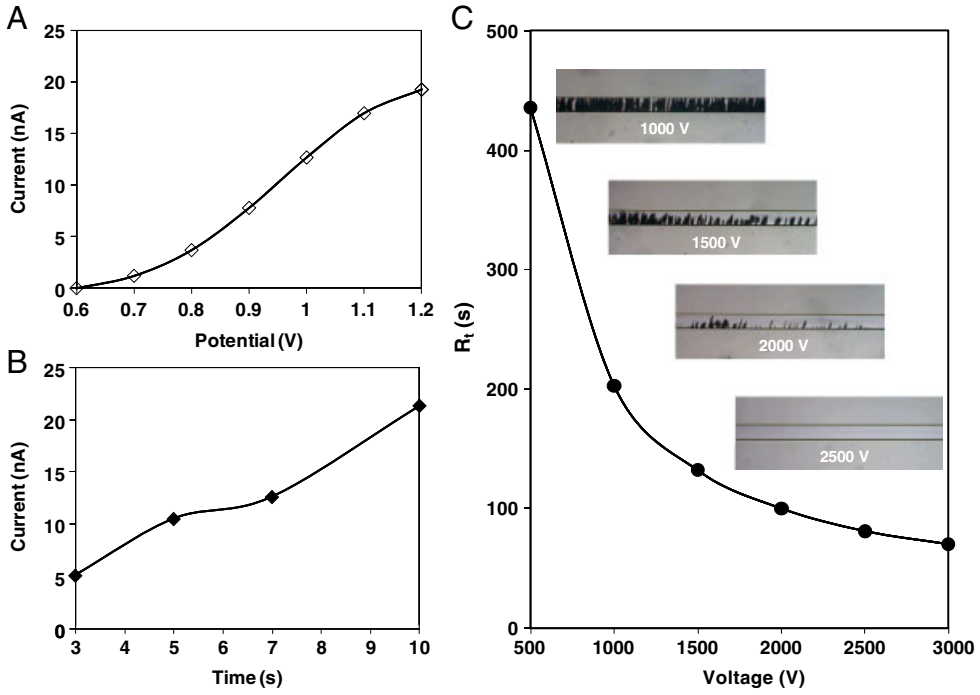

Figure 3. (A) Hydrodynamic study for the detection potential optimization. (B) Optimization of injection time. (C) Optimization of pumping voltage with retention times measured at different pumping voltages with photographs of the channel section with retained MBs. General conditions: Phenol concentration, 200 μM; electro-osmotic flow voltage, 1.5 kV; injection voltage, 1.5 kV; injection time, 10 s; detection potential, 1.1 V; detection potential, 1.1 V; running buffer, 10 mM phosphate at pH 8.

increased. A detecting potential of 1.1 V was chosen as optimal, also taking into account the background signal (results not shown) which resulted significantly high at a potential of 1.2 V.

Fixing the detection potential at 1.1 V and pumping voltage at 1500 V, injection time was investigated. Figure 3B shows the signal recorded for phenol detection, varying the injection time from 3 to 10 s. Increasing the injection time increases the amount of phenol introduced in the channel and therefore as expected higher signals were recorded with the highest obtained using 10 s injection. For injection times longer than 10 s, the broadening effect of the peaks (results not shown) started to be significant and therefore no optimal for the application.

Pumping voltage for this type of device is a very important parameter because not only regulates the flow at which substrate passes through the retained magnetic particles (MB bed) and the flow at which the product reaches the detector, but also has a profound effect on the stability of the MB bed. Separation voltages that are too low could generate broad peaks and with long retention times, whereas separation voltages that are too high could generate a flow, able to remove and wash away all the particles trapped by the magnet. Figure 3C shows the results of two separate experiments. First of all, the effect of the applied pumping voltage on the time necessary to phenol to reach the detector at the channel outlet was evaluated. For this experiment, as expected, increasing the pumping voltage reduced phenol retention time with a big difference between 500 and 1500 V, whereas from 1500 to 3000 V the retention time reduction is less significant. A separate experiment was also carried out in order to evaluate the effect of the pumping voltage on the stability of the MB bed. To visualize this effect, photographs of an MB bed have been taken after the application of pumping voltages between 1000 and 2500 V (see photographs in Fig. 3C). It is clear that by applying voltages lower than 1000 V, all the particles remain trapped by the magnet and fill the channel entirely. Applying a pumping voltage of 1500 V, the particles still remain trapped but forced by the flow tend to fill only the portion of the channel volume closest to the magnet generating a longer but equally stable MB bed. Finally, separation voltages higher than 1500 V start to generate flows too high for the magnetic field and an increased number of particles is washed away. It can be seen that only few particles remain trapped by the magnet at applied pumping voltage of 2000 V, whereas no particle is present at 2500 V. A good combination between reasonable analysis times with high particle retention resulted to be with the applied pumping voltage of 1500 V which was selected as the optimal.

3.2 Influence of paramagnetic bead parameters

In order to evaluate the applicability of the method, preliminary tests have been carried out using AP-modified MBs. One of the advantages of using magnetic particles as in-chip solid support for immunoreactions is that by the manipulation of magnetic field together with the application of the electro-osmotic flow, the bioreaction surface can be easily renewed. Multianalysis procedures could be performed on the same device by following these steps: (i) particle loading, (ii) immunoreactions on trapped particles, (3) detection of the enzyme product, and (iv) washing/releasing of particles. Supporting Information Fig. S3 shows this on-chip renewal of the bioreaction surface in a simple

way. The chip device was prepared introducing in reservoirs I and III, phenol (200 μM), and phenyl phosphate (500 μM), respectively. Reservoir II was filled as usually with running PBS buffer (10 mM). Using this setup and applying the optimized condition (1500 V, pumping voltage; 10 s, injection time; and 1.1 V detection voltage), EC signal was recorded injecting either phenol or phenyl phosphate. As shown in Supporting Information Fig. S3A, no EC signal was recorded when phenyl phosphate was injected. This confirmed that phenyl phosphate is electroinactive. After this experiment, AP-MBs (1 μm diameter, 10^5 particles) were loaded and positioned 1 cm further than the chip channel cross. Recording again the signals generated by the injection of phenol and phenyl phosphate resulted that in this case a signal also appeared after the injection of phenyl phosphate (Supporting Information Fig. S3B). This demonstrates that the presence of AP in the channel produced phenol by passing phenyl phosphate. It can also be seen in the electropherogram S3B that the signal generated by phenyl phosphate converted to phenol by AP has a slightly longer retention time. This could be due to the fact that before the conversion into phenol in the particle ''zone,'' phenyl phosphate migrates more slowly than phenol having a lower electrophoretic mobility, and also to the extra time needed by the enzyme to convert phenyl phosphate into phenol. Also, it can be noted that the signal generated by phenol has a slightly longer retention time compared with that of the first experiment. This is because the presence of magnetic particles inside the channel, as physical hindrance, slightly reduces the electro-osmotic flow. The last experiment consisted in recording again both signals but only after washing away the magnetic particles. As shown in Supporting Information Fig. S3C, magnetic and electrophoretic manipulations allowed a perfect cleaning of the channel since no signal was recorded when phenyl phosphate was injected. The device is therefore ready to be used with renewed bioreaction surface. In all the described experiments, phenol was always injected to check the functionality of the device and to have a reference signal.

Once demonstrated that the device is able to detect the enzymatic product of the reaction occurring inside the microchannel, the size and number of loading particles was optimized. Figure 4 shows the signal recorded when different numbers of particles of 1 and 2.8 μm diameter size were loaded (for particles of 1 μm diameter, see also Supporting Information Video 1). It has to be pointed out that according to the manufacturer' specifications, the binding capacity of streptavidin magnetic particles for biotinylated protein is slightly higher for the particle of 1 μm diameter despite the lower geometrical surface. Approximatively, 6×10^5 and 8×10^5 biotinylated AP can be bond to one streptavidin-MB of 2.8 and 1.0 μm, respectively (www.invitrogen.com). This must be due to a different distribution or density of streptavidin molecules linked to the particles. Keeping this in mind, it is clear from the graph shown in Fig. 4 that for a small number of particles loaded (10^2–10^4), the signal generated resulted similar for both types of particles increasing proportionally with the number of particles. From 10^4 to 10^7 particles of 2.8 μm size, the signal recorded increased less consistently reaching satura-

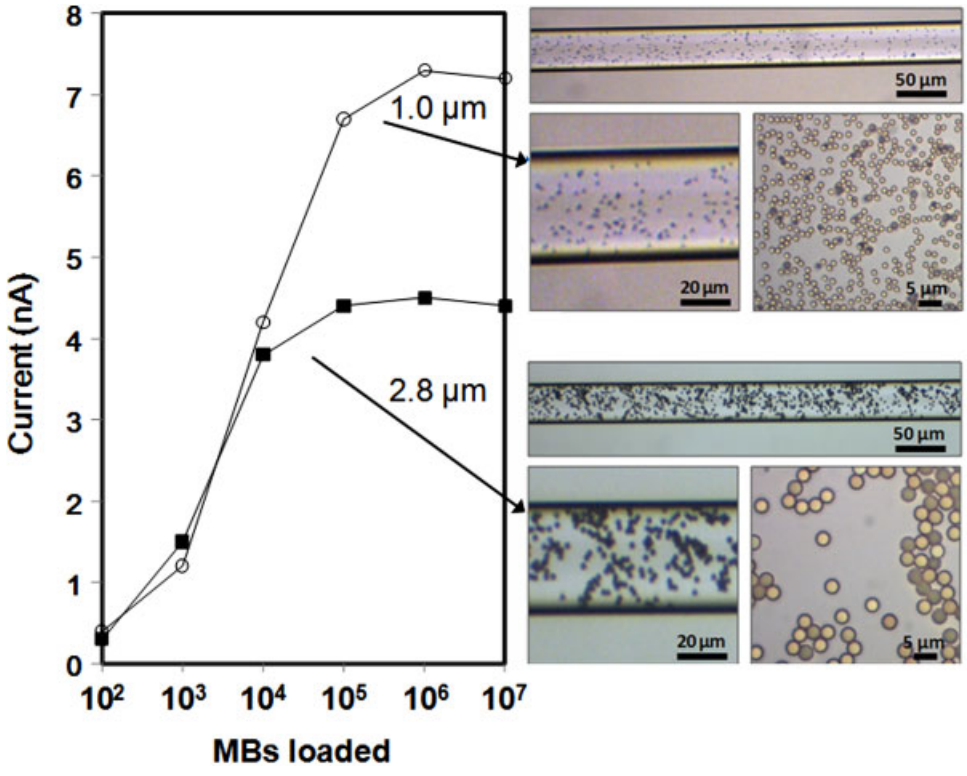

Figure 4. MB dimension study. EC phenol signals generated by MB–AP of 1 and 2.8 μm diameter, loaded, and retained inside the channel by the magnet. Photographs of the beads inside the channel are also shown at different magnifications. General conditions: phenyl phosphate concentration, 500 μM; electro-osmotic flow voltage, 1.5 kV; injection voltage, 1.5 kV; injection time, 10 s; detection potential, 1.1 V; and running buffer, 10 mM phosphate at pH 8.

tion using 10^5 particles. For the same range, using particles of 1.0 μm diameter, the signal increased significantly reaching saturation only for 10^6 particles. This is because the section/volume of channel that can be occupied by MBs being retained steadily by a 3 mm size permanent magnet is filled approximatively by 10^5 and 10^6 particles of 2.8 and 1.0 μm, respectively. In other words, the particles in excess from the values where saturation is reached start to be located at a distance from the magnet too long to be hold at the optimized pumping voltage (1500 V). (see also Supporting Information Video 2). Offering larger active surface and therefore more active enzyme at the given channel volume, the particles of 1.0 μm size generated higher signals and were therefore selected to carry out the rabbit IgG immunoassay. Pictures of the two types of particles inside the channel at different magnifications are also shown in Fig. 4. A number of particles of 10^5 were selected as the optimal in order to be sure that all the particles introduced are trapped effectively by the magnet increasing, in this way, reproducibility of the loading operation.

3.3 Spectrophotometric and EC detection for rabbit IgG immunoassay

Analytical utility of the microchip device loaded with paramagnetic bead was demonstrated on the detection of rabbit IgG model antigen. Off-channel preparation of sandwich-type immunocomplex on paramagnetic beads of 1 μm size is explained in detail in Section 2. Two sets of MB–immunocomplexes have been prepared in parallel using standard rabbit IgG solutions at the concentration between 0.0032 and 2 μg/mL. One set of MB–immunocomplexes was used to perform the spectrophotometric analysis and the other set was used for the on-chip EC analysis. With regard to the spectrophotometric detection, after the final washing step, MB–immunocomplexes were resuspended in 150 μL of ready-to-use p-NPP substrate solution, and incubated at room temperature until the color was developed. Figure 5A shows the absorbance measured after stopping the reaction with NaOH 2 M and transferring the solution (without the MB–immunocomplexes) to a 96-well plastic plate. The MB–immunocomplexes to be used for the EC detection were resuspended in PBS running buffer (10 mM, pH 8.0). The optimized number of MBs (10^5) was then loaded inside the microchip, following the procedure described in Section 2. Phenyl phosphate, 0.5 mM, introduced in reservoir I (Fig. 1C) was used as a substrate to generate phenol. Figure 5B shows the EC signals recorded with MB–immunocomplexes prepared with different rabbit IgG concentrations. It appears clear that the EC detection performed using the microchip device resulted comparable to the spectrophotometric detection despite the fact that with the microchip device an extremely lower number of particles were used and also with a shorter response time. Inset in Fig. 5B shows typical electropherograms recorded using different concentrations of rabbit IgG.

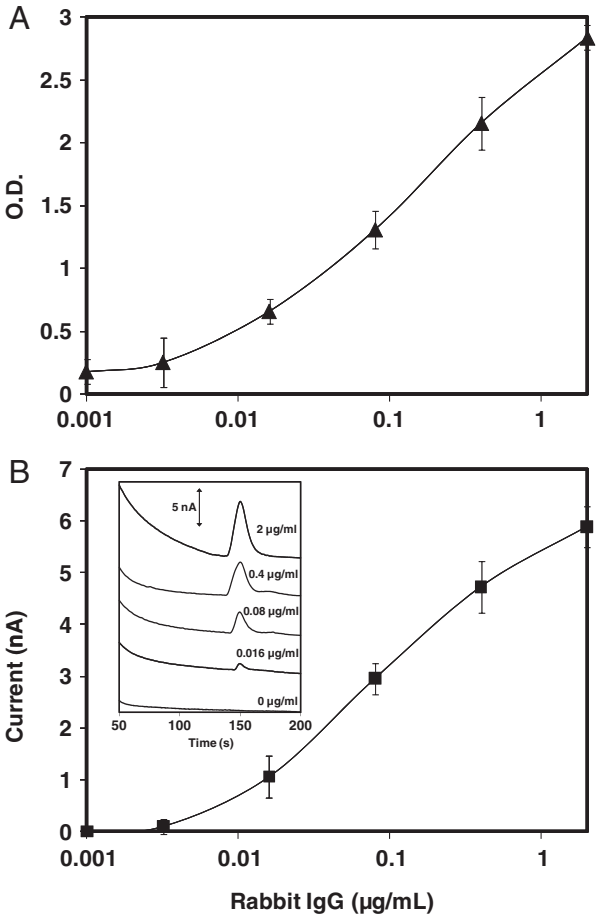

Figure 5. Off-chip spectrophotometric (A) and on-chip EC (B) detection of rabbit IgG. Inset (B) electropherograms recorded using different rabbit IgG standard solutions in the sandwich-type immunoassay on MBs. General conditions for the EC detection: MBs loaded, 10^5; phenyl phosphate concentration, 500 μM; electro-osmotic flow voltage, 1.5 kV; injection voltage, 1.5 kV; injection time, 10 s; detection potential, 1.1 V; and running buffer, 10 mM phosphate at pH 8.

As a measure of the reproducibility in the preparation of the enzymatic reactor, the EC signals generated by five different MB–immunocomplexes prepared with the fixed antigen concentration of 0.08 μg/mL have been considered. The optimized amount of particles (10^5) from each of the five MB–immunocomplexes have been loaded inside the channel and the EC signals generated by passing phenyl phosphate resulted to be with a RSD lower than 10%. It should be noted that this value not only takes into account the reproducibility of the MB–immunocomplex preparation, but also includes the reproducibility of the MB loading operation inside the channel.

Having demonstrated the applicability of the device for analytical purposes, further investigations should be focused mainly in improving the automation of the operations and in the integration of the entire immunoassay protocol. With

regard to the first issue, investigations are currently undergoing with the aim to optimize a loading procedure by means of the electrokinetic pumping, using one of the reservoirs as MB source. Designing a multireservoir chip, it is possible to perform on-chip, the complete immunoassay procedure, from the introduction of the particle as solid-specific support, incubation with sample/detecting antibody, washing steps, to the final detection. Considering the extremely reduced amount of reagent used, the large surface-to-volume ratio and the optimal flowing conditions generated by the electrophoresis device, all the specific immunoreactions would occur in much shorter time, reducing in this way the overall analytical procedure time.

4 Concluding remarks

The combination of paramagnetic particles with microchip electrophoresis, external magnetic field manipulations, and coupled to EC detection resulted extremely promising with regard to the application to protein analysis. The use of an external permanent magnet, easy to be manipulated, allowed a reproducible loading and efficient control of magnetic particles used as solid support for immunoassay. The experiments performed demonstrated the applicability of the device for multianalysis setup since electrophoretic and magnetic manipulations allow the renewing of the immuno-specific support. Very sensitive amperometric detection allowed quantification of the antigen rabbit IgG comparably with the spectrophotometric method but with a number of particles and therefore immuno reactants consumed, extremely lower. In addition to the lower reagent consumption, inherent miniaturization and versatility represent the main advantages of the developed device which in the future could be used as a universal bioanalytical tool. The total analysis procedure, entirely performed with the microchip device, including all the incubations and washing steps is presently under investigation, and this would certainly give an impressive versatility to this bioanalytical device. It could be successfully adopted not only for protein quantification, but also for DNA analysis and environmental applications.

The authors acknowledge funding from the "Ministerio de Ciencia e Innovación" (Madrid, Spain) for Projects MAT 2008-03079/NAN and CSD2006-00012 "NANOBIOMED" (Consolider-Ingenio 2010).

The authors have declared no conflict of interest.

5 References

[1] Manz, A., Graber, N., Widmer, H. M., *Sens. Actuat. B Chem.* 1990, *1*, 244–248.

[2] Dodge, A., Fluri, K., Verpoorte, E., de Rooij, N. F., *Anal. Chem.* 2001, *73*, 3400–3409.

[3] Yang, T., Jung, S.-Y., Mao, H., Cremer, P. S., *Anal. Chem.* 2001, *73*, 165–169.

[4] Lai, S., Wang, S., Luo, J., Lee, L. J., Yang, S.-T., Madou, M. J., *Anal. Chem.* 2004, *76*, 1832–1837.

[5] Hosokawa, K., Omata, M., Sato, K., Maeda, M., *Lab Chip* 2006, *6*, 236–241.

[6] Kawaguchi, H., *Prog. Polym. Sci.* 2000, *25*, 1171–1210.

[7] Kruis, F. E., Fissan, H., Peled, A., *J. Aerosol. Sci.* 1998, *29*, 511–535.

[8] Sato, K., Tokeshi, M., Odake, T., Kimura, H., Ooi, T., Nakao, M., Kitamori, T., *Anal. Chem.* 2000, *72*, 1144–1147.

[9] Verpoorte, E., *Lab Chip* 2003, *3*, 60N–68N.

[10] Pamme, N., *Lab Chip* 2006, *6*, 24–38.

[11] Gijs, M. A. M., *Microfluid. Nanofluid.* 2004, *1*, 22–40.

[12] Pumera, M., Castañeda, M. T., Pividori, M. I., Eritja, R., Merkoçi, A., Alegret, S., *Langmuir* 2005, *21*, 9625–9629.

[13] Ambrosi, A., Castañeda, M. T., Killard, A. J., Smyth, M. R., Alegret, S., Merkoçi, A., *Anal. Chem.* 2007, *79*, 5232–5240.

[14] de la Escosura-Muñiz, A., Maltez-da Costa, M., Merkoçi, A., *Biosens. Bioelectron.* 2009, *24*, 2475–2482.

[15] Liu, G. D., Wang, J., Kim, J., Jan, M. R., Collins, G. E., *Anal. Chem.* 2004, *76*, 7126–7130.

[16] Wellman, A. D., Sepaniak, M. J., *Anal. Chem.* 2006, *78*, 4450–4456.

[17] Fan, A. P., Lau, C. W., Lu, J. Z., *Anal. Chem.* 2005, *77*, 3238–3242.

[18] Zacco, E., Pividori, M. I., Alegret, S., Galve, R., Marco, M. P., *Anal. Chem.* 2006, *78*, 1780–1788.

[19] Jiang, G. F., Harrison, D. J., *Analyst* 2000, *125*, 2176–2179.

[20] Kwakye, S., Baeumner, A., *Anal. Bioanal. Chem.* 2003, *376*, 1062–1068.

[21] Huang, C.-J., Lin, H.-I., Shiesh, S.-C., Lee, G.-W., *Biosens. Bioelectron.* 2010, *25*, 1761–1766.

[22] Vojtíšek, M., Iles, A., Pamme, N., *Biosens. Bioelectron.* 2010, *25*, 2172–2176.

[23] Choi, J. W., Oh, K. W., Thomas, J. H., Heineman, W. R., Halsall, H. B., Nevin, J. H., Helmicki, A. J., Henderson, H. T., Ahn, C. H., *Lab Chip* 2002, *2*, 27–30.

[24] Lacharme, F., Vandevyver, C., Gijs, M. A. M., *Anal. Chem.* 2008, *80*, 2905–2910.

[25] Bronzeau, S., Pamme, N., *Anal. Chim. Acta* 2008, *609*, 105–112.

[26] Liu, Y.-J., Guo, S.-S., Zhang, Z.-L., Huang, W.-H., Baigl, D., Chen, Y., Pang, D.-W., *J. Appl. Phys.* 2007, *102*, 084911–084916.

[27] Leea, Y.-F., Lienb, K.-Y., Lei, H.-Y., Leea, G.-B., *Biosens. Bioelectron.* 2009, *25*, 745–752.

[28] Furdui, V. I., Harrison, D. J., *Lab Chip* 2004, *4*, 614–618.

[29] Sivagnanam, V., Song, B., Vandevyver, C., Bünzli, J.-C. G., Gijs, M. A. M., *Langmuir* 2010, *26*, 6091–6096.

[30] Llopis, X., Pumera, M., Alegret, S., Merkoçi, A., *Lab Chip* 2009, *9*, 213–218.

[31] Martinez, N. A., Schneider, R. J., Messina, G. A., Raba, J., *Biosens. Bioelectron.* 2010, *25*, 1376–1381.

[32] Hervás, M., López, M. A., Escarpa, A., *Analyst* 2009, *134*, 2405–2411.

[33] Harrison, D. J., Fluri, K., Seiler, K., Fan, Z. H., Effenhauser, C. S., Manz, A., *Science* 1993, *261*, 895–897.

[34] Effenhauser, C. S., Manz, A., Widmer, H. M., *Anal. Chem.* 1993, *65*, 2637–2642.

[35] Manz, A., Effenhauser, C. S., Burggraf, N., Harrison, D. J., Seiler, K., Fluri, K., *J. Micromech. Microeng.* 1994, *4*, 257–265.

[36] Jakeway, S. C., de Mello, A. J., Russell, E. L., *Fresenius J. Anal. Chem.* 2000, *366*, 525–539.

[37] Lacher, N. A., Lunte, S. M., Martin, R. S., *Anal. Chem.* 2004, *76*, 2482–2491.

[38] Tanyanyiwa, J., Leuthardt, S., Hauser, P. C., *Electrophoresis* 2002, *23*, 3659–3666.

[39] Wang, J., Pumera, M., *Anal. Chem.* 2002, *74*, 5919–5923.

[40] Vandaveer, W. R., Pasas-Farmer, S. A., Fischer, D. J., Frankenfeld, C. N., Lunte, S. M., *Electrophoresis* 2004, *25*, 3528–3549.

[41] Wang, J., Escarpa, A., Pumera, M., Feldman, J., *J. Chromatogr. A* 2002, *952*, 249–254.

Superhydrophobic Alkanethiol-Coated Microsubmarines for Effective Removal of Oil

Maria Guix,[†,‡,⊥] Jahir Orozco,[†,⊥] Miguel García,[†,§,⊥] Wei Gao,[†] Sirilak Sattayasamitsathit,[†] Arben Merkoçi,[‡] Alberto Escarpa,[§] and Joseph Wang[†,*]

[†]Department of Nanoengineering, University of California—San Diego, La Jolla, California 92093, United States , [‡]ICREA & Catalan Institute of Nanotechnology, Campus University Autónoma of Barcelona, E-08193 Bellaterra, Barcelona, Spain, and [§]Department of Analytical Chemistry and Chemical Engineering, University of Alcalá, E-28871 Alcalá de Henares, Madrid, Spain. [⊥]These authors have contributed equally to this work.

ABSTRACT

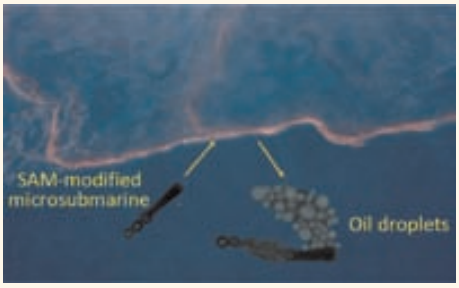

We demonstrate the use of artificial nanomachines for effective interaction, capture, transport, and removal of oil droplets. The simple nanomachine-enabled oil collection method is based on modifying microtube engines with a superhydrophobic layer able to adsorb oil by means of its strong adhesion to a long chain of self-assembled monolayers (SAMs) of alkanethiols created on the rough gold outer surface of the device. The resultant SAM-coated Au/Ni/PEDOT/Pt microsubmarine displays continuous interaction with large oil droplets and is capable of loading and transporting multiple small oil droplets. The influence of the alkanethiol chain length, polarity, and head functional group and hence of the surface hydrophobicity upon the oil—nanomotor interaction and the propulsion is examined. No such oil—motor interactions were observed in control experiments involving both unmodified microengines and microengines coated with SAM layers containing a polar terminal group. These results demonstrate that such SAM-Au/Ni/PEDOT/Pt micromachines can be useful for a facile, rapid, and efficient collection of oils in water samples, which can be potentially exploited for other water—oil separation systems. The integration of oil-sorption properties into self-propelled microengines holds great promise for the remediation of oil-contaminated water samples and for the isolation of other hydrophobic targets, such as drugs.

KEYWORDS: superhydrophobic · microsubmarine · nanomachine · self-assembled monolayer · environmental remediation · oil collection · liquid—liquid interface · self-propulsion

Self-propelled catalytic nanomotors, capable of converting energy into movement and forces,[1−6] have shown considerable promise for diverse practical applications. Particularly attractive are tubular microengines owing to their efficient bubble-induced propulsion in complex biological media and high ionic-strength environments.[4,7,8] Such chemically powered nanomotors have been commonly prepared by top-down photolithography, e-beam evaporation, and stress-assisted rolling of functional nanomembranes into conical microtubes.[5] Alternatively, a simplified membrane-template electrodeposition protocol can be used for mass production of high-performance catalytic microtubular engines.[9,10] The resulting microengines are smaller in size (~8 μm long), require low fuel concentrations (down to 0.2% H_2O_2), and move at an ultrafast speed (over 1400 body lengths/s). These template-fabricated microtubes commonly consist of a polymer/Pt bilayer and require additional Ni and Au layers for their magnetic guidance and facile functionalization (*e.g.*, with receptors), respectively. A judicious modification of the outer Au surface by molecular bioreceptors, *e.g.*, DNA probes,[11] aptamers,[12] antibodies,[13] or lectins,[14] has thus been shown useful for diverse target-isolation sensing applications. Considerable efforts have also been devoted toward the use of catalytic nanomotors for targeted drug delivery.[15]

In this paper we demonstrate the first example of using functionalized nanomachines toward environmental remediation of contaminated water. In particular, we illustrate how the deliberate modification of the rough outer surface of microengines with highly hydrophobic long-chain self-assembled alkanethiol monolayers offers considerable promise for the capture, transport, and removal of oil droplets from water samples. Oil is a major source of ocean pollution and groundwater contamination. The presence of oils in wastewaters as a product of various manufacturing processes is common in different industries. Furthermore, episodes of major water pollution, caused by oil spillage, result in the release

* Address correspondence to josephwang@ucsd.edu.

Received for review March 16, 2012 and accepted April 5, 2012.

Published online April 05, 2012
10.1021/nn301175b

of millions of tons each year. For example, the 1989 *Exxon Valdez* and 2010 *Deepwater Horizon* incidents spilled millons of gallons of crude oil.[16,17] The removal of oils and organic solvents from contaminated water is thus of considerable importance for minimizing the environmental impact of these pollutants.

Substantial efforts have thus been devoted to develop effective tools toward the remediation and cleanup of oil spills. Although oils in wastewater plants are mostly removed by a mechanical separation, other methods have been proposed to address related pollution episodes.[18,19] However, most of these methods lack the desired selectivity and efficiency and are not cost-effective or environmentally friendly. Accordingly, the development of new highly effective oil–water separation methods is highly desired.

Different synthetic and natural materials have been proposed as possible sorbents for oil removal. Surfaces with superhydrophobic properties have recently attracted particular interest for oil–water separation owing to their high efficiency and selectivity,[18–22] although their high cost, complex preparation processes, and scalability issues have hindered their practical applications.[16] These hydrophobic surfaces tend to repel water while strongly interact with nonpolar or oily liquids, which firmly adhere to textured interfaces.[21] Both the micronano-hierarchical texture and the chemical composition are essential for promoting the superhydrophobic character necessary for effective oil removal. The surface polarity and roughness are thus expected to influence the extent of the oil–surface interaction.[23,24] Self-assembled monolayers (SAMs), formed by the spontaneous and strong chemisorption of alkanethiols at gold or silver surfaces, have been particularly useful for transforming these surfaces into superhydrophobic interfaces.[24] Guo *et al.*[25] reported that ZnO hydrophilic surfaces become superhydrophobic after exposure to an octadecanethiol solution. Tailoring the length of the alkanethiol chain has allowed the control of the surface polarity and hence tuning the partition of hydrophobic drugs.[26] The choice of the ending functional group is also vital for tailoring the polarity of the SAMs. For example, water contact angle studies reveal that methyl-terminated SAMs lead to hydrophobic surfaces, while hydroxyl-terminated ones provide wettable surfaces.[27] However, there are no reports of integrating these oil-sorption properties into self-propelled microengines and using such superhydrophobic nanomotors to facilitate the capture, transport, and separation of oil droplets. Autonomously moving synthetic nanomotors have recently been employed for the pick-up and transport of diverse payloads, ranging from cancer cells to drug-loaded polymeric spheres,[12,14] but not in connection to the isolation of oily contaminants.

The method herein presented is based on the creation of a SAM-modified microtubular engine able to strongly interact with oily liquids *via* adhesion and permeation onto its long alkanethiol coating. As illustrated in Figure 1, the new catalytic microsubmarine is template-prepared by electroplating poly(3,4-ethylenedioxythiophene) (PEDOT)/Pt bilayer followed by e-beam deposition of Ni/Au and subsequent functionalization with the SAM. In particular, dodecanethiol-coated Au/Ni/PEDOT/Pt microsubmarines are shown in the following sections to offer an effective capture and transport of oil droplets from aqueous media. The influence of the alkanethiol chain length upon the oil–nanomotor interaction and the collection efficiency has been examined using SAMs of different chain lengths, *i.e.*, hexanethiol (C6), dodecanethiol (C12), and octadecanethiol (C18). The optimal C12 superhydrophobic SAM-coated microsubmarine has shown a strong prolonged interaction with large oil droplets (attached to the glass-slide surface) along with the effective pickup and transport of multiple small oil droplets present in an oil-contaminated water sample. Unmodified microengines did not show such affinity to oil droplets. These results demonstrate that SAM-functionalized microsubmarines can be useful for facile, rapid, and highly efficient collection of oils in water samples. This high oil-adsorption ability indicates considerable potential for environmental remediation of oil-contaminated water samples and other contaminated water systems.

RESULTS

The fabrication of the oil-sorption hydrophobic microsubmarines, depicted in Figure 1, involves a template-based electrodeposition of a PEDOT/Pt bilayer microtube and e-beam vapor deposition of the Ni and Au outer layers, essential for the magnetic navigation control and surface functionalization, respectively. As illustrated in Figure 1A(d), such functionalization involves the formation of a superhydrophobic layer by self-assembly of long alkanethiol chains on the rough outer gold surface. A SEM image of the unmodified microengine (Figure 1B) indicates a rough surface, characteristic of nitrate-doped PEDOT films.[10] The template fabrication process results in 8 μm long microtubes that are substantially smaller than common rolled-up tubular microengines.[28] The relatively similar dimensions of microsubmarine and oil droplets (which range from ~1 to ~100 μm, depending on the emulsion composition) permit convenient real-time optical visualization of the oil–microengine interaction. Similar to recently developed PANI/Pt microengines,[9] the new template-prepared PEDOT/Pt microtubes were propelled efficiently in different media *via* the expulsion of oxygen bubbles generated from the catalytic oxidation of hydrogen peroxide fuel at their inner Pt layer.[10] Several factors, such as additional Ni and Au layers, influence the microengine speed.

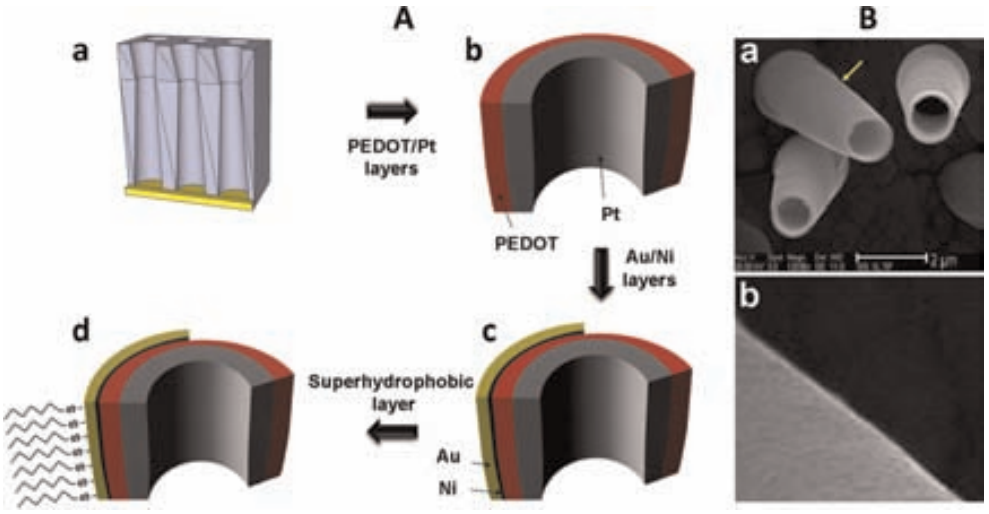

Figure 1. Fabrication and modification of the SAM-Au/Ni/PEDOT/Pt micromotors for environmental remediation. (A) A Cyclopore polycarbonate membrane is used as a template (a), PEDOT and Pt layers are electroplated into the template (b), Au and Ni layers are sputtered by e-beam (c), and a superhydrophobic layer is formed on the microsubmarine surface by incubation in a 0.5 mM *n*-dodecanethiol ethanolic solution (d). (B) SEM image of the resulting PEDOT/Pt microsubmarine (a) with a zoom-in of the zone highlighted with a yellow arrow (b).

TABLE 1. Average Speed of the Microsubmarine upon Each Step Involved in the Fabrication Process and Pick-up of Oil Droplets

microsubmarine step	speed, μm/s
PEDOT/Pt	420
Au/Ni/PEDOT/Pt	200
SAM/Au/Ni/PEDOT/Pt	105
SAM/Au/Ni/PEDOT/Pt/few (1—5) droplets	20—50
SAM/Au/Ni/PEDOT/Pt/numerous droplets	10—20

For example, and as expected for polymer/Pt microengines,[14] the fast speed of the PEDOT/Pt microengines (~420 μm/s average) is reduced by up to 50% after the e-beam deposition of the outer Ni/Au layers.

The resulting Au/Ni/PEDOT/Pt microsubmarines were then immersed in a 0.5 mM dodecanethiol ethanolic solution for 30 min to form the hydrophobic monolayers on the outer gold surface, as illustrated in Figure 1D (see Methods Section in the Supporting Information for additional details). Such surface modification of the Au/Ni/PEDOT/Pt microsubmarine resulted in an additional ~50% speed reduction, reflecting the partial blocking of the inner Pt catalytic layer.[29] However, the reduced speed is sufficient for transporting large cargoes in a manner analogous to our previously reported Au/Ni/PANI/Pt microengines.[14] Table 1 summarizes the changes in the microsubmarines' speed due to each different step involved in the fabrication process.

Figure 2A and Supporting Video S1A (right side) show the Au/Ni/PEDOT/Pt micromotor approaching, contacting, and spinning around a stained olive oil drop firmly attached to a glass slide (see additional details in the Supporting Information). The strong interaction between the SAM-modified microsubmarine and an oil

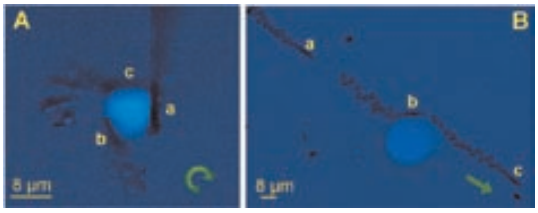

Figure 2. SAM-modified (A) and unmodified (B) microsubmarines in the presence of a stained olive oil droplet (attached to a glass slide). Images, taken from video 1, show (in a single overlaid image) the following sequential steps: approaching, contacting, and spinning around (A, a—c) the droplet and approaching, contacting, and leaving (B, a—c) the oil droplet, respectively. Fuel conditions (final concentration): 0.4% NaCh and 10% H_2O_2. Arrows indicate the microsubmarine trajectory.

droplet results in a continuous spinning of the modified engine around the droplet with an accelerated speed ranging up to 200 μm/s. It should be pointed out that such continuous high-speed spinning is observed even after a prolonged 20 min period. These data also confirm that the hydrogen peroxide fuel and the sodium cholate (NaCh) surfactant, essential for the microsubmarine movement, do not compromise its interaction with the oil droplet or the integrity of the SAM. In contrast, no such interaction is observed using an unmodified microsubmarine (Figure 2B and Supporting Video S1 left side). This bare Au/Ni/PEDOT/Pt micromotor moves rapidly, while approaching, contacting, and bypassing the droplet. Supporting Video S1B shows different unmodified microsubmarines contacting, but not interacting, with olive oil droplets of different sizes (from 5 to 25 μm; attached to a glass slide).

Efficient capture and transport of oil droplets has been observed when the modified microsubmarine navigates in contaminated water samples containing

small "free-floating" oil droplets. Figure 3 and Supporting Video S2 illustrate the capture and transport of multiple small olive oil droplets by the SAM-modified microsubmarine. The longer the navigation time, the more oil droplets are collected and confined onto the surface of the self-propelled micromotor. While around 5 droplets (1.7 ± 0.4 μm size) are captured and transported in Figure 3A (and starting Supporting Video S2) after a 12 s navigation, around 40 droplets are attached to the motor surface following 80 s (Figure 3A(d) and ending Supporting Video S2). These observations demonstrate that these SAM-modified microengines provide high towing force for transporting efficiently approximately 10-fold their volume and indicate considerable potential for oil removal applications. As expected from the increased drag force (Stokes's law),[30] the speed of the micromachine decreases upon increasing the cargo size (*i.e.*, number of captured droplets). This is illustrated in Figure 3B, which displays the dependence of the microsubmarine speed on the number of transported oil droplets. The speed rapidly decreases from 26 to 12 μm/s upon increasing the number of droplets from 7 to 30 and then more slowly to 11 μm/s for 43 droplets. As common for nanomotor-based cargo pickup, the optimal motor speed will provide a trade-off between sufficient contact time and large contact rate.[31,32]

Particularly attractive is the ability to tailor the polarity of the microsubmarine surface *via* a judicious choice of the chain length of the *n*-alkanethiol coating and hence their capture and transport properties. Chain length, head groups, preparation time, and other conditions (*e.g.*, temperature) give rise to different SAM packing densities, configurations, and polarity.[33] The influence of the alkanethiol chain length on the oil–nanomotor interaction was thus examined by modifying the microengine with SAMs of different alkanethiol lengths (C6, C12, and C18). A considerable difference in the microsubmarine–oil droplet interaction was observed using C6 and C12 SAM-coated microsubmarines. Notice, for example, the strong microsubmarine–oil interaction of the C12-modified microengine spinning around a large olive oil droplet (Figure 2B and Supporting Video S1A, right part) compared to the weaker interaction experienced by the C6-modified motor, where no spinning around the droplet is observed (Supporting Figure 1A and Supporting Video S3). Similarly, Supporting Information Figure 2 and Video S4 illustrate the higher number of captured oil droplets using the C12 SAM modification (C) compared to the lower number of droplets attached to the C6-modified motor (B) and to the absence of captured droplets using the unmodified microsubmarine (A). These results are consistent with the different surface wettability properties observed in contact angle studies of *n*-alkanethiols of different lengths.[33,34] On the basis of the higher hydrophobic character of long-chain thiols, C18 SAM-coated microsubmarines are

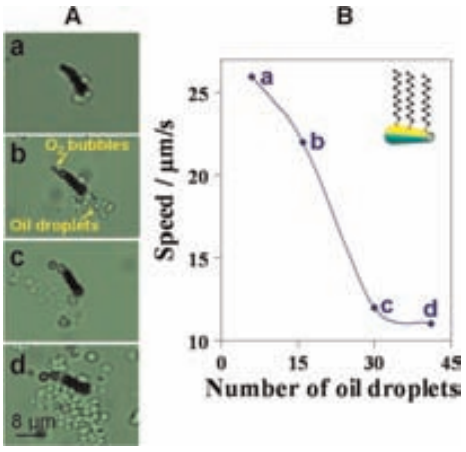

Figure 3. Dodecanethiol (C12-SAM)-modified microsubmarine carrying floating olive oil droplets. (A) Images a–d were taken from video 2 after navigating in the water–oil (10% fuel) solution for 5, 12, 66, and 80 s, respectively (conditions, as in Figure 2). (B) Dependence of the microsubmarine speed upon the number of cargos (olive oil droplets). Inset: Cartoon of the dodecanethiol-modified microsubmarine.

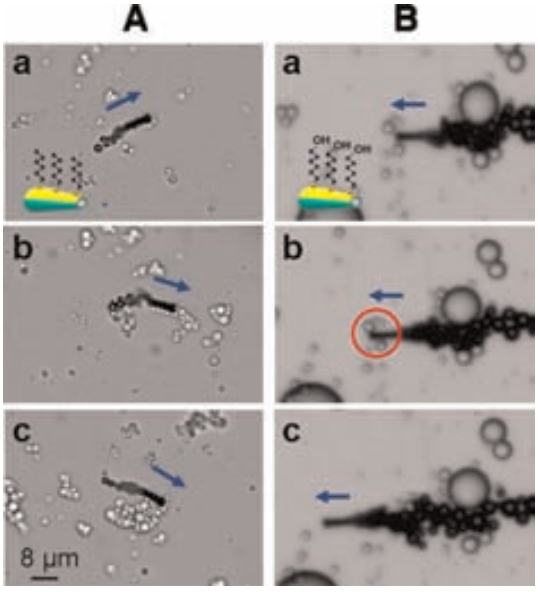

Figure 4. C6-SAM-modified microsubmarines with different head functional groups interacting with small olive oil droplets. Hexanethiol-modified microsubmarines are able to confine a payload of multiple oil droplets (A) (a, b, and c, time-lapse images at different navigation times: 11, 50, and 73 s (for A) and 6.57, 6.66, and 6.71 s (for B)). The corresponding mercaptohexanol-modified counterparts (B) are not able to pick up such droplets (a, b, and c images correspond to approaching, contacting, and leaving the droplets). A(a) and B(a) insets: cartoons of the respective SAM-modified microsubmarines. Arrows indicate the direction of the microsubmarine movement.

expected to offer higher oil-adsorption capabilities. However, such C18 SAM-modified microsubmarines hardly move owing to greater blocking of the inner Pt catalytic layer expected in the presence of longer alkanethiols.[29] Selective modification using alkane isonitriles[35] may be used to minimize the Pt blocking by the alkanethiol SAM, thus retaining microengine speed.

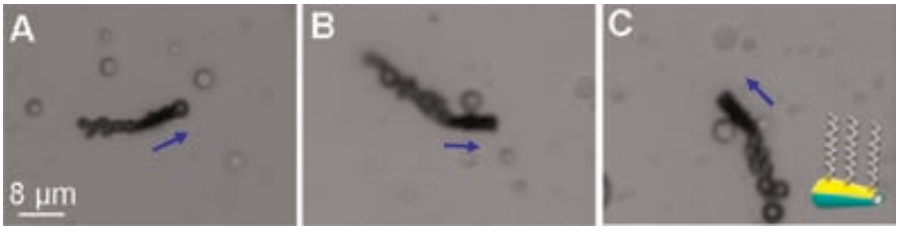

Figure 5. SAM-modified microsubmarine carrying floating droplets of motor oil in a fuel-enhanced oil-contaminated water sample. Images taken from video 6 after 78 s navigation in the fuel-enhanced solution (conditions, as in Figure 2). (A, B, C) Time-lapse images showing the microsubmarine approaching, contacting, and carrying the droplets, respectively. Inset: Cartoon of the dodecanethiol-modified microsubmarine. Arrows indicate the direction of the microsubmarine movement.

The influence of the SAM headgroup and hence surface polarity on the microsubmarines–oil interaction was examined by comparing the behavior of microengines coated with C6 SAM containing methyl and hydroxyl terminal groups using different time scales. Figure 4A(a–c) and Supporting Video S5 illustrate small droplets attached to the hexanethiol-modified microsubmarine upon navigating in the sample. In contrast, and as expected from wettability measurements using hydroxyl-terminated SAM,[27] the mercaptohexanol-modified microsubmarines do not interact with the large or small olive oil droplets upon rapidly contacting them (Supporting Figure 1B and Figure 4B, a–c). It is remarkable that even prolonged navigation of the mercaptohexanol-modified microsubmarines does not lead to any capture of the oil droplets. Clearly, and as expected,[27] the polarity of the head functional group strongly influences the interaction between the modified microsubmarines and the oil droplets and represents another key consideration (besides the chain length) when modifying the outer microengine surface.

Toward a practical utility of this new microsubmarine approach, we examined the ability of the dodecanethiol-modified microsubmarine to collect and transport motor oil in an oil-contaminated water sample. Figure 5 and the corresponding Supporting Video S6 clearly illustrate that the SAM-coated microsubmarines display an "on the fly" capture upon contacting the small droplets of motor oil that are floating in the contaminated water sample. These results demonstrate the potential of the superhydrophobic-modified microsubmarines for facile, rapid, and highly efficient collection of oils in oil-contaminated water samples.

CONCLUSIONS

We have presented the first example of using artificial nano/microscale machines for environmental remediation applications and specifically the tailoring of the surface of such self-propelled machines to interact strongly with oily liquids. The new SAM-Au/Ni/PEDOT/Pt micromotors thus offer a facile, rapid, and highly efficient collection and transport of oil droplets in aqueous environments through the interaction with the hydrophobic alkanethiol monolayer coating. Comparison of different alkanethiol modifiers indicates that the dodecanethiol (C12-SAM)-modified microsubmarines offer the most favorable performance in terms of oil recovery and propulsion. Such high oil-adsorption ability indicates considerable promise for the cleanup of contaminated water samples. The extent of the micromotor–oil interaction and the collection efficiency can be tuned by controlling the surface hydrophobicity through the use of different chain lengths and head functional groups. The new microsubmarine capability was demonstrated either by a strong interaction between the modified nanomotor and large oil droplets (attached to a glass slide) or by the collection and transport of multiple free-floating small olive oil and motor oil droplets present in a contaminated water sample. These micromotor–oil interactions can be exploited in the suitable final disposition of oily wastes (or other organic solvents) by collecting them in a controlled fashion within a certain spatially separated zone. Simultaneous parallel movement of multiple SAM-modified microsubmarines holds promise for improving the efficiency of oil-removal processes. Practical large-scale oil cleaning operations would require the use of motors propelled by their own natural environment[36,37] or driven by an external (magnetic or electrical) control.[38,39] The new superhydrophobic microswimmers offer also considerable promise for the isolation of hydrophobic molecules, *e.g.*, drugs, or for transferring target analytes between liquid–liquid immiscible interfaces, and hence great potential for diverse analytical microsystems. Multifunctional coatings of mixed (or multi) layers, coupling the preferential partition of hydrophobic compounds into the SAMs with additional functions (e.g., biocatalysis), could lead to additional advantages toward on-the-fly "capture and destroy" operations.

EXPERIMENTAL SECTION

Synthesis of Multilayer Microsubmarines. The multilayer microtubes were prepared using a common template-directed electrodeposition protocol.[9,10] A cyclopore polycarbonate membrane, containing 2 μm maximum diameter conical-shaped micropores (Catalog No. 7060-2511; Whatman, Maidstone, U.K.), was employed as the template. A 75 nm gold film was

first sputtered on one side of the porous membrane to serve as working electrode using the Denton Discovery 18. The sputter was performed at room temperature under vacuum of 5×10^{-6} Torr, dc power of 200 W, and Ar flow of 3.1 mT. Rotation speed is 65 μm/s. Sputter time is 90 s. A Pt wire and an Ag/AgCl with 3 M KCl were used as counter and reference electrodes, respectively. The membrane was then assembled in a plating cell with an aluminum foil serving as contact. Poly(3,4-ethylenedioxythiophene) microtubes were prepared by modifying the previously described method.[10] Briefly, PEDOT microtubes were electropolymerized up to 0.1 C at +0.80 V from a plating solution containing 15 mM EDOT monomer, 50 mM SDS, and 7.5 mM KNO_3, all of them prepared from Sigma-Aldrich reagents. The inner Pt tube was deposited galvanostatically at −2 mA for 600 s from a commercial platinum plating solution (Platinum RTP; Technic Inc., Anaheim, CA, USA). The sputtered gold layer was completely removed by mechanical hand polishing with 3−4 μm alumina slurry. Incomplete removal will result in bubbles emerging from the smaller opening of the microengine (yet without compromising its performance). Finally, microengines were collected by centrifugation at 6000 rpm for 3 min and washed repeatedly with methylene chloride, followed by ethanol and ultrapure water (18.2 MΩ cm), three times of each, with a 3 min centrifugation following each wash. The microtube suspension was evaporated onto glass slides before the sequential deposition of 10 nm of Ti (adhesion layer), 15 nm of Ni (magnetic layer), and 15 nm of Au (functionalization layer) over the microtubes by using electron beam deposition. These additional steps provide the necessary magnetic directional control and the appropriate gold surface for the later modification with self-assembled monolayers.

Microsubmarine Modification. The external gold surface of the microsubmarines was modified by immersion in 0.5 mM dodecanethiol in absolute ethanol (from Sigma-Aldrich), after which the resulting monolayer-modified microsubmarines were washed with Milli-Q water and isolated by centrifugation at 6000 rpm during 4 min. All experiments were carried out at room temperature. Study of the chemical structure effect, *e.g.*, length chain and terminal groups, on the speed was performed with different thiols, including hexanethiol, mercaptohexanol, dodecanethiol, and octadecanethiol, all received from Sigma-Aldrich and dissolved in ethanol. Bare microsubmarines without the monolayer were also used as control experiments.

Equipment. Template electrochemical deposition of microtubes was carried out with a CHI 661D potentiostat (CH Instruments, Austin, TX, USA). An inverted optical microscope (Nikon Eclipse Instrument Inc. Ti-S/L100), coupled with a 40× objective, using a Hamamatsu digital camera C11440 and NIS-Elements AR 3.2. software, was used for capturing movies at a frame rate of 20 frames per second. The speed of the microengines was tracked using a NIS-Elments tracking module, and the results were statistically analyzed using Origin software.

Experimental Procedure. In order to self-propel the catalytic microsubmarines around different oil droplets or capture such droplets, an emulsion containing Milli-Q water/oil sample/6% sodium cholate (NaCh) (2:2:1) was first prepared. A known volume of this solution was spread on a glass slide, and an equal volume of a solution containing the microsubmarines and the same volume of hydrogen peroxide was added to get a final concentration of 0.4% NaCh and 10% H_2O_2. Microsubmarines approach the oil droplets either to spin them around for several minutes (up to 20) or to pick up and carry them. Experiments were performed using olive and motor oils dispersed in Milli-Q water. Initial experiments were carried out with Nile-red-stained olive oil for improved visualization under microscopy. However, the dye was not used in most subsequent experiments, as the water−oil interface was sufficiently distinguishable without such staining.

Conflict of Interest: The authors declare no competing financial interest.

Acknowledgment. This work was supported by the National Science Foundation (NSF Award Number CBET 0853375) and NATO Science for Peace and Security Program (SfP 983807). M. Guix acknowledges the support from Spanish MICINN. J. Orozco and M. García are thankful for funding from a Beatriu de Pinós postdoctoral fellowship (Government of Catalonia) and University of Alcalá (Madrid), respectively.

Supporting Information Available: Supporting videos and detailed methods. This material is available free of charge *via* the Internet at http://pubs.acs.org.

REFERENCES AND NOTES

1. Paxton, W. F.; Kistler, K. C.; Olmeda, C. C.; Sen, A., St.; Angelo, S. K.; Cao, Y.; Mallouk, T. E.; Lammert, P. E.; Crespi, V. H. Catalytic Nanomotors: Autonomous Movement of Striped Nanorods. *J. Am. Chem. Soc.* **2004**, *126*, 13424–13431.
2. Ozin, G. A.; Manners, I.; Fournier-Bidoz, S.; Arsenault, A. Dream Nanomachines. *Adv. Mater.* **2005**, *17*, 3011–3018.
3. Fournier-Bidoz, S.; Arsenault, A. C.; Manners, I.; Ozin, G. A. Synthetic Self-Propelled Nanorotors. *Chem. Commun.* **2005**, *41*, 441–443.
4. Wang, J. Can Man-Made Nanomachines Compete with Nature Biomotors?. *ACS Nano* **2009**, *3*, 4–9.
5. Pumera, M. Electrochemically Powered Self-Propelled Electrophoretic Nanosubmarines. *Nanoscale* **2010**, *2*, 1643–1649.
6. Campuzano, S.; Kagan, D.; Orozco, J.; Wang, J. Motion-Driven Sensing and Biosensing Using Electrochemically Propelled Nanomotors. *Analyst* **2011**, *136*, 4621–4630.
7. Mei, Y.; Solovev, A. A.; Sanchez, S.; Schmidt, O. G. Rolled-up Nanotech on Polymers: From Basic Perception to Self-Propelled Catalytic Microengines. *Chem. Soc. Rev.* **2011**, *40*, 2109–2119.
8. Huang, G.; Wang, J.; Mei, Y. Material Considerations and Locomotive Capability in Catalytic Tubular Microengines. *J. Mater. Chem.* **2012**, *22*, 6519–6525.
9. Gao, W.; Sattayasamitsathit, S.; Orozco, J.; Wang, J. Highly Efficient Catalytic Microengines: Template Electro-synthesis of Polyaniline-Platinum Microtubes. *J. Am. Chem. Soc.* **2011**, *133*, 11862–11864.
10. Gao, W.; Sattayasamitsathit, S.; Uygun, A.; Pei, A.; Ponedal, A.; Wang, J. Polymer-Based Tubular Microbots: Role of Composition and Preparation. *Nanoscale* **2012**, *4*, 2447–2453.
11. Kagan, D.; Campuzano, S.; Balasubramanian, S; Kuralay, F; Flechsig, G.; Wang, J. Functionalized Micromachines for Selective and Rapid Isolation of Nucleic Acid Targets from Complex Samples. *Nano Lett.* **2011**, *11*, 2083–2087.
12. Orozco, J.; Campuzano, S.; Kagan, D.; Zhou, M.; Gao, W.; Wang, J. Dynamic Isolation and Unloading of Target Proteins by Aptamer-Modified Microtransporters. *Anal. Chem.* **2011**, *83*, 7962–7969.
13. Balasubramanian, S.; Kagan, D.; Hu, C. J.; Campuzano, S.; Lobo-Castaño, M. J.; Lim, N.; Kang, D. Y.; Zimmerman, M.; Zhang, L.; Wang, J. Micromachine-Enabled Capture and Isolation of Cancer Cells in Complex Media. *Angew. Chem. Int. Ed.* **2011**, *50*, 4161–4164.
14. Campuzano, S.; Orozco, J.; Kagan, D.; Guix, M.; Gao, W.; Sattayasamitsathit, S.; Claussen, J. C.; Merkoçi, A.; Wang, J. Bacterial Isolation by Lectin-Modified Microengines. *Nano Lett.* **2012**, *12*, 396–401.
15. Kagan, D.; Laocharoensuk, R.; Zimmerman, M.; Clawson, C.; Balasubramanian, S.; Kang, D.; Bishop, D.; Sattayasamitsathit, S.; Zhang, L.; Wang, J. Rapid Delivery of Drug Carriers Propelled and Navigated by Catalytic Nanoshuttles. *Small* **2010**, *6*, 2741–2747.
16. Biswas, S.; Chaudhari, S. K.; Mukherji, S. Microbial Uptake of Diesel Oil Sorbed on Soil and Oil Spill Clean-up Sorbents. *J. Chem. Technol. Biotechnol.* **2005**, *80*, 587–593.
17. Machlis, G. E.; McNutt, M. K. Scenario-Building for the Deepwater Horizon Oil Spill. *Science* **2010**, *329*, 1018–1019.
18. Zhu, Q.; Pan, Q.; Liu, F. Facile Removal and Collection of Oils from Water Surfaces through Superhydrophobic and Superoleophilic Sponges. *J. Phys. Chem. C* **2011**, *115*, 17464–17470.
19. Cheng, M.; Gao, Y.; Guo, X.; Shi, Z.; Chen, J. F.; Shi, F. A Functionally Integrated Device for Effective and Facile Oil Spill Cleanup. *Langmuir* **2011**, *27*, 7371–7375.

20. Yao, X.; Song, Y.; Jiang, L. Applications of Bio-Inspired Special Wettable Surfaces. *Adv. Mater.* **2011**, *23*, 719–734.
21. McHale, G.; Shirtcliffe, N. J.; Aqil, S.; Perry, C. C.; Newton, M. I. Topography Driven Spreading. *Phys. Rev. Lett.* **2004**, *93*, 036102.
22. Zhang, J.; Pu, G.; Severtson, S. J. Fabrication of Zinc Oxide/Polydimethylsiloxane Composite Surfaces Demonstrating Oil-Fouling-Resistant Superhydrophobicity. *ACS Appl. Mater. Interfaces* **2010**, *2*, 2880–2883.
23. Shirtciffe, N.; McHale, G.; Newton, M. I.; Chabrol, G.; Perry, C. C. Dual-Scale Roughness Produces Usually Water-Repellent Surfaces. *Adv. Mater.* **2004**, *16*, 1929–1932.
24. Fragoso, A.; Laboria, N.; Latta, D.; Sullivan, C. K. O. Electron Permeable Self-Assembled Monolayers of Dithiolated Aromatic Scaffolds on Gold for Biosensor Applications. *Anal. Chem.* **2008**, *80*, 2556–2563.
25. Guo, M.; Diao, P.; Cai, S. Highly Hydrophilic and Superhydrophobic ZnO Nanorod Array Films. *Thin Solid Films* **2007**, *515*, 7162–7166.
26. Wang, J.; Wu, H.; Angnes, L. On-Line Monitoring of Hydrophobic Compounds at Self-Assembled Monolayer Modified Amperometric Flow Detectors. *Anal. Chem.* **1993**, *65*, 1893–1896.
27. Faucheux, N.; Schweiss, R.; Lutzow, K.; Werner, C.; Groth, T. Self-Assembled Monolayers with Different Terminating Groups as Model Substrates for Cell Adhesion Studies. *Biomaterials* **2004**, *25*, 2721–2730.
28. Sanchez, S.; Solovev, A. A.; Schulze, S.; Schmidt, O. G. Controlled Manipulation of Multiple Cells using Catalytic Microbots. *Chem. Commun.* **2011**, *47*, 698–700.
29. Floridia, M. A.; Rubert, A. A.; Benítez, G. A.; Fonticelli, M. H.; Carrasco, J.; Carro, P.; Salvarezza, R. C. Alkanethiol Adsorption on Platinum: Chain Length Effects on the Quality of Self-Assembled Monolayers. *J. Phys. Chem. C* **2011**, *115*, 17788–17798.
30. Wang, J. Cargo-Towing Synthetic Nanomachines: Towards Active Transport in Microchip Devices. *Lab Chip* **2012**, DOI: 10.1039/C2LC00003B.
31. Katira, P.; Hess, H. Two-Stage Capture Employing Active Transport Enables Sensitive and Fast Biosensors. *Nano Lett.* **2010**, *10*, 567–572.
32. Agarwal, A.; Katira, P.; Hess, H. Millisecond Curing Time of a Molecular Adhesive Causes Velocity-Dependent Cargo-Loading of Molecular Shuttles. *Nano Lett.* **2009**, *9*, 1170–1175.
33. Mendoza, S. M.; Arfaoui, I.; Zanarini, S.; Paolucci, F.; Rudolf, P. Improvements in the Characterization of the Crystalline Structure of Acid-Terminated Alkanethiol Self-Assembled Monolayers on Au(111). *Langmuir* **2007**, *23*, 582–588.
34. Offord, D. A.; John, C. M.; Linford, M. R.; Griffin, J. H. Contact Angle Goniometry, Ellipsometry, and Time-of-Flight Secondary Ion Mass Spectrometry of Gold Supported, Mixed Self-Assembled Monolayers Formed from Alkyl Mercaptans. *Langmuir* **1994**, *10*, 883–889.
35. Lee, T. R.; Laibinis, P. E.; Folkers, J. P.; Whitesides, G. M. Heterogeneous Catalysis on Platinum and Self-Assembled Monolayers on Metal and Metal Oxide Surfaces (Note a). *Pure Appl. Chem.* **1991**, *63*, 821–828.
36. Gao, W.; Uygun, A.; Wang, J. Hydrogen-Bubble-Propelled Zinc-Based Microrockets in Strongly Acidic Media. *J. Am. Chem. Soc.* **2012**, *134*, 897–900.
37. Zhao, G.; Seah, T. H.; Pumera, M. External-Energy-Independent Polymer Capsule Motors and Their Cooperative Behaviors. *Chem. Eur. J.* **2011**, *17*, 12020–12026.
38. Zhang, L.; Abbott, J. J.; Dong, L.; Peyer, K. E.; Kratochvil, B. E.; Zhang, H.; Bergeles, C.; Nelson, B. J. Characterizing the Swimming Properties of Artificial Bacterial Flagella. *Nano Lett.* **2009**, *9*, 3663–3667.
39. Loget, G.; Kuhn, A. Electric Field-Induced Chemical Locomotion of Conducting Objects. *Nat. Commun.* **2011**, *2*, 535, DOI: 10.1038/ncomms1550.

Supporting Information

Superhydrophobic Alkanethiol-Coated Microsubmarines for Effective Removal of Oil

Maria Guix[1,2,‡], *Jahir Orozco*[1,‡], *Miguel García*[1,3,‡], *Wei Gao,*[1] *Sirilak Sattayasamitsathit,*[1] *Arben Merkoçi,*[2] *Alberto Escarpa*[3] *and Joseph Wang*[1]*

[1]Department of Nanoengineering, University of California-San Diego, La Jolla, CA 92093, USA

[2]ICREA & Catalan Institute of Nanotechnology, Campus University Autónoma of Barcelona, E-08193 Bellaterra, Barcelona, Spain

[3]Department of Analytical Chemistry and Chemical Engineering, University of Alcalá, E-28871 Alcalá de Henares, Madrid, Spain.

*E-mail: josephwang@ucsd.edu

SI FIGURES CAPTIONS

SI Figure 1. Absence of interaction of hexanethiol (A) and mercaptohexanol (B)-modified microsubmarine with big olive oil droplets. Images taken consecutively after 11 s navigation time when the modified microsubmarine is approaching (a), contacting (b) and leaving (c) the big olive oil droplets (conditions, as in Figure 2). Inset the corresponding SAM-modified microsubmarine. Arrows indicate direction of the movement.

SI Figure 2. Effect of thiol length chain on the SAM-modified microsubmarine-oil droplets interaction. Unmodified microengine (A) and microsubmarine modified with hexanethiol (B) and dodecanethiol (C) SAMs. Images taken after approximately the same

‡ These authors have contributed equally to this work.

time of navigation in the fuel solution (conditions, as in Figure 2). Arrows indicate direction of the movement.

SI VIDEOS CAPTIONS

Supporting Video S1A. Interaction of C12-modified (left side) and undodified (right side)-microsubmarines with stained big olive oil droplets (attached to a glass slide).

Supporting Video S1B. Interaction of unmodified microengines with olive oil droplets of different sizes.

Supporting Video S2. C12-modified microsubmarines carrying small free-swimming olive oil droplets. Interaction through time.

Supporting Video S3. Interaction of C6-modified microsubmarines with big olive oil droplets.

Supporting Video S4. Interaction of microsubmarines modified with C6 SAMs of different head functional groups with big olive oil droplets: hexanethiol (A) and mercaptohexanol (B).

Supporting Video S5. Effect of thiol length chain on the SAM-modified microsubmarine-oil droplets interaction. Unmodified microengine (A) and microsubmarine modified with hexanethiol (B) and dodecanethiol (C) SAMs.

Supporting Video S6. C-12-modified microsubmarine cleaning motor oil from an oil-contaminated water sample.

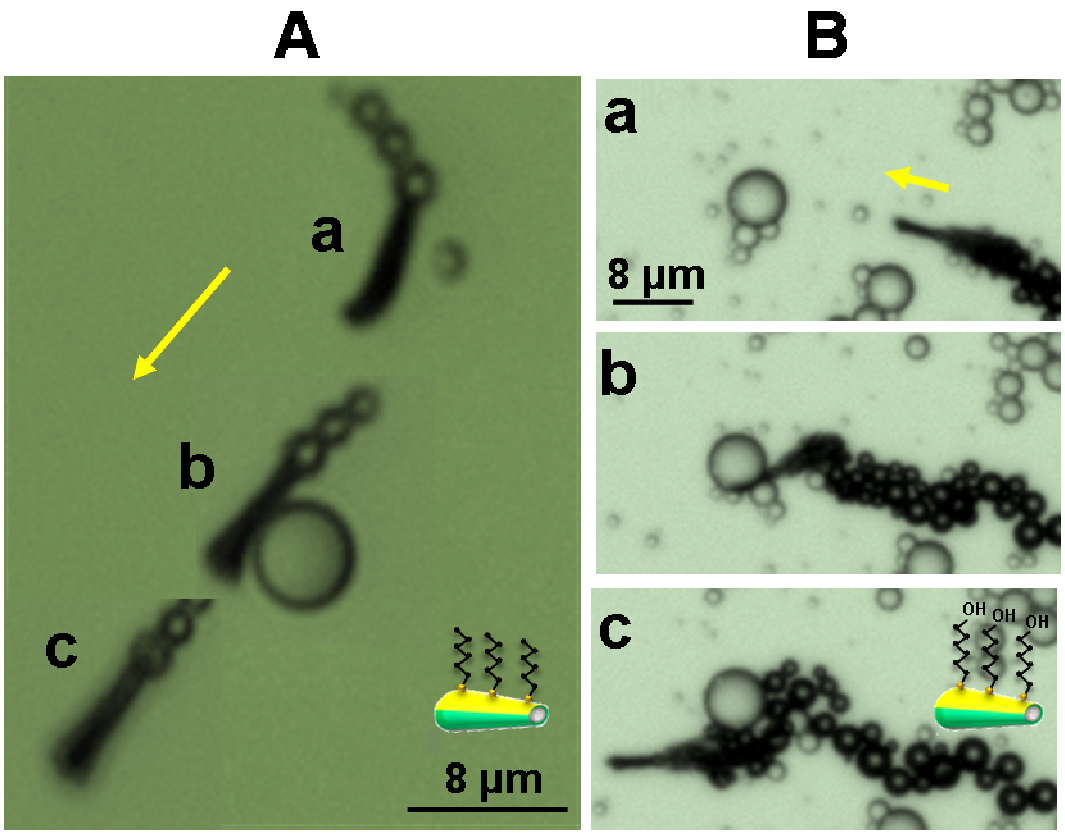

SI Figure 1. Absence of interaction of hexanethiol (A) and mercaptohexanol (B)-modified microsubmarine with big olive oil droplets. Images taken consecutively after 11 s navigation time when the modified microsubmarine is approaching (a), contacting (b) and leaving (c) the big olive oil droplets (conditions, as in Figure 2). Inset the corresponding SAM-modified microsubmarine. Arrows indicate direction of the movement.

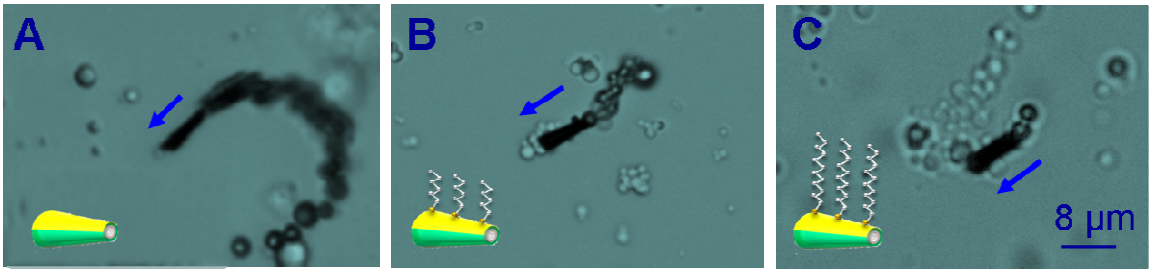

SI Figure 2. Effect of thiol length chain on the SAM-modified microsubmarine-oil droplets interaction. Unmodified microengine (A) and microsubmarine modified with hexanethiol (B) and dodecanethiol (C) SAMs. Images taken after approximately the same time of navigation in the fuel solution (conditions, as in Figure 2). Arrows indicate direction of the movement.